TECHNISCHE UNIVERSITÄT MÜNCHEN
FAKULTÄT FÜR CHEMIE
LEHRSTUHL FÜR ORGANISCHE CHEMIE II

Design and synthesis of novel inhibitors for human protease ClpXP and substrate identification of human and *S. aureus* ClpXP

Dissertation zur Erlangung des akademischen Grades eines
Doktors der Naturwissenschaften von

Thomas Frederik Gronauer

TECHNISCHE UNIVERSITÄT MÜNCHEN
FAKULTÄT FÜR CHEMIE
LEHRSTUHL FÜR ORGANISCHE CHEMIE II

Design and synthesis of novel inhibitors for human protease ClpXP and substrate identification of human and *S. aureus* ClpXP

Thomas Frederik Gronauer

Vollständiger Abdruck der von der Fakultät für Chemie der Technischen Universität München zur Erlangung des akademischen Grades eines

Doktors der Naurwissenschaften (Dr. rer. Nat.)

genehmigten Dissertation.

Vorsitzender:		Prof. Dr. Franz Hagn
Prüfer der Dissertation:	1.	Prof. Dr. Stephan A. Sieber
	2.	Prof. Dr. Kathrin Lang

Die Dissertation wurde am 27.11.2020 bei der Technischen Universität München eingereicht und durch die Fakultät für Chemie am 05.01.2020 angenommen.

Meiner Familie und meinen Freunden gewidmet

DANKSAGUNG

An dieser Stelle möchte ich meinen Dank an all diejenigen in meinem Umfeld richten, die zum erfolgreichen Gelingen dieser Arbeit beigetragen haben.

Zunächst möchte ich mich bei PROF. STEPHAN A. SIEBER dafür bedanken, dass ich meine Doktorarbeit unter seiner Ägide anfertigen durfte. Ausgebildet als reiner organischer Chemiker durfte ich an seinem Lehrstuhl die Kombination aus organischer Synthese und biochemischer Anwendung kennen und schätzen lernen. Ich möchte mich ebenso dafür bedanken, dass ich an einer Vielzahl von Forschungsthemen und Konferenzen teilnehmen konnte und seinerseits stetes Vertrauen in meine Arbeit genoss. Die durch Ihn geschaffenen strukturell und finanziell einmaligen Rahmenbedingungen bilden die beste Grundlage, um die eigenen Ideen verwirklichen und Neues entdecken zu können.

Des Weiteren danke ich meiner Prüfungskommission, welche sich kritisch mit dieser Dissertation auseinandergesetzt und diese eingehend begutachtet hat.

DIETRICH MOSTERT, KONSTANTIN ECKEL und MARTIN PFANZELT möchte ich meinen Dank aussprechen, dieser Arbeit auf sprachlicher und inhaltlicher Ebene die Mängel ausgetrieben zu haben.

Ohne den Input und die Expertise von Kooperationspartner*innen in und außerhalb des Arbeitskreises hätte ich diese Arbeit nicht anfertigen können. Mit MELANIE MANDL, MARTINA MEßNER, PROF. JOHANNA PACHMAYR und PROF. ANGELIKA VOLLMER möchte ich meinen Kollaborationspartnerinnen von der LMU für die erfolgreiche Zusammenarbeit beim ClpP-Projekt danken. MALTE WINNACKER danke ich für die Einführung in die Welt der makromolekularen Chemie. Ein großer Dank geht an meine Kollegen WOLFGANG HEYDENREUTER und CAROLIN GLEIßNER für die gelungene Kooperation beim Neocarzilin-Projekt. TUAN-ANH NGUYEN und PROF. KATHRIN LANG möchte ich für die gemeinsame Suche nach neuen ClpP-Substraten danken. ANH, Dir ganz speziell danke ich für deine Ausdauer und Beharrlichkeit bei den Western Blot Experimenten.

Bei FRANZISKA MANDL, BARBARA EYERMANN und ANGELA WEIGERT-MUÑOZ möchte ich mich für die gemeinsamen Erfahrungen bei der Betreuung der HPLCs bedanken. MARTIN PFANZELT danke ich für die Expertise und Seinen allgäuer Stoizismus beim gemeinsamen Bewältigen von IT-Problemen.

Mit Kolleg*innen an einem gemeinsamen Projekt zu arbeiten, erleichtert die eigene Aufgabe ungemein. Durch den regen Austausch in ungezählten Kaffee- und Kuchenpausen bin ich dem ClpP-Team, bestehend aus MARIA DAHMEN, CHRISTIAN FETZER, MATTHIAS STAHL, MATHIAS HACKL, MARKUS LAKEMEYER, ANJA FUX, DÓRA BALOGH, BARBARA EYERMANN, PATRICK ALLIHN, KONSTANTIN ECKEL und TILL REINHARDT zu höchstem Dank verpflichtet. Insbesondere MARKUS LAKEMEYER, der ClpP lebt wie kein anderer möchte ich für Seinen Wissensdurst und seine Erfahrungen, die er großzügig mit mir teilte, in höchstem Maße danken.

Eine große Stärke des Arbeitskreises ist das Gemeinschaftsgefühl, welches sich in gemeinsamen Unternehmungen, sportlichen Betätigungen und ausgelassenen Feiern entwickelt hat. Dies schlägt sich in einer überaus angenehmen Arbeitsatmosphäre nieder, welche die Herausforderungen des Laboralltags mühelos überstehen lässt. Es war mir eine wahre Freude die letzten Jahre in dieser Umgebung arbeiten zu dürfen. Vielen Dank an NINA BACH, ISABEL WILKINSON, FRANZISKA

MANDL, CAROLIN GLEIßNER, ROBERT MACSICS, STUART RUDDELL, DÓRA BALOGH, INES HÜBNER, JOSEF BRAUN, JAN-NIKLAS DIENEMANN, ALEXANDRA GEIßLER, DAVIDE BOLDINI, PATRICK ALLIHN, KONSTANTIN ECKEL, DIETRICH MOSTERT, MARTIN PFANZELT, THERESA RAUH, ANGELA WEIGERT-MUÑOZ, TILL REINHARDT, STEPHAN HACKER, MICHAEL ZOLLO und PATRICK ZANON.

Nicht zu vergessen sind natürlich alle Kolleg*innen, die während meiner Zeit ausgeschieden sind. Ihnen möchte ich dafür danken, dass sie den Lehrstuhl zu dem gemacht haben was er heute ist. Vielen Dank an PAVEL KIELKOWSKI, ANNABELLE HOEGL, IGOR PAVLOVIĆ, MATHIAS HACKL, MATTHIAS STAHL, VADIM KOROTKOV, PHILIPP LE, ELENA KUNOLD, WEINING ZHAO, KYU-MYUNG LEE, MARIA DAHMEN, MEGAN WRIGHT, JAN VOMACKA, JOHANNES LEHMANN, MARKUS LAKEMEYER, WOLFGANG HEYDENREUTER, ANJA FUX, BARBARA EYERMANN, JONAS DRECHSEL, VOLKER KIRSCH und LISA LEWALD.

Den aktuellen Masterand*innen JOHANNES WENGER, MICHAELA FIEDLER, MARKUS SCHWARZ, DARIO MRDOVIĆ und PATRICK RAUNFT wünsche ich für die Zukunft alles Gute und viel Erfolg.

Ganz speziell möchte ich den Mitgliedern des Labor B für die unterhaltsamen Jahre, jeden Ratschlag und Tipp und die anregenden Diskussionen danken. Angefangen bei FRANZISKA MANDL, MATHIAS HACKL und WEINING ZHAO, die bereits während meiner Masterarbeit für Ablenkung vom Laboralltag sorgten. Der zweiten Generation an Sitznachbarn, die ich erleben durfte, möchte ich ebenso danken. BARBARA EYERMANN, mit der ich den größten Teil der Zeit einen Schreibtisch teilen durfte, möchte ich für die angenehme Arbeitsatmosphäre und jeden aufmunternden Plausch danken. In gleicher Weise trugen PATRICK ALLIHN und ANGELA WEIGERT-MUÑOZ zur positiven Stimmung in Lab B bei und im letzten Jahr hat DOKTOR STUART RUDDELL die Reihe an grandiosen Sitznachbarn vervollkommnet.

Der mittäglichen Kaffeerunde bestehend aus DIETRICH MOSTERT, CAROLIN GLEIßNER, MARTIN PFANZELT, RAMONA ABSMEIER und VOLKER KIRSCH danke ich für die Überbrückung der temporären, geistigen Inaktivität nach den Essen in der Mensa.

Ein großer Dank geht an alle, die bei sportlichen Betätigungen für Ausgleich vom Arbeitsalltag gesorgt haben. Der Boulder-Gang um PATRICK ZANON, THERESA RAUH, PATRICK ALLIHN, TILL REINHARDT und STUART RUDDELL danke ich für die Motivation frühmorgens auf der Matte des Kletterzentrums zu stehen. Den Fahrradfahrer*innen CAROLIN GLEIßNER, STUART RUDDELL, TILL REINHARDT, PATRICK ALLIHN, THERESA RAUH, CHRISTOPHER DODT und MARIE-LENA JOKISCH danke ich für den ein oder anderen Windschatten, der die Fahrt nach Garching erleichtert hat.

Die Zusammenarbeit mit zahlreichen Forschungspraktikant*innen hat mir ausgesprochen viel Freude bereitet und hat einen wesentlichen Beitrag zu dieser Arbeit geleistet. Für den Fleiß und die Motivation möchte ich mich insbesondere bei JOHANNES GROßKOPF, NAZIFA HAMIDZADA, JULIA FRIEDERICH, NINA WICHMANN, IMKE LEMMER, TONI MURNAUER, SEBASTIAN FENZL, JOHANNES WENGER, PHILIPP SCHLOZ, STEFANIE NADLER, TIM RHEINFRANK und JONAS RACKL bedanken. Viel Erfolg auf Eurem weiteren Weg.

Ein besonderer Dank gebührt KATJA BÄUML, MONA WOLFF und allen Auszubildenden für Ihre Geduld und Ausdauer, den täglichen Laborbetrieb am Leben zu erhalten. CHRISTINA BRUMER möchte ich einen großen Dank aussprechen, für Ihre Hilfe in allen organisatorischen und bürokratischen Fragen.

Zu guter Letzt gebührt der allergrößte Dank den Menschen, die mir am allernächsten stehen. Meinen Eltern MARIA und WERNER GRONAUER und meiner Schwester LAURA SYED möchte ich für Ihre bedingungslose Unterstützung, das Vertrauen und den Rückhalt danken. Ihr steht in allen Lebenssituationen hinter mir und gebt mir stets Sicherheit. Meiner Freundin SOPHIA möchte ich für die gemeinsame Zeit, ihr Verständnis und die liebevolle Unterstützung danken. Du bist zugleich mein Ruhepol und Antrieb in allen Lebenslagen.

ABSTRACT

Cancer is the most common cause of death in western developed countries, second only to cardiovascular diseases. Acute myeloid leukemia, a treacherous cancer that impairs the development of blood cells demonstrates only a poor survival rate. Medication normally includes a combination of the nucleoside analog cytarabine and agents of the class of anthracyclines that were introduced in the 1960s and 70s. Since then, several new agents have been investigated, resulting in the kinase inhibitor Gleevec from Novartis as a novel potent drug adding to the standard regimen. Nevertheless, novel chemotherapeutic agents and strategies are urgently needed. Caseinolytic protease P (ClpP) is a barrel-shaped serine protease composed of two heptameric rings that are stacked back to back. Together with the hexameric chaperone ClpX, it forms a complex (ClpXP) that is able to degrade damaged proteins which might otherwise harm the cell. In its function as a potential stress response regulator, ClpXP was recently found to be a promising target for the development of novel approaches to treat acute leukemias. Inhibition of ClpP showed reduction in cell viability of AML cells, however current ClpP inhibitors lack physico-chemical properties to become potential drug candidates.

In this thesis, a novel generation of chemical tools for the manipulation of human ClpP activity is introduced. A high-throughput screen, initially targeted to identify small molecular inhibitors for *Staphylococcus aureus* ClpP, revealed phenyl esters with a characteristic naphthofuran scaffold as potent novel compound class for human ClpP inhibition. Dissection of structural key features led to the development of an activity-based probe that enabled *in situ* investigation of cellular targets in chemical proteomics experiments. Lastly, this resulted in meaningful insights into the bioactivity of this new compound class which showed promising anti-proliferative and anti-migratory effects in human cancer cells.

Since ClpXP is able to degrade a variety of different substrates, it is not only important to possess a potent handle for activity manipulation, but also to gain a deeper knowledge about the entirety of target proteins. Therefore, the second chapter focusses on the identification of novel substrates and interactors of human ClpXP. For this purpose, several ClpP-mutants bearing a photoactivatable amino acid in different positions were generated by site-directed mutation using amber codon suppression. In a mass-spectrometry-based approach, UV-light induced trapping of substrates and interactors in live cells allowed for the discovery of new protein substrates. These results make a valuable contribution to better understand the influence of ClpP in human cells.

In the third chapter, a similar approach was applied to uncover potential protein substrates of *Staphylococcus aureus* ClpXP. Here, a peculiar feature of phenyl ester peptidomimetics was utilized. Initially, phenyl esters were optimized for ClpXP inhibition by the introduction of a peptide scaffold to mimic natural substrates. However, certain scaffolds showed a considerable stimulation of ClpXP activity by simultaneously occupying the active site serines in substoichiometric concentrations. This characteristic was used to trap ClpP substrates by phenyl ester peptidomimetics modified with a photoreactive moiety. Mass spectrometry analysis of these trapped proteins revealed several new protein substrates associated to *S. aureus* virulence confirming the importance of ClpXP in virulence regulation.

ZUSAMMENFASSUNG

Krebs ist nach Herz-Kreislauf-Erkrankungen die zweithäufigste Todesursache in westlichen Industrieländern. Die akute myeloische Leukämie, eine tückische Krebsart, die die Entwicklung von Blutzellen beeinträchtigt, weist nur eine geringe Überlebensrate auf. Die Behandlung umfasst gewöhnlich eine Kombination aus dem Nukleosidanalogon Cytarabin und Wirkstoffen aus der Klasse der Anthrazykline, die in den 1960er und 70er Jahren eingeführt wurden. Seither wurde eine Reihe an neuartigen Substanzen untersucht. Der Kinaseinhibitor Gleevec von Novartis zeigte dabei hohe Wirksamkeit und wurde der Standardbehandlung hinzugefügt. Nichtsdestotrotz werden dringend weitere neue chemotherapeutische Wirkstoffe und Strategien benötigt.

Die caseinolytische Protease P ist eine fassförmige Serinprotease, welche aus zwei heptameren Strukturen besteht, die zusammen als Doppelring angeordnet sind. Gemeinsam mit dem hexameren Chaperon ClpX bildet sie einen Komplex, der in der Lage ist, schadhafte Proteine abzubauen, welche andernfalls die Zelle schädigen könnten. In seiner Funktion als potentieller Stressreaktionsregulator wurde ClpXP kürzlich als vielversprechender Ansatzpunkt für die Entwicklung neuer Strategien zur Behandlung von Leukämien entdeckt. Die Inhibition von ClpP zeigte eine Verminderung der Proliferation von AML-Zellen. Allerdings fehlen derzeitigen ClpP-Inhibitoren die physikochemischen Eigenschaften, um aussichtsreiche Arzneimittelkandidaten zu werden.

In dieser Arbeit wird eine neue Generation von chemischen Strukturen zur Beeinflussung der ClpP-Aktivität in menschlichen Zellen vorgestellt. Ein Hochdurchsatz-Screening, das ursprünglich darauf abzielte, niedermolekulare Inhibitoren für *Staphylococcus aureus* ClpP zu identifizieren, stieß auf Phenylester mit einer charakteristischen Naphthofuran-Struktur, welche eine potente neue Wirkstoffklasse für die selektive Inhibition von humanem ClpP darstellten. Eine Untersuchung von strukturellen Schlüsselmerkmalen führte zur Entwicklung einer aktivitätsbasierten Sonde, die die intrazelluläre Untersuchung von Zielproteinen in chemischen Proteomik-Experimenten ermöglichte. Letztendlich führte dies zu wichtigen Erkenntnissen über die Bioaktivität dieser neuen Verbindungsklasse, welche vielversprechende antiproliferative und antimigratorische Wirkungen aufwies.

Da ClpXP in der Lage ist, eine Vielzahl verschiedener Substrate abzubauen, ist es einerseits nicht nur wichtig, über ein potentes Werkzeug zur Aktivitätsmanipulation zu verfügen, sondern auch ein grundlegendes Wissen über die Gesamtheit der Zielproteine aufzubauen. Aus diesem Grund werden im zweiten Kapitel Ansätze zur Identifizierung neuer Substrate und Interaktoren von humanem ClpXP vorgestellt. Zu diesem Zweck wurden mehrere ClpP-Mutanten, die eine photoaktivierbare Aminosäure an verschiedenen Positionen aufweisen, durch gerichtete Mutation unter Verwendung von Amber-Codon-Suppression erzeugt. In einem Massenspektrometrie-

basierten Ansatz ermöglichte das, durch UV-Licht induzierte Trapping von Substraten und Interaktoren in lebenden Zellen, die Entdeckung neuer Proteinsubstrate. Diese Ergebnisse leisten einen wertvollen Beitrag, um den Einfluss von ClpP in menschlichen Zellen besser zu verstehen.
Im dritten Kapitel wurde ein ähnlicher Ansatz angewandt, um potenzielle Proteinsubstrate von *Staphylococcus aureus* ClpXP zu identifizieren. Dabei wurde eine Besonderheit von Phenylester-Peptidomimetika genutzt. Ursprünglich wurden Phenylester für die Hemmung von ClpXP durch die Einführung eines Peptidgerüsts zur Nachahmung natürlicher Substrate optimiert. Bestimmte Strukturen zeigten jedoch eine ungewöhnliche Stimulation der ClpXP-Aktivität bei gleichzeitiger Bindung der katalytisch aktiven Zentren in sub-stöchiometrischen Konzentrationen. Diese Eigenschaft wurde genutzt, um ClpP-Substrate durch Phenylester-Peptidomimetika, die mit einer photoreaktiven funktionellen Gruppe modifziert wurden, einzufangen. Die massenspektrometrische Analyse dieser eingefangenen Proteine ergab mehrere neue Substrate, die mit der Virulenz von *S. aureus* in Verbindung stehen und dadurch die Bedeutung von ClpXP bei der Virulenzregulation verdeutlichen.

GENERAL REMARKS

The work for this doctoral thesis was conducted in the time between February 2016 and September 2020 at the Chair of Organic Chemistry II under supervision of Prof. Dr. Stephan A. Sieber.

Parts of this dissertation are based on the following publication and manuscript in preparation:

Chapter 2:

Design and synthesis of tailored human caseinolytic protease P inhibitors

Thomas F. Gronauer, Melanie M. Mandl, Markus Lakemeyer, Mathias W. Hackl, Martina Meßner, Vadim S. Korotkov, Johanna Pachmayr, Stephan A. Sieber

Chemical Communications, 2018, 54, 9833-9836.

Reproduced by permission of The Royal Society of Chemistry.

Chapter 3:

Manuscript in preparation

Conference presentation

Design and synthesis of tailored human caseinolytic protease P inhibitors

Thomas F. Gronauer, Melanie M. Mandl, Markus Lakemeyer, Mathias W. Hackl, Martina Meßner, Vadim S. Korotkov, Johanna Pachmayr, Stephan A. Sieber

Gordon research seminar and conference: High Throughput Chemistry and Chemical Biology, June 02 – June 07 2019, New London (NH) USA

Research topics that are not covered in this thesis

Neocarzilin A Is a Potent Inhibitor of Cancer Cell Motility Targeting VAT-1 Controlled Pathways

Carolin M.-L. Gleissner, Carolin L. Pyka, Wolfgang Heydenreuter, Thomas F. Gronauer, Carina Atzberger, Vadim S. Korotkov, Weiting Cheng, Stephan M. Hacker, Angelika M. Vollmar, Simone Braig, Stephan A. Sieber

ACS Central Science, 2019, 5, 7, 1170.

Polyamid/PEG Blends as Biocompatible Biomaterials for the Convenient Regulation of Cell Adhesion and Growth

Malte Winnacker, Andreas J. G. Beringer, Thomas F. Gronauer, Hicran H. Güngör, Leonhard Reinschüssel, Bernhard Rieger, Stephan A. Sieber

Macromolecular Rapid Communications, 2019, 40, 1900091.

Sustainable Polyesteramides and Copolyamides: Iinsights into the Copolymerization Behavior of Terpene-Based Lactams

Malte Winnacker, David H. Lamparelli, Carmine Capacchione, Hicran H. Güngör, Lucas Stieglitz, Katia S. Rodewald, Matthias Schmidt, Thomas F. Gronauer

Macromolecular Chemistry and Physics, 2020, 2000110.

TABLE OF CONTENTS

1

Introduction

1 Introduction

According to a recent estimate, a reference human body contains about $3.0 \cdot 10^{13}$ cells.[1] With 84%, erythrocytes represent the numerical majority of human cells, while 75% of cell mass is provided by adipocytes and myocytes.[2] Regardless of which cell type of the human body, cells are usually composed of the same fundamental elements. A nucleus that harbors the genetic information, essential for reproduction and construction of all other parts of the cell, the endoplasmic reticulum as site of synthesis and modification of proteins and lipids and the Golgi apparatus as transport system for proteins. Lysosomes and peroxisomes are the main recycling sites for intracellular debris and mitochondria provide the cell with energy by oxidation of carbohydrates resulting in generation of ATP.[3] Various neurodegenerative diseases are connected to mitochondrial dysfunction such as Parkinson's and Alzheimer's disease as well as multiple sclerosis.[4–6] Due to the presence of high concentrations of oxygen inside mitochondria, these organelles are constantly exposed to oxidative stress and require a machinery that averts potential damage. The last resort for severely damaged mitochondria is a process called mitophagy, where cells initiate a salvage pathway that leads to selective removal and recycling of mitochondria by the autophagosome.[7] However, since decay and biogenesis afford a great amount of resources, nature has evolved ways to circumvent the point of no return.

Damaged, misfolded or otherwise not correctly translocated mitochondrial proteins are processed by a variety of proteins that can be subdivided according to their location inside mitochondria. The organelle comprises a unique architecture with two membranes enclosing the mitochondrial matrix, creating an additional intermembrane space. For each subsection a select choice of chaperones and proteases is responsible for protein homeostasis. Their role and functions are thoroughly detailed in a very comprehensive review.[8] In the mitochondrial matrix, the task of protein quality control is performed primarily by ATP-dependent oligomeric proteins LonP1 and ClpXP.[9] The former degrades misfolded, oxidized and damaged proteins into smaller peptides which are further processed into amino acids by oligopeptidases like PITRM1.[8] It shows significant sequence homology to its mouse and yeast congeners, which was used to investigate its regulatory role for mitochondrial genome expression and stability.[10] The role of protease ClpXP is detailed in the following chapter and represents the unifying subject of this thesis.

1.1 Caseinolytic protease P

In the cytosol of human cells, a large protein complex termed 26S proteasome is responsible for degradation of dispensable proteins. It consists of a cylindrical 20S core subunit which contains the catalytically active sites and is capped on both apical sites by 19S ring structures that regulate recognition of target proteins.[11,12] Prior to degradation, proteins designated for proteolytic disassembly are marked by a string of ubiquitin, serving as recognition motif of the 19S subunit.[13] In 2004, the work for elucidation of the role and function of ubiquitin-regulated protein degradation was honored with the Nobel prize in chemistry.[14] Based on these eminent findings, numerous applications have since emerged that paved the way for the development of novel strategies to tackle various human diseases. Bortezomib, the first proteasome inhibitor, was found to covalently bind to the active site threonine of certain *β*-subunits and is currently used as a chemotherapeutic agent by inducing apoptosis in malignant cells.[15] A very elegant approach developed by the groups of *Raymond Deshaies* and *Craig Crews* made use of the ubiquitylation machinery to trigger degradation of specific proteins targeted by chimeric molecules. In this way, degradation of any disease-causing protein might be feasible.[16]

A structurally similar, albeit less complex relative of the 26S proteasome is the mitochondrial caseinolytic protease P (ClpP). It is composed of two heptameric rings that are stacked back-to-back to form a barrel-shaped compartment shielding a cavity with fourteen catalytically active sites consisting of a classical serine-histidine-aspartate triad.[17] The spatial dimension of a ClpP tetradecamer is described to be 50 Å in height and 90 Å in diameter.[18] Human ClpP is encoded by a nuclear gene on chromosome 19p13.3 and is expressed as a 277 amino acid sequence into the cytosol with a C-terminal 56 amino acid bearing mitochondrial targeting sequence.[17,19] After transport to the mitochondrion, human proClpP is assumed to be translocated to the mitochondrial matrix by TOMM22 and TIMM22/23, where it is processed to its mature form.[20] It is further presumed that removal of the mitochondrial targeting sequence is accomplished by mitochondrial processing peptidase MPP. Experiments have shown that the ClpP sequence is additionally reduced by an eight amino acid containing sequence, catalyzed by mitochondrial intermediate peptidase (MIPEP).[20] Ultimately, a member of the family of aminopeptidases cleaves the remaining leucine-residue to give rise to the mature protease.[20]

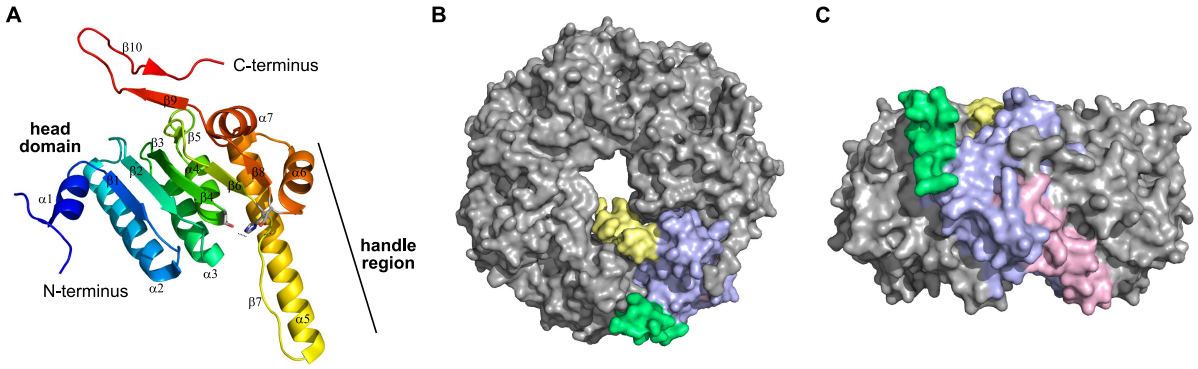

Figure 1.1 Structural features of human ClpP (PDB-identifier: 1TG6).[21] A) Rainbow representation of hClpP monomer from N-terminus to C-terminus. Active site residues are depicted as sticks. B) Top and C) side view of human ClpP heptamer with one ClpP monomer highlighted with N-terminus (pale yellow), C-terminus (lime green), head-domain (light blue) and α5-helix (light pink).

After processing, each ClpP monomer is composed of 221 amino acids that arrange in seven alpha-helices and ten *β*-sheets with a C-terminal extension of 28 amino acids that is not essential for activity.[22] The remaining 193 amino acids form a structure that resembles a hatchet with the blade composed of helices 1-4 and parallel *β*-sheets 1,2,3,5 and 7 which are perpendicular to *β*-sheets 4,6 and 8 (Figure 1.1).[22] The handle is composed of helix α5 and *β*-sheet 7. Contacts of α-helices 2,3,4,6 and 7 to the *β*-sheets are formed by tucking into the folds generated between the *β*-sheets. Altogether, each ClpP monomer can be divided into three structural regions, the globular head-domain, the handle and the N-terminal loop.[23] Contacts among the monomers are established by the head domains by packing of helices α2 and α3 of one monomer against the *β*1-sheet of another. Further contacts are made by α2 and α1 of two adjacent subunits as well as α5 with *β*2 and α7.[23] Tetradecameric ClpP is formed by intercalation of two heptamers resulting in contacts of each handle region with the corresponding opposite ring. The lateral wall of ClpP tetradecamer is build up by the flexible α5 helix through hydrophobic contacts of the side chains with sheet *β*7. Hydrogen bonding between *β*7 and α6 and a salt bridge between Arg170 and Glu169 further strengthens the interactions.

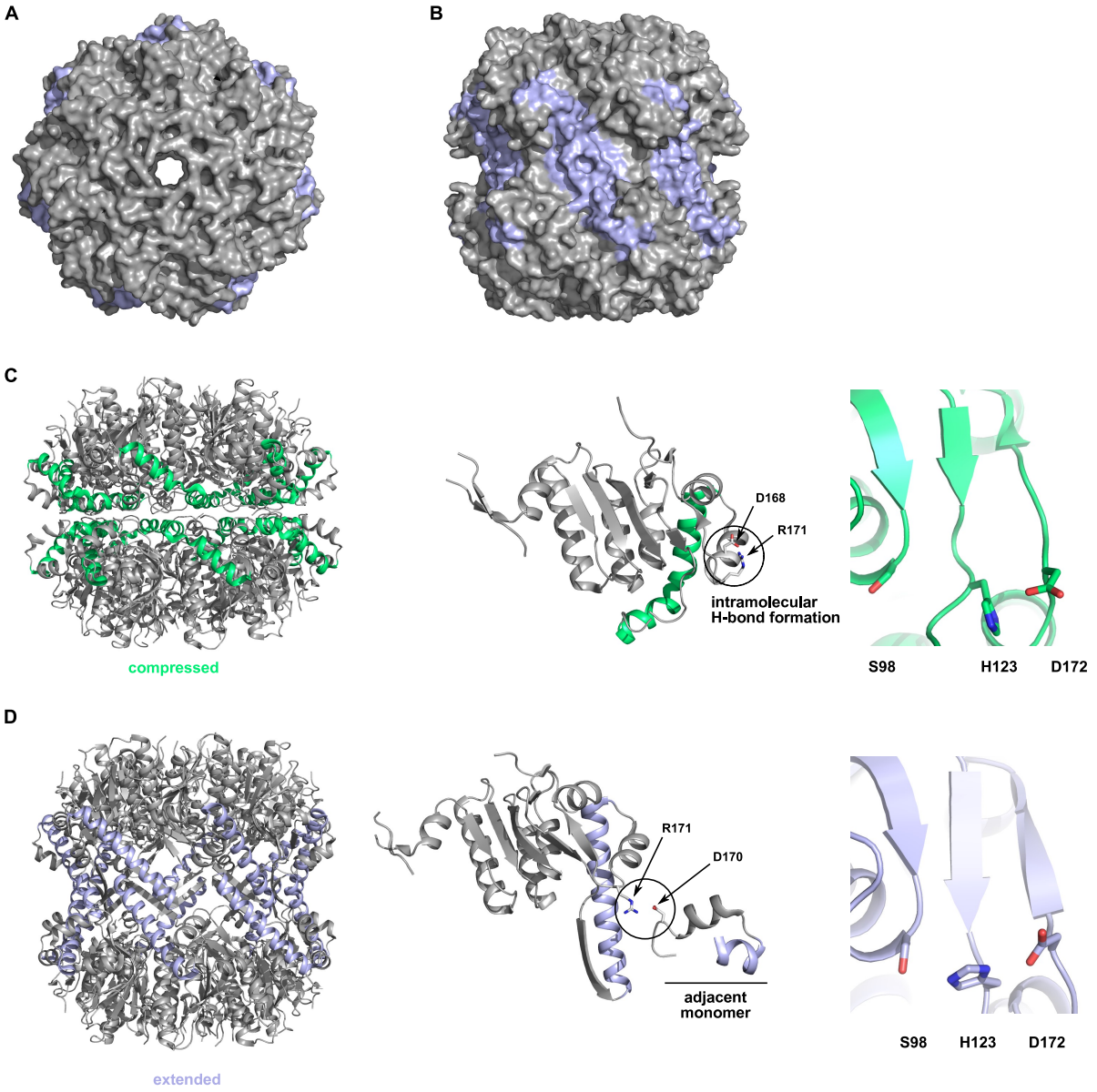

Figure 1.2 Structure of tetradecameric SaClpP in A) top view and B) side view in the extended state. α5-Helices are highlighted in light blue. (PDB-identifier: 3V5E).[24] C) SaClpP tetradecamer in the compressed state (PDB-identifier: 3QWD)[25] with α5-helices highlighted in lime green (left). SaClpP monomer displaying kinked α5-helix and amino acid residue R171 forming an intramolecular hydrogen bond with D168 (middle). Active site residues are misaligned in the compressed state (right). D) Tetradecamer in its extended state with α5-helices highlighted in light blue (left). Monomer with straight α5-helix and intermolecular connection of two heptameric rings by residues R171 and D170 of an adjacent monomer (middle). Active site residues are aligned in the extended state (right).

Interestingly, in ClpP from *Staphylococcus aureus* the salt bridge network was discovered to be essential for tetradecamer formation and activity (Figure 1.2).[24] The interface between monomers of adjacent rings is controlled by a so-called arginine sensor. In each monomer, the sensor is composed of Arg171 of one ring and Asp170 of the other and impacts the orientation of side chains influencing the intercalation of the handle regions and the functional alignment of the active site residues (Figure 1.2D). Thus, three different states of ClpP tetradecamers could be identified. An extended state, a compressed form and a compact state where ClpP is in transition between extended and compressed form.[26] In the extended state, Arg171 of one monomer forms a hydrogen

bond with Asp170 of the opposite subunit, resulting in extension of the tetradecamer and alignment of the catalytic triad. The compressed state is created by hydrogen bond connection between Arg171 and Asp168 on the same monomer subunit, leading to a misalignment of the active site.[24] This switch between extended/active and compressed/inactive state makes it tempting to assume a mechanism in which ClpP switches between extended and compressed states to laterally release fragments of degraded proteins.

Independent of the organism, ClpP always features a catalytic triad that is composed of serine, histidine and aspartic acid.[17] Inside the barrel, fourteen of such sites are located in a cleft at the connection of the head and handle domain (Figure 1.1A).[27] The N-terminus of each monomer extrudes above the barrel-shaped chamber, forming the rim of the axial pore which is narrowed to 12 – 20 Å by residues Glu8, Arg15 and Tyr17.[22,27] This accounts for the fact that ClpP on its own can only degrade short peptides with <15 residues.[28]

In order to degrade larger proteins, ClpP establishes a complex with a chaperone of the AAA+ family (ATPase Associated with diverse cellular Activities). In mammalian cells, the role of substrate recognition and ATP-dependent unfolding is fulfilled by protein ClpX. However, other organisms encode a plethora of other proteins, accomplishing the same function. ClpX is composed of a large domain and a small domain that are connected by a short hinge. The ATPase assembles as a hexamer with an axial pore that is formed by the large domain. Loop regions extending from the large domain are responsible for gripping and translocating substrate proteins in an ATP-dependent manner.[29] In a complex with ClpP it does not only stimulate ClpP activity through allosteric effects on its conformation, but also promotes interactions between ClpP heptamers.[28] ClpX binds to the apical side of ClpP forming a continuous substrate channel. Here, binding to the peptidase subunit occurs primarily through hydrophobic interactions of a short amino acid sequence (IGF loop) with lipophilic pockets on the apical surface of ClpP.[30] One contradictory feature of the ClpXP degradation machinery is the apparent hexamer-heptamer symmetry mismatch. In the last years, extensive research has improved the comprehension of this peculiarity. More recently, the binding interface between ClpX and ClpP2 from *Listeria monocytogenes* was illuminated by cryogenic electron microscopy (cryo-EM).[31] The findings indicate that the chaperone attaches to the peptidase by interaction of six IGF-loops with the corresponding ClpP counterparts, with omission of one ClpP monomer. Together with the stretching of one IGF-loop this results in a tilted plane relative to the ClpP axis. Further highly dynamic interactions are established by an entrance pore surrounding pore-2 loops with N-terminal loops of ClpP2 (Figure 1.3).[31]

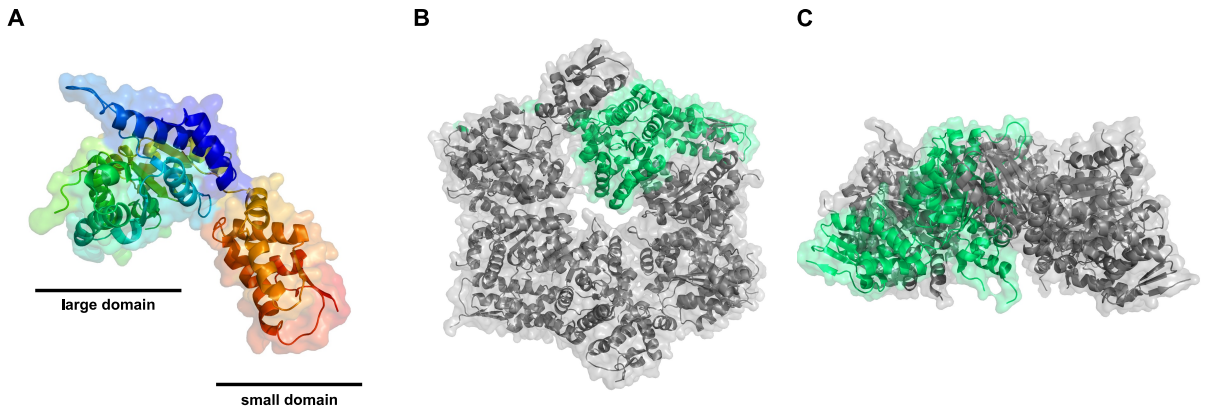

Figure 1.3 Crystal structure of *E. coli* ClpX, depicted in its cofactor bound form (PDB identifier: 3HWS).[32] A) ClpX monomer depicting its large and small domain. B) Top view and C) side view of the ClpX hexameric structure with one monomer highlighted in lime green.

In ClpX from *Neisseria meningitides* it was shown that substrate engagement predominantly occurs by conserved pore-1 loops that are located in the upper part of the entrance pore. Especially one residue, Tyr153, establishes close contacts with the protein substrate. It was proposed that by subsequent ATP-binding and hydrolysis, conformational changes lead to a threading of the peptide into the core subunit.[33] The kinetic background of this process was further examined by an approach using optical tweezers. Here, ClpXP and an appropriate substrate is clamped between two molecular optical reporters which are used to observe ClpX pulling steps.[34]

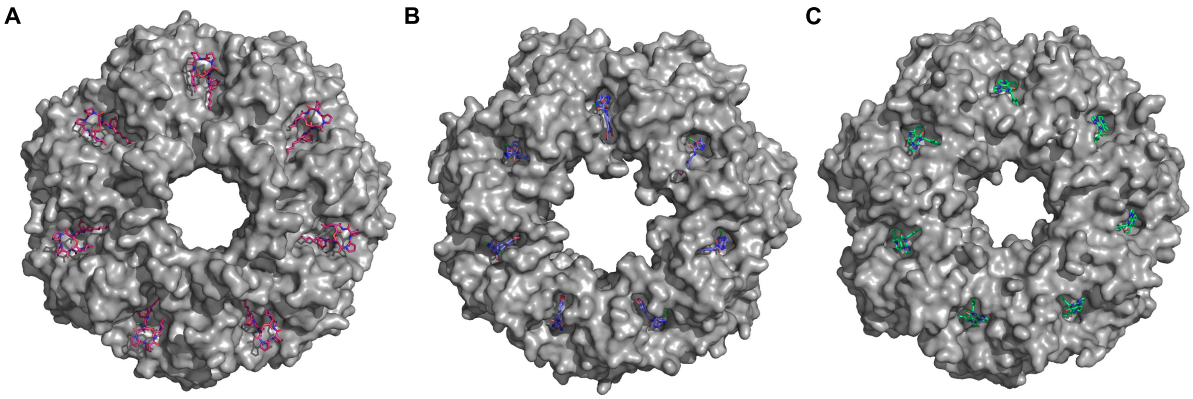

Figure 1.4 Small molecule activators bind to the apical site of ClpP and induce pore opening. A) Crystal structure of ADEP bound to SaClpP (PDB-identifier: 6TTZ).[35] B) Binding of D9 (PDB-identifier: 6H23)[36] and C) compound ONC201 to hClpP (PDB-identifier: 6DL7).[37]

Interestingly, small molecules can exert the same influence on ClpP activity as ClpX. Over the years, several species-selective chemical scaffolds have been identified that exhibit a stimulating effect on ClpP. In 2005, *Brötz-Oesterhelt et al.* could show that the stimulating character of acyldepsipeptides can be exploited as a novel class of antibiotics.[38] By binding to the hydrophobic sites on the head domain of ClpP, ADEPs outcompete ClpX and provoke a conformational change resulting in opening of the axial pore. The enlarged pore facilitates entrance of surrounding proteins entailing unspecific proteolysis and depletion of essential proteins (Figure 1.4).[30] The same picture

is observed with activator ACP1b, which was identified to stimulate bacterial ClpPs from a variety of different organisms.[39] In 2018, the selective human activator D9 was described and one year later the cytotoxic effect of imipridone ONC201 was related to overactivation of human ClpP. Together with its more effective congener ONC212, it is currently under investigation in clinical trials.[36,40]

In the past decades, ClpXP has attracted a great number of research groups leading to investigations that successfully expanded the knowledge about this fascinating entity. Ongoing studies further shed light on the cellular role of ClpP by manipulation of its catalytic activity.

1.2 Activity-based protein profiling

In the field of chemical biology, activity-based protein profiling (ABPP) has emerged as a powerful tool to investigate protein function within a complex biological environment by exploiting the catalytic activity of enzymes.[41] These cellular catalysts accelerate reaction rates of molecules by providing ideal conditions for the reaction in a confined space. Most of the time, one or more amino acid residues actively participate in conversion of a substrate molecule.[3] Therefore, these active sites express elevated reactivity and can be addressed by a suitable small molecule with appropriate affinity.[42] In drug discovery, this approach proved to be exceptionally useful, as phenotypic screenings of natural products can be further substantiated by determination of the cellular target. Since the first experiments which strived for the identification and localization of serine proteases[43,44] the technology has evolved dramatically under *Cravatt et al.*[45,46] and *Bogyo et al.*[42,47] and is now applied for identification of proteins with various active site residues.

Structurally, these activity-based probes (ABP) are composed of three characteristic features. A reactive functional group that is selective for the catalytic amino acid residue of a specific enzyme class, a linker and a biologically silent reporter tag (Figure 1.5A).[41] As reactive centers of enzymes typically contain a nucleophilic residue, the warhead of an ABP must exhibit an electrophilic functional group. A key factor thereby is to provide balance between reactivity and selectivity. Warheads with excessive reactivity will lead to unselective labeling and high false positive rates, while low reactivity excludes potentially essential targets.[48]

ABPP has been applied to address a variety of enzyme classes. For instance, fluorophosphonates[49] and arylphosphonates[50] have been used to profile serine hydrolases, while epoxides[47] and acyloxymethylketones[51] exhibited selectivity for cysteine proteases. In contrast, an inverse approach that exploits the broad reactivity of iodoacetamide enabled the global discovery of ligandable cysteines in human[52] and bacterial proteomes.[53]

A major benefit of ABPP is the applicability in live cells that allows the investigation of target proteins in their native environment. Solubility issues, limited permeability and steric demand of the reporter group, however, restricts the application of ABPs. Thus, the reporter tag is usually attached to the probe after incubation and cell lysis *via* an appropriate orthogonal reaction. For this, *Staudinger ligation*,[54] *tetrazine ligation*[55] and copper-assisted 1,3-dipolar *Huisgen*-cycloaddition[45,56] have proved to be suitable ways to introduce such an entity. Due to its relatively high reaction rate, high selectivity as well as applicability in aqueous solutions the so-called *click*-reaction of a terminal alkyne with an alkyl-azide is today the most frequently used ligation method.[56,57] Additionally, introduction of an alkyne-tag to the structure of a natural product represents only a minor alteration.

To allow visualization of labeled proteins, the cells are lysed and a reporter consisting of a fluorescent molecule coupled to an azide moiety is clicked to the alkyne tag of the probe. Separation by sodium dodecyl sulfate polyacrylamide gel electrophoresis (SDS-PAGE) with subsequent fluorescence scanning enables analysis of the labeled proteome (Figure 1.5B).

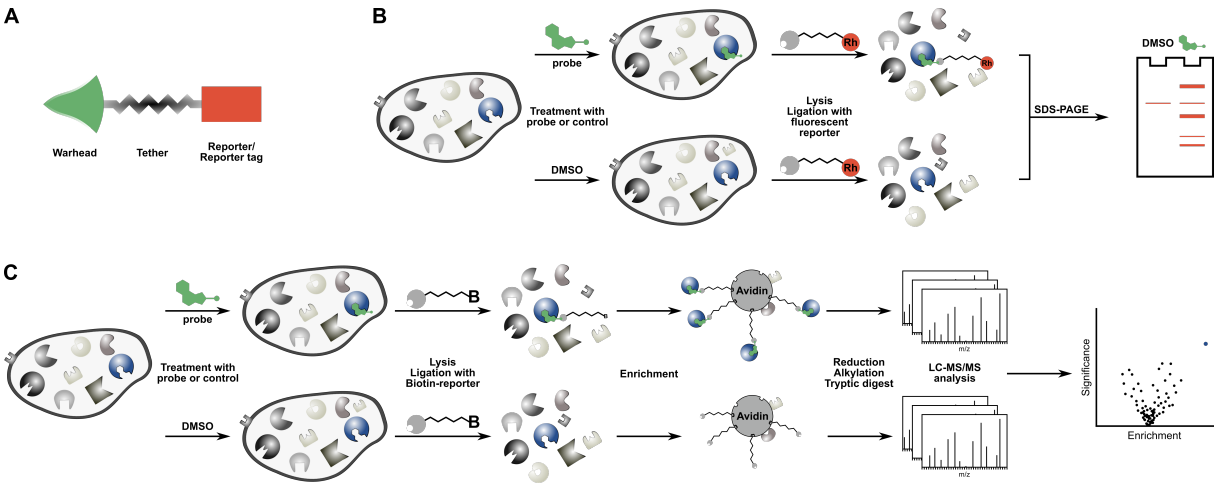

Figure 1.5 A) Simplified structure of a classical activity-based probe, containing a reactive moiety that is connected to a reporter molecule or a reporter tag. B) Schematic representation of a gel-based activity-based protein profiling workflow. Cells are treated either with probe or compound vehicle as a control, cells are further lysed and a fluorescent reporter is attached *via* bioorthogonal ligation. Visualization is achieved by SDS-PAGE. C) Workflow representing a classical MS-based ABPP experiment. Cells are incubated with compound or control, ligated to biotin and labeled proteins are enriched using streptavidin-agarose beads. Reduction, alkylation and tryptic digest generates peptides that are analyzed by LC-MS/MS.

For quantitative analysis, labeled proteins are clicked to a biotin-azide conjugate (Figure 1.5C). After protein precipitation and re-solubilization, the high affinity of biotin to streptavidin is utilized for enrichment of protein-biotin adducts.[58] In a gel-free approach, cysteine residues of enriched proteins are further reduced and alkylated before they are digested with an appropriate protease.[41] After desalting of eluted peptides, quantification and identification is performed by liquid chromatography coupled to tandem mass spectrometry (LC-MS/MS).

Unfortunately, small molecules that do not bind covalently to their target protein fail to enrich proteins by the above-mentioned approach. To circumvent this obstacle, probes are further modified to contain a functional group for UV-light induced crosslinking.[59] This photoactivatable moiety can be of various composition depending on the structural available space and appropriate irradiation wavelength. Common photoreactive groups that are applied in photoaffinity labeling are summarized in Figure 1.6.[60]

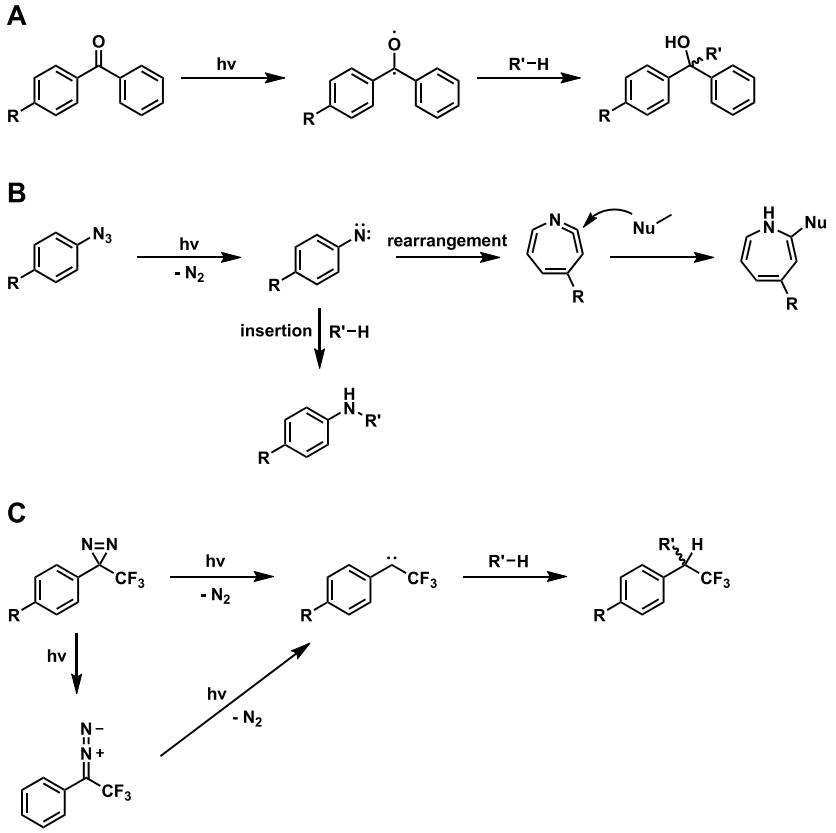

Figure 1.6 Mechanism of photocrosslinking for A) benzophenones, B) arylazides and C) aryldiazirines after UV-irradiation. R' represents any alkyl or aryl residue or hetero atom. R indicates connection of the photoreactive moiety to an ABP.

Upon irradiation with UV-light of wavelengths $\lambda \geq 320$ nm, benzophenones form triplet diradicals that are able to insert into C-H-bonds. It was hypothesized that this diradical abstracts a hydrogen radical from the amino acid backbone or side chain and the resulting carbon radical further reacts with the radical from the photocrosslinker.[61] The fact that triplet radicals from aryl ketones do not efficiently react with water poses a major advantage for this type. However, the large size of this photoreactive group and reversibility of the excitation limits its application.[61] Aryl azides have been the most frequently used photoaffinity labels, because of their stability in the dark and their synthetically simple accessibility. Irradiation with UV-light in the range of $\lambda = 250 – 350$ nm leads to generation of a nitrene which rapidly forms an azacycloheptatetraene through intramolecular ring expansion.[59,60] This intermediate is highly electrophilic but less reactive compared to nitrenes and carbenes and thus, cannot insert into C-H-bonds like benzophenones. Interestingly, introduction of electronwithdrawing moieties like fluorine atoms leads to a lowering of the rate of ring expansion and an increase in nitrene labeling efficiency.[60] Drawbacks of arylazides are the short excitation wavelength that may induce damage to biological molecules and the susceptibility to reduction to the amine by cellular reducing agents.[62] Nowadays, aryldiazirines as well as alkyldiazirines constitute the most widely used photocrosslinking groups. Irradiation of aryldiazirines with UV-light in the range of $\lambda = 350 – 355$ nm either leads to fragmentation to the

corresponding carbene by release of molecular nitrogen or rearrangement to the diazo compound.[61,62] The electrophilic carbene is highly reactive and is readily quenched by surrounding water leading to reduced photocrosslinking efficiency. Nonetheless, it is also able to insert into C-H-bonds and showed high insertion efficiency in a non-aqueous environment. The generation of the diazo compound leads to substantial loss of reactivity, although it slowly decomposes to the singlet carbene. The propensity to undergo side reactions could be limited by introduction of a trifluoromethyl group.[60,61] In summary, this photoreactive group poses a valuable photocrosslinking moiety due to its small size, chemical inertia regarding temperature, pH and redox conditions and its high excitation wavelength.[62]

In an affinity-based protein profiling approach, all three photoreactive groups possess one major drawback. Generation of highly reactive intermediates offers the opportunity to crosslink uninvolved proteins, leading to potential false-positive hits (photomes). This background labeling was further examined by a variety of photoreactive moiety containing scaffolds of low molecular weight, resulting in an inventory of repeatedly emerging proteins.[63] In turn, this list of photome hits can be used as a control in affinity-based protein profiling experiments to avert possible incorrect conclusions.

2

Synthesis and evaluation of novel human ClpP inhibitors

This chapter is based on the publication "*Design and synthesis of tailored human caseinolytic protease P inhibitors*" published by Thomas F. Gronauer, Melanie M. Mandl, Markus Lakemeyer, Mathias W. Hackl, Martina Meßner, Vadim S. Korotkov, Johanna Pachmayr, Stephan A. Sieber in *Chemical Communications*, 2018, 54, 9833-9836.

Contributions

MMM and MM performed cell viability assays, Nicoletti assays and migration assays, as well as western blot experiments. K_{obs}/[I] determination was conducted by MWH and apparent IC_{50} values were determined by ML. ClpP expression strains were created by Matthias Stahl and ssrA-tagged eGFP was graciously provided by ML. TFG synthesized all compounds, performed activity assays and conducted mass spectrometry experiments. SAS and TFG prepared the manuscript with input from all other authors.

2 Synthesis and evaluation of novel human ClpP inhibitors

This chapter is based on the publication "Design and synthesis of tailored human caseinolytic protease P inhibitors" published in Chemical Communications, 2018, 54, 9833-9836.

2.1 Relevance of ClpP in human cells and diseases

Human ClpP is associated with a variety of different malignancies such as *Perrault* syndrome or acute myeloid leukemia (AML). The former represents a rare autosomal recessive disorder which constitutes in premature ovarian failure and congenital sensorineural hearing loss in both sexes.[64] It is suggested to be caused by biallelic recessive mutations in *CLPP* resulting in substitutions of amino acids Thr145 and Cys147 with proline and serine, respectively. Both amino acids are part of the β-3 strand which is responsible for hydrogen bond formation. Thr145 can form a hydrogen bond with Leu159 which is abrogated for the mutant proline whereas the cysteine to serine mutation is proposed to deteriorate hydrophobicity in this side chain. These mutations ultimately influence the hydrophobic cleft which is important for ClpX binding thus impeding ClpXP complex formation. In the end this results in compromised mitochondrial protein homeostasis.[65,66] Conversely, in AML differences occur on transcription level rather than in sequence composition. ClpP expression levels were increased in almost half of all observed malignant cells from 511 primary AML samples but also in other malignancies such as multiple myeloma, chronic myeloid leukemia, prostate cancer and sarcomas.[67] Knockdown of ClpP *via* short hairpin RNA (shRNA) in cell lines overexpressing ClpP such as K562, TEX and OCI-AML2 resulted in reduced viability. In addition, chemical inhibition of ClpP by β-lactones also induced cell death to these cancer cells while cells with a basal ClpP expression remained unaffected.[67,68] In accordance with previous studies it was rationalized that reduction of viability is connected to deterioration of mitochondrial metabolism and oxidative phosphorylation.[67,69,70] Furthermore, treatment with β-lactones resulted in delayed growth of OCI-AML2 cells in xenografted mice, thus suggesting ClpP as an attractive target for a subset of leukemias.[67]

2.2 Inhibition of ClpP

In 2008, *trans*-β-lactones were initially reported to effectively inhibit proteolytic activity of bacterial ClpP establishing the first class of potent ClpP inhibitors.[71,72] The strained ring system of the cyclic esters provides the required reactivity for nucleophilic attack of the active site serine which is higher in β-lactones compared to the β-lactam congener.[72,73] Here, compound **D3** stood out by displaying an extraordinarily rapid binding to SaClpP.[72] Further investigations revealed that especially the hydrophobic nature of the side chain R^1 beneficially contributes to the binding affinity by interacting with the hydrophobic pocket adjacent to the active site serine, thus facilitating

nucleophilic attack. Configuration of *trans*-β-lactones also proved to be crucial for reactivity which can be explained by interaction with the oxyanion hole which is only satisfied by the structural geometry of the (*S*,*S*)-isomers.[74] Although β-lactones exhibit excellent potency to inhibit ClpP activity and treatment of malign mammalian cells revealed potent effects the propensity to hydrolyze in aqueous solutions limits their application as therapeutics.[67]

Therefore, *Hackl et al.* attempted to discover novel ClpP inhibitors that would contain improved selectivity and stability. By assessing more than 137,000 compounds in an unbiased high-throughput screen for their ability to block SaClpP peptidase activity phenyl esters were discovered as a novel generation of inhibitors. The most potent compound **AV170** was four-fold more effective at the lowest concentration tested compared to previously described standard inhibitors **D3** and **E2**.[75] All active phenyl esters share a similar structural motif with a planar aromatic carboxylic acid moiety that is connected *via* an ester bond to a phenolic leaving group. The mode of action for binding of these compounds to their protein target ClpP was proposed to undergo by nucleophilic attack on the ester group leading to elimination of the phenolic leaving group (Figure 2.1).

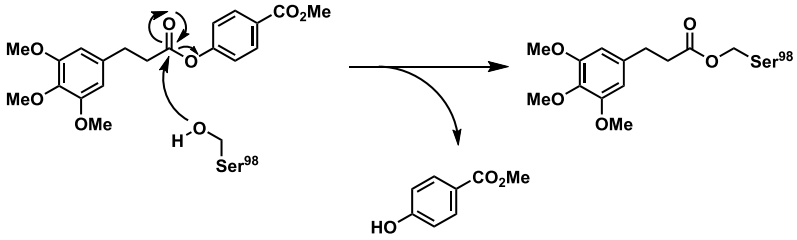

Figure 2.1 Proposed mechanism for covalent modification of ClpP by phenyl esters as proposed by *Hackl et al.*[75]

Molecular docking revealed that tri-methoxyphenylpropanoic acid with its tri-substituted aromatic ring comprises privileged binding properties to the hydrophobic cleft leading to an excellent alignment of the ester with the oxyanion hole. Further attempts to stabilize the phenyl ester and shield it from unintended hydrolysis by installation of a methyl group in α-position to the acyl group resulted in discovery of a stereogenic switch with compounds **ML89** and **ML90**. While (*S*)-configured **ML90** modified all active sites of the ClpP tetradecamer (*R*)-configured **ML89** only modified half of all active sites and, moreover, led to a disassembly of the two heptameric rings. Substitution of one methoxy group of the acid moiety of **AV170** by a propargylic group resulted in probe **ML16**. In an ABPP approach, this compound showed improved selectivity for ClpP over the previous standard **D3** in a complex proteome.[75]

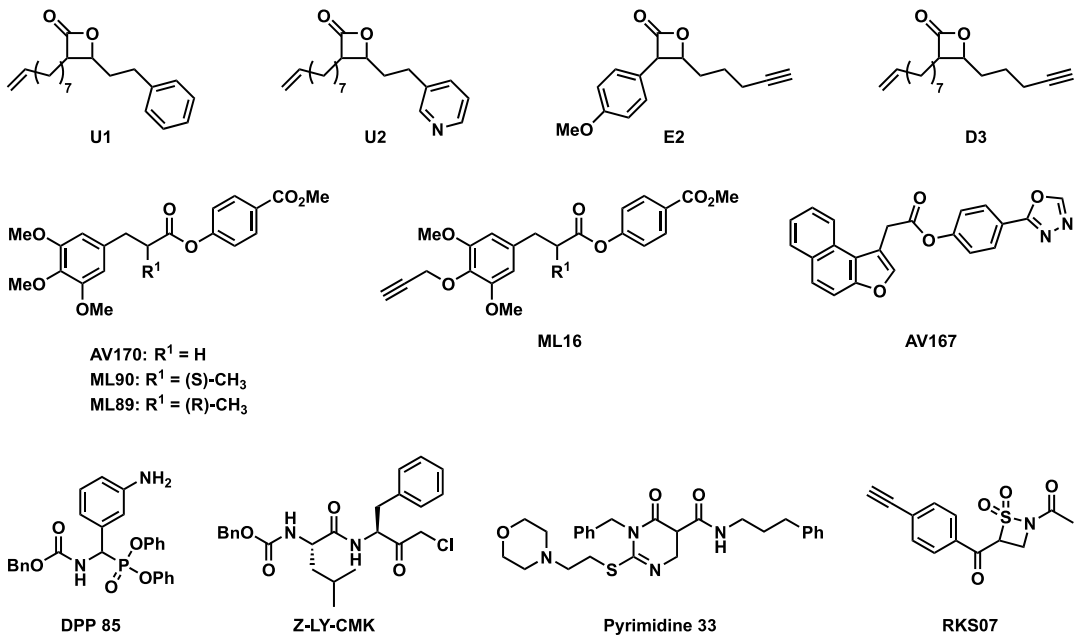

Figure 2.2 Chemical structures of reported ClpP inhibitors.

Until 2015, no selective human ClpP inhibitor has been reported, however in the above-mentioned high-throughput screen one compound stood out of six initial hits displaying superior inhibitory activity against hClpP which even exceeded that of *β*-lactones.[75,76] Compound **AV167** exhibits a characteristic naphthofuran motif on the acid moiety of the phenyl ester and a 1,3,4-oxadiazolyl *para*-substituted phenol as leaving group. It was the only phenyl ester that not only inhibited SaClpP but also its human congener (Figure 2.3A).

ClpP is expressed as a widely conserved protein in a variety of species exhibiting different substrate specificity which naturally also impacts the structures of potential inibitors.[77] Therefore, a variety of inhibitors exists next to phenyl esters which all exhibit their own selectivity and reactivity on a variety of different ClpPs.[78] Of note are the α-amino diphenyl phosphonates[79], selective for *Escherichia coli* (*E. coli*) ClpP, which introduced another selective inhibitor besides chloromethyl ketone ***Z*-LY-CMK**.[80] Additionally, substituted pyrimidines displayed selectivity for *P. falsiparum* ClpP after discovery in *in silico* docking studies and also impaired apicoplast development in the second cell cycle.[81] The binding mode however has to be unveiled. A rather destructive inhibition mode was uncovered by *Gersch et al.* using *β*-sultams to inhibit *S. aureus* ClpP. Here, compound **RKS07** binds to the active site serine *via* the sulfone group generating a leaving group that ultimately results in elimination and demise of the active site.[82]

In the following chapter the discovery of new human ClpP inhibitors will be detailed along with the results of a structure activity relationship study (SAR) as well as bioactivity and chemical proteomics experiments.

2.3 SAR of AV167

Ever since ClpP was found to be an attractive therapeutic target for acute myeloid leukemia and the present *β*-lactones displayed only insufficient selectivity for ClpP and low stability in aqueous solution, discovery of new potent pharmacological leads were indispensable.[67] In a HTS, initially designed to identify novel structural scaffolds for the inhibition of SaClpP, one compound stood out of the mass which comprised a characteristic naphthofuranyl moiety. **AV167** was the only compound showing promising results against human ClpP in initial peptidase activity assays and was therefore selected for a SAR study to analyze key structural motifs of the compound in order to optimize it for hClpP inhibition and to uncover suitable positions for attachment of a handle for target identification.

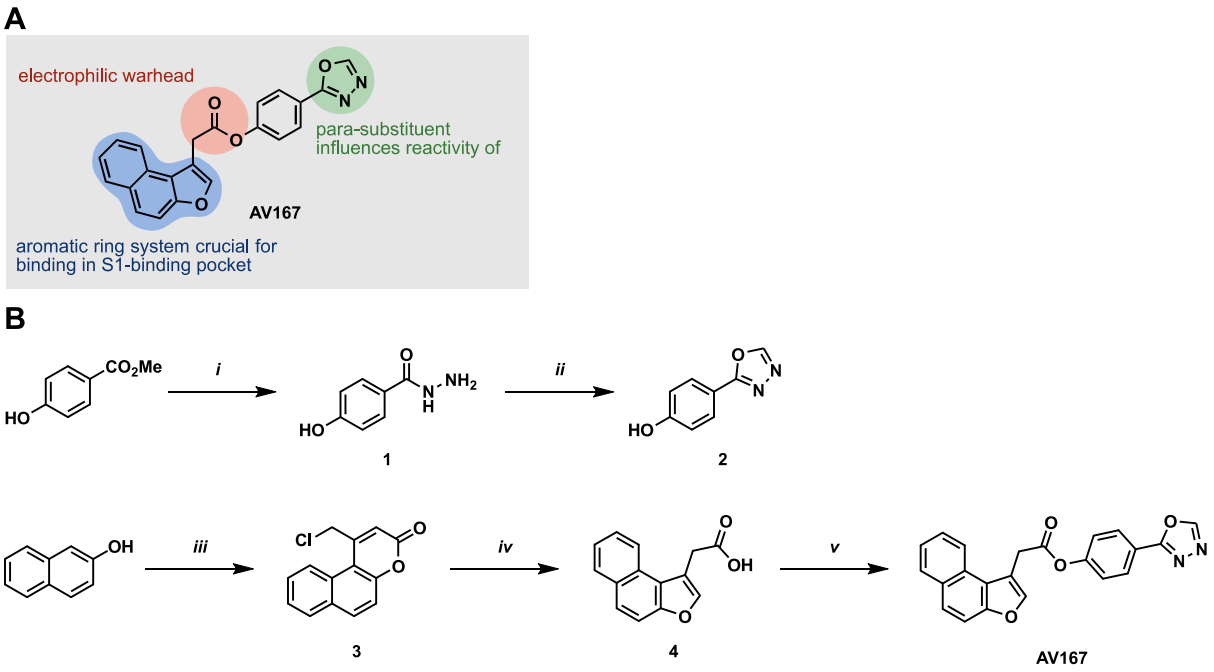

Figure 2.3 A) Key structural features of initial hit **AV167**. B) Synthesis of compound **AV167**: i) $N_2H_4 \cdot H_2O$ (4.00 eq.), rfx, 5 h, 93%; ii) $CH(OEt)_3$ (12.0 eq.), rfx, 18 h, 87%; iii) ethyl 4-chloroacetoacetate (1.14 eq.), conc. H_2SO_4, 0 °C → RT, 3 h, 92%; iv) 6 M $NaOH_{aq}$ (18.6 eq.), 80 °C, 20 h, 96%; v) EDCI (1.32 eq.), DMAP (0.50 eq.), **2** (1.20 eq.), DCM, RT, 17 h, 21%.

First, parent compound **AV167** was synthesized and validated for ClpP inhibition. For this, the phenolic leaving group was synthesized in a two-step synthesis. Starting with methyl 4-hydroxybenzoate heating with hydrazine hydrate gave the appropriate hydrazide **2** which was further reacted with triethoxymethane to yield the heterocycle substituted phenol.[83,84] the naphthofuranyl moiety was synthesized starting with a procedure described by *Abd-El-Aziz*[85] using 2-naphthol and ethyl 2-chloroacetylacetate in concentrated sulfuric acid to give benzocoumarin **3** *via Pechmann reaction*. Treatment with 6 M aqueous sodium hydroxide resulted in ring contraction *via* rearrangement and gave the appropriate naphthofuranylacetic acid **4**.[86] Simplicity and reproducibility of these reactions serve as an ideal starting point for further structure activity

relationship studies (Figure 2.3B). The final compound was achieved by esterification using 1-Ethyl-3-(3-dimethylaminopropyl)carbodiimide (EDCI) and catalytic amounts of dimethylaminopyridine (DMAP). For the following structure activity relationship study, potency of synthesized structures against ClpP activity was assessed using a fluorometric enzyme assay. In this peptidase assay the ability of ClpP to cleave the fluorogenic substrate Suc-L-Y-AMC (Succinate-leucine-tyrosine-7-amino-4-methylcoumarin, upon inhibitor treatment was tested and compared to a DMSO-treated negative control. Upon cleavage of the amide bond between tyrosine and the fluorogenic reporter by ClpP 7-amino-4-methylcoumarin (AMC) is released which emits light at $\lambda = 440$ nm upon excitation ($\lambda = 380$ nm), thus offering a direct correlation between fluorescence and proteolytic activity. The amount of cleaved AMC is plotted against time and the initial slopes of the resulting curves were determined by linear regression and normalized to a DMSO control.

2.3.1 Synthesis of phenol derivatives

Potency of phenyl esters towards ClpP inhibition heavily relies on the reactivity of the ester. This is largely influenced by the tendency of the phenol to stabilize the negative charge generated upon cleavage of the ester. Therefore, variation of the substitution pattern of the phenolic leaving group should provide insights into the influence of the *para*-substituent in order to fine-tune the reactivity of phenyl esters. As an electron-withdrawing substituent in *para*-position to the hydroxy group lowers the pK_a of the phenol OH-group, thus stabilizing a negative charge of the phenolate, two different functional groups, a methylsulfonyl-, nitro- and methylester group were chosen to substitute the heterocyclic oxadiazole.[87] To assess the influence of an electrondonating group the heterocycle was replaced by a methoxy group. To reflect a state without *para*-substituent plain phenol was used. Synthesis of all inhibitors was performed by esterification of naphthofuranylacetic acid with the corresponding phenol. (Figure 2.4A)

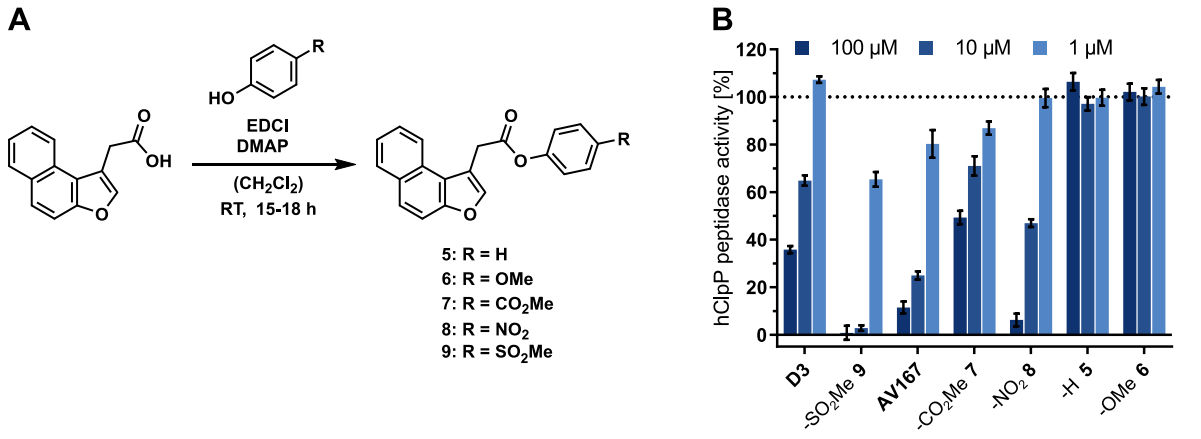

Figure 2.4 A) Synthesis of phenyl esters with varying phenolic leaving groups: EDCI (1.50 eq.), DMAP (0.50 eq.), substituted phenol (1.20 eq.), RT, o/n, **5**: 54%; **6**: 70%; **7**: 53%; **8**: 29%; **9**: 21%. B) Results from hClpP peptidase activity assay ($hClpP_{monomer}$

concentration 1 μM, fluorogenic substrate: Suc-L-Y-AMC, 200 μM). Each data set represents six technical replicates from two independent experiments (mean ± SD).

Peptidase assay results proved to reflect the pK_a values of the corresponding leaving group which decline in the order OMe > H > NO_2 > CO_2Me > SO_2Me.[87] Phenyl ester **5** with a phenol leaving group did not show any potency to inhibit ClpP actvity as did its methoxy substituted congener. Electron withdrawing effect exerted onto the aromatic ring by a nitro group converted to higher potency of the corresponding phenyl ester. This was even more pronounced with a methyl ester substituent and a methylsulfonyl group even surpassed the inhibitory effect of parent compound **AV167**. (Figure 2.4B) These findings underline the substantial influence of the *para*-substituent of the leaving group and accentuate the challenge that accompanies the development of reactive but stable phenyl esters.

2.3.2 Synthesis of acid derivatives

To dissect the structure of **AV167** for critical enzyme recognition motifs and to explore the structural space for the introduction of an alkyne tag for target identification *via* ABPP the naphthofuranylacetic acid moiety was functionalized. Introduction of a methoxy group in 7-position of the naphthofuranyl moiety should warrant information about the accessibility of such compounds to the S1 binding pocket. Synthesis of compound **12** was performed analogous to **AV167** with 7-methoxynaphthol as starting material (Figure 2.5).

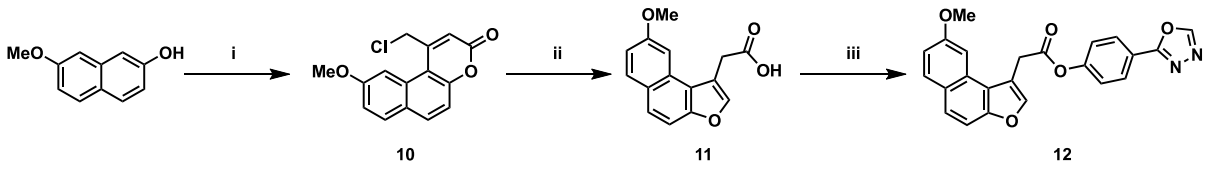

Figure 2.5 Synthesis of methoxy-substituted naphthyl-derivative of **AV167**. i) ethyl 4-chloroacetoacetate (1.14 eq.), conc. H_2SO_4, 0 °C → RT, 3 h, 47%, ii) 6 M $NaOH_{aq}$ (18.6 eq.), 80 °C, 20 h, 95%; iii) EDCI (1.50 eq.), DMAP (0.50 eq.), **2** (1.20 eq.), DCM, RT, 24 h, 43%.

Peptidase activity assay revealed that modification at this site of the molecule leads to a complete abolition of inhibition potency (Figure 2.6D).

ClpP features a deep hydrophobic S1-binding site adjacent to the active site serine which provides only limited space for binding of an effector.[74,88] As shown above, already a small extension to the aromatic ring system suffices to induce dramatic loss of function. Therefore, reduction of the aromatic ring system to gain additional space for the introduction of a benign tag was further investigated. For this, substituted phenols were reacted in the same synthesis strategy as described before to generate substituted phenyl esters with a reduced aromatic ring size. Phenol, 4-methylphenol, 3-methoxyphenol and 4-methoxyphenol, respectively, were reacted with ethyl 4-chloroacetoacetate in 70% (v/v) $H_2SO_{4(aq)}$ to the appropriate coumarin which was further

converted by alkaline supported rearrangement to the benzofuranylacetic acids.[89] EDCI mediated esterification with catalytic amounts of DMAP and 1,3,4-(oxadiazolyl)phenol gave phenyl esters **19-22** which were subjected to evaluation in ClpP peptidase assay.

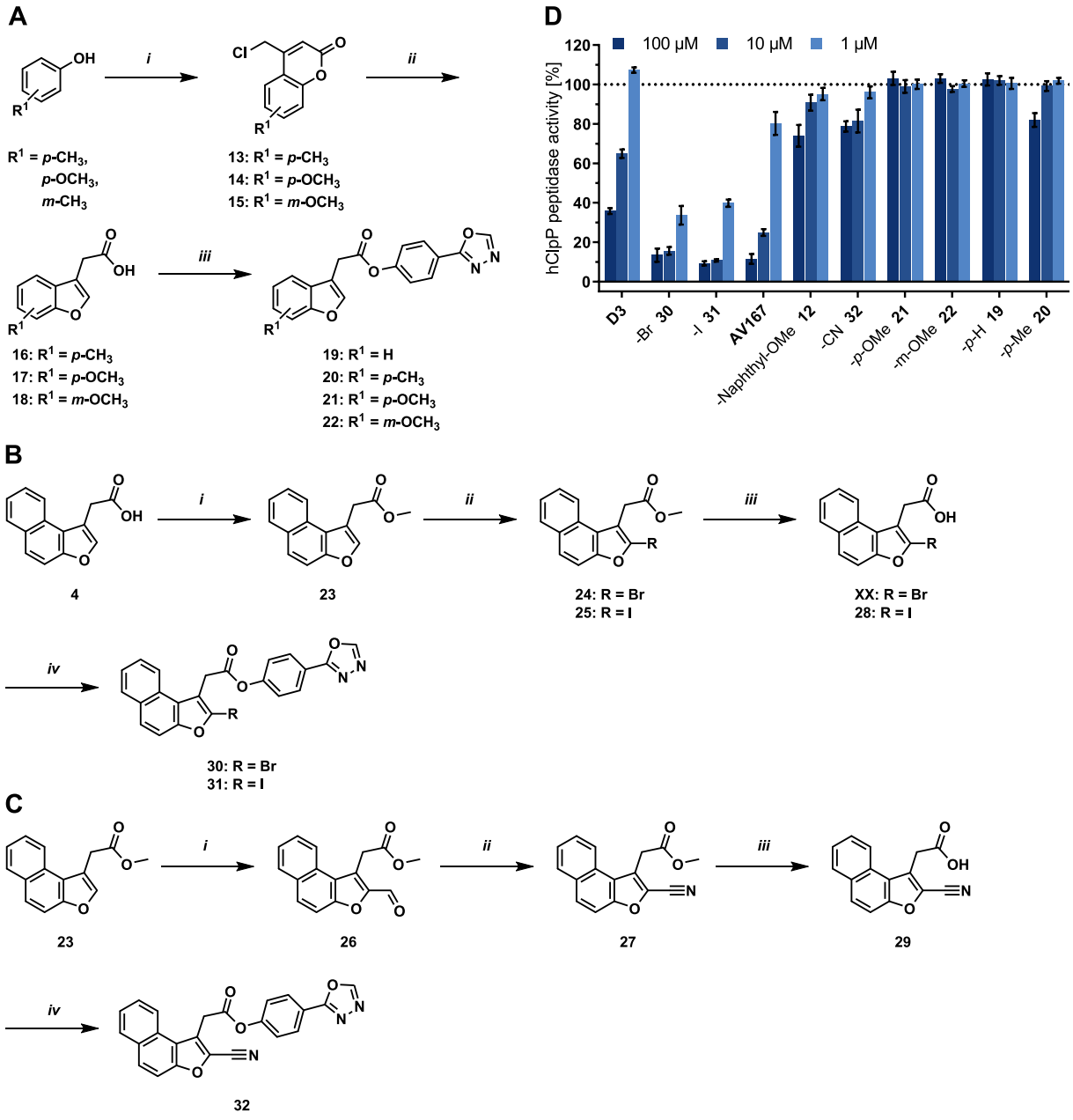

Figure 2.6 A) Synthesis route of substituted benzyl-derivatives of **AV167**. i) ethyl 4-chloroacetoacetate (1.00 eq.), 70% (v/v) $H_2SO_{4(aq)}$, 0 °C → RT, 18 h, **13**: 74%; **14**: 31%; **15**: 51%; ii) 1 M $NaOH_{aq}$, rfx, 1 h, **16**: 63%; **17**: 82%; **18**: 56%; iii) EDCI (2.00 eq.), DMAP (0.50 eq.), **2** (1.20 eq.), DCM, 16 – 21 h, **19**: 50%: **20**: 10%; **21**: 85%; **22**: 23%. B) Synthesis of **AV167** derivatives subtituted on 2-position of furanyl-ring. i) conc. H_2SO_4 (cat.), MeOH, rfx, 5 h, 96%; ii) **24**: NBS (1.09 eq.), $CHCl_3$/MeCN 1:1; -8 °C, 1 h, 90%; **25**: NIS (1.10 eq.), $CHCl_3$/MeCN 1:1, -10 °C, 1 h, 19%; iii) 1 M $LiOH_{aq}$ (1.20 eq.), THF, RT, 18 h, 95%; iv) EDCI (1.50 eq.), DMAP (0.50 eq.), **2** (1.20 eq.), DCM, RT, 16 h, **30**; 5% over two steps, **31**: 73%. C) Synthesis of nitril-derivative. i) DMF (23.1 eq.), $POCl_3$ (5.80 eq.), 0 °C → RT, 7 h, 43%; ii) $NH_2OH \cdot HCl$ (6.22 eq.) pyridine (9.47 eq.) Ac_2O (2.00 eq.), 95 °C, 2 h, 95%; iii) 1 M $LiOH_{aq}$ THF, RT, 18 h, 82%; iv) EDCI (1.50 eq.), DMAP (0.50 eq.), **2** (1.20 eq.), DCM, RT, 17 h, 26%. D) Peptidase activity assay results with hClpP ($hClpP_{monomer}$ concentration 1 µM, fluorogenic substrate: Suc-L-Y-AMC, 200 µM). Each data set represents six technical replicates from two independent experiments (mean ± SD).

Here, none of the compounds exhibited potency against ClpP peptidase activity (Figure 2.6D). Apparently, the extended aromatic ring system is crucial for the affinity to the binding pocket and any modification to either ring size or decoration has adverse effects on the interaction.
As the naphthyl structure must be preserved and the phenolic leaving group cannot be modified with an alkyne tag only the α-position to the furanyl-*O* allowed for modification.
Therefore, phenyl esters were synthesized that were substituted with a bromine, iodine and a nitrile group. Synthesis of these naphthofuranylacetic acids commenced with protection of the carboxylic acid by esterification with methanol. Halogenated compounds were generated by reaction with the appropriate *N*-halosuccinimide according to a slightly modified procedure by *Ando et al.*[90] For the introduction of a nitrile group compound **23** was formylated in a *Vilsmeyer-Haack reaction* following the procedure by *Chan et al.*[91] and the resulting aldehyde was further converted with hydroxylamine and acetic anhydride in pyridine to the corresponding nitrile.[92] In preparation for esterification with 4-(1,3,4-(oxadiazol-2-yl))phenol methyl esters **28** and **29** were cleaved with aqueous LiOH solution similar to a known procedure.[93] Phenyl esters **30-32** were then tested in the aforementioned peptidase assay. Compounds **30** and **31** exhibited superior inhibitory effects compared to the parent compound **AV167** whereas phenyl ester **32** did not show any inhibition (Figure 2.6D). Clearly, substitutions in α-position to the furanyl-*O* lead to compounds that are active, however changes have to be minor to be tolerated. As electron rich groups are tolerated at this position it was speculated that introduction of an alkyne tag might also be suitable.

2.3.3 Synthesis of probe derivatives

For target identification of ClpP inhibitors based on compound **AV167** introduction of an alkyne tag was presumed to be most beneficial at the α-position to the furanyl-*O*. Therefore, starting from brominated methyl ester **23**, *Sonogashira* coupling with TMS-acetylene according to a patent[94] yielded alkynylated methyl ester **33**. Deprotection of the methyl ester also resulted in cleavage of the TMS-group, thus reducing the overall number of steps.[93] The resulting carboxylic acid provided a basis for esterification with different phenols to hone reactivity of corresponding phenyl esters. This led to compounds **35-40** which comprise essentially the same leaving groups that were already introduced in chapter 2.3.1.

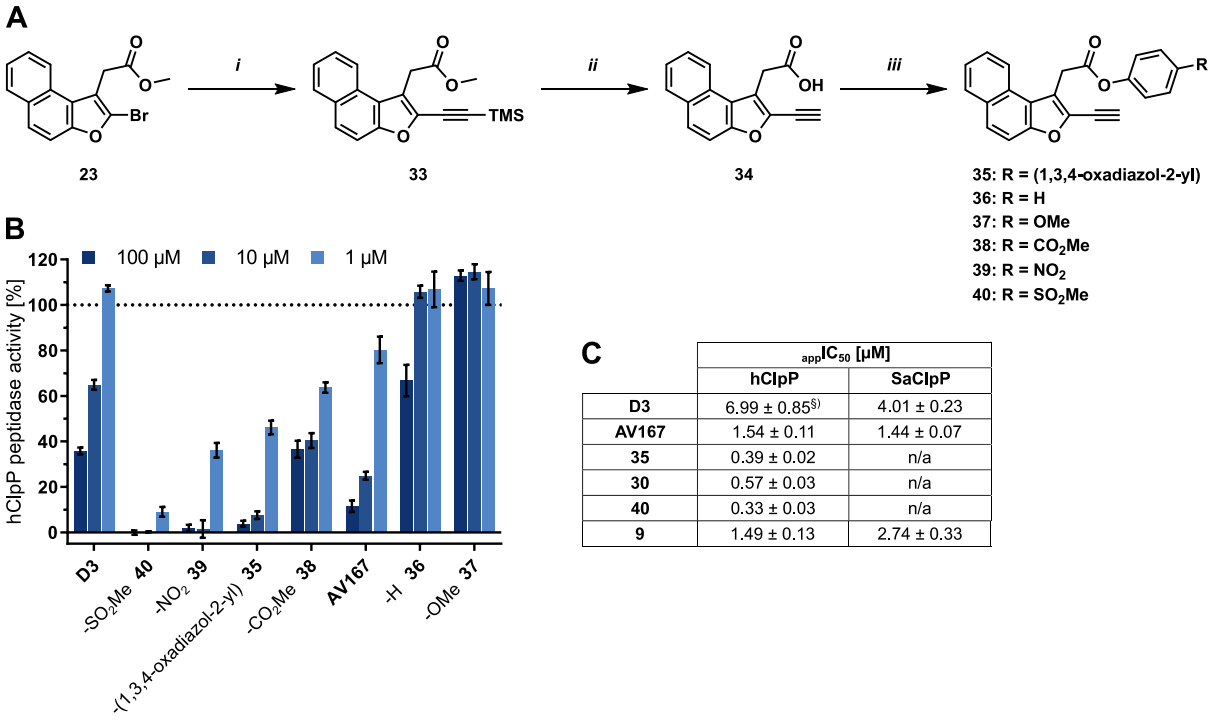

C

	appIC50 [µM]	
	hClpP	SaClpP
D3	6.99 ± 0.85§)	4.01 ± 0.23
AV167	1.54 ± 0.11	1.44 ± 0.07
35	0.39 ± 0.02	n/a
30	0.57 ± 0.03	n/a
40	0.33 ± 0.03	n/a
9	1.49 ± 0.13	2.74 ± 0.33

Figure 2.7 A) Synthesis of probe derivatives with varying leaving groups. i) $Pd(PPh_3)_4$ (1.8 mol-%), CuI (0.27 eq.), TMS-acetylene (2.00 eq.), NEt_3 (1.10 eq.), THF, RT, 20 h, 86%; ii) 1 M $LiOH_{aq}$ (1.20 eq.), THF, RT, 24 h, 93%; iii) EDCI (1.50 eq.), DMAP (0.50 eq.), **2** (1.20 eq.), DCM, RT, 18-22 h, **35**: 49%; **36**: 68%; **37**: 72%; **38**: 48%; **39**: 28%; **40**: 61%. B) Results from hClpP peptidase activity assay ($hClpP_{monomer}$ concentration 1 µM, fluorogenic substrate: Suc-L-Y-AMC, 200 µM). Each data set represents six technical replicates from two independent experiments (mean ± SD). C) Apparent IC_{50} values of selected inhibitors for human and *S. aureus* ClpP. Inhibitors were incubated with 1 µM $ClpP_{monomer}$ at 32 °C (SaClpP) or 37 °C (hClpP) for 15 min prior to addition of fluorogenic substrate Suc-L-Y-AMC, 200 µM). Apparent IC_{50} curves were generated by fitting a nonlinear regression curve to the data points representing results from at least six replicates (mean ± SD, § 35% residual peptidase activity).

As expected, among these new probes all compounds with activated ester moieties including a *p*-nitro, *p*-methyl ester or *p*-methylsulfonyl substituted phenol showed potent inhibition profiles when tested in the peptidase activity assay. Electron-donating groups in *para*-position led to poor inhibitors again highlighting the relevance of an activated phenyl ester (Figure 2.7B). Strikingly, probes **35**, **39** and **40** showed a substantial reduction even at concentrations as low as 1 µM providing even higher inhibition potency than parent compound **AV167**. This was most pronounced for compound **40** eliciting a residual ClpP activity of 10%. In addition, apparent IC_{50} measurements not only confirmed a higher potency of phenyl ester **AV167** compared to *β*-lactone **D3** but substituted phenyl esters **35**, **30** and **40** also showed elevated potency compared to **AV167** and species selectivity over SaClpP towards hClpP (Figure 2.7 C). Together with the influence of the phenolic leaving group on inhibitor potency these results confirm a synergistic effect of the substitution pattern of the naphthofuran ring.

All alkyne containing phenyl ester probes were further tested in another ClpP activity assay as well as the corresponding non-alkynylated compound of **40**. ClpP, on its own, is only capable to degrade small peptides of up to 6 amino acids[95] however for degradation of larger proteins the peptidase subunit associates with a chaperone of the AAA+ family (ATPases associated with diverse cellular

activities) which leads to pore opening and active transport of substrate proteins.[96,97] So far, several small molecules have been identified that can take over the task of pore-opening resulting in uncontrolled proteolysis of surrounding unfolded or weakly folded proteins. Especially for bacterial ClpP acyldepsipeptides (ADEPs) have been proven to achieve a reliable activation.[38] Furthermore, certain ADEP fragments (Figure 2.8B) also induce activation of human ClpP which can be exploited to measure the proteolytic activity of hClpP upon inhibitor binding.[98] In this assay, casein, a soluble natural substrate of many proteases is labeled with fluorescein isothiocyanate (FITC) and serves as reporter for proteolytic efficiency. In a Förster resonance energy transfer (FRET) based assay ADEP-fragment activated hClpP is able to cleave this protein construct which leads to a reduction of fluorescence quenching and thus to an increase in fluorescence.[99] The measured signal is plotted against time and the slope of the resulting curve is determined *via* linear regression.

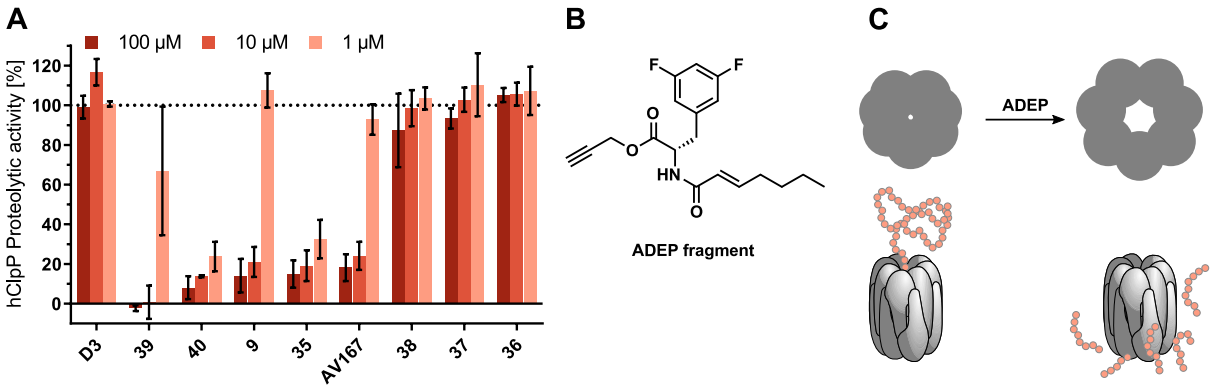

Figure 2.8 A) Results from FITC-Casein assay. hClpP is incubated first with inhibitors in three different concentrations (100 µM, 10 µM, 1 µM), then with acyldepsipeptide fragment (B, 10 µM). FITC-Casein substrate (2 µM) is added and increase in fluorescence is recorded. Each data-set represents results from six replicates obtained from two independent experiments (mean ± SD). B) Structure of ADEP fragment. C) Acyldepsipeptides induce pore opening of ClpP facilitating degradation of proteins by the peptidase subunit.

Again, compounds that contain a strong electron withdrawing substituent in *para*-position of the phenol displayed the highest potency to block proteolytic activity of hClpP while *β*-lactone **D3** showed no activity at all. A valuable finding was revealed when ClpP was first incubated with ADEP-fragment following addition of phenyl esters. Here, ClpP inhibition by phenyl esters could not be detected leading to the assumption that ADEP-fragment binding somehow influences the geometry of the S1 binding site. This was further corroborated by intact protein mass spectrometry data which demonstrate a reduced binding of phenyl ester **35** to ClpP when introduced after incubation with ADEP-fragment.

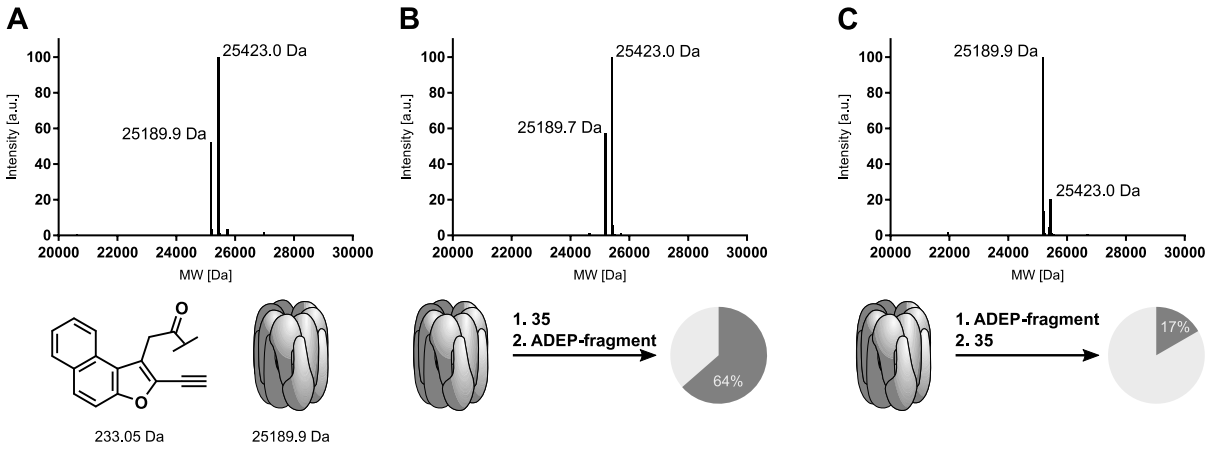

Figure 2.9 Intact protein mass spectrometry of human wild-type ClpP (25189.9 Da) with phenyl ester probe **35**. The protein was incubated with excess of inhibitor at 37 °C for 15 min. A) Incubation with 10-fold excess of **35** leads to modification of 66% ($hClpP_{monomer}$ concentration: 1 µM, **35**: 10 µM), B) IP-MS after incubation with **35** and ADEP fragment does not change extent of modification of hClpP by phenyl ester **35**. C) Incubation with ADEP fragment prior to incubation with phenyl ester drastically reduces the extent of modification.

To further substantiate the peptidase and FITC-casein assay results, a select choice of phenyl esters was tested in another protease activity assay in presence of ClpX.[100] Here, *E. coli* ClpX is used which is able to form a functionally active complex with hClpP. For activity assessment, degradation of enhanced green fluorescent protein (eGFP) is monitored. Equipped with a ssrA-tag that is recognized by EcClpX as degron eGFP is readily cleaved by the EcClpX-hClpP complex under ATP-hydrolysis resulting in a decrease of fluorescence (Figure 2.10).[101]

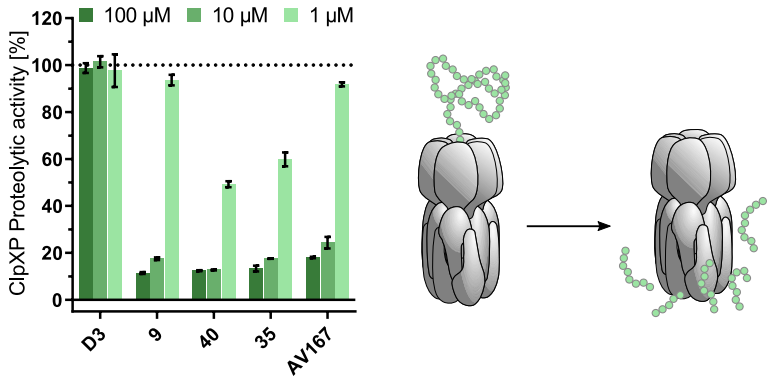

Figure 2.10 GFP degradation assay with ClpXP (2.8 µM $hClpP_{monomer}$ in the presence of 2.4 µM $EcClpX_{monomer}$ and 0.4 µM eGFP-ssrA) and selected phenyl esters. Each data-set represents results from three replicates (mean ± SD).

All tested phenyl esters exhibited strong inhibition of ClpXP proteolytic function down to concentrations of 1 µM for **35** and **40** surpassing the effect of *β*-lactone **D3**.

In summary, the presented SAR study could show that potency of the initial hit **AV167** to inhibit ClpP can further be elevated by modification of the *para*-substituent of the phenolic leaving group and the decoration of the acid motif. Especially the introduction of strong electron withdrawing groups on the phenol moiety proved to be a valuable handle to fine-tune phenyl ester reactivity and can further be enhanced by incorporation of similar substituents like a trifluoromethylsulfonyl,

ammonium or cyano group. The introduction of more substituents in *meta*- and *ortho*-position to further decrease electron density in the aromatic ring system could also yield more reactive phenyl esters, however detrimental effects to the compound's stability will be inevitable. A more efficient approach lies in the modification of the acid motif. Here, introduction of an alkyne group in 2-position of the naphthofuran ring displayed 4-fold enhancement of compound activity compared to parent compound **AV167**. Further attempts to investigate the interaction of phenyl esters with the binding site could result in compounds with even higher affinity.

Compounds **35** and **40** exhibited the highest activity in peptidase and protease assays and provide metabolically realtively stable substituents on the phenolic leaving group. Therefore, these compounds were selected for further validation in cell-based experiments.

2.4 Target identification with phenyl ester based probes

2.4.1 Modification of ClpP by 35 and AV167

Phenyl esters proved to be active as ClpP inhibitors in *in vitro* experiments. To validate that ClpP is covalently modified intact protein mass spectrometry experiments were conducted. For this wild-type hClpP was incubated with the corresponding phenyl ester at room temperature for one hour and was further analyzed by mass spectrometry. Formation of the acyl-enzyme complex with compounds **35** and parent compound **AV167** could successfully be shown with increasing concentration of phenyl ester (Figure 2.11). **AV167** modifies hClpP to up to 78% at 10-fold excess whereas **35** modifies ClpP to a substantial extent already at 1:1 ratio. Interestingly, modification with **35** only reaches 61% at 10-fold excess and decreases again for higher concentrations. Combining this outcome with the peptidase assay results it can be shown that modification of only half of all active sites by **35** already results in full inhibition confirming its high potency.

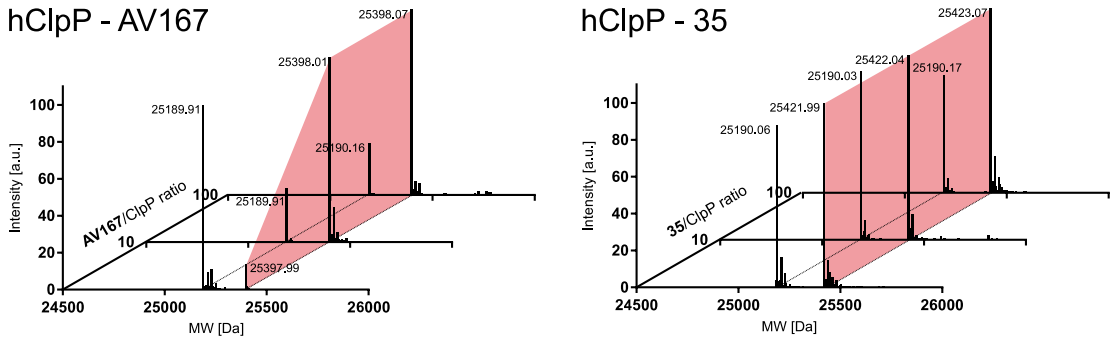

Figure 2.11 Intact protein mass spectrometry results after incubation of hClpP (1 µM $hClpP_{monomer}$) for 1 h with varying concentrations of **AV167** or phenyl ester probe **35**. Modification of hClpP with **35** reaches 61% at 10-fold excess whereas parent compound **AV167** modifies hClpP to a maximum of 78%.

2.4.2 Gel-based *in vitro* labeling

The identification of protein targets of a chemical compound is a crucial requirement in order to illuminate the mode of action for a given phenotype that results from application of a small molecule. As phenyl esters contain an electrophilic reactive moiety it is of great importance to ensure target specificity and minimize off-target binding events. To assess whether phenyl esters are able to address ClpP in a complex environment, a hClpP expressing *E. coli* strain was labeled with all available phenyl ester probes. For this, bacteria were grown until they reached an optical density (OD, λ = 600 nm) of 0.5-0.6 and protein expression was induced by addition of isopropyl-*β*-D-thiogalactopyranoside (1:2,000 from 0.5 M stock in water). Bacteria cells were grown for further 3 h and uninduced cells served as negative control. Afterwards bacteria suspensions were brought to an OD_{600} = 40, aliquoted and incubated with phenyl esters or DMSO as a negative control at room temperature for 1 h. Cells were lysed by sonication and cytosolic fractions were incubated with TAMRA-N_3 to attach the fluorescent dye *via* copper(I)-catalyzed alkyne-azide cycloaddition.[56,102,103] Labeled proteins were separated by sodium dodecyl sulfate polyacrylamide gel electrophoresis (SDS-PAGE) and visualized by fluorescence read-out.

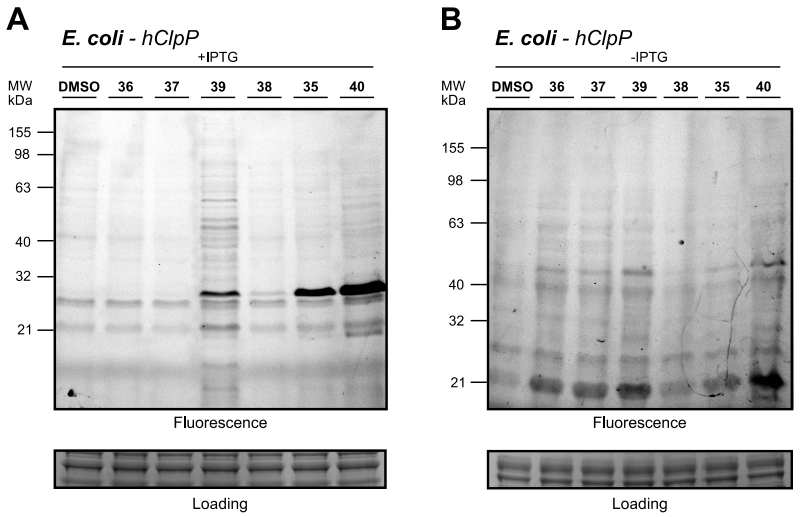

Figure 2.12 Labeling of recombinantly expressed hClpP in *E. coli* Rosetta2 expression strain. A) After induction of expression with IPTG, ClpP is only labeled by most reactive phenyl ester probes **35**, **39** and **40**. B) Without induction of expression only background labeling of fluorescence dye is detectable.

Labeling experiments clearly show a dependence on ester reactivity and ability to label hClpP as was already demonstrated *in vitro* (Figure 2.12). Phenyl esters **36** and **37** exhibit no labeling of hClpP which is in accordance with peptidase activity results. **38** bearing a methyl ester in *para*-position on the phenolic leaving group that slightly activates the phenyl ester presents minor labeling efficiency. Compounds **35**, **39** and **40** show pronounced labeling capability with **40** exhibiting the highest signal intensity. Again, these results perfectly match findings obtained from peptidase and protease assays. Concomitantly, higher electrophilicity of the ester corresponds to increased off-target

binding which is reflected by additional bands appearing in **39** and **40** labeling. In the case of **39** promiscuity may also arise from unstable metabolites caused by reductive breakdown of the *p*-nitro group.[104] Out of all tested phenyl ester probes compound **35** exhibits most promising selectivity and reactivity towards hClpP and was therefore chosen for further investigation.

In order to verify the results of labeling experiments in hClpP expressing *E. coli*, recombinant hClpP was further labeled *in vitro* with varying concentrations of compound **35**. After incubation at room temperature for 1 h probes were reacted with TAMRA-N_3 *via Click* reaction.

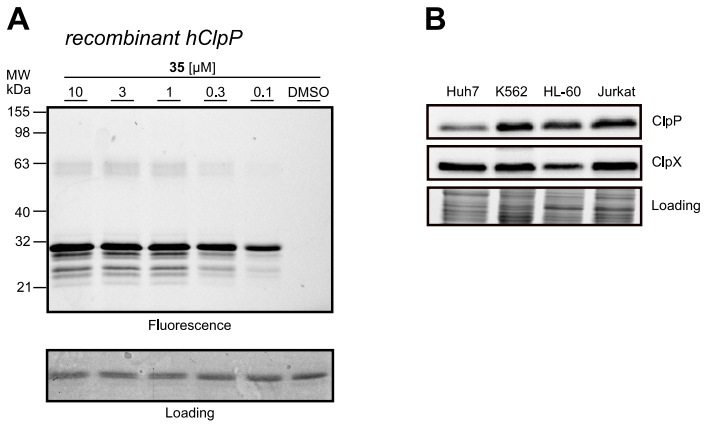

Figure 2.13 A) Labeling of recombinantly expressed hClpP with phenyl ester probe **35** reveals one distinct band at ≈32 kDa. Additional bands indicate self-degradation of ClpP, observable by bands with lower molecular weight. One band at 63 kDa putatively derives from ClpP-dimers. B) Comparison of ClpX and ClpP expression levels in various cell lines by Western blotting.

Fluorescence gels demonstrate a prominent band at around 32 kDa matching the molecular weight of the band from *E. coli* labeling experiments (Figure 2.13A). Furthermore, bands with a lower molecular weight were marked which represent truncated forms of ClpP monomers that result from self-degradation. The minor protein band at 63 kDa most likely constitute uncommonly stable ClpP dimers that endured heating to 95 °C. Following this, labeling in various different human cell lines was attempted. Prior to this, western blot experiments revealed high abundance of ClpP in Huh7, K562 and Jurkat cell lines (Figure 2.13B). Therefore, first analytical gel-based labeling experiments were conducted in Huh7 and Jurkat cells.

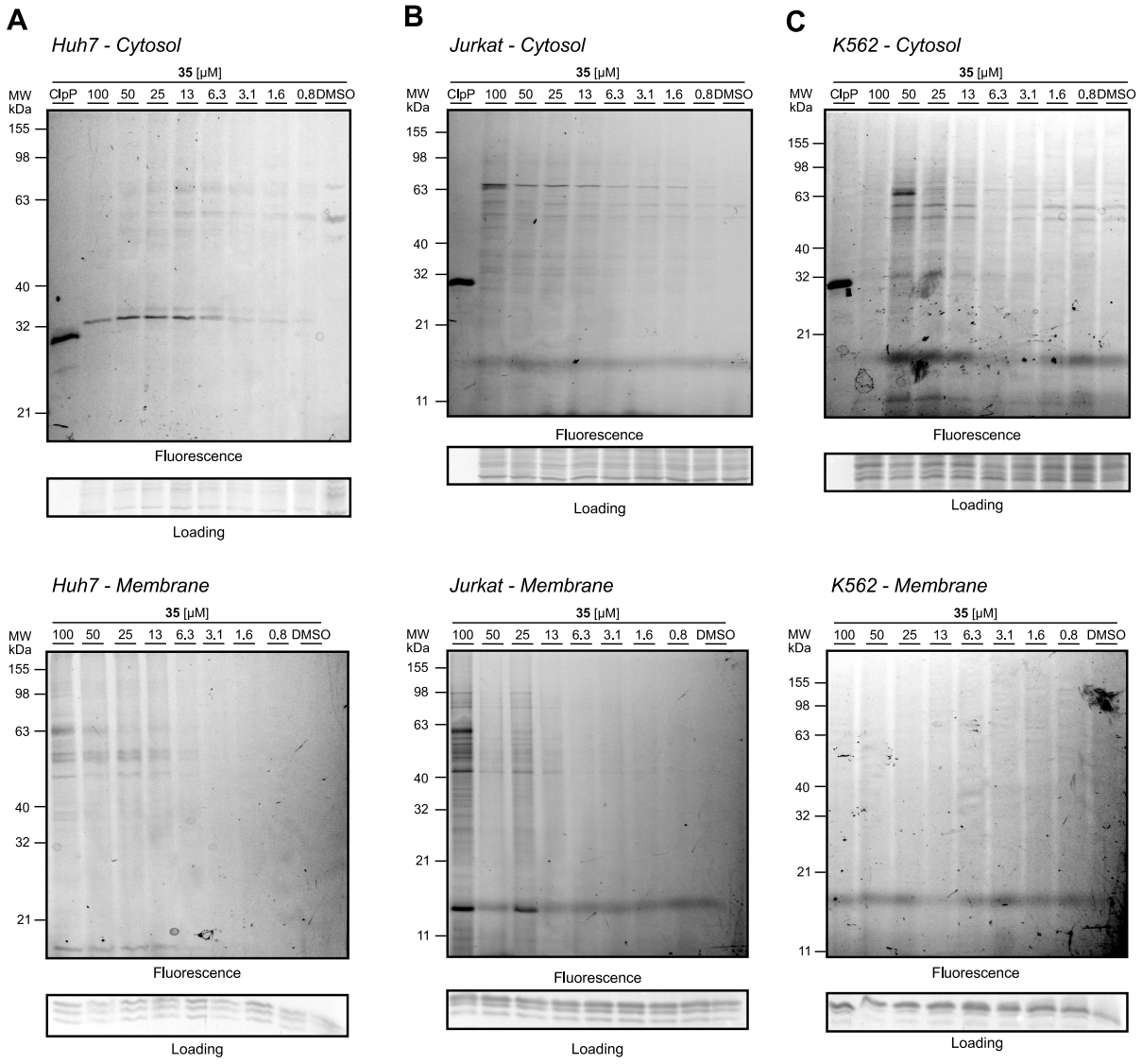

Figure 2.14 Analytical labeling with phenyl ester **35** in A) Huh7 B) Jurkat and C) K562. Labeling experiments were conducted in live cells with varying concentrations for 1 h at 37 °C. Cytosolic and membrane fractions were separated prior to *Click*-reaction with fluorescent dye TAMRA-N_3.

Labeling with **35** in Huh7 revealed one distinct band in the cytosolic fraction appearing at 32 kDa. This protein is labeled concentration dependently down to a concentration of 1.6 µM, however it did not fully align with recombinant hClpP used as a positive control (Figure 2.14A). The underlying mass difference may arise from two different ClpP monomers. While recombinant ClpP was expressed in its mature form without the mitochondrial targeting sequence resulting in a molecular mass of around 25 kDa, native cytosolic ClpP still contains a 56 amino acid long N-terminus that is cleaved upon mitochondrial transit.[17,105] The resulting mass difference therefore might result from labeling of cytosolic hClpP. In the membrane fraction only limited unspecific binding could be detected with probe **35**. For Jurkat cells one band slightly above 63 kDa exhibits a similar concentration dependent labeling (Figure 2.14B). As shown in labeling experiments with recombinant ClpP this band might be evoked by a dimer of ClpP-monomers that weren't separated or possess an unusual high affinity. Again labeling in membrane fraction only led to unspecific

binding at high probe concentrations. Labeling with **35** in cytosolic fraction of K562 resulted in rather inconsistent labeling patterns (Figure 2.14C). Labeling with 100 μM did not show any labeling which might originate from low solubility in aqueous solution. Only labeling with 50 μM **35** provoked a band at 63 kDa while lower concentration did not show any labeling distinguishable from the background. Interestingly, the membrane fraction also did not provide any labeled bands.

As **40** was identified as more reactive probe labeling was also conducted with this probe in Huh7, Jurkat and K562 (Figure 2.15).

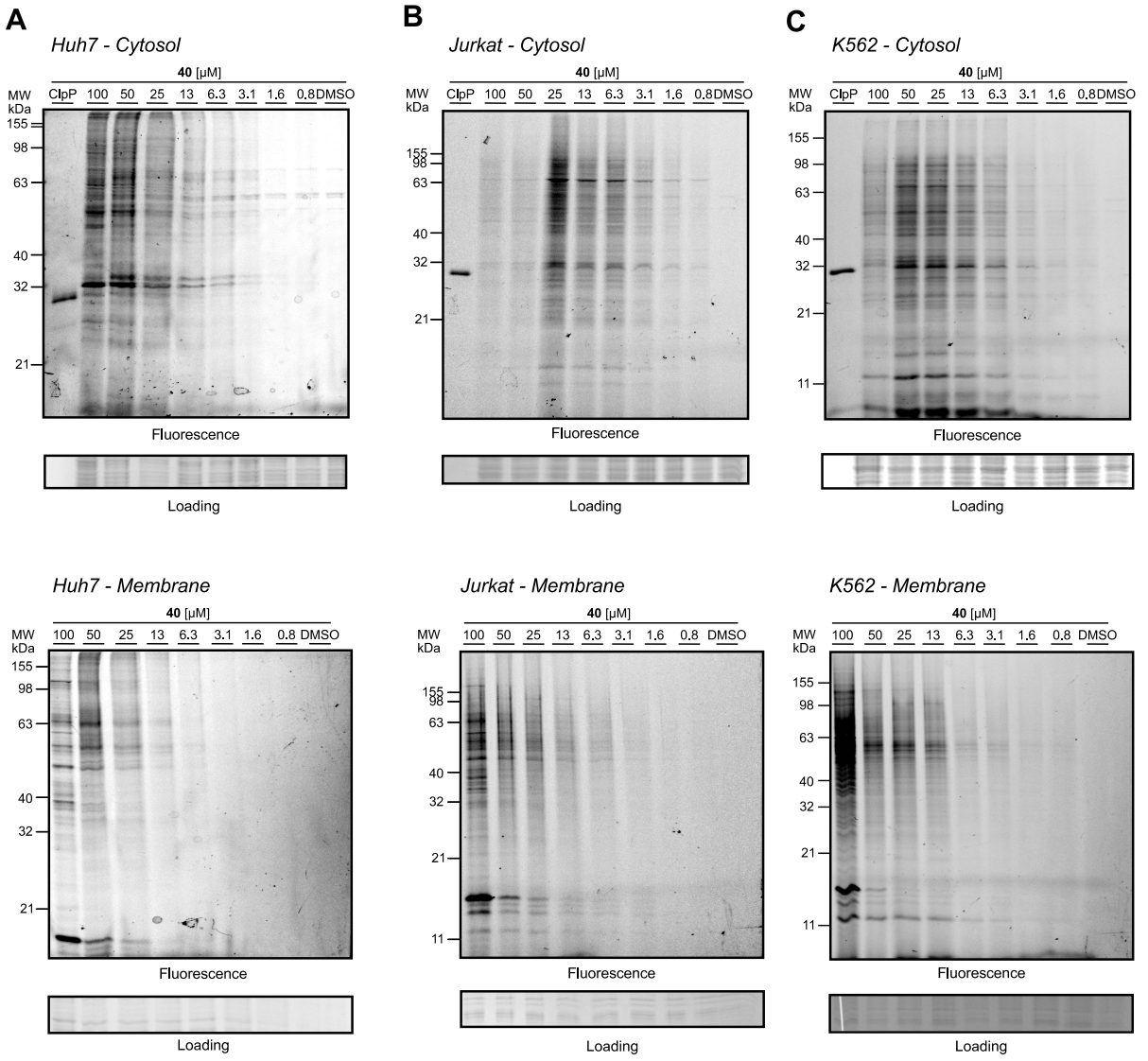

Figure 2.15 Analytical labeling with phenyl ester **40** in A) Huh7 B) Jurkat and C) K562. Labeling experiments were conducted in live cells with varying concentrations for 1 h at 37 °C. Cytosolic and membrane fractions were separated prior to *Click*-reaction with fluorescent dye TAMRA-N_3.

The high reactivity of **40** is reflected in fluorescence gels as in all cell lines background binding strongly superimposes labeling of hClpP. In Huh7 concentration dependent labeling of one band at 32 kDa mirrors labeling with **35**. However, background binding of probe **40** diminishes the

selectivity. In the membrane fractions of Huh7 as well as Jurkat and K562 one distinct band with molecular weight <21 kDa is only observable at concentrations between 100 and 25 µM. In cytosolic fractions of K562 and Jurkat binding of a variety of proteins predominates while a band corresponding to ClpP at 32 kDa is only slightly visible. Labeling of **40** at concentrations of 100 and 50 µM in Jurkat cells is impeded by the hydrophobic nature of the compound leading to precipitation.

In conclusion, analytical gel-based labeling experiments indicate that phenyl ester probes **35** and **40** are able to bind hClpP in a complex mammalian proteome especially in Huh7 cells, however high reactivity of phenyl esters leads to increased off-target binding.

2.4.3 MS-based identification of phenyl ester off-targets

Gel-based labeling experiments with probe **35** exhibited promising results in Huh7 cells. In this cell line **35** was able to label a protein with around 32 kDa in the background of a complex human proteome. To elucidate the identity of the distinct band appearing in Huh7 labeling, a gel-free labeling approach was applied. For this, Huh7 cells were grown until a confluency of 70-80% and were treated with 20 µM **35** or DMSO as a control at 37 °C for 1 h. Afterwards, cells were lysed and probes were reacted with biotin-azide for affinity enrichment. After incubation with avidin-agarose beads, enriched proteins were reduced, alkylated and digested with trypsin. Peptides were subjected to LC-MS/MS measurement and were analyzed *via* label-free quantification.[106] After statistical evaluation with Perseus software, enrichment factors were plotted against p-values to visualize proteins that are targeted by phenyl ester probes.

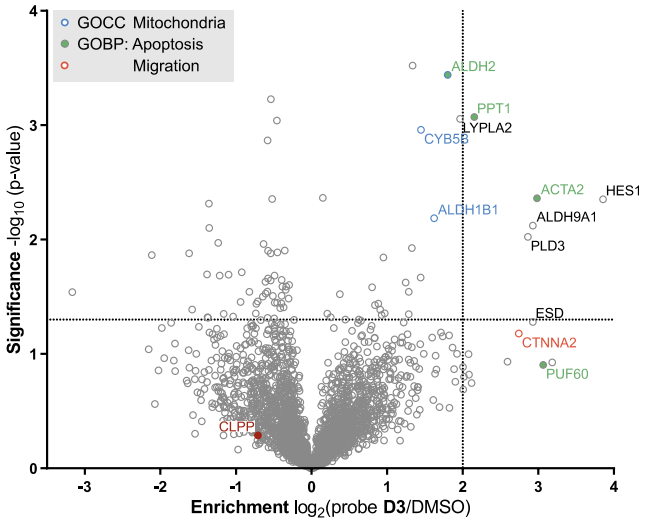

Figure 2.16 Gel-free quantitative ABPP experiments with *β*-lactone **D3** in Huh7 cells (20 µM **D3**, 1 h labeling, 37 °C) depicted as volcano plot representation with enrichment factors plotted against significance of enrichment. Graphs represent data from four technical replicates per state. Two sample student's *t*-test was performed by comparison of compound treated samples with DMSO as single control group with Benjamini-Hochberg FDR correction set to 0.05. Cut-off lines were set at a minimum $\log_2$ change of 2 with a minimum *p*-value of 0.05. Color codes express connection of protein targets with cell compartment (GOCC) and biological processes (GOBP) determined by gene ontology analysis.

Labeling with **35** in Huh7 showed only minor enrichment of hClpP to almost 4-fold compared to DMSO control, surpassing the effect of current gold standard **D3** which showed no enrichment at all (Figure 2.16). Interestingly, when incubated with Jurkat cells hClpP could be significantly enriched almost 8-fold compared to the negative control (Figure 2.17B). Strikingly, both labeling experiments in Jurkat and Huh7 exhibit a large number of other prominent targets which suggests that the highly electrophilic probe is of limited selectivity in human proteome.

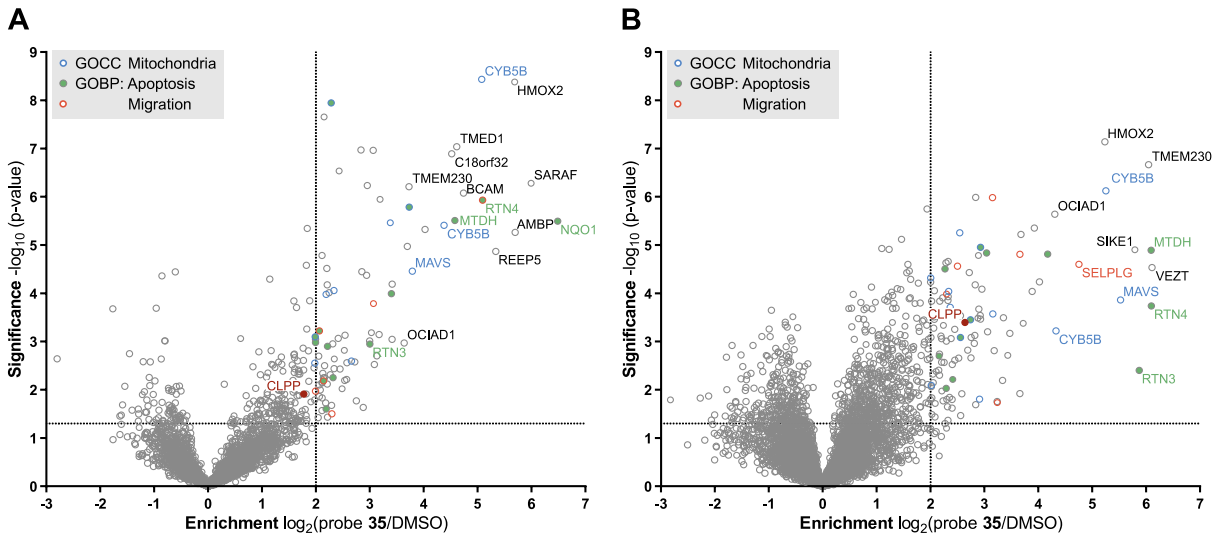

Figure 2.17 Gel-free quantitative ABPP experiments with **35** in A) Huh7 and B) Jurkat cells (20 µM **35**, 1 h labeling, 37 °C) depicted as volcano plot representation with enrichment factors plotted against significance of enrichment. Graphs represent data from eight technical replicates for each state for Huh7 and four technical replicates per state for Jurkat cells. Two sample student's *t*-test was conducted by comparison of labeled group with DMSO as single control group. False discovery rate was determined by Benjamini-Hochberg procedure setting correction to 0.05. Cut-off lines were set at a minimum $\log_2$ change of 2 with a minimum *p*-value of 0.05. Color codes express connection of protein targets with cell compartment (GOCC) and biological processes (GOBP) determined by gene ontology analysis.

Among these off-targets, proteins that are highly enriched in both cell lines are heme oxygenase 2 (HMOX2) which is responsible for conversion of heme to biliverdin[107] and transmembrane protein 230 (TMEM230) which is associated with Parkinson's disease and is suggested to mediate PARP1-linked apoptotic cell death.[108] Further proteins that are associated with apoptosis are protein MTDH[109] as well as RTN3[110,111] whose down-regulation is suggested to induce programmed cell-death and attenuates the anti-apoptotic activity of Bcl-2. Overexpression of the former was shown to block serum starvation-induced apoptosis through *Ras* and PI3K-AKT pathway. Recurring mitochondrial proteins contain cytochrome b5 type B (CYB5B) which is involved in various metabolic and anabolic processes by providing reductive potential[112–114] and the mitochondrial antiviral-signaling protein MAVS which mediates innate immune response through activation of NF-$\varkappa$B and IRF3 upon virus infection.[115] Besides the listed targets that reappear in both treated cell lines a plethora of proteins is additionally enriched by **35**, a fact that demands for optimization of the molecular scaffold of **35** to enhance cellular selectivity for mitochondrial hClpP.

2.5 ClpP inhibitors 35 and 40 display cytotoxic, anti-proliferative and anti-migratory effects

ClpP was previously reported to serve as a potential target for treatment of acute myeloid leukemia. Inhibition by *β*-lactones resulted in decreased viability of cells with high expression profiles of ClpP.[67] With a new generation of selective ClpP inhibitors in hand phenyl esters were tested for their potency to impede viability and migration of cancer cells.

First, compounds **35** and **40** were tested for their ability to reduce cell viability in Huh7 cells after treatment for 48 h and 72 h, respectively. CellTiterBlue® assay was used to assess the amount of viable cells by fluorescence readout of the dye resorufin, the metabolic product of resazurin in viable cells.[116] Both phenyl esters exhibited reduction of viability to 50% after treatment for 72 h with concentrations of 30 μM while treatment for 48 h revealed superior potency of **35** compared to **40** (Figure 2.18A).

Whether cells died after induction of apoptosis or in an uncontrolled manner was investigated using an assay described by *Nicoletti et al.*[117] Here, the amount of DNA is measured by flow cytometry after incubation with a DNA intercalating agent and fluorescence intensity is plotted against cell count. Presence of a sub-G_1 peak indicates apoptotic cells.[118] Clearly, upon incubation with 30 μM **35** for 48 h almost half of all cells induced apoptosis while the same effect was caused by **40** only at slightly higher concentrations of 50 μM (Figure 2.18B).

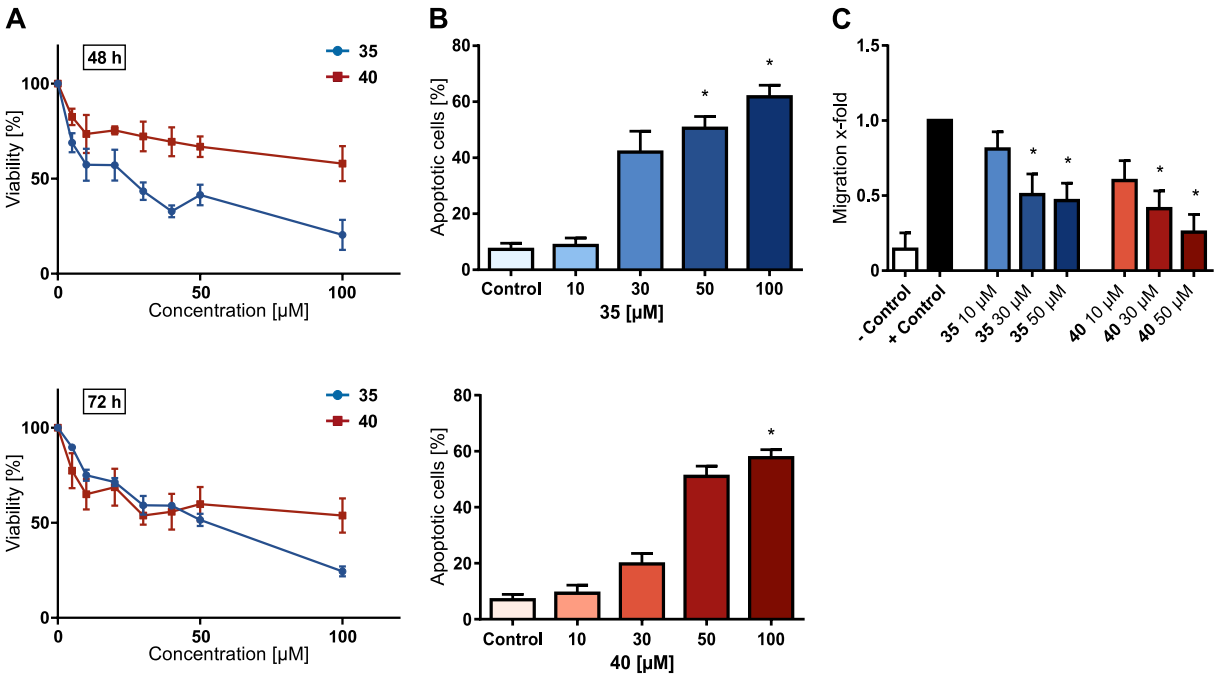

Figure 2.18 A) hClpP inhibitors **35** and **40** reduce cell viability of Huh7 cells after treatment for 48 h and 72 h (determined by CellTiterBlue® assay). Graphs depict results from nine technical replicates from three independent experiments (mean ± SD). B) Upon treatment with **35** and **40** for 42 h Huh7 cells induce programmed cell-death. Apoptosis was measured using flow cytometry and quantifying subG1 population after treatment with propdium iodide (* $p < 0.05$, mean ± SEM, one-way ANOVA, Tukey's multiple comparison, n = 3). C) hClpP inhibitors **35** and **40** diminished migration ability of Huh7 after treatment for 16 h (mean ± SEM, * $p < 0.05$, one-way ANOVA, Dunnet's test, n = 3).

Next, influence of phenyl esters on migration of adherent cells was tested. For this, chemotaxis related migration of Huh7 cells was investigated using a Boyden chamber setup.[119] By excluding nutrients from the culture medium, cells are forced to actively move towards an area with higher concentration of growth factors.[120] At concentrations of 30 μM phenyl ester probes **35** and **40** proved to effectively inhibit cell migration to half of its maximum (Figure 2.18C).

2.6 Conclusion

ClpP is a promising target for selective eradication of cancer cells as it is overexpressed in a variety of malign cells and is thought to be involved in fundamental pathways such as protein homeostasis.[121] As already shown by *Brötz-Oesterhelt et al.* overactivation of bacterial ClpP by acyldepsipeptides led to uncontrolled proteolysis and eventually cell death.[122] Similarly, however with an antipodal approach inhibition of ClpP by *β*-lactones showed reduction of skin abscesses in a murine model caused by *S. aureus*.[123] *Cole et al.* were able to show that a very similar *β*-lactone could also induce ClpP expression-level dependent cell death in a variety of leukemia cells as well as anti-AML activity in a xenograft model of human leukemia.[67]

In a high-throughput screen, initially designed for the discovery of novel bacterial ClpP inhibitors, compound **AV167** stood out by effectively inhibiting human ClpP. Structure-activity relationship studies on the phenyl ester core structure culminated in novel inhibitors that exceeded potency of **AV167** to inhibit peptidase and proteolytic activity and proved to be useful for activity-based protein profiling. Compound **40** inhibited ClpP peptidase activity almost completely at concentrations as low as 1 μM and reduced proteolytic activity to 20% at concentrations of 10 μM. The less reactive compound **35** was then applied in activity-based protein profiling to validate the effective target engagement in a human proteome. While ClpP could be successfully targeted among the protein background and showed superior labeling compared to gold standard **D3**, several off-targets were identified. Therefore, the influence on viability and migration cannot be completely attributed to the inhibition of ClpP by phenyl esters. Hence, further optimization of this compound class in regard to cellular selectivity and stability against undesired hydrolysis is required. One step towards this goal was accomplished by *Tan et al.*[124] with the introduction of a boronic acid as a novel warhead for *in vitro* inhibition of human ClpXP.

3

Identification of substrates of human ClpP

This chapter is based on a manuscript in preparation.

Contributions

Organic synthesis, genetic encoding of the unnatural amino acid and protein expression were conducted by Tuan-Anh Nguyen in the laboratories of Prof. Kathrin Lang, TU München. TFG conducted mass-spectrometry based experiments and corresponding analysis as well as enzyme activity assays.

3 Identification of substrates of human ClpP

This chapter is based on a manuscript in preparation. Organic synthesis, genetic encoding of the unnatural amino acid and protein expression were conducted by Tuan-Anh Nguyen in the laboratories of Prof. Kathrin Lang, TU München.

3.1 Introduction

3.1.1 Function and known substrate scope of ClpXP in human cells

Primarily known as the cellular power-house, mitochondria play a pivotal role in the late stage of ATP generation.[125] Metabolism of fats and carbohydrates ultimately results in the generation of a proton gradient extending across the mitochondrial membrane that in turn propels ATP synthesis.[126] The consecutive electron transport through complexes I-IV in the electron transfer chain (ETC) is susceptible for generation of reactive oxygen species (ROS) *via* electron leakage culminating in damaged and misfolded proteins.[127] To counteract accumulation of dysfunctional proteins a signaling cascade is initiated, resulting in overexpression of chaperones and enzymes that process or degrade affected proteins.[128] Caseinolytic protease P is believed to contribute to this so-called mitochondrial unfolded protein response (^{mt}UPR) by either signaling *via* degraded substrates or controlled degradation of specific proteins under stress conditions.[129–132] ClpP is specifically addressed to mitochondria by a signaling sequence which is cleaved upon translocation, thus indicating a critical role in this cellular compartment.[17] To further capture the function of ClpXP in human cells it is not only important to find tools to manipulate the protease's activity but to inventory its potential interactors, substrates and targets.

Recent efforts to explore ClpXP substrates in eukaryotes are manifold and were focused on three major approaches.[133]

The method of spatial trapping of protein substrates inside the self-compartmentalized protease was first introduced by *Flynn et al.* using *E. coli* ClpXP. Here, identification of novel protein substrates was enabled by abrogating the catalytic activity of ClpP *via* mutation of the active site serine to alanine combined with affinity purification of the bait and its trapped substrates.[134] The same approach was applied by *Fischer et al.* in the fungal strain *Podospora anserina (P. anserina)* to investigate the substrate scope of human ClpP in an eukaryotic environment. Here, the inactive mutant of human ClpP that is able to form a peptidase-chaperone complex with PaClpX was used. Affinity purification coupled with LC-MS/MS analysis enabled the comparison of protein abundance between wild-type and inactive ClpP. Proteins of the tricarboxylic acid cycle (TCA) and components of the pyruvate dehydrogenase (PDH) as well as subunits of the electron chain complex I were among the substrates found by this method.[135]

In the same year *Cole et al.* conducted a study to elucidate the influence of ClpXP on leukemia cells. Besides the discovery that β-lactones reduce viability of AML cells by impeding ClpP's proteolytic activity the group set out to identify interactors of ClpP by using the BioID mass spectrometry method.[136,137] Here, the protein of interest is fused to the biotin conjugating enzyme BirA R118G (BirA*) which is able to promiscuously biotinylate lysine residues of proteins within a certain proximity to the bait protein. Affinity purification followed by LC-MS/MS analysis revealed ClpX as a major interactor as well as components of the respiratory chain and enzymes involved in mitochondrial metabolism.[67]

A very similar approach was accomplished by *Fux et al.* exploiting the broad reactivity of succinimides with lysine residues. Two succinimide moieties connected *via* a MS-cleavable tether render a crosslinking scaffold which can be applied to a target enzyme in a complex environment. Crosslinking of the bait protein with interactors in close vicinity coupled with classical co-immunoprecipitation experiments leads to a powerful tool for the investigation of protein-protein interactions.[138] Applied in human K562 and HepG2 cells a plethora of interaction partners of ClpXP could be identified. A great share of these proteins were of mitochondrial origin and also coincided with already reported interactors.

In between *Szczepanowska et al.* reported further putative ClpXP substrates by comparing proteomes from murine heart mitochondria in presence and absence of ClpP. Deletion of ClpP led to a down-regulation of mitochondrial respiratory chain I subunit proteins while elements of the mitochondrial translation machinery where highly upregulated.[139]

Further investigations indicate that ClpP participates in the quality control of respiratory chain proteins such as members of protein complex I (CI)[140] and complex II (CI)[141]. Others propose a connection of ClpP loss in muscle cells to decreased expression of proteins involved in ^{mt}UPR and therefore attenuation of respiratory protein complex activity.[142]

3.1.2 Genetic code expansion

Cellular processes rely to a vast extent on proteins interacting with one another. In order to understand the underlying mechanisms and resulting pathways it is crucial to identify and annotate such protein-protein interactions (PPi). To date, a variety of different approaches have been reported that enable characterization of transient interactions between proteins. The three key technologies so far are i) yeast two-hybrid (Y2H) assay ii) affinity purification mass spectrometry and iii) BioID.[143] All these technologies have seen various implementation and improvements over the years and all possess their own advantages and drawbacks. While the Y2H may show high false-positive and false-negative interactions it also represents an inexpensive, economic technology. Recently, parallelization of BioID and AP-MS resulted in the Multiple Approaches Combined

(MAC)-tag workflow which allows the analysis of PPi's by both methods using one single construct.[143] Nonetheless, since interactions between proteins are almost always of transient nature capturing these contacts can still be arduous. A loophole to this fragile system poses the formation of a permanent bond between involved protein partners. This approach requires modification of the protein of interest at a position that is close to the binding site but simultaneously distant enough that binding can still occur. In recent years, expansion of the genetic code permitted the site-specific incorporation of a multitude of unnatural amino acids (UAA) with a variety of different side chains.[144,145] In this way, protein sequences can be altered to exhibit an unnatural amino acid that is able to establish a covalent bond between interacting proteins. For site-specific incorporation an orthogonal aminoacyl tRNA synthetase (aaRS) is necessary that is able to recognize an unnatural amino acid and successfully loads it onto a corresponding tRNA. The aaRS/tRNA pairs used in these approaches mostly make use of the amber stop codon (TAG) for incorporation during mRNA translation.[146] The high substrate side chain acceptance of pyrrolysyl-tRNA synthetase (PylRS) which usually incorporates the 22nd proteinogenic amino acid pyrrolysine in bacteria and methanogenic archaea proved particularly useful for introduction of novel amino acid scaffolds.[144,147] Directed evolution towards a specific aaRS/tRNA pair generally involves several selection steps which are time-consuming in human cells and are therefore typically conducted in single-cell microorganisms like *E. coli* or *S. cerevisiae* and can be transferred without loss of orthogonality.[144] So far, various studies have demonstrated that incorporation of photocrosslinker containing amino acids into proteins is feasible and have described their exploitation for identification of interaction partners.[148–150]

3.1.3 Scope of this work

In this chapter a novel approach is described that allows the identification of human ClpXP substrates by simultaneously minimizing the accompanying structural alteration to the proteolytic subunit. Previous studies relied on either inactive ClpP subunits or extensive alterations to the cellular environment such as entire deletion of the target protein. Site-specific modification of each ClpP subunit by an unnatural amino acid bearing a photoactivatable moiety enables UV-light induced trapping of proteins within the peptidase subunit. Modification with a short HA-tag allows for systematic enrichment of the bait protein followed by identification of trapped proteins *via* mass spectrometry. In this context, various ClpP-mutants were tested for their efficiency to trap substrate proteins.

Previous studies suggested a connection between ROS-induced protein damage and ClpP mediated initiation of the mitochondrial unfolded protein response. Therefore, cells with an efficient ClpP trap were treated with rotenone, a known inhibitor of complex I of the ETC, and the influence on ClpP's substrate scope was investigated.

3.2 Experimental results and discussion

3.2.1 Synthesis of unnatural amino acid diaziK (dK) and site specific incorporation

As previously described by *Chou et al.*[149] and *Ai et al.*[148] N^6-((2-(3-methyl-3*H*-diazirin-3-yl)ethoxy) carbonyl)-L-lysine can be synthesized in a four step synthesis (Figure 3.1) from 4-hydroxybutan-2-one and can readily be incorporated in a variety of enzymes such as glutathione S-transferase (GST) or cyclin-dependent kinase 5 (Cdk5). Here, the photoactivatable moiety was utilized to freeze the dimeric state of GST in *E. coli* or to capture the natural substrate of Cdk5, p21-activated kinase 1 (Pak1), in mammalian cells.

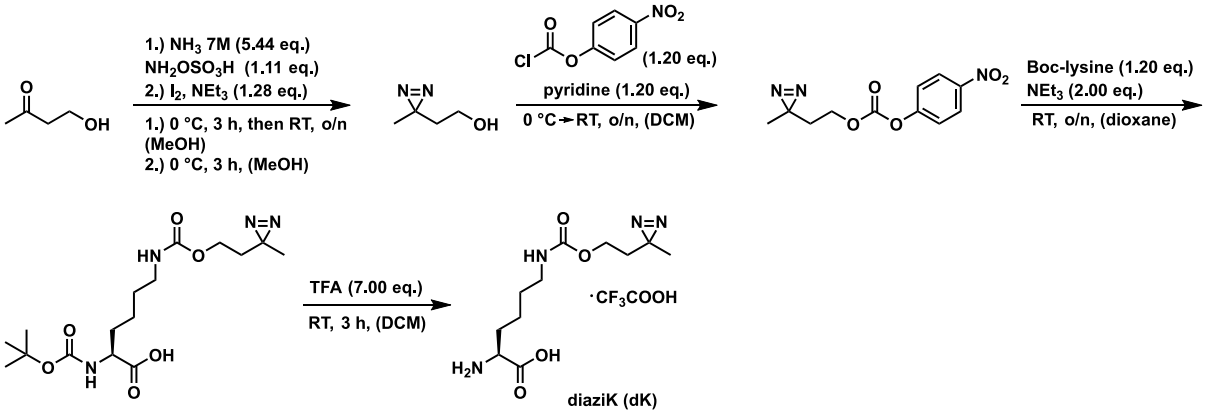

Figure 3.1 Synthesis of unnatural amino acid diaziK (dK) according to a slightly modified procedure published by *Chou et al.*[149]

By screening a panel of PylRS variants a novel synthetase for incorporation of dK was identified by directed evolution. The corresponding aaRS/tRNA pair was further utilized to incorporate dK into hClpP with a C-terminal His-tag for purification. For application in biochemical activity assays the N-terminal 56 amino acid bearing mitochondrial guiding sequence was omitted. Appropriate positions for the site-directed incorporation were selected based on structural evaluation of hClpP crystal structure (PDB identifier: 1TG6, Figure 3.2). Substrate proteins are generally recognized by the specific chaperone and enter the peptidase subunit from the apical site. Inside the hollow chamber protein degradation is catalyzed by 14 active sites. Taking this into account photocrosslinking moieties need to be located on the inner wall of the barrel-shaped protease directed towards the central cavity. The length of the tether that connects the protein backbone with the crosslinking component is yet another crucial feature that has to be carefully adjusted for successful trapping of substrate proteins. At the same time, alterations on the amino acid sequence level must be limited to a minimum to maintain structural integrity of the protein complex.

Seven positions were selected for site-directed incorporation of the corresponding amino acid with six mutation sites residing inside the catalytic barrel. Two mutation sites are chosen on residues connecting the β1 sheet with the α2 helix, three mutations on the junction of β1 sheet and α3 helix and another mutation of amino acid residue S181 residing close to the active site on β7 sheet (SH1-

6, Figure 3.2). In order to gather information about proteins that closely interact with ClpP amino acid residue K261 which protrudes from the side of the barrel was mutated as well (Figure 3.2).

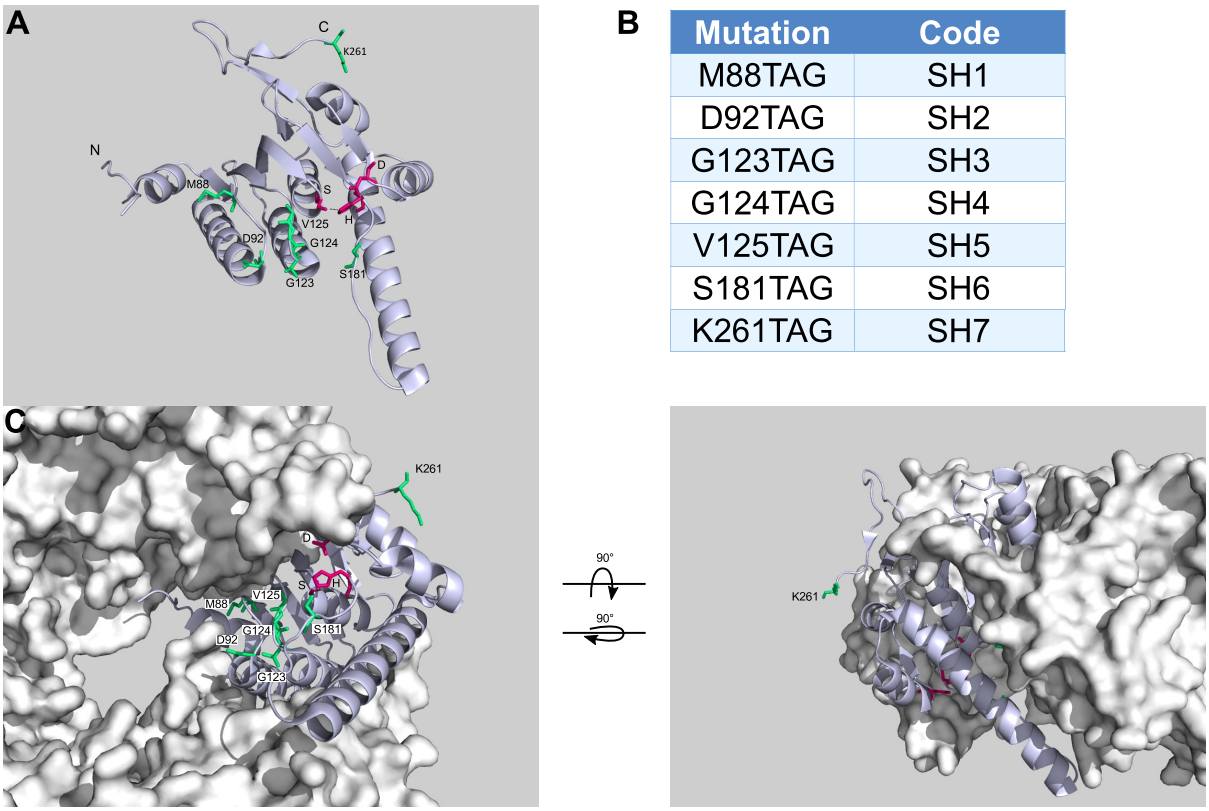

Mutation	Code
M88TAG	SH1
D92TAG	SH2
G123TAG	SH3
G124TAG	SH4
V125TAG	SH5
S181TAG	SH6
K261TAG	SH7

Figure 3.2 A) Representation of hClpP monomer (PDB-entry: 1TG6)[151] with mutation sites highlighted as stick models in limegreen. Active site residues are colored as stick models in hotpink and N- and C terminii are marked with N and C, respectively. B) List of mutated residues and their corresponding codes in the following experiments. C) Representation of one heptameric ClpP ring from bottom and side view.

Subsequently, all seven mutant hClpPs as well as wild-type hClpP were expressed in amber suppression experiments in *E. coli* expression strains. Size exclusion chromatography (SEC) analysis with a calibrated SEC column revealed equal elution profiles for all variants indicating correct assembly of the protein complex and no major structural influence of UAA incorporation (Figure 3.3A). Following this, hClpP mutants were assessed for their ability to build a proteolytically active complex with chaperone EcClpX and to cleave ssrA-tagged eGFP as described in chapter 2. Residual proteolytic activity of the mutants was normalized to wild-type hClpP. All tested mutants showed similar activity compared to the wild-type except for the mutants in which glycines were exchanged for the UAA (Figure 3.3B). A possible explanation for this observation may be the prejudicial position of the mutation sites in the loop region next to the catalytic triad leading to a partial distortion of the active site. Nevertheless, these mutants will also be implemented in further experiments.

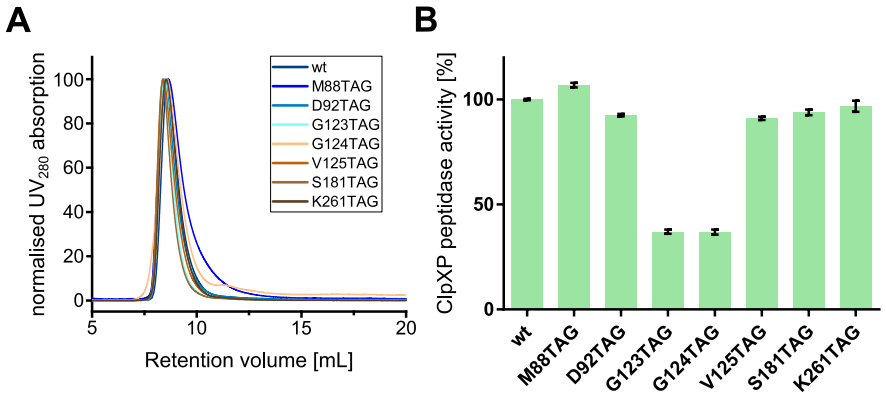

Figure 3.3 A) Elution profiles of mutant ClpP and wild-type ClpP reveal no detrimental influence of UAA incorporation on oligomerization state. B) Results from ClpXP GFP-degradation assay (2.8 µM $hClpP_{monomer}$ in the presence of 2.4 µM $EcClpX_{monomer}$ and 0.4 µM eGFP-ssrA). Activity of mutant ClpPs was normalized to activity of wild-type ClpP. Each data-set represents results from three replicates (mean ± SD).

3.2.2 *In situ* trapping experiments with hClpP mutants

With functional $ClpP^{TAG}$ traps in hand, first *in situ* trapping experiments were conducted in human cell line Hek293T. A schematic overview of the approach is depicted in Figure 3.4

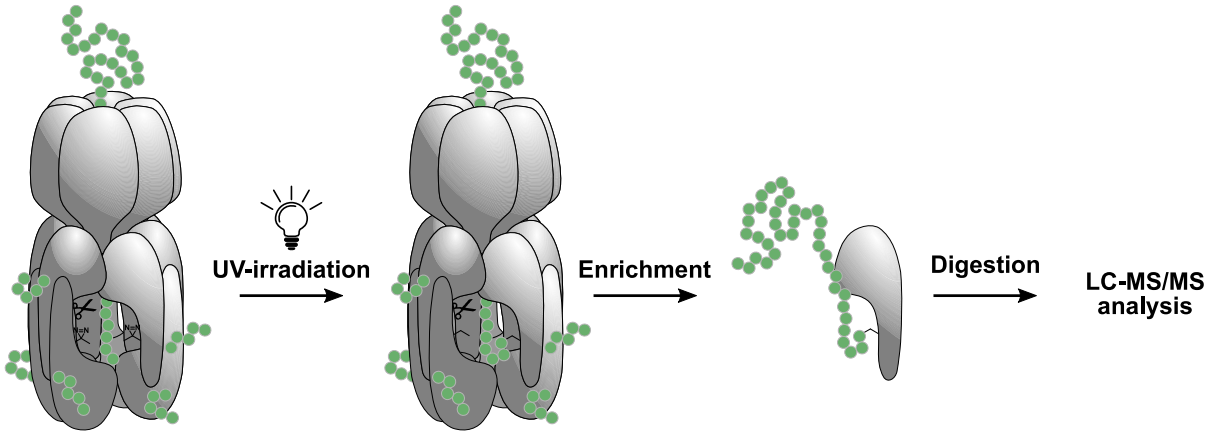

Figure 3.4 Schematic representation of in situ trapping experiments. Proteins presented to the peptidase core are crosslinked to ClpP-subunits upon UV-irradiation. Substrate-bait adducts are then purified *via* an enrichment tag on each ClpP subunit. Further digestion of ClpP and bound substrates enables identification by LC-MS/MS.

Inside mitochondria, ClpP mutants form tetradecamer complexes and constitute a functional protease with the corresponding chaperone ClpX. Substrate proteins are recognized by ClpX and are translocated in the inner cavity of ClpP. *In vitro* experiments could show that the proteolytic subunit is functional and degrades protein substrates like its native equivalent. Meanwhile, UV-light exposure leads to activation of the diazirine moiety within mutant ClpP monomers resulting in short-lived, highly reactive carbenes that can insert in C-H-bonds of proximal amino acid side chain residues. Due to the concentration of protein substrates within the protease compartment and the presence of 14 activatable functional groups high chances for successful photocrosslink are expected. Solely quenching of the reactive intermediate by surrounding water molecules or the amino acid residues of the protease itself should account for attenuation of photocrosslinking

events. For further analysis, negative control samples are added wherein treatment with UV-light is omitted.

Each ClpP monomer is constructed to bear a C-terminal HA-tag that extends from the proteolytic subunit. This short amino acid sequence derived from the hemagglutinin epitope YPYDVPDYA from influenza virus A[152] allows for protein purification *via* enrichment with specific antibodies while simultaneously exhibiting only minor changes to the protein. Hence, after lysis of UV-treated and untreated cells, cytosolic fractions were incubated with monoclonal HA-antibody conjugated agarose beads. Enriched proteins were subsequently digested by trypsin and further prepared for LC-MS/MS analysis.

Statistical evaluation was performed by two-sample student's *t*-test with UV-treated samples and untreated samples as single negative control (n = 3). Results were visualized by plotting enrichment factors against significance of enrichment for each mutant. Cut-off criteria for enriched proteins were defined as $\log_2 = 1$ (2-fold enrichment over UV-untreated samples) for enrichment with p-values higher than $-\log_{10} = 1.3$ (Figure 3.5, Appendices).

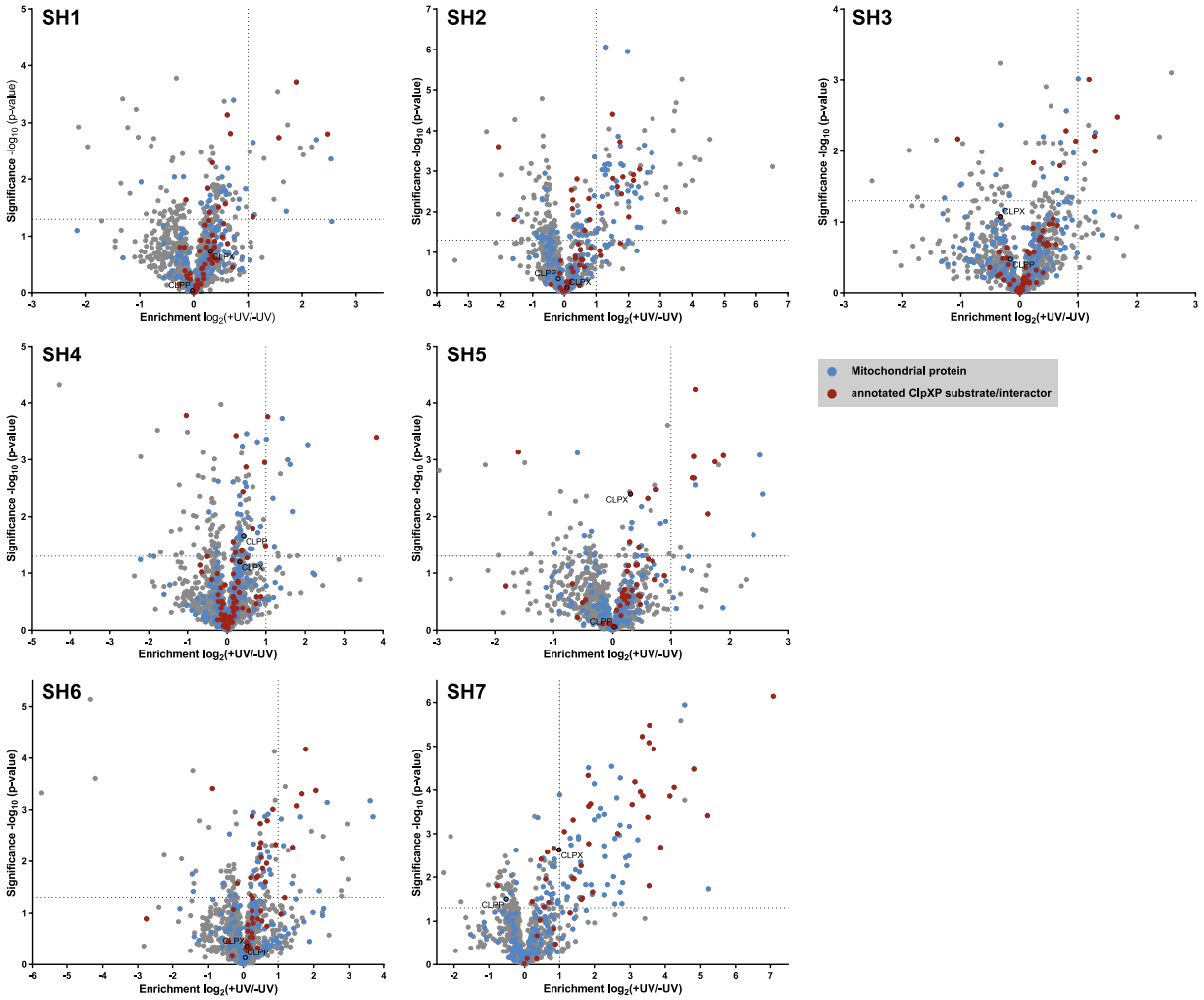

Figure 3.5 A) Graphical representation of trapping experiments with ClpP mutants SH1-7. Enrichment factors are plotted against significance of enrichment. Graphs represent data from three technical replicates for each state. Two sample student's *t*-test was conducted by comparison of UV-treated group with UV-untreated as single control group. False discovery rate was determined by Benjamini-Hochberg procedure setting correction to 0.05. Cut-off lines were set at a minimum $\log_2$ change of 1 with a minimum *p*-value of 0.05. Proteins that are annotated as members of mitochondrial compartment are colored in blue. Proteins colored in red indicate known ClpP substrates.

In all ClpP mutants the majority of enriched proteins are of mitochondrial origin (marked in blue), which indicates correct import of mutant ClpPs in mitochondria and full maturation. However, mutants SH1-7 clearly show different trapping efficiencies which is observable in the level of enrichment. While mutants SH1, SH3 and SH4 only exhibit one to four already annotated ClpP substrates with low enrichment ratios, mutants SH2 and SH7 feature a high number of annotated proteins with enrichment of up to 128-fold. Concordant with *in vitro* results ClpP mutants, SH3 and SH4 are also the lowest performing variants in the GFP degradation assay.

3.2.3 Pathway analysis of enriched proteins

After this first quality check enriched proteins were subjected to network analysis using the String v11 database.[153] With this tool, network patterns can be revealed to provide a broader overview over the pathway involvement of ClpP. Network analyses for mutants SH2 and SH7 are presented

as graphical examples and are discussed in more detail while all other mutants are subsequently interpreted as a whole (Figure 3.6, Figure 3.7, Figure 3.8).

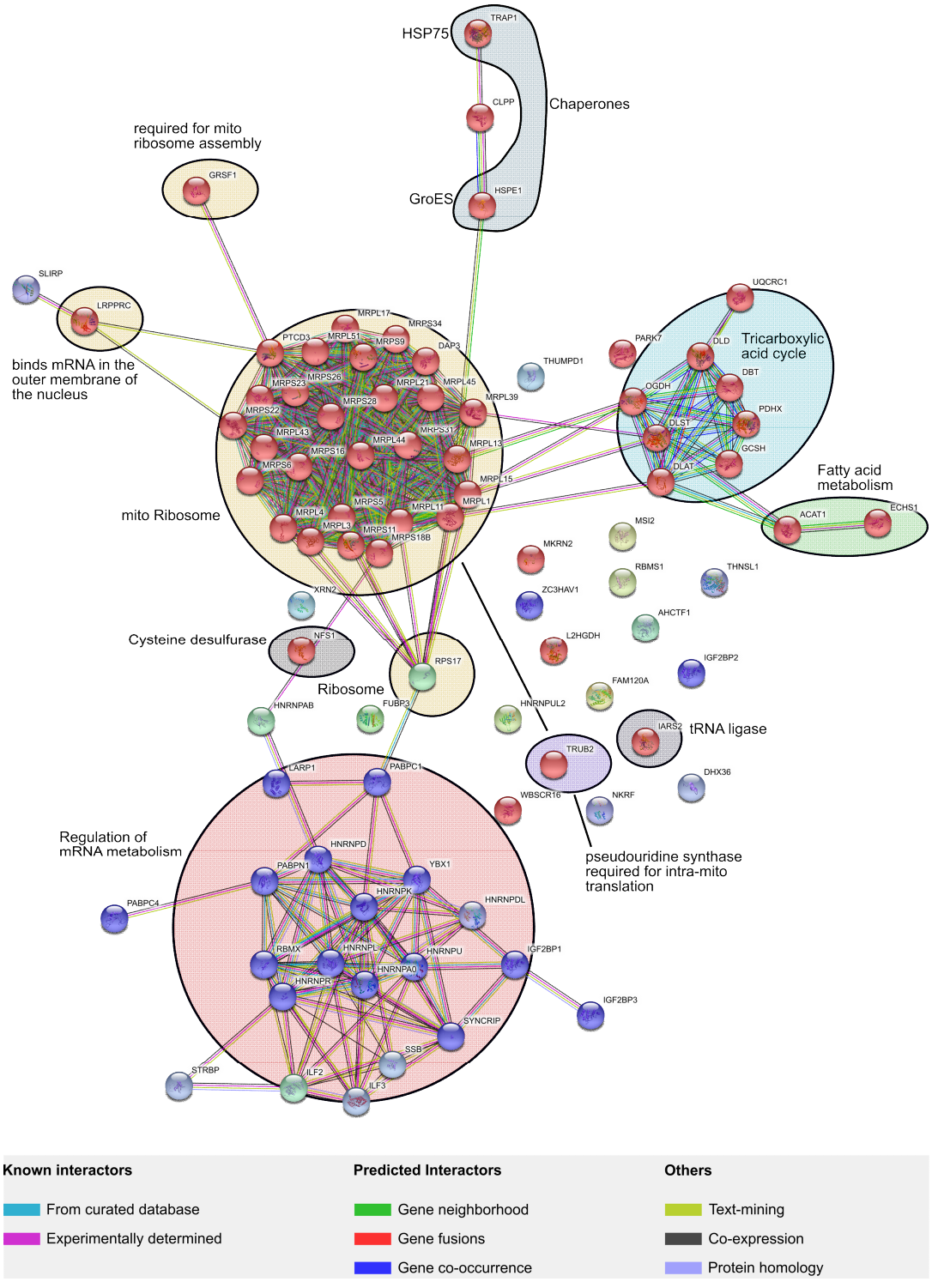

Figure 3.6 Network analysis for proteins that were enriched by ClpP mutant SH2 using String v11 database.[153] The network displays connections between identified proteins based on evidence found in literature as indicated in the legend. Minimum required interaction score was set to 0.7 (high confidence). Mitochondrial proteins are marked with red spheres. Blue spheres indicate members of the regulatory pathway of RNA metabolism. Proteins are further clustered and named for their collective pathway affiliation.

At first glance three major pathways are overrepresented in trapping experiments with ClpP mutant SH2. With 25 proteins annotated as mitoribosomal subunits, the mitochondrial translation machinery appears to be a major target of ClpP. This finding is substantiated by a study from *Szczepanowska et al.*[154] describing a significant upregulation of mitoribosomal subunits in murine ClpP knockout cells compared to their wild-type congener.

In the same study, increased abundance of mitochondrial chaperone Trap1 and protein LRPPRC (Leucine-rich pentatricopeptide repeat containing protein) was detected. Trap1 was also shown to co-localize with a survivin-ClpXP complex in co-immunoprecipitation experiments, corroborating the results from this trapping experiment.[155] Furthermore, Trap1 is involved in downregulation of respiratory chain activity by binding and inhibiting succinate dehydrogenase (SDH), another protein which is also destabilized in absence of ClpXP.[155,156]

Protein LRPPRC exhibits RNA binding ability and is crucial for stability and polyadenylation of mitochondrial mRNA, underlining ClpP's involvement in mitochondrial translation pathways.[157]

Another link to protein translation regulation is demonstrated by a cluster which is composed of various heterogeneous nuclear ribonucleoproteins (HNRNP). Interestingly, these proteins are annotated as members of the nucleic compartment and should consequently be beyond the range of ClpP. Nevertheless, findings by *Fischer et al.*[135] already suggested HNRNPA2B1, a member of the family of ribonucleoproteins, to be a ClpP target.

The third major cluster containing putative ClpP substrates is composed of members of the tricarboxylic acid cycle (TCA-cycle) coinciding with findings of several other studies.[135,154,158] Apart from protein DBT (Lipoamide acyltransferase component of branched-chain alpha-keto acid dehydrogenase complex) all proteins of this cluster were already annotated as ClpP substrates. As protein DBT was found with six out of seven mutant ClpPs and was not annotated as ClpP substrate before this protein is highly likely to represent a novel target of ClpP. This finding is further substantiated as DBT constitutes the branched-chain α-keto acid dehydrogenase complex (BCKDC) together with known ClpP substrate DLD and an α-ketoacid decarboxylase.

In total, 40 of the 85 enriched proteins were already annotated as ClpP substrates or interactors (Appendix). Of the remaining 45 proteins nine proteins, including DBT, were found to be of mitochondrial origin. These potential new ClpP substrates will be discussed in more detail at a later point.

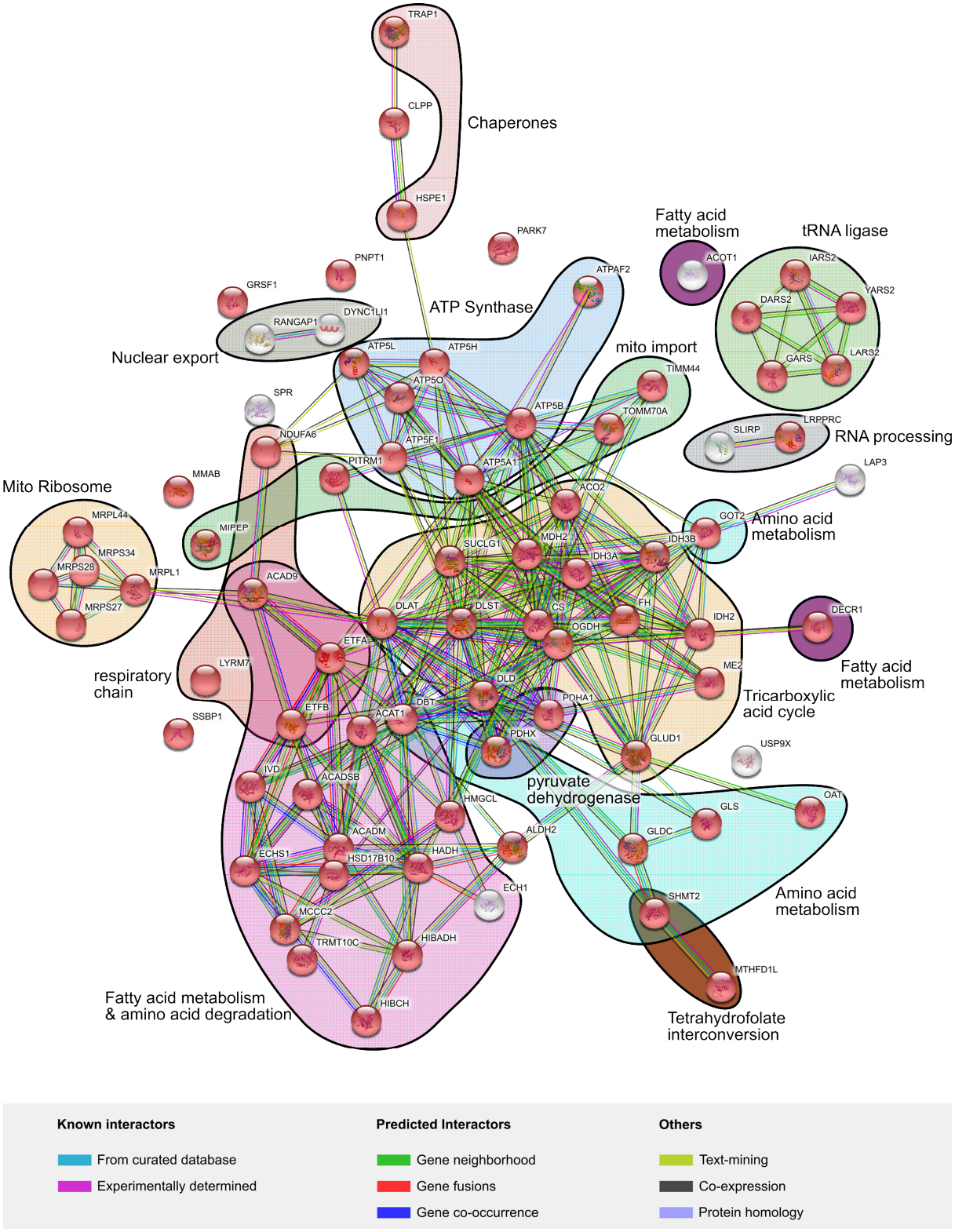

Figure 3.7 Network analysis for proteins that were enriched by ClpP mutant SH7 using String v11 database.[153] The network displays connections between identified proteins based on evidence found in literature as indicated in the legend. Minimum required interaction score was set to 0.7 (high confidence). Red spheres indicate proteins of mitochondrial origin. Proteins are further clustered and named for their collective pathway affiliation.

Network analysis for ClpP mutant SH7, that exhibits the photoreactive moiety on the outside of the proteolytic barrel reveals a similar picture as for mutant SH2 (Figure 3.7). Of note, this ClpP mutant is also able to trap proteins that merely interact with ClpP and do not necessarily represent actual substrates. Unfortunately, these proteins cannot be differentiated and hits that were identified with mutant SH7 will only be specified as putative substrates or interactors. In this way, several new clusters appear when trapping was conducted with mutant SH7 as well as known clusters containing members of the tricarboxylic acid cycle and subunits of the mitochondrial ribosome. In contrast, proteins of the heterogeneous ribonucleoprotein cluster are missing. Nonetheless, it is noteworthy that 57 of 79 proteins that were enriched by mutant SH7 were previously annotated as putative ClpP substrates and of these 79 proteins, 72 proteins are located primarily in mitochondria. Of the 22 proteins that were not annotated as ClpP substrates so far, 17 proteins are assigned to mitochondria. All in all, overrepresented clusters include members of fatty acid and amino acid degradation/metabolism pathways as well as proteins of the ATP synthase and tRNA ligase. Concordant with SH2 mutant, chaperones Trap1 and HSPE1 are also enriched. Members of the respiratory chain have been recently added to the pool of ClpP substrates.[40] Of these, NDUFA6, ETFB and ACAD9 could also be found by this approach.

Figure 3.8 summarizes the trapping experiments for the remaining ClpP mutants SH1 and SH3-6. Overall the number of enriched proteins is significantly lower for each mutant, however several cluster reoccur. Again TCA cycle is represented by every ClpP mutant emphasizing the regulatory role of ClpP in this pathway. Mitoribosomal subunits, fatty acid metabolism associated proteins, as well as chaperones Trap1 and HSPE1 are also enriched by several ClpP mutants. Whether mitochondrial translocation and import proteins from the TIMM and TOMM family are actual ClpP substrates has to be further examined since trapping might also occur when ClpP mutants are actively transported from the cytosol to the mitochondrial lumen.

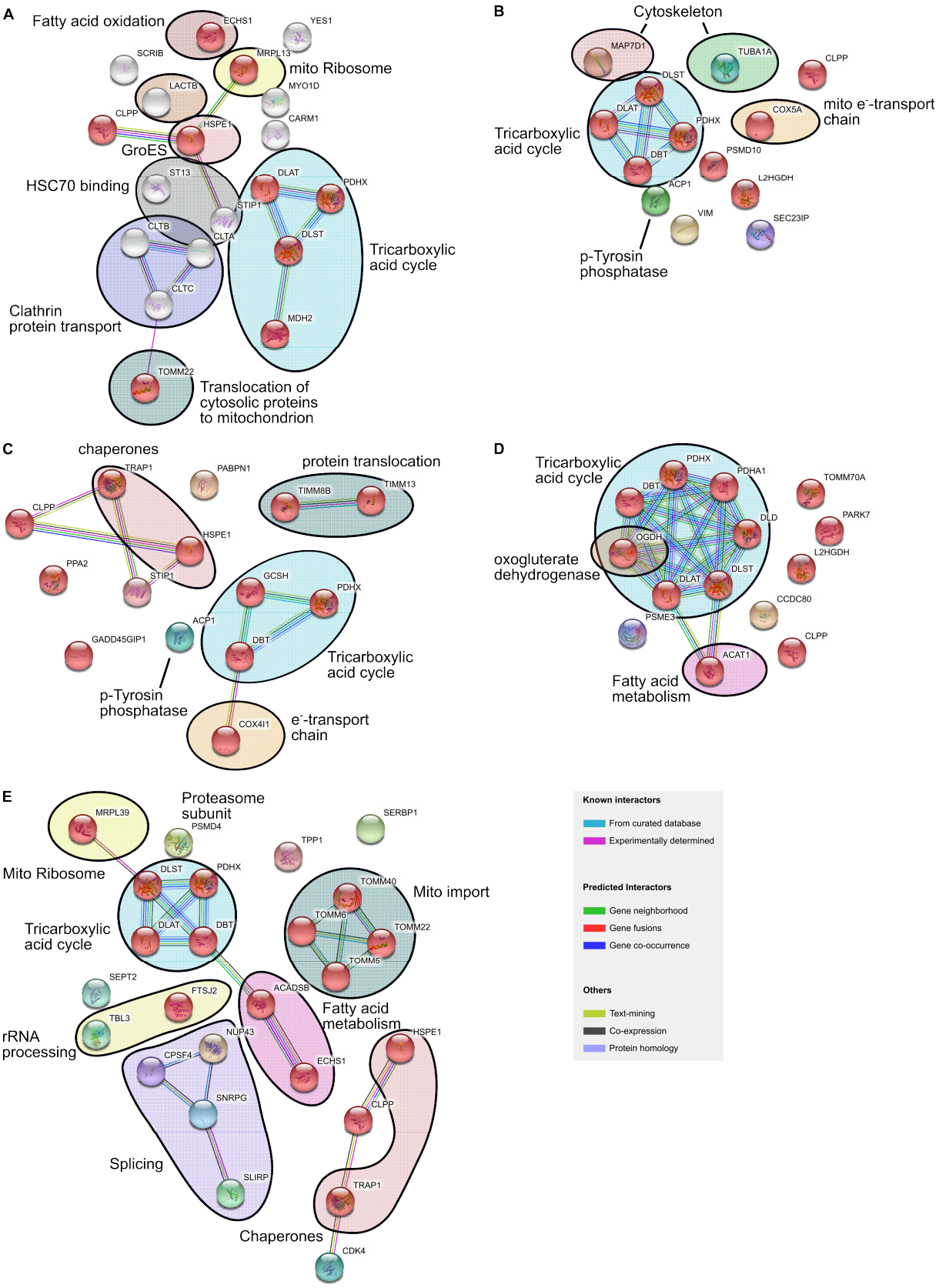

Figure 3.8 Network analysis for proteins that were enriched by ClpP mutants A) SH1, B) SH3, C) SH4, D) SH5, E) SH6 using String v11 database.[153] The network displays connections between identified proteins based on evidence found in literature as indicated in the legend. Red spheres indicate proteins of mitochondrial origin. Proteins are further clustered and named for their collective pathway affiliation.

In summary, diazirine photocrosslinking experiments with ClpP mutants led to the identification of 182 putative ClpP substrates (Figure **3.9**). Of these, 86 proteins were previously identified and annotated by different techniques as ClpP substrates or interactors which serves as a proof of concept for this approach. The remaining 96 hits can be seen as potential new ClpP substrates or interactors, however, two thirds are not attributed to mitochondria. 33 proteins can be further classified as members of mitochondrial import receptors, subunits of the mitochondrial ribosome and ATP synthase, proteins with tRNA ligase activity and components of the TCA-cycle and amino acid degradation system. Seven proteins demonstrate various enzymatic activities that cannot be assigned to any of the other.

The fact that these pathways have recently been shown to be linked to ClpP activity supports the discovery of novel substrates. Nonetheless, validation of these targets is indispensable and will be conducted by an orthogonal technique such as western blot or MS-based selected reaction monitoring (SRM).[159,160]

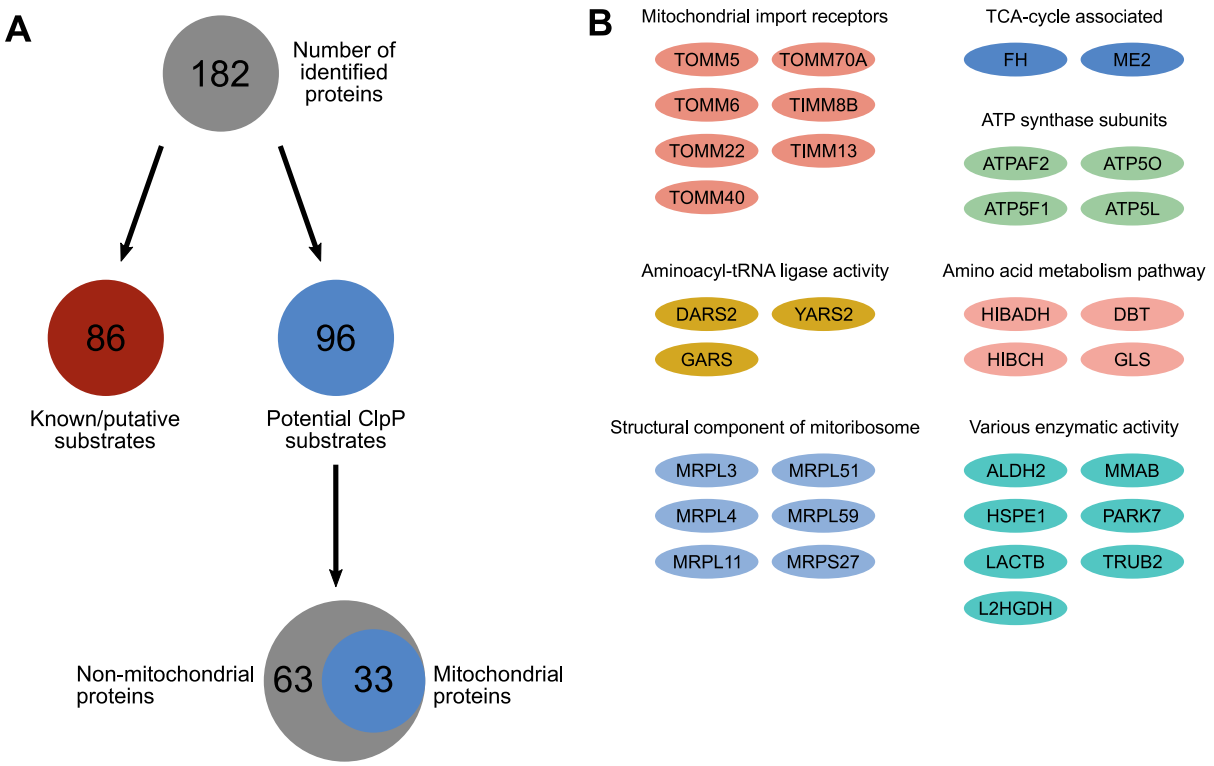

Figure 3.9 A) Flowchart representing number of identified proteins and putative new substrates. B) Putative new ClpP substrates and their affiliation to biological processes.

3.2.4 Identification of ClpP substrates in rotenone treated cells

The electron transport chain in inner mitochondrial membranes is composed of four complexes (CI-IV) that catalyze electron transfer from NADH to dioxygen (Figure 3.10).[161] Directly coupled to these redox processes is the transfer of protons into the intermembrane space, generating a proton gradient across the inner mitochondrial membrane. This proton gradient is then harnessed by complex V for the generation of ATP.[126] Associated with the consecutive electron passage through these large protein complexes is a high potential for side reactions. Especially the electron transport in the peripheral arm of complex I (CI) is prone to electron leakage and ROS production. A large portion of these reactive species, however, is rapidly scavenged by mitochondrial peroxiredoxins PRDX-3 and PRDX-5 and glutathione (GSH) together with glutathione peroxidase, preventing damage to other proteins. Still, proteins affected by reactive oxygen species need to be effectively cleared in order to maintain a steady energy supply. A study by *Szczepanowska et al.* recently showed that ClpP plays a crucial role in maintaining a functional electron transport chain. It is suggested that selective removal and degradation of damaged subunits of CI averts potential adverse effects of accumulated dysfunctional proteins.[140]

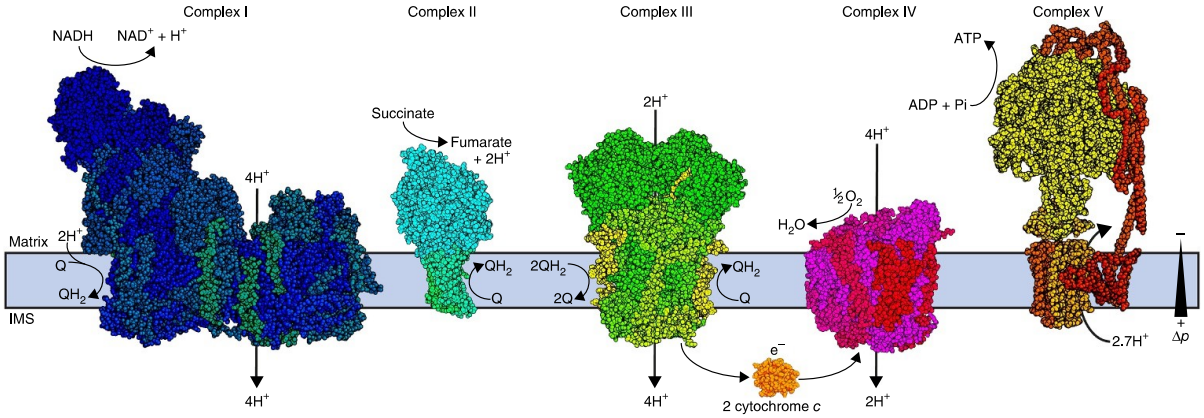

Figure 3.10 Graphical representation of members of the mitochondrial electron transport chain assembled from various species(CI, ovine, CII, porcine, CIII-CV, bovine). The blue rectangle indicates the inner mitochondrial membrane (IMS) that provides the basis for establishment of a proton gradient (Q, ubiquinone, QH_2, ubiquinol). Printed with permission.[126]

To investigate if and how ClpP changes its substrate scope with elevated levels of reactive oxygen species, the above-mentioned trapping approach was applied upon triggering ROS-production by the known CI inhibitor rotenone.

Aside from others, rotenone is one of the most well-characterized inhibitors of complex I of the electron transport chain. It is suggested to act by binding to the ubiquinone channel of the ND1 subunit, thus inhibiting the downstream electron transfer from iron-sulfur cluster N2 onto ubiquinone (Q).[161]

In the following, experiments were conducted with mutants SH2 and SH7 in the same manner as described in chapter 3.2.2. Prior to UV-light induced trapping, cells were incubated with 1 µM rotenone for 6 h. Afterwards samples were further processed by HA-antibody-agarose bead mediated enrichment followed by several washing steps to eliminate unspecifically bound proteins. Peptide samples from tryptic digestion were further desalted and subjected to mass spectrometry analysis. Statistical evaluation was performed by two-sample student's *t*-test with UV-treated samples and untreated samples as single negative control (n = 3). Results were visualized by plotting enrichment factors against significance of enrichment for each mutant. Cut-off criteria for enriched proteins were defined as $\log_2 = 1$ (2-fold enrichment over UV-untreated samples) for enrichment with p-values higher than $-\log_{10} = 1.3$.

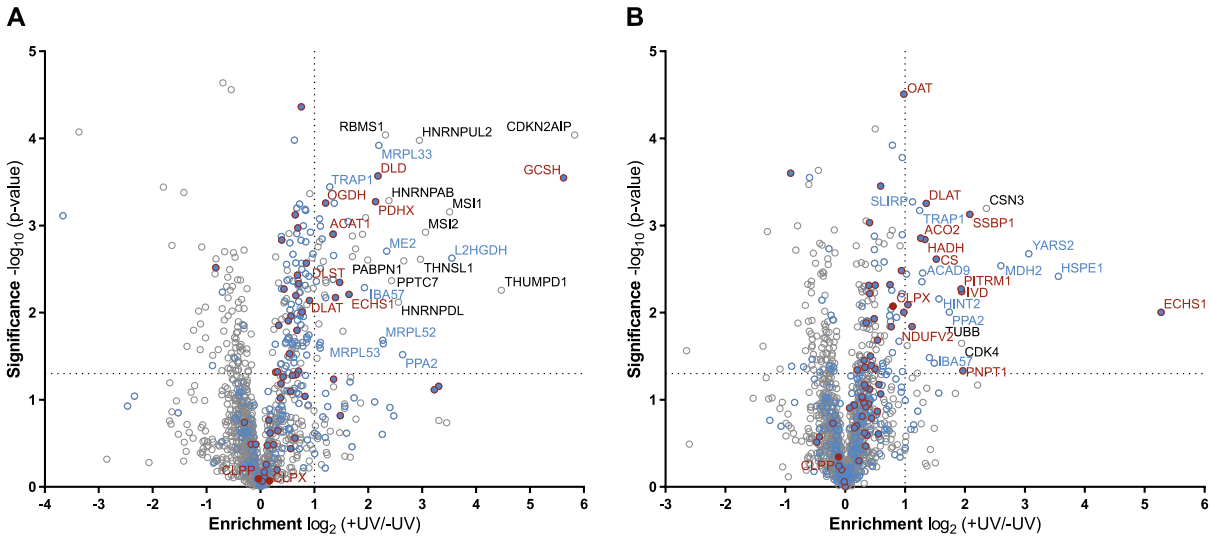

Figure 3.11 Graphical representation of trapping experiments with ClpP mutant A) SH2 and B) SH7. Enrichment factors are plotted against significance of enrichment. Graphs represent data from three technical replicates for each state. Two sample student's *t*-test was conducted by comparison of UV-treated group with UV-untreated as single control group. False discovery rate was determined by Benjamini-Hochberg procedure setting correction to 0.05. Cut-off lines were set at a minimum $\log_2$ change of 1 with a minimum p-value of 0.05. Proteins that are annotated as members of mitochondrial compartment are colored in blue. Proteins colored in red indicate known ClpP substrates or interactors.

Quality control of trapping experiments with mutant SH2 and SH7 revealed that the bait protein ClpP was not enriched and that a high proportion of enriched proteins are linked to mitochondrial origin. From this promising starting point, enriched proteins were compared to results from trapping experiments without rotenone treatment. For rotenone treated mutant SH2, 56 proteins showed an enrichment of 2-fold or higher. Of these, 18 proteins were uniquely found in the rotenone treated SH2 variant. For rotenone treated SH7 mutant, 28 proteins were enriched with 10 uniquely found in rotenone treated samples. (Appendix, Table 8.8, Table 8.9).

Among the putative new substrates of ClpP mutant SH2, 11 proteins are annotated as members of mitochondria (Figure 3.12). These include various mitoribosomal subunits of which MRPL18 and MRPL54 were already annotated as putative ClpP substrates or interactors. Proteins HSD17B10

and TRMT10C, or MRPP2 and MRPP1, respectively, constitute together with MRPP3 the mitochondrial ribonuclease P complex that cleaves tRNA molecules at their 5'-ends.[162] Protein BCKDHA is involved in the catabolism of branched-chain amino acids and in this function forms a complex with DLD, another known ClpP substrate/interactor.[163] PPTC7 and IBA57 are both involved in the maturation of ETC subunits. The protein phosphatase PTC7 regulates biosynthesis of coenzyme Q_{10}[164], while IBA57 forms complexes with members of the iron-sulfur cluster assembly machinery (ISC) to promote maturation of [4Fe-4S]-cluster containing proteins.[165,166]The latter is of particular interest as it was previously shown that ClpXP degrades members of ETC complex I which contain multiple iron-sulfur cluster for electron transfer.

Trapping with ClpP mutant SH7 only exhibits three proteins that were enriched over the non-treated mutant. Among these IBA57 was also found in mutant SH2 corroborating this target as putative ClpP substrate. The histidine triad nucleotide binding protein 2 shows acyl-AMP hydrolase and phosphoramidase activity.[167] Protein NDUFV2 is a member of the peripheral arm of complex I in the electron transport chain containing the flavin mononucleotide (FMN) cofactor site as well as five iron-sulfur cluster. Due to its function as primary entry gate for electron transfer, NDUFV2 and neighboring proteins NDUFS1 and NDUFV1 are susceptible sites for ROS production. Only recently, it could be shown that these proteins are rapidly exchanged and degraded by ClpXP when CI is stalled by dysfunctional N-modules.[140]

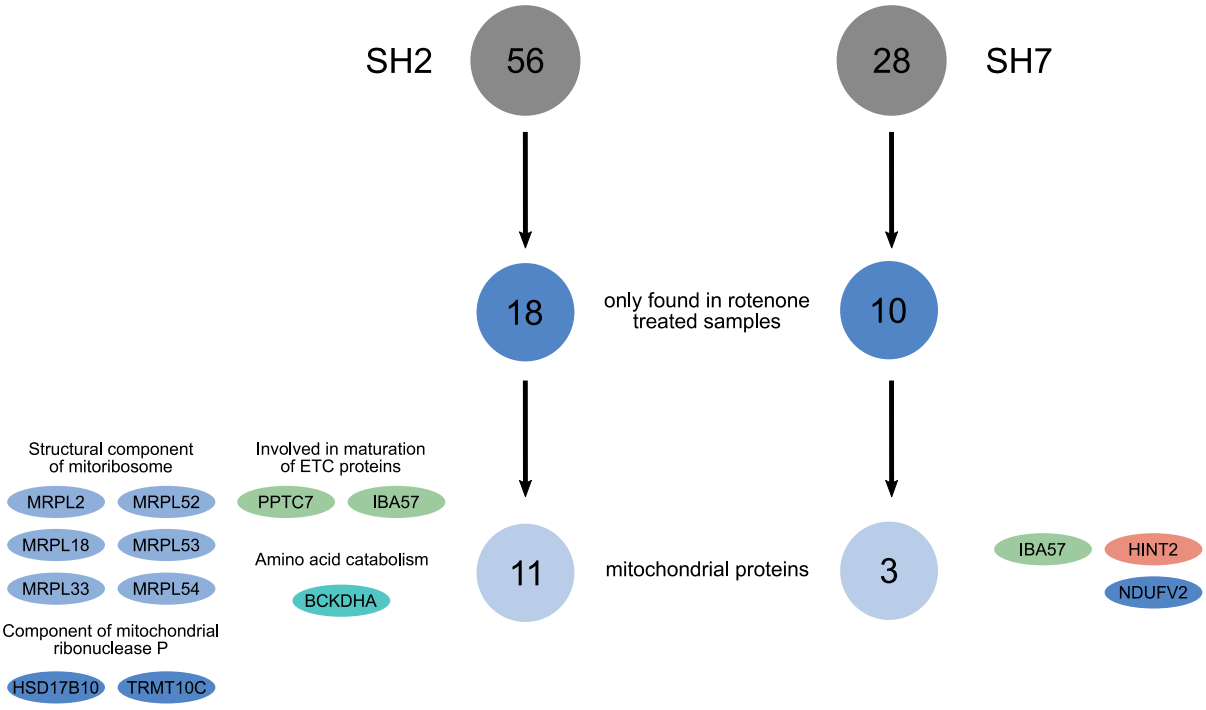

Figure 3.12 Flowchart representing results from trapping experiments with ClpP mutants SH2 and SH7 in rotenone treated Hek293T cells.

In summary, several putative new substrates of ClpXP could be identified after rotenone induced ROS-generation using photocrosslinking ClpP mutants. Of great interest, protein NDUFV2, a member of the electron transport chain could be significantly enriched, however only by mutant SH7 that bears the photocrosslinking on the outside of the proteolytic barrel and thus can also trap mere interactors of ClpP that are not necessarily substrates. The fact that protein IBA57 could be found by both ClpP mutants strengthens the assumption that ClpXP is also involved in a regulatory function of maturation of iron-sulfur cluster containing proteins.

3.3 Conclusion and outlook

Recently, various novel approaches have accounted for a steady increase in the number of putative ClpXP substrates and interactors. While the first technique made use of catalytically inactive ClpP mutants[135], further attempts using whole proteome analysis with ClpP knockout cells[139,140,168–170], proximity labeling of interactors and substrates[138,158] and manipulation of ClpP by overactivation[20,40] led to a surge of potential new substrates and interactors.

In this chapter, a novel complementary approach using ClpP mutants harboring an artificial amino acid with a photoactivatable crosslinking moiety was introduced. The site-specific introduction of unnatural amino acid N^6-((2-(3-methyl-3*H*-diazirin-3-yl)ethoxy) carbonyl)-L-lysine at seven different positions by amber codon suppression resulted in ClpP mutants that successfully established tetradecameric complexes. Except for mutants SH3 and SH4, bearing the mutation site in a fragile part of the ClpP monomer, all ClpP variants showed proteolytic activity. When applied in *in situ* trapping experiments in Hek293T cells, mutants exhibited variable efficiency to trap proteins presented to the protease.

Altogether 182 proteins could be identified by seven ClpP mutants of which 86 were already annotated by other trapping techniques, corroborating the validity of our approach. A substantial number of proteins were annotated as members of mitochondria and of these 33 proteins could be classified as potential new ClpP substrates.

With the introduction of a mutant that carries the photocrosslinking moiety on the outside of the barrel-shaped protease it is further possible to identify proteins that merely interact with ClpP. Interestingly, this mutant exhibited the highest number of enriched proteins, exemplifying the importance of ClpP in a multitude of pathways.

Further experiments revealed an altered substrate scope of ClpP when rotenone-induced ROS-generation is elevated. Here, a member of the iron-sulfur cluster assembly could be identified as well as the known substrate NDUFV2.

Further experiments need to be conducted to confirm the identified proteins as ClpP substrates. For this, western blotting or selected reaction monitoring-based proteomics represent suitable orthogonal techniques.

4

Identification of substrates of *S. aureus* ClpP

Contributions

TFG conducted all synthetical and biochemical experiments. Proteins SaClpP and SaClpX were graciously provided by Barbara Eyermann.

4 Identification of substrates of SaClpP

4.1 Introduction

Humans are inhabited by an estimated number of $3.9 \cdot 10^{13}$ bacterial cells that mostly coexist peacefully next to their eukaryotic neighbors.[2] A great share of these permanent companions reside in the gastrointestinal tract but also cover the skin and occupy the saliva, mucosa and conjunctiva.[1] Especially in the intestinal mucosa they thrive in commensal or mutualistic relationship by executing protective and structural functions or by providing the host with nutrients and short-chain fatty acids which positively affect differentiation and proliferation of intestinal epithelial cells.[171] Some species however have the ability to cause life-threatening diseases when they reach a certain quorum or have otherwise the chance to evade the host immune system. For this, pathogens have evolved a plethora of strategies to circumvent the natural boundaries in order to colonize the host. Some are capable of perceiving the number of congeners by a system called quorum sensing to initiate an orchestrated attack by simultaneously expressing virulence factors.[172,173] Others excrete proteins that aid in adhesion to tissue and blood cells or actively damage cell tissue.[174] Great attempts have been conducted to overcome microbial infections initiated by the serendipitous discovery of penicillin in 1928 by Sir Alexander Fleming.[175] The golden era of antimicrobial discovery in the 1950s has long since passed and more and more so far treatable infections have become a substantial peril. This is essentially due to the extensive underuse, overuse and misuse of antimicrobials.[176] Bacteria face a constant flood of antimicrobials which eliminate most pathogens, however those who are able to endure develop resistances. The constant selection pressure favors survival of bacteria with mutations leading to structural variation of the antibiotic targets or minimization of the amount of drug by metabolism or active efflux and reduced uptake.[177] A major task for fundamental research and pharmaceutical companies therefore lies in the development of novel effective strategies to overcome bacterial resistance formation.

4.2 Virulence association in Staphylococcus aureus

One major protagonist of nosocomial infections is the gram-positive bacterium *Staphylococcus aureus* (*S. aureus*) which was first identified 1880 by Sir Alexander Ogston in pus of infected wounds and named because of its physical appearance after the greek term *staphylé* meaning a "bunch of grapes".[178,179] Further investigated by Friedrich Rosenbach in 1884 the microbe was ultimately termed after the golden appearance of isolated cultures.[180] 30% of all humans persistently carry *S. aureus* in their nasopharynx or other parts of the body tolerating their existence without suffering from symptoms. However, when the peaceful balance is disturbed invasive infections can arise.

These can range from mild skin infections to life-threatening diseases like pneumonia, sepsis or infective endocarditis to name a few.[179]

Pathogenicity of *S. aureus* is considered to be organized by a substantial number of secreted proteins and cell-surface anchored proteins. These greatly differ in their expression level dependent on the growth phase. Exoproteins are produced especially in the post-exponential phase while surface-anchored proteins are generated substantially in the exponential phase.[181] Examples for secreted proteins are the hemolysins α, *β* and *γ* which specifically affect blood cells. Hemolysin α (hla/hly) is a hollow barrel shaped protein that forms pores in lysosomes and erythrocytes causing leakage of cytosolic contents and ultimately leading to lysis and demise of the affected cell.[182] The beta-form (hlb) exhibits phospholipase C activity provoking sphingomyelin degradation of the erythrocyte membrane eventually leading to cell lysis.[183] The *γ*-form (hlgAB, hlgCB) belongs to yet another family called bicomponent pore forming toxins (PFT) or leukocidins for their preference to target leukocytes.[184] They share key structural and mechanistic features with α-hemolysin but comprise two structural components HlgA or HlgC and HlgB that successively engage and oligomerize in the cellular membrane.[185–187] Further leukocidins are known (LukSF-PV, LukED, LukAB, LukMF', LukPQ) which are associated with infections in various sepecies.[184,188–190]

Further examples for extracellular toxins are secreted proteases (exfoliative toxins ETA, ETB, ETC and ETD), lipases (SAL1, SAL2)[191] and phospholipase PI-PLC[192], coagulases and staphylokinase.

Exfoliative toxins are responsible for staphylococcal scalded skin syndrome (SSSS) by selectively cleaving the glutamate-glycine bond in protein desmoglein 1 which is required for the cell-to-cell adhesion.[193,194] Lipases generally hydrolyze extracellular lipids and have been shown to contribute to biofilm formation in a murine infection model, however their exact function in pathogenicity is still unclear.[195] The coagulases Coa and von Willebrand factor binding protein (vWbp) are non-enzymatic proteins that bind to prothrombin forming staphylothrombin. This leads to the activation of the zymogen which in the end is highly active in converting fibrinogen to fibrin.[196,197] The following coagulation of host blood plasma helps *S. aureus* to build a protective shield of eosinophilic pseudocapsules to evade host immune cells in abscesses.[174] In contrast, staphylokinase binds to plasmin which activates plasminogen inducing breakdown of fibrin clots facilitating bacterial dissemination.[184,198]

Another class of toxins produced by *S. aureus* strains are the so-called superantigens which can further be classified into T-cell and B-cell superantigens. The T-cell superantigens (SAg) again are grouped in staphylococcal enterotoxins (SE), staphylococcal enterotoxin-like (SE-*l*) superantigens and toxic shock syndrome toxin-1 (TSST-1) which express unique stability features towards heat, proteolysis or dessication.[199] SAgs manipulate the host immune system by crosslinking the V*β* T-cell receptor (TCR) on a T-cell with the major histocompatibility complex (MHC) class II of an antigen-

presenting cell (APC) resulting in activation of T-cell proliferation.[184,200] Eventually this can lead to a massive release of cytokines resulting in toxic shock syndrome and lethal shock.[201]

The only known example for B-cell superantigens is represented by staphylococcal protein A (spA). This protein subverts the innate immune system of the host by binding the Fc domain of immunoglobulins thus disrupting opsonization and impeding phagocytosis.[202] Furthermore it acts as a natural B-cell toxin inducing caspase-dependent apoptosis.[203]

Further proteins that are displayed on the cell surface are accumulated under the term MSCRAMM (microbial surface components recognizing adhesive matrix molecules) and can be divided into two groups. Those that are related to the clumping factor A (ClfA) and those that share similarity with the Collagen-binding protein family (Cna) of *S. aureus*. They all share the common motif to bind to the extracellular matrix of the host. They bind either by docking, locking and latching to fibrinogen (dock-lock-latch, DLL) or by binding to collagen *via* the collagen-hug (CH).[204]

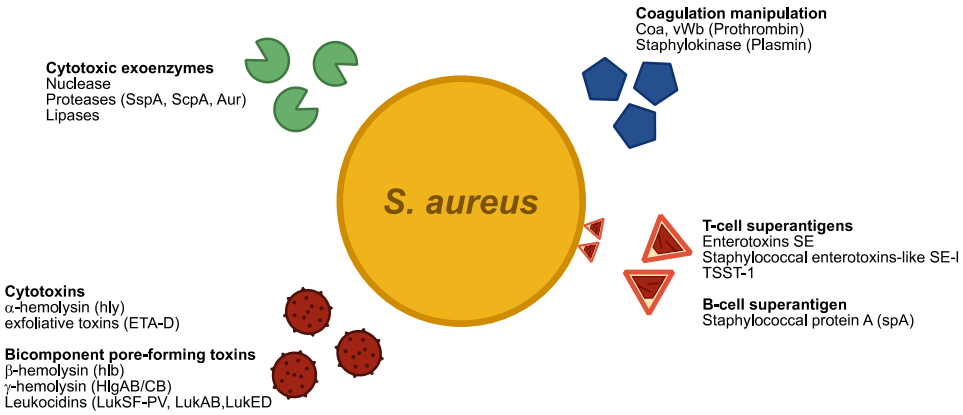

Figure 4.1 Overview of selected virulence factors expressed by *S. aureus* strains.

The list of enzymes and proteins mentioned above stand exemplary for the extensive repertoire developed by *S. aureus* in order to colonize, exploit and harm a host organism and represent only a glimpse of this pathogen's arsenal. To capture virulence associated proteins of *S. aureus* in its entirety various review articles are recommended.[184,187,199,204]

Virulence factors are largely controlled by regulators which initiate and adapt their expression depending on cell density and diverse microenvironments.[205] Examples include sae (*S. aureus* exoprotein expression) which regulates the expression of α and *β*-hemolysins, DNase and coagulase while simultaneously not interfering with production of proteases, lipase, staphylokinase, or enterotoxin A.[206] The two component system (TCS) srrA-srrB (staphylococcal respiratory response A and B) is considered to repress virulence factor expression under low-oxygen conditions while disruption of *srrB* results in increased levels of RNAIII, a major regulator for expression of exoproteins and cell wall associated proteins.[207] Another TCS arlR-arlS (autolysis-related locus R and S) represses the production of various secreted proteins (α and *β*-hemolysin, lipases, coagulases,

serine protease ssp and protein A) by downregulating the transcription of the corresponding genes while at the same time being regulated by the two global regulators agr and sarA.[208] The importance of the *agr* system (accessory gene regulator) as a controlling entity must be emphasized since it is linked to the regulation of more than 70 genes including 23 virulence factors.[172,209,210] It is composed of four proteins AgrA, AgrB, AgrC and AgrD which are encoded on transcript RNAII whose transcription is modulated by promoter P2. Two of these proteins, AgrA and AgrC, form a two component system functioning as sensor and regulator proteins.[211] AgrD contains the so-called auto-inducing protein (AIP) sequence and forms a propeptide that is processed by membrane bound AgrB to generate the mature AIP.[210] AIPs again are secreted and can be sensed by surrounding bacteria population by a process called quorum sensing.[212] When a certain quorum of bacteria is reached AIP bind to the surface bound AgrC which in turn undergoes autophosphorylation and activates response regulator AgrA.[211] Trans-autophosphorylation of AgrC and subsequent phosphorylation of AgrA is a widely accepted assumption but an ultimate proof has to be adduced.[210] The phosphorylated AgrA eventually induces transcription by binding to promoter P2 thus closing the positive feedback loop in the *agr* system (Figure 4.2).

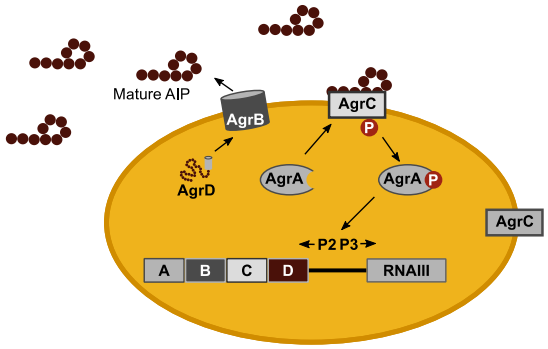

Figure 4.2 Schematic representation of accessory gene regulator (agr) feedback loop. Adapted from *George et al.*[210].

AgrA concomitantly binds to the P3 promoter inducing transcription of RNAIII. This multifunctional regulator impacts the stability and translation of mRNAs encoding a plurality of virulence factors.[213,214] By cleaving the mRNA of repressor of toxins (Rot) and therefore regulating the translation of Rot RNAIII exerts major influence on expression of toxins like *tst* and *sed*.[214,215] Besides its function as regulator RNAIII itself also encodes for protein δ-hemolysin (hld) a member of the so-called phenol-soluble modulins (PSM) which exhibits amphipathic properties providing it with the ability to lyse cells similar to detergent.[216–218]

Another layer of regulating function is created by the protease ClpXP which is proposed to play a pivotal role in regulating the expression of genes that encode for proteins involved in pathogenicity. This includes factors associated with virulence, stress response and overall physiology of *S. aureus*.[181,219,220] Studies on ClpP and ClpX deletion models suggest the regulation of virulence

factor production by *agr* signaling.[181,214] Selective chemical inhibition of ClpXP by *β*-lactones showed downregulation of *δ*-hemolysin and AgrC, both connected to the two-component signaling pathway that activates RNAIII transcription. α-Toxin and its corresponding transcriptional regulators SarR and AgrA were also down-regulated while the repressor of toxins Rot was up-regulated, consolidating the role of ClpP in virulence factor expression.[212] Although a direct evidence of Rot being a substrate of ClpXP still needs to be illustrated, these findings already claim a principle role of ClpXP in virulence factor control and propose *β*-lactones as a way to subvert them.

β-lactones are selective ClpP-inhibitors

Initially *trans-β*-lactones were found to target a variety of proteins in non-pathogenic *Listeria welshimeri* and *Bacillus subtilis*[221] when in the same year activity-based protein profiling (ABPP) with lipophilic *β*-lactone probes revealed an exceptional selectivity for ClpP in *S. aureus* by binding the active site-serine.[222] The influence of ClpP inhibition on expression of virulence factors was further validated and extended however the inherent tendency to hydrolyze under basic conditions impedes this molecule class from further application as antivirulence agent. As described in chapter 2 an unbiased high-throughput screen was conducted to search the chemical space for new entities that would show 1) high inhibitory potency against ClpP peptidase activity, 2) improved structural stability and integrity and 3) high selectivity in a complex environment.[223] The most active compounds featured a phenyl ester moiety as common motif (Figure 2.2). Among these, compound **AV170** stood out in terms of its ability to not only inhibit ClpP peptidase but also to impair the proteolytic function of ClpXP.[223] To investigate target engagement in the environment of a bacterial cell modification of **AV170** with a propargyl ether gave compound **ML16** which was applied in an ABPP approach to prove ClpP as a unique target in *S. aureus*.[223] Further modification of the parent compound revealed a unique mode of action. Depending on the configuration of the methyl-substituent in compounds **ML90** and **ML89** either full modification and inhibition of the tetradecamer or de-oligomerization into heptameric rings occurred.

ClpP in its nature as peptidase is able to cleave small peptides. Therefore, *Lakemeyer et al.* refined the structures of **ML89**/**ML90** which inherently share amino acid-like features to eventually receive dipeptide mimics. These N-Boc-capped dipeptide phenyl esters showed inhibitory activity in a GFP-degradation assay with ClpXP when the residue facing the S1 pocket exhibits a spacious aromatic ring system like the Tmo-group of the parent compound or the indol scaffold of tryptophan. The S2-pocket permitted more structural diversity for the second amino acid represented by the consistent inhibitory potency of different residues ranging from hydrophobic scaffolds to polar side chain residues. Surprisingly, three compounds showed a mild to high

enhancement of ClpXP activity while simultaneously presenting modest to good inhibitory potency of ClpP peptidase alone, depending on the buffer system. Analytical size exclusion chromatography showed that activators 34, 49 and 50 locked the ClpXP complex in its $ClpX_{12}P_{14}$ state with ClpX capping the ClpP tetradecamer on both apical sides.[224] The ability to overactivate the ClpXP complex in combination with stabilization of the proteolytically active complex highly qualifies dipeptide phenyl esters as tool for further investigation of ClpP's pathway affiliation and substrate preference.

4.3 State of affairs and scope of this work

This chapter covers the exploration of novel ClpP substrates in the bacterial pathogen *S. aureus* with the help of tailored peptide phenyl esters. These compounds were recently shown to possess an overactivating effect on *in vitro* proteolysis of GFP by ClpXP.[224] The fact that the peptidolytic function of ClpP can be overactivated by small molecules is already known for more than a decade and was first exemplified by the identification of acyldepsipeptides (ADEP).[38] Further studies revealed that ADEPs bind to hydrophobic pockets at the apical sides of ClpP which are naturally occupied by the IGF loops of chaperone ClpX. This induces a conformational change in the N-terminal region of ClpP thus widening the axial pore allowing larger peptides to enter.[225–227] Substrate specificity is lost since chaperones like ClpX compete with ADEPs for the binding site and are thus not able to assort substrates for the peptidase subunit.[228] In contrast to ADEPs, Tmo-based dipeptide phenyl esters bind covalently to the active site serine of ClpP peptidase subunits presumably tightening the association of the ClpXP complex.[224]

Amongst other approaches, substrate proteins of *S. aureus* ClpP have been previously identified by an elegant method that uses inactive serine-to-alanine mutants of ClpP. These mutants retain $ClpX_{12}P_{14}$ complex formation *in vivo* and ClpX-mediated recognition and translocation of substrate proteins into the proteolytic core, however, due to the lack of active site serine substrates are not degraded and can be identified after affinity enrichment *via* LC-MS.[134,229] In this way 70 substrate proteins could be identified of which one third were reported previously to be unstable in presence of ClpP or actual substrates in other organisms. Of note are the transcriptional regulators CtsR and Spx, the ClpC adaptor proteins McsB and MecA as well as the cell division regulator FtsZ. Further proteins that were grouped as putative ClpP substrates include enzymes involved in DNA metabolism and transcription, various chaperones and proteins involved in metabolism and biosynthesis (Figure 4.3).[229]

In this chapter a new strategy will be reported that attempts the discovery of ClpXP substrates by using modified dipeptide phenyl esters to trap proteins presented to the proteolytic machinery. In this regard disadvantages and unintended biases that may arise from expressing an artificial protein in a native environment may be circumvented.

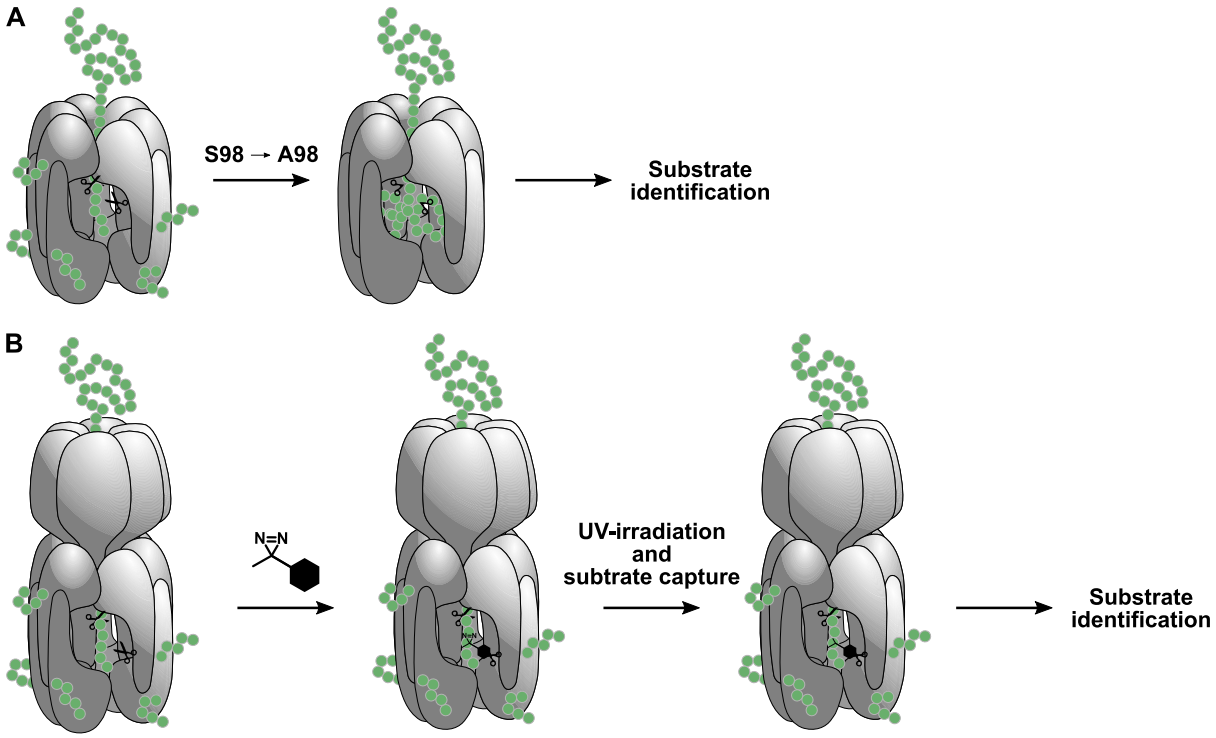

Figure 4.3 Schematic representation of trapping approaches. A) *Frees et al.* reported trapping of substrate proteins using a serine-to-alanine mutant of SaClpP.[229] B) Scope of this work: Incubation of photoactivatable moiety containing phenyl esters with subsequent UV-irradiation should result in capture of ClpP substrates.

4.4 Structural consideration and chemical synthesis

Lakemeyer et al. previously reported overactivating properties of dipeptide phenyl esters on ClpXP which were initially designed to mimic peptides and to inhibit said protease. This unexpected transition of compound characteristics which, in parts, is only attributed to slight structural changes offers the opportunity for exploitation as substrate trapping probes. Boc-protected (*S*)-Met-(*R*)-Tmo-OAr (Activator 34) exhibits moderate overactivation at 10 µM whereas acetylated (*R*)-Tmo phenyl ester (Activator 49) and Boc-(*R*)-Glu(OBn)-(*R*)-Tmo-OAr (activator 50) show increased ClpXP activity to up to 250% at 100 µM and 10 µM, respectively (Figure 4.4). Since overactivation of ClpXP is most pronounced with Boc-(*R*)-Glu(OBn)-(*R*)-Tmo-OAr at low concentrations this scaffold was chosen for transformation into a photoactivatable probe.

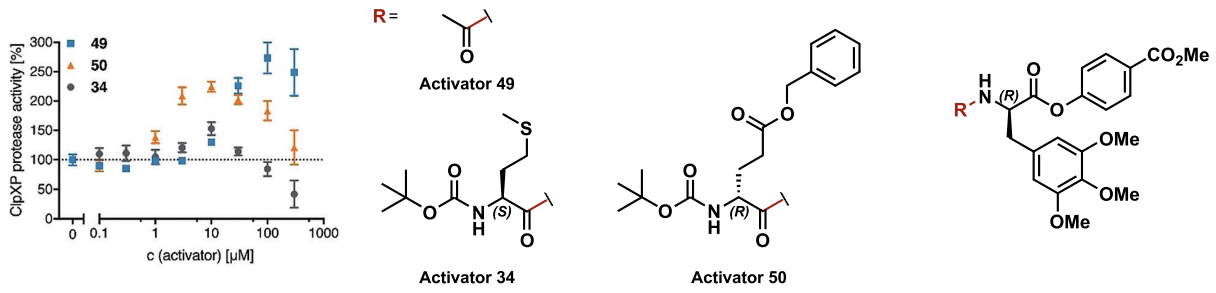

Figure 4.4 Phenyl esters exhibit overactivation in ClpXP-mediated GFP degradation assay. Adapted from *Lakemeyer et al.*[224] with permission.

The structural requirements that are necessary for the development of a photoactivatable probe are 1) the introduction of an alkyne handle for bioorthogonal ligation and 2) insertion of a photoactivatable moiety such as benzophenones, aryl azides or diazrines and 3) a suitable tether that guarantees a sufficient distance to the target protein. Structural evaluation of activator 50 reveals several positions suitable for those modifications (Figure 4.5).

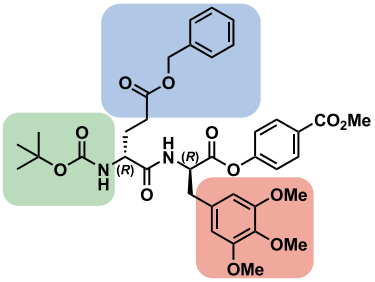

Figure 4.5 Structural features of ClpXP **activator 50**.

The peptide backbone of this compound has to remain unmodified since this structural feature is crucial for binding to ClpP's active site pockets. Likewise, (*R*)/(*R*) configuration of the dipeptide is a prerequisite for the formation of binding affinity to the respective sites of the protein. The phenyl ester moiety provides the warhead for covalent binding to the protein and has to remain unchanged. Moreover, alterations to the phenolic leaving group are only advised if this improves reactivity of the phenyl ester since installation of affinity handles is pointless for a leaving group. This leaves the Tmo-group (3,4,5-trimethoxyalanine), the benzyl protected glutamate and the Boc-protecting group as remaining moieties for modifications. The nature of the N-terminal cap proved to be vital for inhibitory potency of phenyl ester amino acid mimics. Neither amines capped with methyl- nor benzyloxycarbonyl or the structurally very similar pivaloyl-group showed comparable effects on ClpXP protease activity.[224] As both activator 34 and activator 50 exhibit Boc-protected N-termini a short aliphatic residue in form of a propargylic carbamate appears to be a suitable substitute. The Tmo-group features the major interaction with the S1-binding pocket of ClpP. Thus, decoration of this scaffold with a photoreactive group should prove detrimental to the efficacy of photoactivated trapping of substrate proteins. Since the photoactivatable moiety has to be small in size and distant from the bait protein, insertion of an aryl azide or diazirine seems to be most beneficial at the benzyl protecting group of the (*R*)-glutamic acid. Molecules satisfying these parameters are depicted in Figure 4.6.

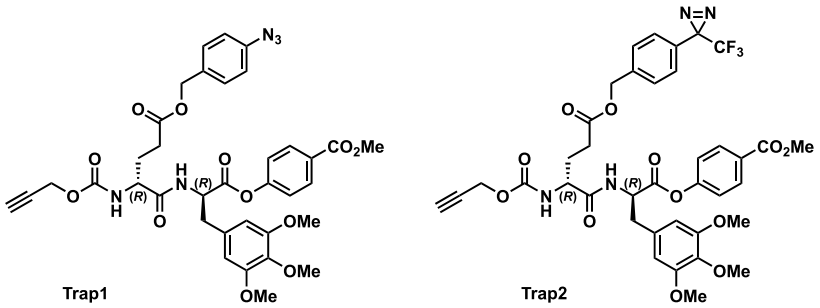

Figure 4.6 Structural representation of phenyl esters equipped with photoactivatable moieties and alkyne-tag for affinity enrichment.

To broaden the application of the photoactivatable dipeptide phenyl ester probe molecules with two different photoreactive moieties were synthesized. In both probes the eastern part is based on the same (*R*)-configured amino acid. Synthesis of this part of the molecule was performed as described previously (Figure 4.7).[224] Starting from 3,4,5-trimethoxybenzaldhyde *Erlenmeyer-Plöchl* synthesis with N-acetyl glycine yielded the oxazolidinone **41** which underwent ring opening by stirring with sodium acetate in methanol. Palladium catalyzed hydrogenation of the double bond gave the *N*-acetyl and methyl ester protected substituted phenylalanine **43** as a racemic mixture. For further synthesis only the (*R*)-configured amino acid was required. Therefore, kinetic resolution with protease Subtilisin A from *Bacillus licheniformis* (Alcalase®, *Sigma Aldrich*) was used to separate the (*R*)-configured enantiomer as the corresponding methyl ester **44**. Deprotection of the amine following reprotection using Boc-anhydride and subsequent deprotection of the methyl ester with aqueous lithium hydroxide was feasible in a one-pot reaction to give Boc-protected amino acid **45**. Esterification with methyl 4-hydroxybenzoate mediated by 1-ethyl-3-(3-dimethylaminopropyl)-carbodiimide (EDCI) and hydroxybenzotriazole (HOBt) yielded phenyl ester **46**. For further solution-phase peptide synthesis phenyl ester **46** was deprotected using an excess of trifluoroacetic acid (TFA) to give amine **47** as the corresponding TFA-salt.

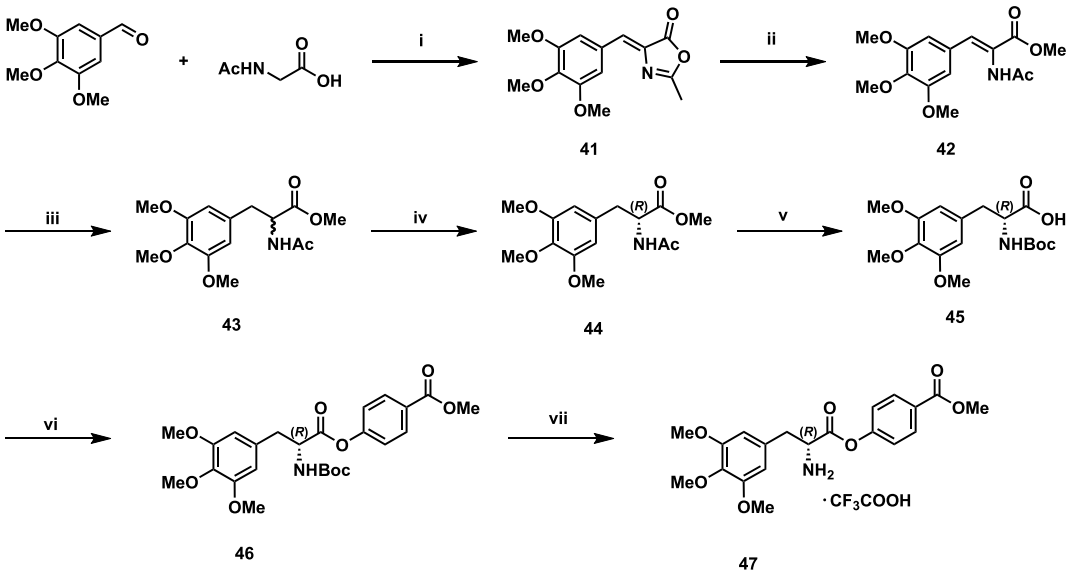

Figure 4.7 Synthesis of eastern fragment of **Trap1** and **Trap2** as described previously.[224] i) NaOAc (1.00 eq.), Ac_2O (1.00 eq.), 60 °C, 5 h, 61%; ii) NaOAc (2.00 eq.), MeOH, RT, 4 h, 89%; iii) Pd/C (10% Pd loading, 3 mol-%), H_2, MeOH, RT, 7 d, 96%; iv) Alcalase® (>2.4 U/g), 0.2 M $NaHCO_3$ buffer, pH = 8.4, 37 °C, 2 h, (R)-**44**-COOMe 47%; (S)-**44**-COOH 47%; v) 1.) DMAP (0.20 eq.), Boc_2O (2.00 eq.), THF, 75 °C, 3 h, 2.) 2 M $LiOH_{aq}$, THF/H_2O (5:4), RT, 5 h, 65% over two steps; vi) 4-methyl hydroxybenzoate (1.05 eq.), EDCI (1.05 eq.), HOBt (1.50 eq.), DIPEA (2.00 eq.), DCM, RT, 19 h, 51%; vii) TFA (9.70 eq.), DCM, 0 °C →RT, 5 h, 97%.

Synthesis of the western part (Figure 4.7) started by protection of the benzylated and *N*-Boc-protected D-glutamate with EDCI, dimethylaminopyridine (DMAP) and *tert*-butanol to give fully protected D-glutamate **49**.[230] Reductive deprotection of the benzyl ester was performed with palladium on charcoal under hydrogen atmosphere.[231] The benzyl alcohol **48** containing the photoreactive azide in *para*-position was synthesized in a single step from 4-amino benzyl alcohol by first diazotization of the amine following displacement with sodium azide.[232] Afterwards, esterification with benzyl alcohol **48** gave benzyl ester **51**[233] which was further deprotected with excess TFA to yield amine **52**. It is worth noticing that deprotection of the Boc-protected amine with TFA also resulted in deprotection of the *t*-butyl ester, however only to a minor degree. Exploiting this side reaction would shorten the synthesis towards the *N*-propargylated D-glutamate, however decomposition of the benzyl ester was also detected vitiating the advantage of this route. Formation of the propargyl carbamate **53** was achieved by reacting the amine with propargyl chloroformate in presence of sodium bicarbonate.[234] Deprotection of the *tert*-butyl ester with excess TFA was accompanied with decomposition of the propargyl carbamate, however sufficient amounts of carboxylic acid **54** could be isolated. To complete synthesis of **Trap1**, solution-phase peptide coupling with [(1-Cyano-2-ethoxy-2-oxoethylidenaminooxy)dimethylamino-morpholino-carbenium-hexafluorophosphat] (COMU) as coupling agent was conducted.

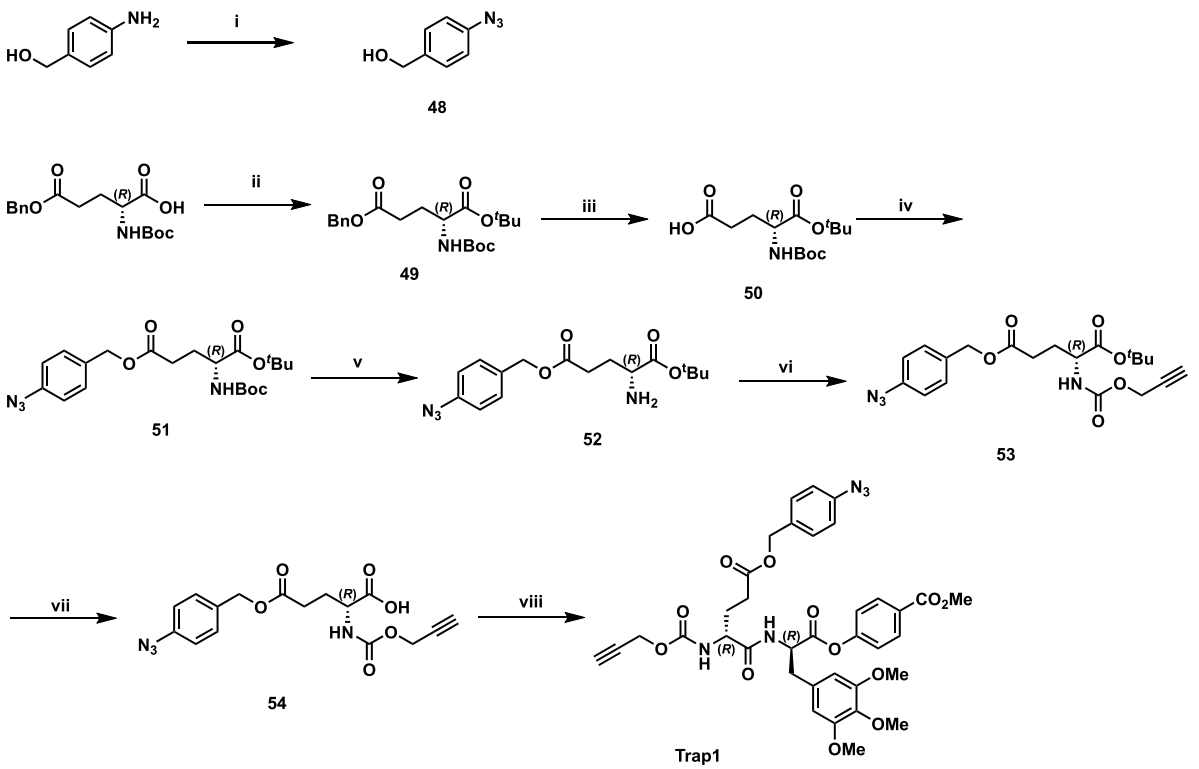

Figure 4.8 Synthesis of the western part resulting in **Trap1**. i) 2 M $H_2SO_{4(aq)}$, $NaNO_2$ (1.50 eq.), NaN_3 (1.50 eq.), 0 °C, 15 min, 97%; ii) *t*-BuOH (5.07 eq.), EDCI (1.00 eq.), DMAP (0.05 eq.), DCM, 0 °C, 1 h then RT, 22 h, 36%; iii) Pd/C (10% Pd-loading, 7 mol-%), H_2, MeOH, RT, 20 h, >99%; iv) (4-azidophenyl)methanol **48** (1.00 eq.), EDCI (2.00 eq.), DMAP (0.50 eq.), DCM, RT, 21 h, 77%; v) TFA (9.70 eq.), DCM, 0 °C → RT, 6 h, 54%; vi) $NaHCO_3$ (2.98 eq.), propargyl chloroformate (2.10 eq.), DCM, 0 °C, 2.5 h then RT, 3 h. 67%; vii) TFA (9.70 eq.), DCM, 0 °C, 4 h, 22%; viii) amine **47** (Figure 4.7, 1.00 eq.), **54** (1.10 eq.), COMU (1.10 eq.), DIPEA (2.00 eq.), DMF, 0 °C, 22 h, 23%.

Synthesis of **Trap2** overall followed the same route as synthesis of **Trap1** with the exception that first the benzyl protecting group on the side chain carboxylic acid of D-glutamate had to be implemented (Figure 4.9). For this, synthesis started from 4-bromo benzyl alcohol with protection of the hydroxyl group with *tert*-butyldimethylsilyl chloride under basic conditions in the presence of imidazol.[235] Lithium-halogen exchange with *n*-butyl lithium (*n*-BuLi) at -78 °C followed by addition of methyl trifluoroacetate resulted in trifluoroacetated silylether **56**.[236] This was further converted to the stereoisomeric (E/Z) mixture of oximes **57** by reaction with hydroxyl amine in the presence of excess pyridine in ethanol. Yields didn't meet the expectations but might be improved by rigorously drying ethanol and pyridine beforehand. However, yields were sufficient to proceed with the synthesis. Oximes **57** were converted to the tosyl-oximes **58** using *para*-toluenesulfonyl chloride in presence of triethylamine with catalytic amounts of DMAP[236] before cyclization with ammonia gave diaziridine **59**. In contrast to the literature[237] the cyclisation reaction was conducted with 7 M ammonia in methanol. Oxidation of the diaziridine to the diazirine **60** was accomplished with iodine in a basic solution of triethylamine in methanol. Following deprotection of silyl ether **60** with tetra-*n*-butylammonium fluoride gave benzyl alcohol **61**[238] which was esterified with *N*-Boc protected D-glutamic acid *t*-butyl ester **50** as described above. In accordance with the synthetic procedure detailed above benzyl ester **62** was further deprotected with TFA, reacted with

propargyl chloroformate in presence of sodium bicarbonate and *t*-butyl ester was deprotected again by using excess amounts of TFA. Lyophilization gave the starting material for the final peptide coupling with compound **47** resulting in the formation of **Trap2**.

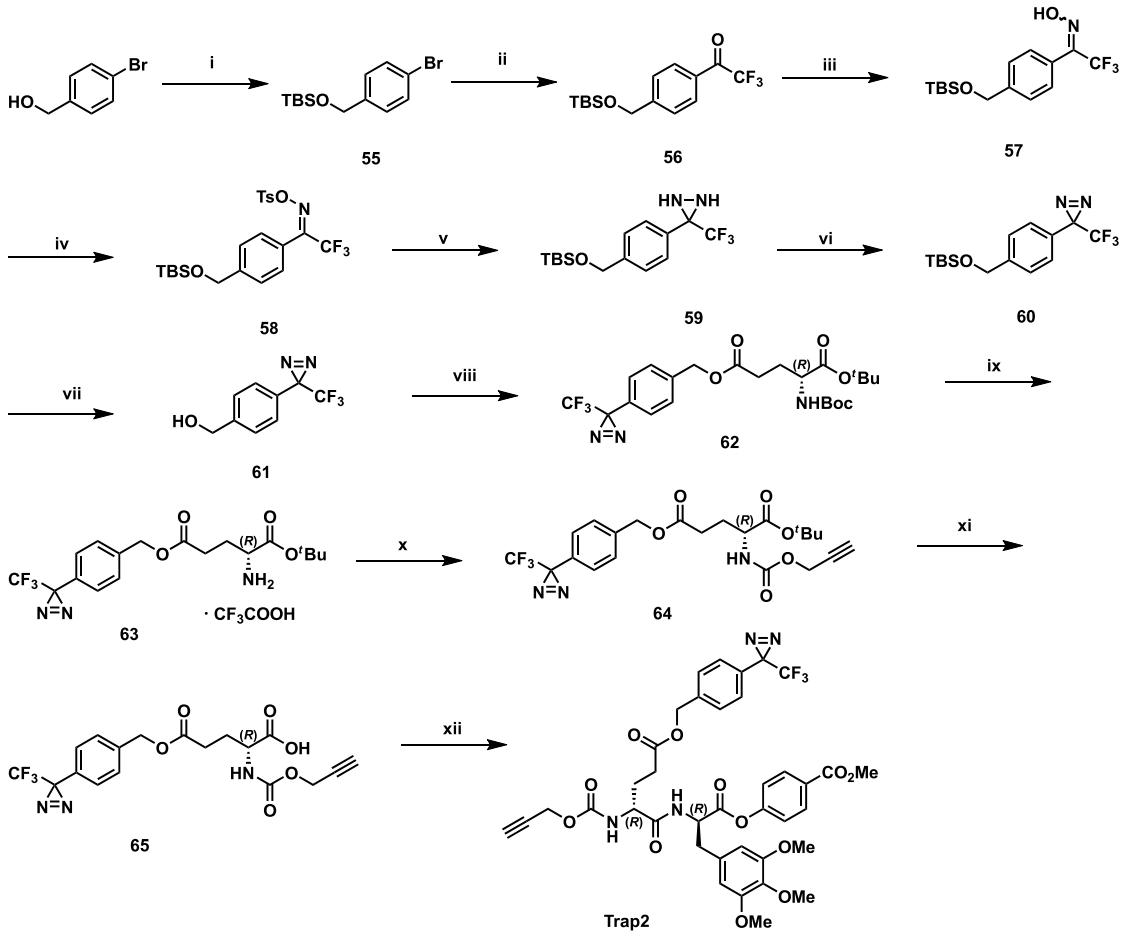

Figure 4.9 Synthesis of western fragment of compound **Trap2**. i) TBDMSCl (1.10 eq.), imidazole (2.00 eq.), DCM, RT, 21 h, >99%; ii) *n*-BuLi (1.20 eq.), CF_3CO_2Me (1.20 eq.), THF, -78 °C, 3.5 h, 92%; iii) $NH_2OH \cdot HCl$ (1.10 eq.), pyridine/EtOH (2:1), 80 °C, 19 h, 37%; iv) NEt_3 (1.30 eq.), DMAP (0.09 eq.), *p*-TsCl (1.20 eq.), DCM, 0 °C → RT, 2 h, 81%; v) NH_3 (7 M in MeOH, 64.9 eq.), 52%; vi) NEt_3 (1.66 eq.), I_2 (1.33 eq.), MeOH, RT, 4.5 h, 79%; vii) TBAF (1.20 eq.), THF, RT, 1 h, 90%; viii) D-glutamate **50** (1.00 eq.), benzyl alcohol **61** (1.20 eq.), EDCI (2.00 eq.), DMAP (0.50 eq.), DCM, RT, 21.5 h, 69%; ix) TFA (9.70 eq.), DCM, 0 °C, 5 h, then RT, 1 h, 58%; x) $NaHCO_3$ (2.98 eq.), propargyl chloroformate (3.05 eq.), DCM, 0 °C, then RT, 7 h, 89%; xi) TFA (9.70 eq.), DCM, 0 °C, 7.5 h, 84%, xii) amine **47** (Figure 4.7, 1.00 eq.), **65** (1.10 eq.), COMU (1.10 eq.), DIPEA (2.00 eq.), DMF, 0 °C → RT, 21 h, 57%.

4.5 Biochemical investigations

4.5.1 Influence of Trap1 and Trap2 on proteolytic activity of SaClpP

Phenyl esters were previously shown to be potent inhibitors of bacterial peptidase ClpP and are considered second generation inhibitors with *trans*-β-lactones being the previous gold standard.[221,223] As described in chapter 2 the covalent modification of phenyl esters is proposed to undergo a nucleophilic attack by the active site serine leading to the *para*-substituted phenol leaving the molecule. The geometry and aromatic nature of the acid moiety was suggested to be etiological for the binding to the S1 binding pocket.[223]

The ability of **Trap1** and **Trap2** to covalently bind and inhibit peptidase activity of ClpP was investigated by measuring the residual proteolytic activity of ClpP upon incubation with phenyl esters. For this, the probes were assessed in an assay similar to the one described in chapter 2 with Ac-Ala-hArg-(*S*)-2-aminooctanoic acid-7-amino-4-carbamoylmethylcoumarin (Ac-Ala-hArg-(*S*)-Aoc-ACC) as the fluorogenic substrate. Experiments were conducted in different buffer systems with PZ-buffer containing dithiothreitol (DTT), glycerol and Mg^{2+} apart from HEPES and KCl. EP-buffer only contained buffering agent HEPES and KCl. In accordance with literature[224] ClpP activity is enhanced in protease buffer (PZ) versus minimal buffer (EP) as depicted in Figure 4.10B. It was also reported that several phenyl esters showed elevated inhibitory potency when tested in EP-buffer compared to PZ-buffer. This effect can be observed when ClpP is incubated with **Trap1** which led to a concentration dependent decrease of ClpP activity that was more pronounced in EP-buffer than in PZ-buffer. Incubation with **Trap2** resulted in only minor inhibition and a negligible buffer effect. Overall both compounds represent only poor inhibitors of SaClpP (Figure 4.10A).

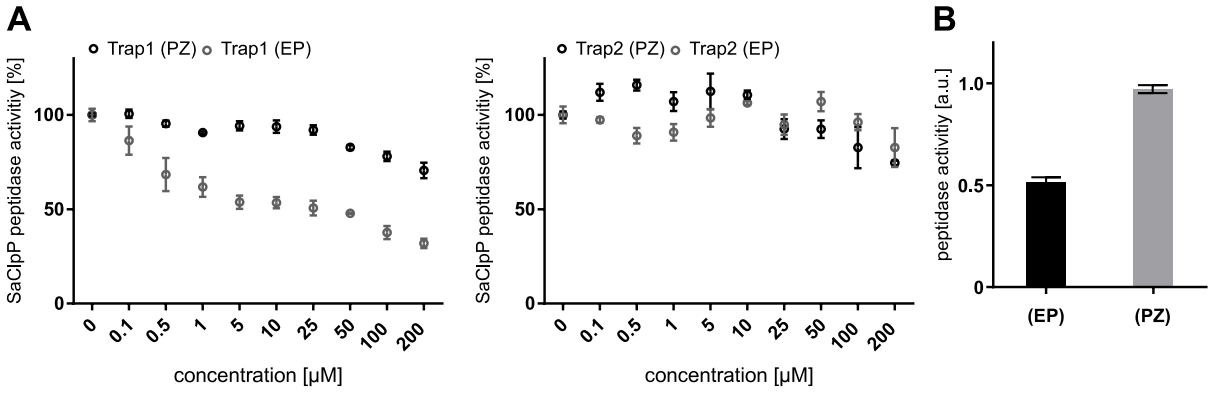

Figure 4.10 A) Results from SaClpP peptidase activity assays ($SaClpP_{monomer}$ concentration 140 nM, fluorogenic substrate: Ac-Ala-hArg-(*S*)-Aoc-ACC, 200 µM, 32 °C) with **Trap1** and **Trap2**. Each data set represents three technical replicates (mean ± SD). B) SaClpP activity is enhanced in protease buffer (PZ) compared to minimal buffer (EP).

On its own, ClpP can only degrade small peptides like the ones used in the peptidase assay, mentioned above.[239] However, *in situ* ClpP usually teams up with a chaperone of the AAA+

superfamily which fulfills functions such as recognition, unfolding and translocation of substrate proteins. As described in chapter 2, GFP-degradation assay can be utilized to investigate residual protease activity upon phenyl ester treatment. Previous phenyl ester based peptide mimics showed unexpected divergence in inhibitory potency ranging from full inhibition at concentrations as low as 1 μM to overactivating features at varying concentrations.[224] For application in substrate trapping experiments **Trap1** and **Trap2** were therefore designed to exhibit stimulating effects on ClpXP protease.

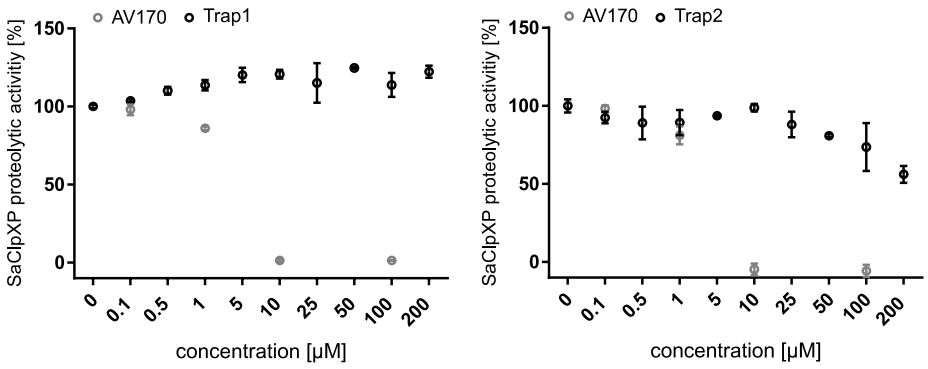

Figure 4.11 Results from SaClpXP protease assay conducted with phenyl esters **Trap1** and **Trap2** (0.2 μM SaClpP in the presence of 0.4 μM SaClpX and 0.4 μM eGFP-ssrA, 32 °C). Each data set represents results from three replicates (mean ± SD).

Indeed, **Trap1** demonstrates minor overactivation to 120% at a concentration of 10 μM or higher. **Trap2**, in contrast, exhibits no stimulating effect but rather an inhibitory effect when reaching higher compound concentrations. Nevertheless, these first results encourage the applicability of phenyl ester based peptide mimics in substrate trapping experiments since the proteolytic function of SaClpXP is not significantly hampered.

4.5.2 Phenyl ester traps modify ClpP

To further consolidate that phenyl esters **Trap1** and **Trap2** affect SaClpXP by binding to the active site serine acyl-enzyme complex formation of ClpP with phenyl esters was verified by intact protein mass spectrometry (IP-MS). Incubation of ClpP with excess amounts of **Trap1** and **Trap2** revealed a buffer-dependent engagement which was intrinsically more distinctive with higher ratios of Trap to protein (Figure 4.12).

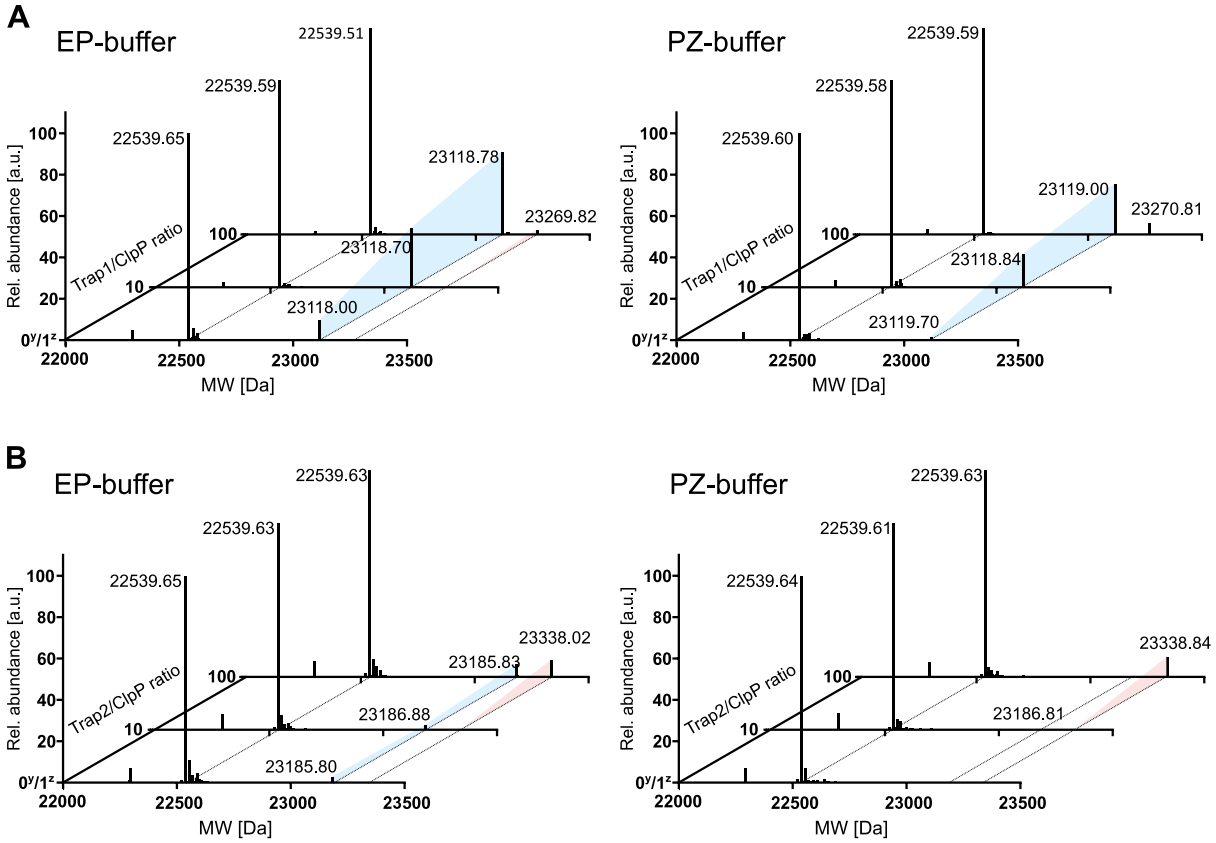

Figure 4.12 Results from intact protein mass spectrometry experiments conducted with varying concentrations of A) **Trap1** and B) **Trap2** (SaClpP concentration: 1 μM) in different buffers (PZ protease buffer and EP minimal buffer). Protein was incubated for 1 h at room temperature prior to LC-MS measurement. Intensities were normalized to the highest peak occurring in each data set. Graphs depict molecular weight plotted against relative abundance. Z-axis depicts varying concentrations of phenyl ester probes **Trap1** and **Trap2**. Pale blue color indicates ClpP-Trap adducts with increasing Trap concentrations. Pale red color indicates non-covalent ClpP-Trap adducts without cleavage of the phenyl ester.

In EP-buffer **Trap1** reaches a maximum of 28% modification compared to unmodified ClpP whereas **Trap2** modifies ClpP only to an extent of maximal 6%. In PZ-buffer modification is significantly lower which is in accordance with peptidase assay results. While **Trap1** modifies ClpP's active site serine to up to 20%, **Trap2** exhibits no binding in this experiment setup. Whether this reflects the actual state *in situ* cannot fully be proven since binding of ClpX was neglected in this experiment setup. Surprisingly, **Trap2** seems to also bind ClpP non-covalently which is observable by the mass adduct of 23338 Da and contradicts the expected mode of action for binding to the active site serine. However, detection of allosterically binding small molecules in intact protein mass spectrometry experiments was previously observed in the case of glutamate synthase.[240] An

explanation for this behavior of phenyl ester **Trap2** is still subject of investigations and can currently only be speculated to be caused by a high affinity of the compound to ClpP.
In summary, intact protein mass spectrometry experiments indicate that phenyl ester based dipeptides bind ClpP after 1 h only to a minor extent. This ostensible disadvantage might prove valuable for *in situ* trapping experiments since a fully modified peptidase could not be proteolytically functional and would impede continuous substrate trapping.

4.5.3 Traps crosslink proteins in *in vitro* assays

First experiments to investigate the ability of phenyl ester traps to capture proteins presented to the ClpXP machinery were conducted *in vitro* with recombinantly expressed SaClpX and SaClpP. For this the setup of the well-established GFP-degradation assay was utilized in order to reduce complexity and to suppress perturbing side effects of a complex protein mixture. Varying concentrations of **Trap1** and **Trap2** were pre-incubated with ClpXP to ensure acyl-enzyme complex formation and afterwards ssrA-tagged eGFP was added. UV-irradiation at $\lambda = 365$ nm was used to photocrosslink the substrate protein, following ligation of phenyl ester probes with TAMRA-azide *via* CuAAC click reaction. Efficacy of GFP trapping was visualized by fluorescence readout after separation of the protein mixture *via* SDS-PAGE. Experiments were conducted in different buffer systems – EP-buffer, PZ-buffer and PZ-buffer lacking DTT. Figure 4.13 depicts fluorescence gels of *in vitro* trapping experiments with **Trap1** including appropriate controls.

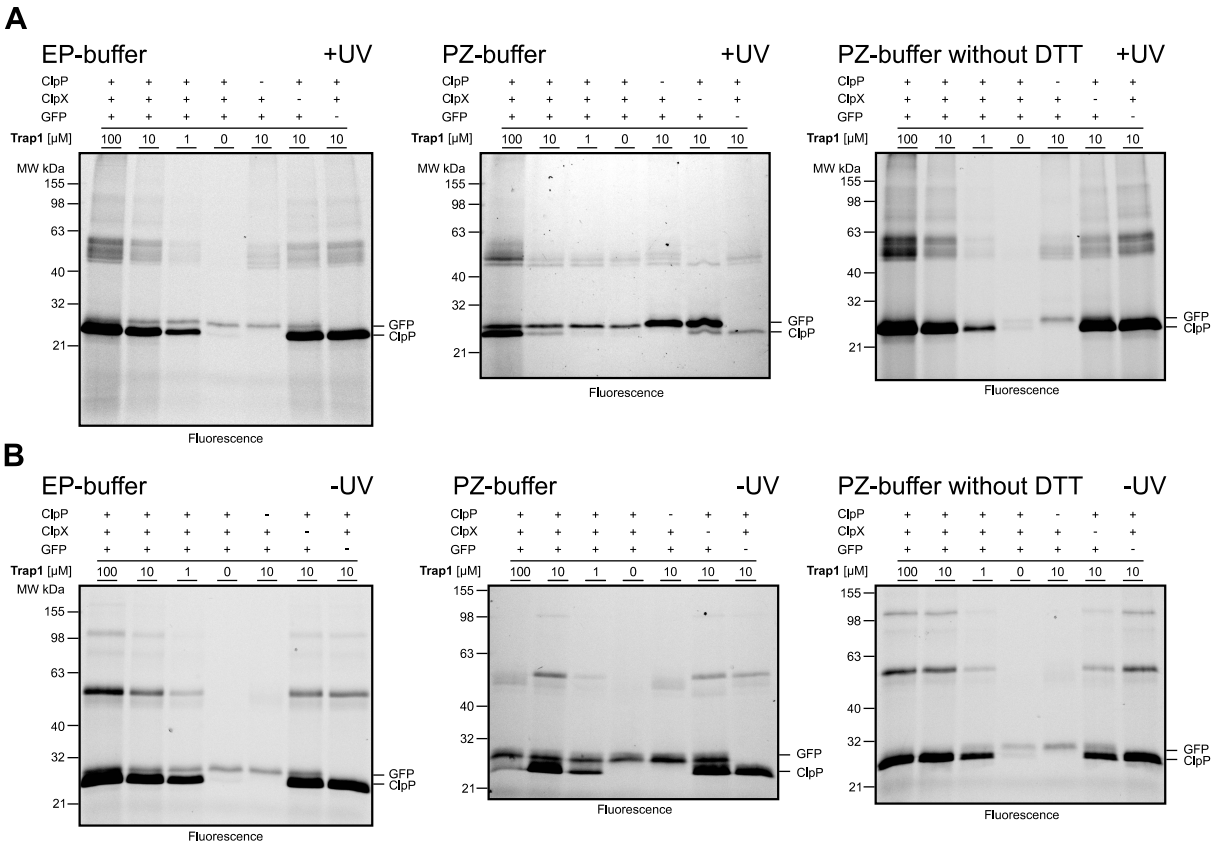

Figure 4.13 Results from analytical labeling and trapping experiments using the GFP-degradation setup with SaClpXP (0.2 µM $SaClpP_{monomer}$, 0.4 µM $SaClpX_{monomer}$, 0.4 µM eGFP-ssrA). Protein mixtures were incubated with **Trap1** for 15 min at 32 °C following UV-irradiation and click reaction with TAMRA-N_3. A) Experiments conducted with **Trap1** in three different buffer systems and UV-irradiation for 30 min. B) Experimental setup without UV-irradiation.

As Trap-treated ClpP is supposed to crosslink GFP leading to a covalent bond between both proteins, a fluorescent band in the range of 50 kDa is expected (25 kDa for ClpP +26.9 kDa for GFP). Experiments in EP-buffer show a concentration dependent labeling of ClpP at a molecular weight of around 25 kDa as well as fluorescent signals of incompletely unfolded GFP running slightly above the ClpP band. Irradiation of probe treated proteins in EP-buffer resulted in additional bands at around 50 kDa which are less prominent in the –UV-control. The controls without **Trap1** or ClpP are in accordance with expectations and reveal no additional band between 21 and 32 kDa. However, bands at ≈50 kDa still appear when ClpP is absent. This might stem from **Trap1** photocrosslinking ClpX since this band is invisible in the –UV control. Overall with this method it is difficult to draw a clear connection between **Trap1** treatment and trapping of GFP as bands at ≈50 kDa may arise either from ClpX or GFP crosslinking.

Experiments in PZ-buffer clearly show increased GFP-levels when ClpP or ClpX are absent indicating that degradation of GFP is functional and dependent on presence of peptidase and chaperone. Furthermore, this proves that GFP degradation is not inhibited by **Trap1** at any concentration. Bands that would correspond to crosslinked proteins are however less observable than in experiments conducted in EP-buffer. Interestingly, in PZ-buffer labeling of ClpP by **Trap1**

is also remarkably less pronounced than in EP-buffer. This can be explained by the composition of PZ-buffer which contains DTT known for its ability to reduce aryl azides.[241] Indeed, when DTT is omitted, labeling of ClpP returns as well as crosslinks after UV-irradiation.

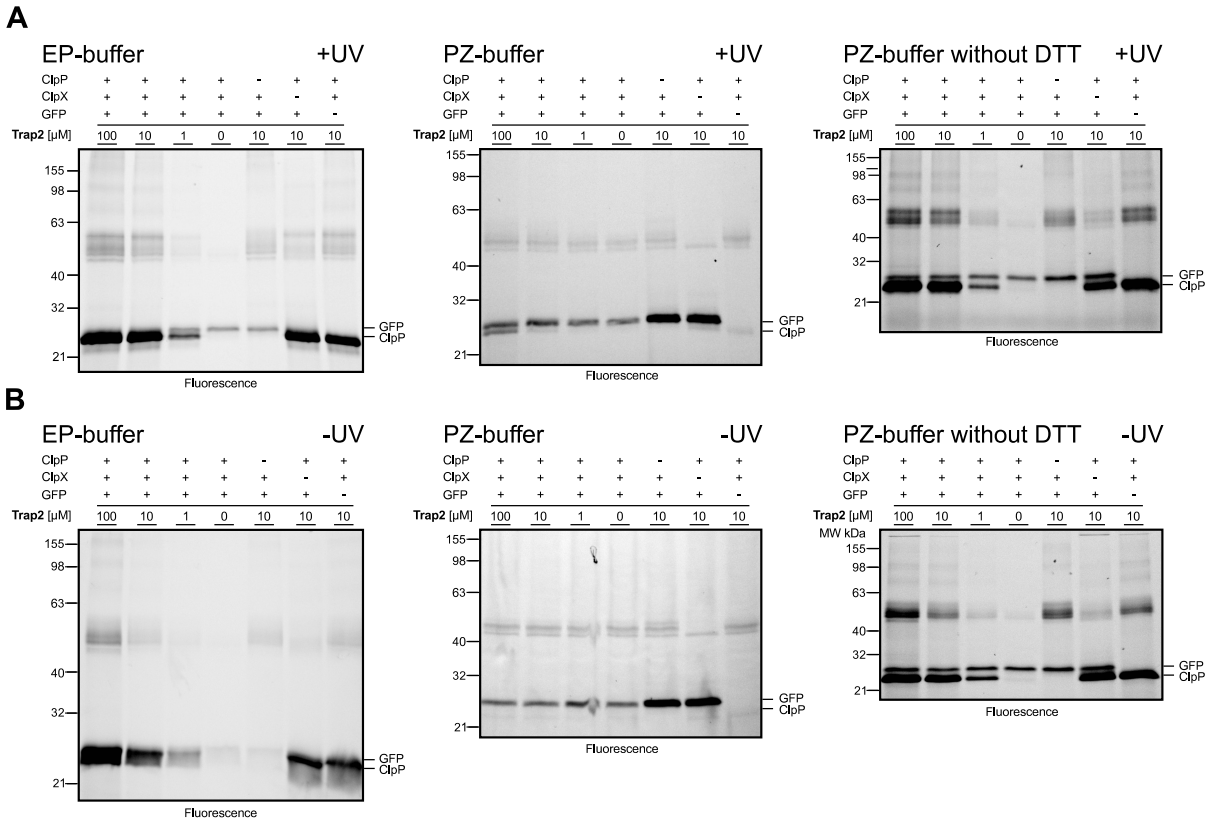

Figure 4.14 Results from analytical labeling and trapping experiments using the GFP-degradation setup with SaClpXP (0.2 µM $SaClpP_{monomer}$, 0.4 µM $SaClpX_{monomer}$, 0.4 µM eGFP-ssrA). Protein mixtures were incubated with **Trap2** for 15 min at 32 °C following UV-irradiation and click reaction with TAMRA-N_3. A) Experiments conducted with **Trap2** in three different buffer systems and UV-irradiation for 30 min. B) Experimental setup without UV-irradiation.

In vitro trapping experiments with **Trap2** reveal a very similar picture when labeling is conducted in EP-buffer. Additional bands at around 50 kDa are observable in the UV-treated samples as well as a concentration dependent labeling of ClpP. Trapping in PZ-buffer exhibits the same effects as with **Trap1**. Labeling of ClpP is diminished due to the influence of DTT and can be recovered by using buffer without DTT.

In order to investigate whether bands at 50 kDa contain crosslinked GFP, western blot analysis was performed using anti-GFP antibodies conjugated to horse radish peroxidase (HRP).

Representative example proteins of trapping experiment with **Trap1** in EP-buffer were blotted and probed with a HRP-conjugated GFP-antibody (Figure 4.15).

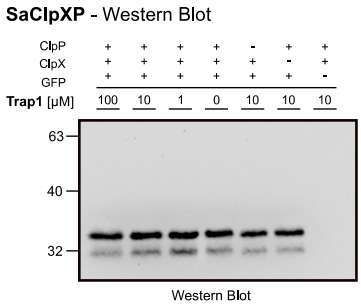

Figure 4.15 Comparison of GFP levels by Western blot upon incubation of SaClpXP with GFP and photocrosslinking with **Trap1**.

Strikingly, no bands within the range of 50 kDa could be assigned to GFP. However, a second band with a higher molecular weight appeared at around 30 kDa. Although these results suggest that phenyl ester traps do not crosslink ClpP to GFP one cannot rule out that the epitope of GFP is not addressable if GFP is cleaved or crosslinked to ClpP.

In summary, *in vitro* trapping experiments support the assumption that phenyl esters **Trap1** and **Trap2** can be used to label ClpP and to crosslink proteins in the vicinity of the protein. However, the identity of emerging bands at 50 kDa is difficult to determine and so far gave only ambiguous results.

4.5.4 Phenyl ester traps label ClpP in *S. aureus*

With **Trap1** and **Trap2** showing excellent behavior towards labeling of ClpP *in vitro*, target engagement in a more complex environment was tested. For this, *S. aureus* NCTC8325 was grown to stationary phase, cell density was adjusted to $OD_{600} = 40$ and bacteria suspensions were incubated for 1 h with various concentrations of either **Trap1** and **Trap2** or DMSO as a control. After lysis and separation of soluble and insoluble protein fractions, phenyl ester probes were clicked to TAMRA-azide and labeled proteins were visualized by fluorescence readout after SDS-PAGE.

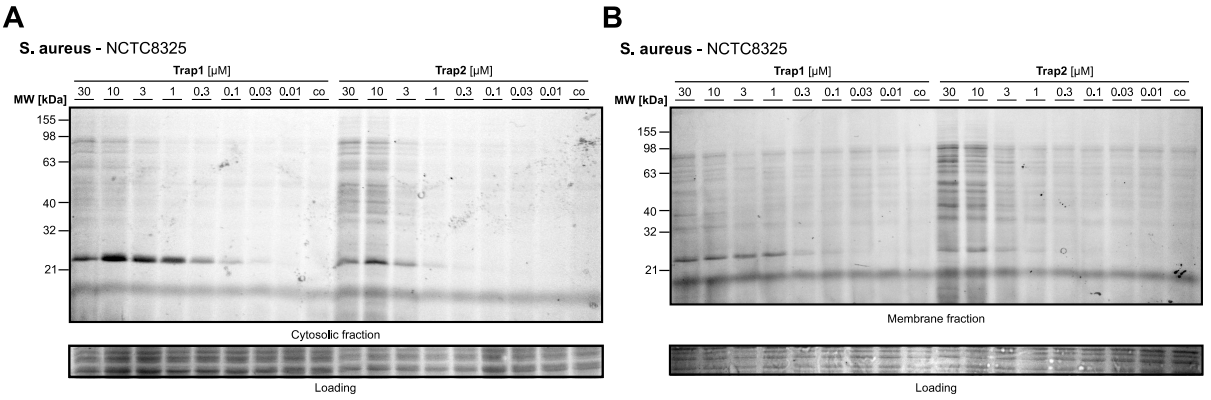

Figure 4.16 Concentration dependent labeling with **Trap1** and **Trap2** in *S. aureus* NCTC8325. A) Labeling in cytosolic fraction. B) Labeling in membrane fraction.

Labeling was performed in both soluble and insoluble fractions of *S. aureus* as depicted in Figure 4.16. Here, **Trap1** shows distinct labeling of one band between 21 and 32 kDa which can be identified as ClpP. Surprisingly, labeling of ClpP by **Trap1** can be visualized at probe concentrations as low as 30 nM illustrating outstanding labeling efficiency. In contrast, **Trap2** does not exhibit this capability, however labeling is still visible at a concentration of 1 µM. A clear difference can also be observed when comparing cytosolic to membrane fractions. ClpP naturally resides as soluble protein in the cytosol and therefore labeling in this fraction is more pronounced than in the insoluble fraction. Hence, for further experiments only the cytosolic fraction was used.

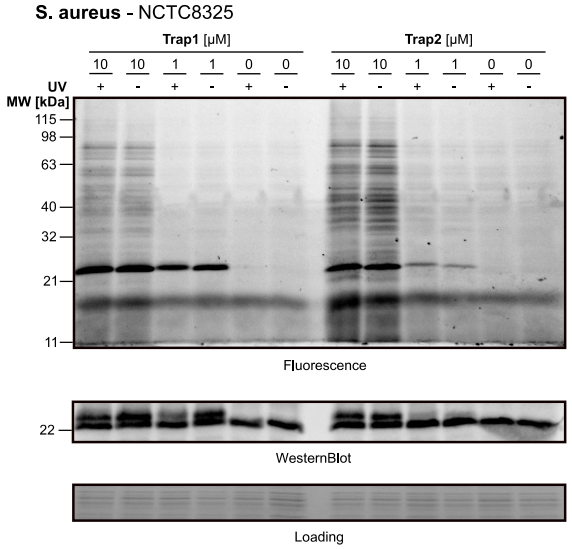

Figure 4.17 Analytical labeling with **Trap1** and **Trap2** in *S. aureus* with subsequent UV-irradiation and corresponding negative controls. Western Blot experiment was performed with SaClpP-antibody and secondary antibody with HRP-function.

First, *in situ* trapping experiments were conducted with both phenyl ester traps using two different concentrations, 10 and 1 µM and DMSO as control. Incubation of bacterial suspension (OD_{600} = 40) for 1 h at 37 °C was followed by an UV irradiation step for 15 min at λ = 365 nm. Cytosolic fractions were reacted with TAMRA-azide by CuAAC click chemistry and proteins were separated *via* SDS-PAGE. Fluorescence readout is depicted in Figure 4.17 and unfortunately revealed no additional bands that would indicate successful crosslinking of substrate proteins. Western Blot analysis also showed no additional bands that would reflect ClpP crosslinked with another protein (Appendix, Figure 8.2). Interestingly, incubation with **Trap1** and **Trap2** results in another band appearing at a slightly higher molecular weight than ClpP. As a second band is not observed when phenyl ester probes are absent and **Trap1** and **Trap2** exhibit a considerable increase in molecular weight of 597 and 664 Da, respectively when bound to ClpP, the additional band most likely reflects the acyl-enzyme complex. Clearly, ClpP monomers are only partially occupied by phenyl ester probes which may explain the fact that no trapping is detected. Nevertheless, MS-

based trapping experiments will be conducted to discern if crosslinking events occur that cannot be detected by SDS-PAGE or immunoblotting.

4.5.5 MS-based ABPP experiments with Trap1 and Trap2

One critical prerequisite for MS-based detection of ClpP substrates by small molecule photo crosslinkers is the effective target engagement by phenyl ester probes **Trap1** and **Trap2**. For this, the probes need to covalently bind ClpP and form a strong connection in a way that the acyl-enzyme complex is stable enough to survive subsequent sample preparation. In order to shed light on this, classical preparative labeling experiments were conducted by applying the same conditions as in gel-based labeling experiments. In detail, bacterial cells were grown to stationary phase and were incubated in triplicates either with 10 µM phenyl esters **Trap1** or **Trap2** or DMSO as a control. Cells were lysed by sonication and labeled proteins were clicked to biotin-azide *via* CuAAC click chemistry. Enrichment of labeled proteins with Avidin-agarose beads was followed by reduction of disulfide bonds with DTT, alkylation of free cysteines with iodacetamide (IAA) and tryptic digestion. Resulting peptides were identified by LC-MS/MS by a label-free quantification approach and raw data were further analyzed using MaxQuant software as well as Perseus for statistical interpretation. For visualization of enriched proteins, scatter plots were generated with Perseus representing enrichment factors on a $\log_2$ scale on the x-axis and p-values in $-\log_{10}$ scale on the y-axis. Proteins exhibiting an enrichment factor greater than 2 and p-value lower than 0.05 were regarded as hits.

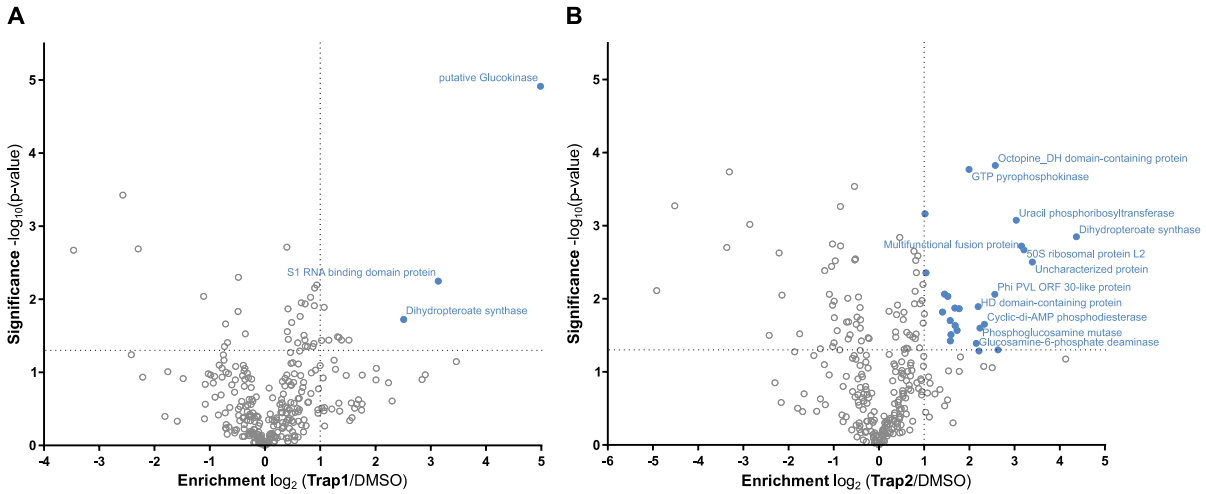

Figure 4.18 Gel-free quantitative ABPP experiment with A) **Trap1** and B) **Trap2** in *S. aureus* NCTC8325 (10 µM probe concentration, 1 h labeling at 25 °C). Volcano plots represent enrichment factors plotted against significance of enrichment. Graphs represent data from three technical replicates for each state. Two sample student's *t*-test was conducted by comparison of labeled group with DMSO as single control group. False discovery rate was determined by Benjamini-Hochberg procedure setting correction to 0.05. Cut-off lines were set at a minimum $\log_2$ change of 1 with a minimum *p*-value of 0.05.

Results of the first MS-based labeling experiments are depicted in Figure 4.18. It is evident that the univocal results of gel-based labeling are not reflected in the scatter plots. Labeling with **Trap1**

resulted in only three proteins passing the cut-off threshold (Table 4.1). These include glucokinase (glck) which is a major component of energy generation in *S. aureus* since it catalyzes the phosphorylation of glucose to glucose-6-phosphate in the cytoplasm.[242] Furthermore, 30S ribosomal protein S1 (rpsA) which is known to participate in translation initiation complex formation in *E. coli* and dihydropteroate synthase (dhps) that is involved in the folate synthesis by catalyzing the generation of 7,8-dihydropteroate were found as enriched proteins.[243,244]

Labeling with **Trap2** unveils considerably more targets than labeling with **Trap1**. Of the identified proteins dihydropteroate synthase is the only protein significantly enriched in both sample sets substantiating it as a possible off-target. Further interesting proteins are the 50S ribosomal protein L2 (rplB) which is required for assembly of the 70S ribosome, tRNA binding and peptide bond formation[245] and the multifunctional fusion protein (secD) which is a part of the general secretory pathway involved in translocation and secretion of proteins such as virulence factors.[246] Proteins that are further characterized include uracil phosphoribosyl transferase (upp) which catalyzes the conversion of uracil to UMP[247] and phosphoglucosamine mutase (glmM) a protein that acts as inhibitor to c-di-AMP-cyclase (dacA) and furthermore catalyzes the conversion of glucosamine-6-phosphate to glucosamine-1-phosphate, an important intermediate of peptidoglycan synthesis.[248,249] Interestingly cyclic di-AMP phosphodiesterase (gdpP) is also significantly enriched, a protein that is suggested to play a role in controlling cell size and which reverses the function of dacA, the protein that is inhibited by glmM.[250] Another protein involved in monosaccharide metabolism which was enriched by **Trap2** is glucosamine-6-phosphate deaminase (nagB), a protein that catalyzes the reaction of glucosamine-6-phosphate to fructose-6-phosphate hereby enabling the conversion of cell wall building blocks for energy generation.[251] In summary, labeling with **Trap2** resulted in enrichment of proteins of the nucleotide synthesis pathway and amino sugar metabolism pathways.

Table 4.1 Enriched proteins from gel-free quantitative ABPP experiments.

Uniprot ID	*Gene name*	*Protein name*	*Enrichment factor (log_2)*	*p-value (log_{10})*	*probe*
Q2FY27	glcK	Glucokinase, putative	4.98569171	4.91635226	Trap1
Q2G0Q7	dhps	Dihydropteroate synthase	4.36849213	2.84924451	Trap1
Q2FYQ2	-	Uncharacterized protein	3.39471054	2.50331771	Trap2
P60430	rplB	50S ribosomal protein L2	3.20661163	2.67032905	Trap2
Q2FXT8	secD	Multifunctional fusion protein	3.1530393	2.72268079	Trap2
Q2FWJ5	rpsA	S1 RNA binding domain protein	3.13607788	2.24921314	Trap1
Q2FWE6	upp	Uracil phosphoribosyltransferase	3.03611946	3.07475282	Trap2
Q2G1W0	gndA	6-phosphogluconate dehydrogenase, decarboxylating	2.57522392	3.82617552	Trap2
Q2FY84	-	Phi PVL ORF 30-like protein	2.56409391	2.06232317	Trap2
Q2G0Q7	dhps	Dihydropteroate synthase	2.5114886	1.72372607	Trap2
Q2G2T6	gdpP	Cyclic-di-AMP phosphodiesterase	2.33301544	1.65267143	Trap2
P0C0V7	glmM	Phosphoglucosamine mutase	2.23564339	1.60043133	Trap2

ClpP was not among these hits. In fact, ClpP was only identified in two out of 6 samples in each labeling experiment. One reason for this could be insufficient cell lysis during sample preparation.

Cell lysis by sonication potentially does not result in full disruption of all bacterial cells. Therefore, lysis was selected as an element for improvement.

Lysostaphin is a zinc-containing monomeric endopeptidase that is secreted from *Staphylococcus simulans* and is known to degrade cell walls of all known staphylococcal species.[252,253] Recombinantly expressed lysostaphin can be added to *S. aureus* cell suspensions to cleave peptidoglycan of the cell wall.

Optimization measures of the previous labeling experiments were therefore conducted by incubating cell suspensions with 5 µL lysostaphin solution (10 mg/mL in 20 mM sodium acetate buffer, pH = 4.5) at 37 °C for 30 min and short sonication with low intensity after labeling with 10 µM **Trap1** or **Trap2** or DMSO as a control in the same way as mentioned above. Click chemistry, affinity enrichment, alkylation, reduction and digestion were also performed as described before. LC-MS/MS analysis followed by protein identification and quantification using MaxQuant provided the results depicted in Figure 4.19.

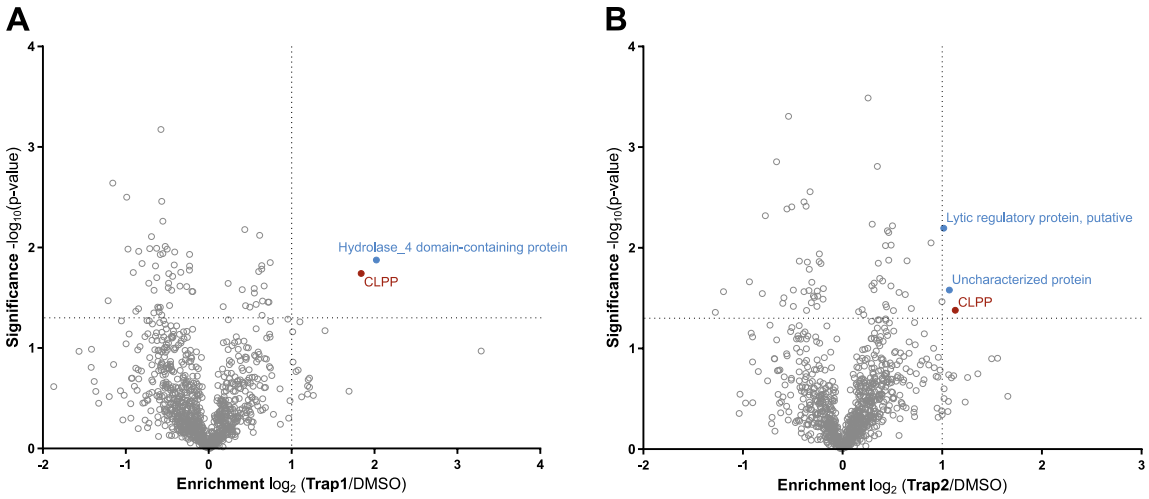

Figure 4.19 Gel-free quantitative ABPP experiment with A) **Trap1** and B) **Trap2** in *S. aureus* NCTC8325 (10 µM probe concentration, 1 h labeling at 25 °C). Volcano plots represent enrichment factors plotted against significance of enrichment. Graphs represent data from three technical replicates for each state. Two sample student's *t*-test was conducted by comparison of labeled group with DMSO as single control group. False discovery rate was determined by Benjamini-Hochberg procedure setting correction to 0.05. Cut-off lines were set at a minimum $\log_2$ change of 1 with a minimum *p*-value of 0.05.

Labeling with **Trap1** and **Trap2** reveals two to almost four-fold enrichment of ClpP over DMSO control. This is in accordance with previous gel-based labeling experiments and confirms the affinity of phenyl ester based probes for ClpP. **Trap1** labeling exhibits merely one other target under these conditions. Hydrolase_4 domain-containing protein is a poorly characterized protein that displays carboxylic ester hydrolase activity which could explain the affinity for the phenyl ester probe.[254] Besides ClpP, **Trap2** also enriches a putative lytic regulatory protein and an uncharacterized protein. However, more details regarding their structure and function are unknown (Table 4.2). Interstingly, dihydropteroate synthase was not enriched anymore using optimized lysis conditions.

Table 4.2 Enriched proteins from quantitative gel-free ABPP experiments.

Uniprot ID	*Gene name*	*Protein name*	*Enrichment factor (log_2)*	*p-value (log_{10})*	*probe*
Q2G0V7	-	Hydrolase_4 domain-containing protein	1.87654379	2.02487691	Trap1
Q2G036	ClpP	ATP-dependent Clp protease proteolytic subunit	1.74181423	1.84111595	Trap1
			1.37993709	1.13135084	Trap2
Q2FW64	-	Uncharacterized protein	1.58077506	1.0715332	Trap2
Q2FWA8	-	Lytic regulatory protein, putative	2.19609504	1.01499812	Trap2

4.5.6 Trapping results with Trap1 and Trap2

Labeling and identification of ClpP by phenyl ester probes **Trap1** and **Trap2** proved to be feasible when appropriate lysis is performed. This positive result enables the use of dipeptide phenyl ester probes for MS-based substrate trapping experiments. For this, bacterial cultures were grown to stationary phase and were subsequently incubated with 10 µM **Trap1** or **Trap2** for 1 h at 25 °C in six replicates each. Afterwards samples were washed and taken up in PBS buffer. For substrate trapping three replicates from each probe treated sample set were irradiated with UV-light (λ = 365 nm) for 15 min and the other three replicates were kept in the dark for the same time serving as controls. In the following UV treated samples are referred to as +UV while controls that were not UV irradiated are termed –UV. Bacteria were subsequently lysed by addition of lysostaphin (5 µL, 10 mg/mL in 20 mM sodium acetate buffer, pH = 4.5) and incubation at 37 °C for 30 min. Labeled proteins were reacted with biotin-azide affinity handle *via* CuAAC click chemistry and after enrichment with avidin-agarose beads proteins were reduced, alkylated and digested on the beads. Peptides were analyzed by LC-MS/MS and raw data were processed using MaxQuant software. Results of trapping experiments are depicted as scatter plots in Figure 4.20.

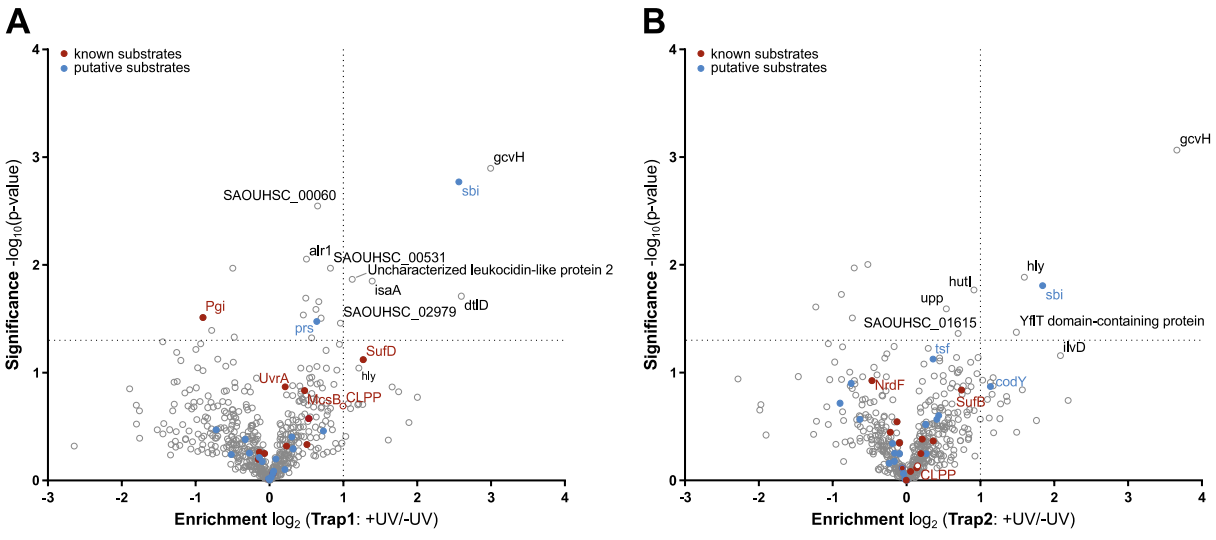

Figure 4.20 Gel-free quantitative ABPP experiment with A) **Trap1** and B) **Trap2** in *S. aureus* NCTC8325 (10 µM probe concentration, 1 h labeling at 25 °C). Samples were UV-irradiated for 15 min after labeling with **Trap1** and **Trap2**. As negative control samples incubated with phenyl ester probes were kept in the dark for 15 min. Volcano plots represent enrichment factors of UV-treated versus untreated samples plotted against significance of enrichment. Graphs represent data from three technical replicates for each state. Two sample student's *t*-test was conducted by comparison of UV treated group with UV untreated as single control group. False discovery rate was determined by Benjamini-Hochberg procedure setting correction to 0.05. Cut-off lines were set at a minimum log_2 change of 1 with a minimum *p*-value of 0.05.

For detection of ClpP substrates UV treated samples were compared to untreated samples. Since both replicate sets were treated with the same amount of phenyl ester probes and the only difference is induced by the treatment with UV-light, higher abundance of proteins should be a result of crosslinking events.

Experiments with **Trap1** reveal several proteins that can be interpreted as substrates of ClpP. These include glycine cleavage system H protein (gcvH) which is responsible for the NAD^+-dependent synthesis of 5,10-methylene-H_4folate (CH_2-THF) by breakdown of glycine. CH_2-THF is then used by serine hydroxymethyltransferase (SHMT) for the synthesis of serine.[255–257] Interestingly, *Fischer et al.* could show in a similar trapping approach as conducted by *Frees et al.*[229] that in the fungal ageing model *Podospora anserina* the fungal equivalent of gcvH (glycine cleavage system H protein, gcsH) is a substrate of human ClpXP.[135] This finding as well as the fact that gcvH is a top hit in **Trap2** labeling too, strengthens the assumption that gcvH might be a substrate of SaClpP.

Another protein that was trapped by **Trap1** as well as **Trap2** is second immunoglobulin-binding protein Sbi. This protein is known to bind the Fc region of IgG in a similar way as protein A representing a major virulence factor critical for host infection and evasion of host immune response.[258,259] It occurs both extracellularly and bound to the cell envelope and exerts its function in both forms.[258] ClpP is well-known to modulate virulence factor expression[212] and the present finding draws a direct link between ClpP and the virulence factor. Furthermore, Sbi was found to be upregulated in a *S. aureus clpp* mutant strain.[181] The fact that Sbi is identified as putative substrate in phenyl ester based trapping further corroborates the assumption by *Frees et al.* who found that a non-mature Sbi carrying a signal peptide exists in parallel to the envelope-associated protein only when ClpP is not present.[260] It is therefore tempting to speculate that ClpP is responsible for the maturation of Sbi by cleaving the signal peptide.

Protein DltD (D-alanylation of lipoteichoic acid D) was enriched by **Trap1** and is involved in cell wall biogenesis by D-alanylation of lipoteichoic acid.[261,262] Further information about structure and function are currently subject of investigations.

Protein isaA (immunodominant staphylococcal antigen A) was also enriched by **Trap1** and represents, together with SceD lytic transglycosylases which are able to cleave peptidoglycan and whose deletion in *S. aureus* led to a decreased biofilm formation.[263,264] Additionally isaA was identified as a major antigen expressed during sepsis caused by *S. aureus*[265,266] and was found to be upregulated in a ClpP deletion model.[219] It is excreted into the extracellular environment as well as being cell-wall bound sharing a key feature with protein Sbi which is speculated to be matured by ClpP.[264] Identifying isaA adds another protein involved in cell wall biogenesis to the list of putative ClpP substrates.

Interestingly, another major virulence factor of *S. aureus* was observed to be a putative substrate of ClpP. α-Hemolysin (hly) was enriched almost four fold compared to UV untreated samples and represents a member of the protein family responsible for lysis of lysosomes and erythrocytes.[182] In wild type *S. aureus* NCTC8325 expression of hly was shown to be strongly induced in transition between post-exponential and stationary phase and is drastically reduced in *clpP* and *clpX* knock out mutant cells.[181] The fact that expression of hly was downregulated when ClpP was chemically inhibited by *β*-lactones[212] together with a drastic reduction of α-hemolysin secretion in *clpP* and *clpX* knock out cells makes it tempting to assume a processing function of ClpP for this special virulence factor. The report about precursor proteins of hly migrating at 44.8 and 44 kDa in SDS-PAGE when precursor processing is inhibited by 2,4-dinitrophenol (DNP) further supports this theory.[267] Nevertheless it must be considered that *clpX* and *clpP* deletion also resembles expression patterns of *agr* mutant strains indicating that *hly* expression might be mediated by the *agr* system.[181]

Further proteins that were identified as putative ClpP substrates but which are rather uncharacterized are YflT domain-containing protein and the uncharacterized leukocidin-like protein 2. The latter interestingly shows a 35% sequence similarity with *γ*-hemolysin representing another member of the hemolysin toxins of *S. aureus*.

Table 4.3 Enriched proteins after tapping experiments with **Trap1** and **Trap2**.

Uniprot ID	*Gene name*	*Protein name*	*Enrichment factor (log_2)*	*p-value (log_{10})*	*probe*
Q2FZZ8	gcvH	Glycine cleavage system H protein	2.9935627	2.897486716	Trap1
			3.65996106	3.065447091	Trap2
Q2FZW3	dltD	Protein DltD	2.59848086	1.71005891	Trap1
Q2FVK5	sbi	Immunoglobulin-binding protein Sbi	2.770798246	2.56462351	Trap1
			1.807438924	1.8426679	Trap2
Q2FV52	isaA	Probable transglycosylase IsaA	1.39174207	1.851381236	Trap1
Q2FWN9	SAOUHSC_02243	Uncharacterized leukocidin-like protein 2	1.11974907	1.866881391	Trap1
Q2G1X0	hly	Alpha-hemolysin	1.5965538	1.885904609	Trap2
Q2G0Z0	SAOUHSC_00371	YflT domain-containing protein	1.48717372	1.37534955	Trap2

In summary, only one protein previously annotated as putative ClpP substrate was found with phenyl ester traps **Trap1** and **Trap2**. All other proteins can therefore only be attributed as putative new ClpP substrates and certainly do not reflect the whole substrate scope of ClpXP. Optimization of trapping conditions as well as measurements in different growth stages will be subject of further experiments.

4.6 Conclusion and Outlook

Phenyl ester based peptide mimics were shown to exhibit unexpected stimulating effects on *S. aureus* ClpXP activity which presumably arises from a tightened ClpX-ClpP interaction.[224] These compounds greatly differ from already known ClpP activators such as ADEPs[227], D9[268] or imipridones[40] which bind to the apical side of ClpP leading to a conformational change and widening of the entrance pore. Phenyl ester based activators, however, paradoxically bind the active site serine and not to an allosteric site. We therefore hypothesized that this phenomenon can be exploited to trap and identify substrates that pass the proteolytic sites of ClpP.

In this regard, phenyl ester dipeptides **Trap1** and **Trap2** were successfully equipped with a photoreactive moiety for UV-induced substrate trapping and an affinity handle for enrichment of trapped proteins. These probes proved to bind covalently to ClpP in a sub-stoichiometrical manner and thus exhibited no interference with the proteolytic activity of ClpP. Moreover, ClpP could be selectively labeled *in situ* meeting an important criterion for further trapping experiments. Ultimately, several new putative substrate proteins could be identified by a MS-based trapping approach. These identified substrates largely consist of virulence associated proteins as well as proteins of the cell wall biogenesis. However, the low number of identified substrate proteins indicates that only the surface of ClpP's substrate scope was touched and further experiments need to be conducted to reveal what lies beneath.

5

Experimental Section

5 Experimental Section

5.1 Material and Methods

5.1.1 Organic Chemistry

All chemicals and reagents were purchased from commercial sources and were utilized without further purification. Solvents of technical grade were distilled once before use for column chromatography. Where necessary crude reagents were also distilled.

Chemical reactions were conducted in oven-dried glassware. For air-sensitive reactions glassware was thoroughly heated under high vacuum and purged with argon three times. Dry solvents and air or water sensitive reagents were handled using disposable syringes which were purged with argon and air sensitive solvents were added to reaction flasks under argon counter flow. Reactions were monitored by LC-MS (MSQ Plus or LTQ-FT Ultra, both *Thermo Fisher Scientific Inc.*, both coupled to a Dionex UltiMate 3000 HPLC) or pre-coated TLC silica gel 60 F_{254} plates (*Merck*) with visual detection under UV light (λ = 254 and 366 nm) or staining with appropriate solutions ($KMnO_4$-stain: 1.50 g $KMnO_4$, 10.0 g K_2CO_3, 1.25 mL $NaOH_{aq}$ 10% (w/v), 200 mL ddH_2O; 2,4-dinitrophenylhydrazine (DNP) stain: 12 g DNP, 60 mL H_2SO_4 (conc.), 80 mL ddH_2O, 200 mL EtOH (95%); Hanessian-stain: 0.5 g $(NH_4)_4Ce(SO_4)_4$, 12 g $(NH_4)_2MoO_4$, 15 mL H_2SO_4 (conc.), 235 mL ddH_2O; Ninhydrin-stain: 0.3 g ninhydrin, 100 mL, *n*-BuOH, 3 mL AcOH). Purification of crude products was achieved by silica column chromatography or flash chromatography (Reveleris X2, *Büchi*) with silica gel 60 (particle size = 40 – 63 µm, *VWR*). Column volumes, diameter and eluents are indicated individually for each synthetic step in the following order: silica gel, volume, column diameter, eluent ratio. Synthesis products that exhibited low lipohilicity were purified by reversed-phase high-performance liquid chromatography (RP-HPLC). For analytical puposes, a Waters 2695 separation module coupled with a Waters PDA 2996 and a Waters XBridge C18 column (3.5 µm, 4.6 x 100 mm, solvent flow: 1.2 mL/min) was used. For preparative separation, a Waters 2545 quaternary gradient module coupled to a Waters PDA 2998 was used. Depending on crude product mass, reversed-phase columns with different sizes were used (P1: YMC Triart C18 (3.5 µm, 10 x 250 mm, flow rate: 10 mL/min), P2: Waters XBridge™ C18 (5.0 µm, 30 x 150 mm, flow rate: 50 mL/min), P3: Waters XBridge™ C18 (10 µm, 50 x 250 mm, flow rate: 130 mL/min)). Product elution was performed with mobile phases consisting of a gradient mixture of water with 0.1% (v/v) TFA (buffer A) and acetonitrile with 0.1% (v/v) TFA (buffer B) or water (buffer C) and acetonitrile (buffer D).

Structure and purity of synthesized compounds were analyzed by nuclear magnetic resonance spectroscopy (NMR) on *Avance-I/III* (AV-HD300, AV-HD400, AV-HD500 or AV-HD500cryo)

systems (*Bruker*) using *Topspin* software (verions 2.1 and 3, *Bruker*). ^{1}H-NMR spectra were recorded at room temperature with deuterated solvents ($CDCl_3$, DMSO-d_6, CD_3CN). Chemical shifts are specified in parts per million (ppm) and are indicated in reference to the residual proton signal of the corresponding solvent ($CDCl_3$: δ = 7.26 ppm, DMSO-d_6: δ = 2.50 ppm, CD_3CN: δ = 1.94 ppm). Coupling constants *J* are reported in hertz (Hz) and multiplicity of the signals is assigned with the following abbreviations: s – singlet, d – doublet, dd – doublet of doublets, dt – doublet of triplets, dq – doublet of quartets, ddd – doublet of doublet of doublets, ddt – doublet of doublet of triplets, t – triplet, td – triplet of doublets, q – quartet, p – quintet. ^{13}C-NMR spectra were obtained with the same instruments operated at 75, 101 or 126 MHz respectively. Chemical shifts were referenced to the solvent signal ($CDCl_3$: δ = 77.16 ppm, DMSO-d_6: δ = 39.52 ppm, CD_3CN: δ = 1.32 ppm). Multiplicity was assigned as follows: q – quartet. ^{19}F-NMR spectra were recorded on *Avance-III* (AV-HD500, *Bruker*) systems operated with 376 MHz and were referenced to the internal standard hexafluorobenzene (δ = 164.64 ppm).

High resolution mass spectrometry was conducted on a LTQ-FT Ultra (*Thermo Fisher Scientific Inc.*) with electrospray ionization (ESI) or atmospheric-pressure chemical ionization (APCI) and coupled to a Dionex Ultimate 3000 HPLC (*Thermo Fisher Scientific Inc.*).

5.1.2 Biochemistry

5.1.2.1 Buffers

In the following, buffers that were used for biochemical experiments are listed. All buffers are aqueous solutions unless otherwise indicated.

Table 5.1 Buffers for biological experiments.

Buffer	***Ingredients***
PBS-buffer	140 mM NaCl 10 mM Na_2HPO_4 2.7 mM KCl 1.8 mM KH_2PO_4 pH 7.4
Lysis buffer	140 mM NaCl 10 mM Na_2HPO_4 2.7 mM KCl 1.8 mM KH_2PO_4 1% (v/v) NP-40 alternative 1% (w/v) sodium deoxycholate pH 7.4
Trypan blue	5 mg/mL trypan blue 9 mg/mL NaCl
Tris-Glycine running buffer (10x) for SDS-PAGE	250 mM Tris/HCl 1.92 M glycine 1% (w/v) SDS pH 8.3
Coomassie stain	0.25% (w/v) Coomassie brilliant Blue R250 9.2% (v/v) AcOH 45.4% (v/v) EtOH
Coomassie destain	10% AcOH 20% EtOH
Laemmli buffer (2x)	63 mM Tris/HCl 139 mM SDS 2% (v/v) glycerol 0.0025% (v/v) bromophenol blue 5% (v/v) mercaptoethanol
PBS-T buffer	140 mM NaCl 10 mM Na_2HPO_4 2.7 mM KCl 1.8 mM KH_2PO_4 0.5% (v/v) Tween-20® pH 7.4
Blotting buffer	48 mM Tris base 39 mm glycine 20% (v/v) MeOH
Western blot blocking buffer	140 mM NaCl 10 mM Na_2HPO_4 2.7 mM KCl 1.8 mM KH_2PO_4 5% (w/v) skim milk 0.5% (v/v) Tween-20® pH 7.4
EcClpX His lysis buffer	50 mM HEPES 300 mM KCl 1 mM DTT 10 mM imidazol 5 mM $MgCl_2 \cdot 6H_2O$ 15% (v/v) glycerol pH 7.6
EcClpX His wash buffer	50 mM HEPES 300 mM KCl 1 mM DTT 40 mM imidazol 15% (v/v) glycerol

	pH 7.6
EcClpX His elution buffer	50 mM HEPES 300 mM KCl 1 mM DTT 300 mM imidazol 15% (v/v) glycerol pH 7.6
EcClpX SEC buffer	50 mM HEPES 300 mM KCl 1 mM DTT 5 mM $MgCl_2 \cdot 6H_2O$ 15% (v/v) glycerol pH 7.6
HsClpP Strep binding buffer	100 mM Tris/HCl 150 mM NaCl 1 mM EDTA pH 8.0
HsClpP Strep elution buffer	100 mM Tris/HCl 150 mM NaCl 1 mM EDTA 2.5 mM desthiobiotin pH 8.0
HsClpP SEC buffer	20 mM HEPES 100 mM NaCl pH 7.0
Peptidase assay buffer (HsClpP), *FITC-Casein assay buffer*	50 mM HEPES 300 mM KCl 1 mM DTT 15% (v/v) glycerol pH 8.0
EP-buffer	100 mM HEPES 100 mM NaCl pH 7.0
PZ-buffer	25 mM HEPES 200 mM KCl 5 mM $MgCl_2 \cdot 6H_2O$ 1 mM DTT 10% (v/v) glycerol pH 7.6
Basic buffer for HA-tag affinity enrichment	50 mM Tris/HCl 150 mM NaCl 1 mM $MgCl_2 \cdot 6H_2O$ pH 7.4 (at 4 °C)
Lysis buffer for HA-tag affinity enrichment	50 mM Tris/HCl 150 mM NaCl 1 mM $MgCl_2 \cdot 6H_2O$ 5% (v/v) glycerol 1% (v/v) NP-40 alternative pH 7.4 (at 4 °C)
Wash buffer for HA-tag affinity enrichment	50 mM Tris/HCl 150 mM NaCl 1 mM $MgCl_2 \cdot 6H_2O$ 5% (v/v) glycerol 0.05% (v/v) NP-40 alternative pH 7.4 (at 4 °C)
Digestion buffer I	50 mM Tris/HCl 2 M urea 5 ng/µL Trypsin (in 50 mM acetic acid) 1 mM DTT pH 8.0
Digestion buffer II	50 mM Tris/HCl 2 M urea 5.5 mM iodoacetamide pH 8.0

5.1.2.2 Media and solutions

Media that were used for culturing of bacterial and human cells are specified in the following table.

Table 5.2 Media for bacterial and human cell culture.

Medium	***Ingredients***
LB-medium	1% (w/v) peptone 0.5% (w/v) yeast extract 0.5% (w/v) NaCl 0.1% pH 7.5
B-medium	1% (w/v) peptone 0.5% (w/v) yeast extract 0.5% (w/v) NaCl 0.1% (w/v) K_2HPO_4 pH 7.5
Dulbecco's Modified Eagle's Medium (DMEM)	D5796 (*Sigma Aldrich*)
Roswell Park Memorial Institute Medium (RPMI)	R0883 (*Sigma Aldrich*)
Iscove's Modified Dulbecco's Medium	I3390 (*Sigma Aldrich*)
Fetal bovine serum (FBS)	F0804 (*Sigma Aldrich*)
L-Glutamine 200 mM solution	G7513 (*Sigma Aldrich*)
Accutase® solution	A6964 (*Sigma Aldrich*)
Trypsin-EDTA solution (10x)	T4174 (*Sigma Aldrich*)
Collagen A solution	L7220 (*Merck*)

5.1.2.3 Antibodies

For western blot analysis the following antibodies were used.

Table 5.3 Primary and secondary antibodies.

Antigene	***Source***	***Dilution***	***Supplier***
HsClpP	Mouse	1:1,000	*Abcam*, Cambridge, UK
HsClpX	Rabbit	1:500	*Abcam*, Cambridge, UK
HRP, goat anti-mouse IgG	Goat	1:,1000	*Santa Cruz Biotechnology*, Dallas TX USA
HRP, goat anti-rabbit IgG	Goat	1:1,000	*DIANOVA GmbH*, Hamburg, Germany
GFP-HRP conjugate	Goat	1:5,000	*Abcam, Cambridge, UK*

5.1.2.4 Human cancer cell lines

Cell lines that were used for labeling experiments and assays are listed in the following table.

Table 5.4 Human cell lines.

Cell line	***Cell type***	***Cultivation***	***Cancer type***
Huh7	adherent	DMEM supplemented with 10% (v/v) FBS, 2 mM L-glutamine	hepato cellular carcinoma
Jurkat	suspension	RPMI supplemented with 10% (v/v) FBS, 2 mM L-glutamine	acute T cell leukemia
HL-60	suspension	IMDM supplemented with 10% (v/v) FBS, 2 mM L-glutamine	acute promyelocytic leukemia
K562	suspension	RPMI supplemented with 10% (v/v) FBS, 2 mM L-glutamine	chronic myelogenous leukemia
Hek293T	adherent	DMEM supplemented with 10% (v/v) FBS, 2 mM L-glutamine	embryonic kidney 293 cells

5.2 Experimental part for chapter 2

5.2.1 Chemical Synthesis

General procedures

General procedure I for the synthesis of esters **AV167**, **5**-**9**, **12**, **19**-**22**, **30**-**32**, **35**-**40**

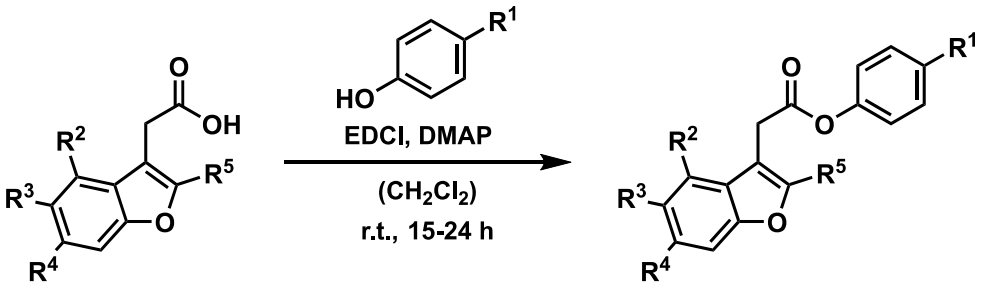

R^1 = H, OMe, CO_2Me, NO_2,
SO_2Me, 1,3,4-Oxadiazol
R^2 = H, -CH=CH-CH=CH-
R^3 = H, -CH=CH-CH=CH-, Me, OMe,
R^4 = H, OMe
R^5 = H, Br, I, -CN, -C≡CH

To a suspension of benzofuranyl/naphthofuranylacetic acid (1.00 eq.) in CH_2Cl_2 (≈ 0.1 M) was added EDCI (1.50 eq.), DMAP (0.50 eq.) and then the appropriate phenol (1.20 eq.). The resulting mixture was stirred at room temperature for 15 – 24 h under argon atmosphere. Afterwards, the reaction mixture was diluted with CH_2Cl_2 and the clear solution was washed with saturated $NaHCO_3$ solution, water and brine. The organic extracts were dried over Na_2SO_4, filtered and evaporated under vacuum. Purification of the crude product was carried out by silica gel column chromatography.

General procedure II for the synthesis of substituted coumarins **13**-**15** and substituted benzo[*f*]coumarins **3** and **10**.

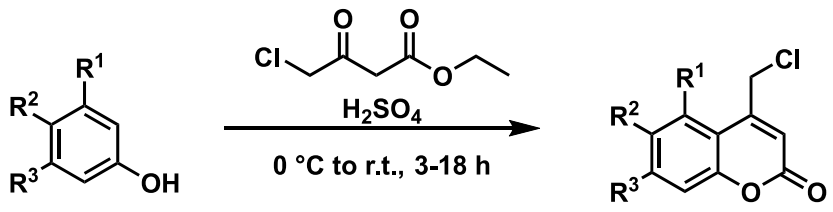

R^1 = H, -CH=CH-CH=CH-
R^2 = H, -CH=CH-CH=CH-, Me, OMe
R^3 = H, OMe

Substituted phenol or naphthol derivatives (1.00 eq.) and ethyl 4-chloroacetoacetate (1.00 eq., 1.14 eq. for naphthol derivatives) were mixed in a round bottom flask. Under ice cooling H_2SO_4 (70% (v/v), ≈ 1 mL/mmol substrate) was added dropwise over a period of 15 min. For naphthol derivatives, concentrated H_2SO_4 (98%, ≈ 0.5 mL/mmol substrate) was used. Following that, the reaction mixture was stirred at room temperature for 18 h; in the case of naphthol substrates the reaction time was 3 h. After completion, the mixture was poured onto ice water and stirred for 1 – 2 h. In this time a precipitate formed which was filtered and washed with cold water. In some cases, silica gel column chromatography was required to isolate the pure product.

General procedure III for the synthesis of substituted benzofuran-3-ylacetic acids **16-18**

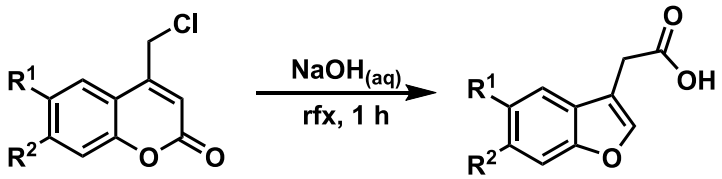

R^1 = H, Me, OMe
R^2 = H, OMe

In a round bottom flask substituted coumarin (1.00 eq.) was suspended in 1 M $NaOH_{aq}$ and heated under reflux for 1 h. Afterwards, the clear solution was cooled to room temperature, acidified with 1 M HCl_{aq} until pH = 5 – 6 was reached and stirred for 30 min. The resulting precipitate was collected by filtration, washed with 1 M HCl_{aq} and water and dried *in vacuo*.

General procedure IV for the synthesis of substituted naphthofuran-1-ylacetic acids **4** and **11**

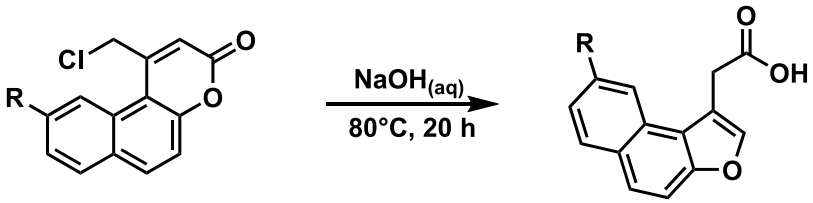

R = H, OMe

In a round bottom flask substituted benzo[*f*]coumarin (1.00 eq.) was suspended in 6 M $NaOH_{aq}$ and heated under reflux for 20 h. Afterwards, the clear solution was acidified with 6 M HCl_{aq} until pH = 5 – 6 was reached and stirred for 30 min. The resulting suspension was extracted with ethyl acetate. Then, the organic layer was washed with water and brine, dried over Na_2SO_4, filtered and evaporated under reduced pressure to give the corresponding naphthofuranylacetic acid.

4-Hydroxybenzohydrazide (1)

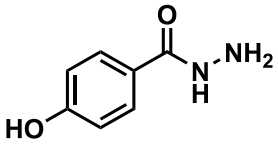

In a 25 mL round bottom flask hydrazine hydrate (98%, 3.24 g, 68.4 mmol, 4.00 eq.) was added to methyl 4-hydroxybenzoate (2.60 g, 17.1 mmol, 1.00 eq.). After refluxing for 5 h, the resulting solid was collected by filtration and dried *in vacuo* to afford the product as a white solid (2.42 g, 15.9 mmol, 93%). **^{1}H-NMR** (DMSO-d_6, 300 MHz, 298 K): δ (ppm) = 4.36 (br s, 2H), 6.77 (d, 2H, ^{3}J = 8.8 Hz), 7.68 (d, 2H, ^{3}J = 8.8 Hz), 9.47 (br s, 1H).**^{13}C-NMR** (DMSO-d_6, 75 MHz, 300 K): δ (ppm) = 114.8, 124.0, 128.8, 156.0, 165.9. **TLC**: R_f = 0.13 (hexane/ethyl acetate = 1:1).

4-(1,3,4-Oxadiazol-2-yl)phenol (2)

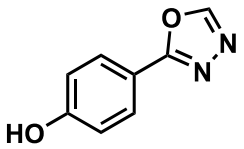

4-Hydroxybenzohydrazide (1.00 g, 6.57 mmol, 1.00 eq.) and triethyl orthoformate (11.7 g, 78.8 mmol, 12.0 eq.) were mixed in a 50 mL round bottom flask and heated under reflux for 18 h. After cooling to room temperature, the remaining triethyl orthoformate was removed *in vacuo*. Purification by column chromatography (SiO_2, 160 mL, 4 cm, hexane/ethyl acetate = 1:1) gave the product (930 mg, 5.73 mmol, 87%) as a white solid. **^{1}H-NMR** (DMSO-d_6, 400 MHz, 298 K): δ (ppm) = 6.95 (d, 2H, ^{3}J = 8.8 Hz), 7.85 (d, 2H, ^{3}J = 8.8 Hz), 9.22 (s, 1H), 10.30 (s, 1H). **^{13}C-NMR** (DMSO-d_6, 101 MHz, 300 K): δ (ppm) = 114.0, 116.2, 128.6, 153.7, 160.8, 163.8. **HRMS** (ESI): m/z calcd for $C_8H_6O_2N_2$ $[M+H]^+$: 163.0500, found: 163.0500. **TLC**: R_f = 0.36 (hexane/ethyl acetate = 1:1).

1-(Chloromethyl)-3*H*-benzo[*f*]chromen-3-one (3)

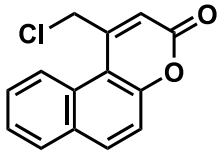

Following general procedure (II), 2-naphthol (2.02 g, 14.0 mmol, 1.00 eq.) and ethyl 4-chloroacetoacetate (2.63 g, 16.0 mmol, 1.14 eq.) were combined in a 50 mL round bottom flask and cooled to 0 °C. After adding concentrated H_2SO_4 (98%, 5 mL) over a period of 30 min, the

reaction mixture was stirred at room temperature for 3 h. Afterwards, the mixture was poured into ice water and stirred for another hour to give an off-white precipitate. The solid was filtered off, washed with cooled water and ether and dried *in vacuo* to give the product (3.16 g, 12.9 mmol, 92%) as an off-white solid. **^{1}H-NMR** (DMSO-d_6, 400 MHz, 298 K): δ (ppm) = 5.07 (s, 2H), 6.75 (s, 1H), 7.50 (d, 1H, ^{3}J = 8.9 Hz), 7.59 (ddd, 1H, ^{3}J = 8.0 Hz, ^{3}J = 6.9 Hz, ^{4}J = 1.0 Hz), 7.71 (ddd, 1H, ^{3}J = 8.6 Hz, ^{3}J = 6.9 Hz, ^{4}J = 1.5 Hz), 7.95 (dd, 1H, ^{3}J = 8.1 Hz, ^{4}J = 1.5 Hz), 8.02 (d, 1H, ^{3}J = 8.9 Hz), 8.42 (d, 1H, ^{3}J = 8.8 Hz). **^{13}C-NMR** (DMSO-d_6, 75 MHz, 300 K): δ (ppm) = 46.0, 112.7, 117.6, 118.0, 125.1, 126.0, 128.7, 129.0, 130.1, 131.5, 134.5, 151.4, 155.3, 160.1. **TLC**: R_f = 0.86 (hexane/ethyl acetate = 1:2).

2-(Naphtho[2,1-*b*]furan-1-yl)acetic acid (4)

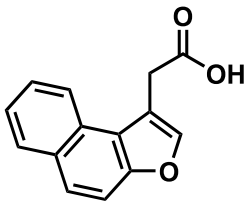

Following general procedure (IV), a suspension of 1-(Chloromethyl)-3*H*-benzo[*f*]chromen-3-one (3.16 g, 12.9 mmol, 1.00 eq.) in $NaOH_{aq}$ (40 mL, 6 M, 0.24 mol) was stirred at 80 °C for 20 h. After cooling to room temperature, the reaction mixture was acidified with HCl_{aq} (35 mL, 6 M, 0.21 mol) and extracted with ethyl acetate (4 · 80 mL). The organic extracts were washed with 80 mL water and brine respectively, dried over Na_2SO_4 and evaporated under vacuum. The title compound was obtained as a brown solid (2.80 g, 12.4 mmol, 96%). **^{1}H-NMR** (DMSO-d_6, 400 MHz, 298 K): δ (ppm) = 4.06 (s, 2H), 7.52 (ddd, 1H, ^{3}J = 8.1 Hz, ^{3}J = 6.9 Hz, ^{4}J = 1.2 Hz), 7.61 (ddd, 1H, ^{3}J = 8.3 Hz, ^{3}J = 6.9 Hz, ^{4}J = 1.4 Hz), 7.78 (d, 1H, ^{3}J = 8.9 Hz), 7.85 (d, 1H, ^{3}J = 9.0 Hz), 8.03 (s, 1H), 8.05 (br d, 1H, ^{3}J = 8.0 Hz), 8.19 (br d, 1H, ^{3}J = 7.9 Hz), 12.62 (s, 1H). **^{13}C-NMR** (DMSO-d_6, 101 MHz, 300 K): δ (ppm) = 30.9, 112.6, 115.7, 121.1, 123.0, 124.3, 125.6, 126.4, 127.9, 128.9, 130.3, 143.6, 152.6, 172,2. **TLC**: R_f = 0.15 (hexane/ethyl acetate = 1:2).

4-(1,3,4-Oxadiazol-2-yl)phenyl-2-(naphtho[2,1-*b*]furan-1-yl)acetate (AV167)

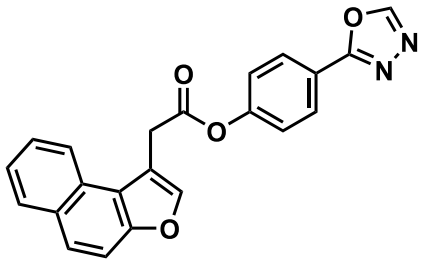

Following general procedure (I), 2-(naphtho[2,1-*b*]furan-1-yl)acetic acid (200 mg, 0.88 mmol, 1.00 eq.) was suspended in dry CH_2Cl_2 (5 mL). Addition of EDCI (224 mg, 1.17 mmol, 1.32 eq.), DMAP (54.0 mg, 0.44 mmol, 0.50 eq.) and then 4-(1,3,4-oxadiazol-2-yl)phenol (172 mg, 1.06 mmol, 1.20 eq.) gave a clear solution which was stirred at room temperature for 17 h. The mixture was diluted with CH_2Cl_2 (10 mL) and subsequently washed with saturated $NaHCO_3$ solution, water and brine. The organic extracts were dried over Na_2SO_4 and evaporated under reduced pressure. Purification by column chromatography (SiO_2, 180 mL, 4 cm, hexane/ethyl acetate = 1:1) gave the product (70.1 mg, 190 µmol, 21%) as a brown solid. **^{1}H-NMR** ($CDCl_3$, 300 MHz, 298 K): δ (ppm) = 4.37 (d, 2H, ^4J = 0.9 Hz), 7.21 – 7.26 (m, 2H), 7.52 (ddd, 1H, ^3J = 8.1, 7.0 Hz, ^4J = 1.2 Hz), 7.64 (ddd, 1H, ^3J = 8.4, 7.0 Hz, ^4J = 1.4 Hz), 7.68 (d, 1H, ^3J = 9.0 Hz), 7.78 (d, 1H, ^3J = 9.0 Hz), 7.86 (s, 1H), 8.00 (*br* d, 1H, ^3J = 8.1 Hz), 8.07 (d, 2H, ^3J = 8.9 Hz), 8.32 (*br* d, 1H, ^3J = 8.4 Hz), 8.44 (s, 1H). **^{13}C-NMR** ($CDCl_3$, 75 MHz, 298 K): δ (ppm) = 32.1, 112.9, 114.1, 121.0, 121.5, 122.6, 122.8, 124.6, 126.3, 126.8, 128.4, 128.7, 129.5, 131.0, 143.1, 152.8, 153.5, 153.7, 169.0. **HRMS** (ESI): *m/z* calcd for $C_{22}H_{14}N_2O_4$ $[M+H]^+$: 371.1023, found: 371.1026. **TLC**: R_f = 0.46 (hexane/ethyl acetate = 1:1).

Phenyl 2-(naphtho[2,1-*b*]furan-1-yl)acetate (5)

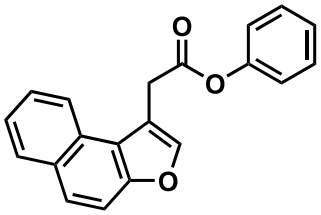

Following general procedure (I), 2-(naphtho[2,1-*b*]furan-1-yl)acetic acid (30.0 mg, 133 µmol, 1.00 eq.) was suspended in dry CH_2Cl_2 (1 mL). Addition of EDCI (38.1 mg, 199 µmol, 1.50 eq.), DMAP (8.19 mg, 67.0 µmol, 0.50 eq.) and phenol (15.1 mg, 160 µmol, 1.20 eq.) gave a clear solution which was stirred under argon atmosphere at room temperature for 16 h. Afterwards, CH_2Cl_2 (2 mL) was added and the reaction mixture was washed with saturated aqueous $NaHCO_3$ solution, water and brine and dried over Na_2SO_4. The solvent was evaporated under reduced pressure and the resulting crude product was purified by column chromatography (SiO_2, 150 mL, 4 cm, hexane/ethyl acetates = 3:1) to give the product (21.7 mg, 71.8 µmol, 54%) as a yellow solid. **^{1}H-NMR** ($CDCl_3$, 300 MHz, 298 K): δ (ppm) = 4.34 (d, 2H, ^4J = 1.0 Hz), 7.06 (d, 2H, ^3J = 7.6 Hz), 7.21 (t, 1H, ^3J = 7.4 Hz), 7.33 – 7.37 (m, 2H), 7.51 (ddd, 1H, ^3J = 8.0, 6.8 Hz, ^4J = 0.9 Hz), 7.63 (ddd, 1H, ^3J = 8.2, 6.8 Hz, ^4J = 1.1 Hz), 7.67 (d, 1H, ^3J = 8.9 Hz), 7.76 (d, 1H, ^3J = 8.9 Hz), 7.86 (s, 1H), 7.99 (d, 1H, ^3J = 8.1 Hz), 8.34 (d, 1H, ^3J = 8.3 Hz). **^{13}C-NMR** ($CDCl_3$, 101 MHz, 300 K):

δ (ppm) = 32.1, 112.9, 114.5, 121.1, 121.6, 123.0, 124.5, 126.2, 126.2, 126.7, 128.5, 129.4, 129.6, 131.0, 143.1, 150.8, 153.7, 169.5. **HRMS** (ESI): *m/z* calcd for $C_{20}H_{14}O_3$ $[M+H]^+$: 303.1014, found: 303.1014. **TLC**: R_f = 0.57 (hexane/ethyl acetate = 3:1).

4-Methoxyphenyl 2-(naphtho[2,1-*b*]furan-1-yl)acetate (6)

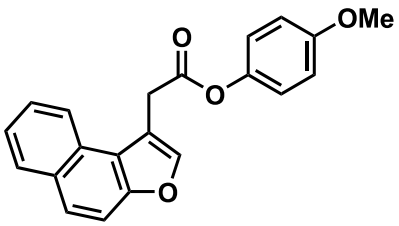

Following general procedure (I), 2-(naphtho[2,1-*b*]furan-1-yl)acetic acid (30.0 mg, 133 μmol, 1.00 eq.) was suspended in dry CH_2Cl_2 (1 mL) and EDCI (38.3 mg, 200 μmol, 1.50 eq.), DMAP (8.19 mg, 67.0 μmol, 0.50 eq.) and 4-methoxyphenol (20.0 mg, 160 μmol, 1.20 eq.) were added. The reaction mixture was stirred under argon atmosphere at room temperature for 15 h. Afterwards, the mixture was diluted with CH_2Cl_2 (2 mL), washed with saturated aqueous $NaHCO_3$ solution, water and brine and dried over Na_2SO_4. The organic solvent was removed under reduced pressure and the crude product was purified by column chromatography (SiO_2, 140 mL, 4 cm, hexane/ethyl acetate = 3:1). The prodcut (31.0 mg, 93.0 μmol, 70%) was isolated as a pale yellow solid. **^{1}H-NMR** ($CDCl_3$, 400 MHz, 298 K): δ (ppm) = 3.77 (s, 3H), 4.32 (d, 2H, ^4J = 1.0 Hz), 6.85 (d, 2H, ^3J = 9.2 Hz), 6.97 (d, 2H, ^3J = 9.2 Hz), 7.51 (ddd, 1H, ^3J = 8.1, 6.9 Hz, ^4J = 1.2 Hz), 7.62 (ddd, 1H, ^3J = 8.3, 6.9 Hz, ^4J = 1.3 Hz), 7.67 (d, 1H, ^3J = 9.0 Hz), 7.76 (d, 1H, ^3J = 9.0 Hz), 7.85 (s, 1H), 7.98 (*br* d, 1H, ^3J = 8.1 Hz), 8.33 (d, 1H, ^3J = 8.4 Hz). **^{13}C-NMR** ($CDCl_3$, 101 MHz, 300 K): δ (ppm) = 32.1, 55.7, 112.9, 114.6, 114.6, 121.1, 122.3, 123.0, 124.5, 126.2, 126.7, 128.5, 129.4, 131.0, 143.1, 144.3, 153.6, 157.5, 169.9. **HRMS** (ESI): *m/z* calcd for $C_{21}H_{16}O_4$ $[M+H]^+$: 333.1119, found: 333.1120. **TLC**: R_f = 0.44 (hexane/ethyl acetate = 3:1).

Methyl 4-(2-(naphtho[2,1-*b*]furan-1-yl)acetoxy)benzoate (7)

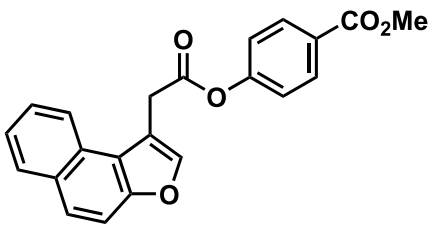

According to general procedure (I), 2-(naphtho[2,1-*b*]furan-1-yl)acetic acid (30.0 mg, 133 μmol, 1.00 eq.) was suspended in dry CH_2Cl_2 (1 mL). EDCI (38.3 mg, 200 μmol, 1.50 eq.), DMAP (8.19 mg, 67.0 μmol, 0.50 eq.) and methyl 4-hydroxybenzoate (24.3 mg, 160 μmol, 1.20 eq.) were

added and the mixture was stirred under argon atmosphere at room temperature for 19 h. Afterwards, the reaction mixture was diluted with CH_2Cl_2 (2 mL), washed with saturated aqueous $NaHCO_3$ solution, water and brine and dried over Na_2SO_4. Purification of the crude product by column chromatography (SiO_2, 130 mL, 4 cm, hexane/ethyl acetates = 3:1) resulted in a white solid (25.4 mg, 70.0 µmol, 53%). **^{1}H-NMR** ($CDCl_3$, 400 MHz, 298 K): δ (ppm) = 3.90 (s, 3H), 4.36 (d, 2H, ^4J = 0.9 Hz), 7.14 (d, 2H, ^3J = 8.9 Hz), 7.52 (ddd, 1H, ^3J = 8.1, 7.0 Hz, ^4J = 1.2 Hz), 7.62 (ddd, 1H, ^3J = 8.3, 7.0 Hz, ^4J = 1.3 Hz), 7.68 (d, 1H, ^3J = 9.0 Hz), 7.77 (d, 1H, ^3J = 9.0 Hz), 7.86 (s, 1H), 7.99 (*br* d, 1H, ^3J = 8.2 Hz), 8.04 (d, 2H, ^3J = 8.9 Hz), 8.31 (br s, 1H, ^3J = 8.3 Hz). **^{13}C-NMR** ($CDCl_3$, 101 MHz, 300 K): δ (ppm) = 32.1, 52.4, 112.9, 114.2, 121.0, 121.6, 122.9, 124.6, 126.3, 126.8, 128.1, 128.4, 129.5, 131.0, 131.3, 143.1, 153.7, 154.3, 166.4, 169.0. **HRMS** (ESI): *m/z* calcd for $C_{22}H_{16}O_5$ $[M+H]^+$: 361.1071, found: 361.1071. **TLC**: R_f = 0.45 (hexane/ethyl acetate = 3:1).

4-Nitrophenyl 2-(naphtho[2,1-*b*]furan-1-yl)acetate (8)

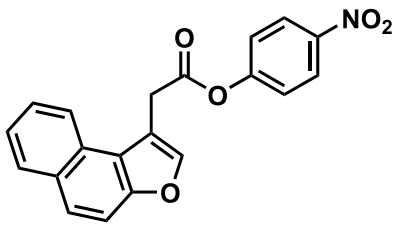

Following general procedure (I), 2-(naphtho[2,1-*b*]furan-1-yl)acetic acid (30.0 mg, 133 µmol, 1.00 eq.) was suspended in dry CH_2Cl_2 (1 mL). Addition of EDCI (38.3 mg, 200 µmol, 1.50 eq.), DMAP (8.19 mg, 67.0 µmol, 0.50 eq.) and 4-nitrophenol (22.3 mg, 160 µmol, 1.20 eq.) gave a clear solution which was stirred under argon atmosphere at room temperature for 19 h. After this time the reaction mixture was diluted with CH_2Cl_2 (2 mL), washed with saturated aqueous $NaHCO_3$ solution, water and brine and dried over Na_2SO_4. After purification by column chromatography (SiO_2, 130 mL, 4 cm, hexane/ethyl acetate = 3:1), the product (13.3 mg, 38.0 µmol, 29%) was isolated as yellow solid. **^{1}H-NMR** ($CDCl_3$, 400 MHz, 298 K): δ (ppm) = 4.38 (d, 2H, ^4J = 0.9 Hz), 7.24 (d, 2H, ^3J = 9.2 Hz), 7.53 (ddd, 1H, ^3J = 8.1, 7.0 Hz, ^4J = 1.2 Hz), 7.63 (ddd, 1H, ^3J = 8.3, 7.0 Hz, ^4J = 1.4 Hz), 7.69 (d, 1H, ^3J = 9.0 Hz), 7.79 (d, 1H, ^3J = 9.0 Hz), 7.86 (s, 1H), 8.00 (*br* d, 1H, ^3J = 8.1 Hz), 8.24 (d, 2H, ^3J = 9.2 Hz), 8.29 (*br* d, 1H, ^3J = 8.4 Hz). **^{13}C-NMR** ($CDCl_3$, 126 MHz, 300 K): δ (ppm) = 32.1, 113.0, 113.9, 120.8, 122.5, 122.7, 124.7, 125.4, 126.4, 126.8, 128.3, 129.6, 131.0, 143.2, 145.6, 153.7, 155.4, 168.7. **HRMS** (APCI): *m/z* calcd for $C_{20}H_{13}NO_5$ $[M+H]^+$: 348.0866, found: 348.0867. **TLC**: R_f = 0.44 (hexane/ethyl acetate = 3:1).

4-(Methylsulfonyl)phenyl 2-(naphtho[2,1-*b*]furan-1-yl)acetate (9)

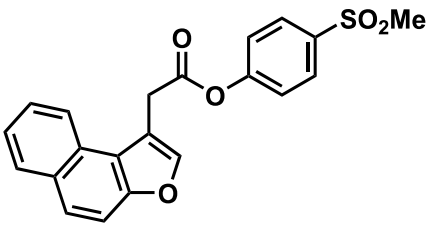

According to general procedure (I), 2-(naphtho[2,1-*b*]furan-1-yl)acetic acid (100 mg, 442 µmol, 1.00 eq.) was dissolved in dry CH_2Cl_2 (3 mL) and EDCI (127 mg, 663 µmol, 1.50 eq.), DMAP (27.0 mg, 221 µmol, 0.50 eq.) and 4-(methylsulfonyl) phenol (91.3 mg, 530 µmol, 1.20 eq.) were added. The resulting brown solution was stirred at room temperature under argon atmosphere for 24 h and then diluted with CH_2Cl_2 (10 mL). The organic phase was washed with saturated $NaHCO_3$ solution, water and brine (10 mL) and dried over Na_2SO_4. After evaporation of the organic solvent the crude product was purified by column chromatography (SiO_2, 220 mL, 4 cm, hexane/ethyl acetate = 3:1). The product (34.8 mg, 91.0 µmol, 21%) was isolated as yellow-brown solid. **^{1}H-NMR** ($CDCl_3$, 400 MHz, 298 K) δ (ppm) = 3.03 (s, 3H), 4.38 (d, 2H, ^4J = 1.0 Hz), 7.25 – 7.29 (m, 2H), 7.52 (ddd, 1H, ^3J = 8.1, 6.9 Hz, ^4J = 1.2 Hz), 7.62 (ddd, 1H, ^3J = 8.3, 7.0 Hz, ^4J = 1.4 Hz), 7.68 (d, 1H, ^3J = 9.0 Hz), 7.78 (d, 1H, ^3J = 9.0 Hz), 7.92 – 7.96 (m, 2H), 7.98 – 8.01 (m, 1H), 8.29 (dd, 1H, ^3J = 8.4 Hz, ^4J = 1.1 Hz). **^{13}C-NMR** ($CDCl_3$, 126 MHz, 300 K) δ (ppm) = 32.08, 44.78, 112.96, 113.92, 120.86, 122.70, 122.73, 124.65, 126.39, 126.78, 128.32, 129.40, 129.54, 130.99, 138.19, 143.17, 153.72, 154.69, 168.86. **HRMS** (ESI) *m/z* calcd for $C_{21}H_{16}SO_5$ $[M+H]^+$: 381.0791, found: 381.0788. **TLC**: R_f = 0.22 (hexane/ethyl acetate = 2:1).

1-(Chloromethyl)-9-methoxy-3*H*-benzo[*f*]chromen-3-one (10)

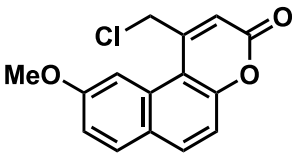

In a 25 mL round bottom flask, 7-methoxy-2-naphthol (500 mg, 2.87 mmol, 1.00 eq.) and ethyl 4-chloroacetoacetate (540 mg, 3.27 mmol, 1.14 eq.) were mixed and cooled to 0 °C. Concentrated H_2SO_4 (98%, 1 mL) was added over a period of 15 min and the reaction mixture was stirred for 3 h at room temperature. Afterwards, the reaction mixture was poured into ice water and stirred for another 3 h. The resulting yellow-brown precipitate was collected by filtration, washed with water and dried *in vacuo*. The crude product was purified by column chromatography (SiO_2, 300 mL, 8 cm, hexane/ethyl acetate = 2:1 → 1:2) to give the product (370 mg, 1.35 mmol, 47%) as a bright yellow

solid. **^{1}H-NMR** ($CDCl_3$, 400 MHz, 298 K): δ (ppm) = 4.01 (s, 3H), 5.01 (s, 2H), 6.63 (s, 1H), 7.24 (dd, 1H, ^3J = 8.9 Hz, ^4J = 2.3 Hz), 7.34 (d, 1H, ^3J = 8.9 Hz), 7.81 – 7.87 (m, 2H), 7.94 (d, 1H, ^3J = 8.8 Hz). **^{13}C-NMR** ($CDCl_3$, 101 MHz, 300 K): δ (ppm) = 45.8, 55. 8, 106.0, 112.1, 115.4, 117.3, 117.6, 126.6, 130.5, 131.4, 134.2, 151.2, 156.1, 160.0. **TLC**: R_f = 0.50 (hexane/ethyl acetate = 2:1).

2-(8-Methoxynaphtho[2,1-*b*]furan-1-yl)acetic acid (11)

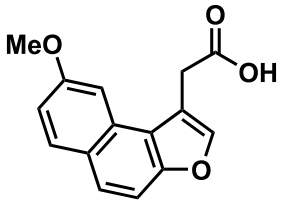

Following general procedure (IV), a suspension of 1-(chloromethyl)-9-methoxy-3*H*-benzo[*f*]chromen-3-one (324 mg, 1.18 mmol, 1.00 eq.) in $NaOH_{aq}$ (8 mL, 6 M, 48.0 mmol) was heated under reflux for 20 h. Afterwards, the mixture was cooled to room temperature and acidified with HCl_{aq} (10 mL, 6 M, 60.0 mmol) until pH = 5 – 6 was reached. The suspension was extracted with ethyl acetate (4 · 15 mL), the organic extracts were washed with water and brine, dried over Na_2SO_4 and evaporated under reduced pressure. The product (288 mg, 1.12 mmol, 95%) was obtained as a brown solid. **^{1}H-NMR** (DMSO-d_6, 400 MHz, 298 K): δ (ppm) = 3.91 (s, 3H), 4.05 (s, 2H), 7.16 (dd, 1H, ^3J = 8.9 Hz, ^4J = 2.5 Hz), 7.57 (d, 1H, ^4J = 2.4 Hz), 7.59 (d, 1H, ^3J = 8.9 Hz), 7.76 (d, 1H, ^3J = 8.9 Hz), 7.95 (d, 1H, ^3J = 9.0 Hz), 7.97 (s, 1H) 12.66 (br s, 1H). **^{13}C-NMR** (DMSO-d_6, 101 MHz, 300 K): δ (ppm) = 30.9, 55.0, 103.0, 110.1, 115.6, 115.8, 120.5, 125.2, 125.4, 129.1, 130.4, 143.2, 153.2, 157.7, 172.5. **TLC**: R_f = 0.29 (CH_2Cl_2, 5% CH_3OH).

4-(1,3,4-Oxadiazol-2-yl)phenyl 2 (8-methoxynaphtho[2,1-*b*]furan-1-yl)acetate (12)

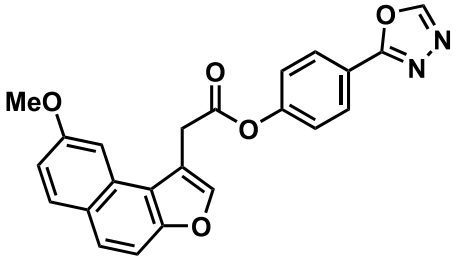

Following general procedure (I), 2-(8-methoxynaphtho[2,1-*b*]furan-1-yl)acetic acid (100 mg, 390 μmol, 1.00 eq.) was suspended in dry CH_2Cl_2 (4 mL). EDCI (112 mg, 584 μmol, 1.50 eq.), DMAP (24.0 mg, 196 μmol, 0.50 eq.) and 4-(1,3,4-oxadiazol-2-yl)phenol (76.0 mg, 469 μmol, 1.20 eq.) were added and the resulting mixture was stirred under argon atmosphere at room temperature for 24 h. After this time the reaction mixture was diluted with CH_2Cl_2 (8 mL), washed

with saturated $NaHCO_3$ solution, water and brine, dried over Na_2SO_4 and evaporated under reduced pressure. The crude product was purified by silica gel column chromatography (SiO_2, 160 mL, 4 cm, hexane/ethyl acetate = 1:1) to give phenyl ester **12** (67.2 mg, 108 µmol, 43%) as a slightly yellow solid. **^{1}H-NMR** ($CDCl_3$, 400 MHz, 298 K): δ (ppm) = 3.95 (s, 3H), 4.33 (d, 2H, J = 0.9 Hz), 7.16 – 7.22 (m, 3H), 7.53 (d, 1H, ^3J = 9.0 Hz), 7.69 – 7.72 (m, 2H), 7.81 (s, 1H), 7.89 (d, 1H, ^3J = 9.0 Hz), 8.11 (d, 2H, ^3J = 8.9 Hz), 8.44 (s, 1H). **^{13}C-NMR** ($CDCl_3$, 101 MHz, 300 K): δ (ppm) = 32.3, 55.6, 103.1, 110.5, 114.0, 116.0, 120.3, 121.5, 126.0, 126.2, 128.7, 129.6, 130.9, 142.9, 152.8, 153.5, 154.4, 158.6, 164.2, 169.2. **HRMS** (ESI): m/z calcd for $C_{23}H_{16}N_2O_5$ $[M+H]^+$: 401.1121, found: 401.1123. **TLC**: R_f = 0.57 (hexane/ethyl acetate = 2:3).

4-(Chloromethyl)-6-methyl-2*H*-chromen-2-one (13)

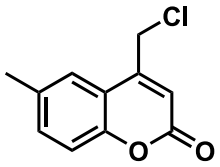

According to general procedure (II) 4-methylphenol (300 mg, 2.77 mmol, 1.00 eq.) was mixed with ethyl 4-chloroacetoacetate (460 mg, 2.77 mmol, 1.00 eq.) in a 50 mL round bottom flask. H_2SO_4 (70% (v/v), 2.5 mL) was added under ice cooling over 15 min. The resulting brown solution was stirred at room temperature for 18 h. Afterwards, the reaction mixture was poured onto ice water to give a greyish precipitate. The solid was filtered off washed with cold water and dried *in vacuo* to yield the product (432 mg, 2.07 mmol, 74%). **^{1}H-NMR** ($CDCl_3$, 400 MHz, 298 K): δ (ppm) = 2.44 (s, 3H), 4.67 (d, 2H, ^4J = 0.9 Hz), 6.56 (s, 1H), 7.28 (virt. s, 1H), 7.38 (dd, 1H, ^3J = 8.5 Hz, ^4J = 1.8 Hz), 7.43 (s, 1H). **^{13}C-NMR** ($CDCl_3$, 101 MHz, 300 K): δ (ppm) = 21.2, 41.4, 116.0, 117.2, 117.4, 124.0, 133.4, 134.4, 149.5, 152.2, 160.6. **HRMS** (ESI): m/z calcd for $C_{11}H_9ClO_2$ $[M+H]^+$: 209.0360, found: 209.0360.

4-(Chloromethyl)-6-methoxy-2*H*-chromen-2-one (14)

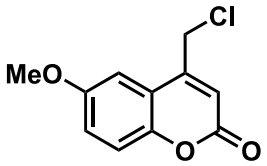

Following general procedure (II), 4-methoxyphenol (300 mg, 2.42 mmol, 1.00 eq.) was mixed with ethyl 4-chloroacetoacetate (400 mg, 2.42 mmol, 1.00 eq.) in a 50 mL round bottom flask and cooled to 0 °C. After addition of H_2SO_4 (70%, 2.5 mL) the reaction mixture was allowed to warm to room temperature and stirred for 18 h. After this time the mixture was poured onto ice water with

additional stirring for 1 h. The crude product was purified by column chromatography (SiO_2, 190 mL, 4 cm, hexane/ethyl acetate = 2:1) to give the product (277 mg, 1.23 mmol, 31%) as a bright yellow solid. **^{1}H-NMR** ($CDCl_3$, 300 MHz, 298 K): δ (ppm) = 3.87 (s, 3H), 4.65 (d, 2H, ^4J = 0.9 Hz), 6.58 (s, 1H), 7.09 (d, 1H, ^4J = 2.8 Hz), 7.15 (dd, 1H, ^3J = 9.0 Hz, ^4J = 2.9 Hz), 7.32 (d, 1H, ^3J = 9.0 Hz). **^{13}C-NMR** ($CDCl_3$, 75 MHz, 300 K): δ (ppm) = 41.5, 56.1, 107.4, 116.5, 117.9, 118.6, 119.5, 148.4, 149.2, 156.3, 160.5. **HRMS** (ESI): *m/z* calcd for $C_{11}H_9ClO_3$ $[M+H]^+$: 225.0309, found: 225.0309. **TLC**: R_f = 0.52 (hexane/ethyl acetate = 2:1).

4-(Chloromethyl)-7-methoxy-2*H*-chromen-2-one (15)

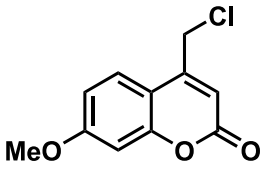

According to general procedure (II), 3-methoxyphenol (300 mg, 2.42 mmol, 1.00 eq.) was combined with ethyl 4-chloroacetoacetate (400 mg, 2.42 mmol, 1.00 eq.) in a 50 mL round bottom flask. Under ice cooling H_2SO_4 (70%, 3 mL) was added and the reaction mixture was stirred at room temperature for 18 h. Afterwards, the mixture was poured onto ice water and was stirred for 1 h. The crude product was filtered off and recrystallized from ethanol to afford the title compound (276 mg, 1.23 mmol, 51%) as colourless solid. **^{1}H-NMR** (DMSO-d_6, 400 MHz, 298 K): δ (ppm) = 3.87 (s, 3H), 4.99 (d, 2H, ^4J = 0.7 Hz), 6.50 (s, 1H), 7.01 (dd, 1H, ^3J = 8.8 Hz, ^4J = 2.5 Hz), 7.04 (d, 1H, ^4J = 2.4 Hz), 7.76 (d, 1H, ^3J = 8.8 Hz). **^{13}C-NMR** (DMSO-d_6, 101 MHz, 300 K): δ (ppm) = 41.3, 56.0, 101.1, 110.4, 112.0, 112.3, 126.4, 150.8, 155.2, 160.0, 162.6.

2-(5-Methylbenzofuran-3-yl)acetic acid (16)

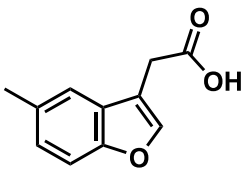

According to general procedure (III), 4-(chloromethyl)-6-methyl-2*H*-chromen-2-one (427 mg, 2.05 mmol, 1.00 eq.) was suspended in $NaOH_{aq}$ (15 mL, 1 M, 15.0 mmol) and heated under reflux for 1 h. After cooling to room temperature, the reaction mixture was acidified with HCl_{aq} (15 mL, 1 M, 15.0 mmol) and stirred for 1 h. The resulting greyish precipitate was collected by filtration washed with water and dried *in vacuo*. The product (245 mg, 1.29 mmol, 63%) was obtained as a greyish solid. **^{1}H-NMR** (DMSO-d_6, 400 MHz, 298 K): δ (ppm) = 2.39 (s, 3H), 3.65 (d, 2H, ^4J =

0.9 Hz), 7.12 (dd, 1H, ^3J = 8.4 Hz, ^4J = 1.7 Hz), 7.36 – 7.38 (m, 1H), 7.43, (d, 1H, ^3J = 8.4 Hz), 7.83 (s, 1H), 12.45 (s, 1H). **^{13}C-NMR** (DMSO-d_6, 101 MHz, 300 K): δ (ppm) = 20.9, 29.0, 110.8, 113.7, 119.7, 125.4, 127.8, 131.4, 143.5, 152.9, 171.9. **HRMS** (ESI): *m/z* calcd for $C_{11}H_{10}O_3$ [M-H]$^-$: 189.0557, found: 189.0556.

2-(5-Methoxybenzofuran-3-yl)acetic acid (17)

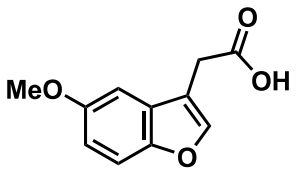

Following general procedure (III), 4-(chloromethyl)-6-methoxy-2*H*-chromen-2-one (272 mg, 1.21 mmol, 1.00 eq.) was suspended in $NaOH_{aq}$ (15 mL, 1 M, 15.0 mmol) and heated under reflux for 1 h. The resulting pale yellow solution was acidified with 1 M HCl_{aq} until pH ≈ 5 was reached. A white precipitate formed which was collected by filtration, washed with water and dried under reduced pressure. The product (205 mg, 994 µmol, 82%) was isolated as a white solid. **^{1}H-NMR** (DMSO-d_6, 400 MHz, 298 K): δ (ppm) = 3.66 (d, 2H, ^4J = 0.8 Hz), 3.78 (s, 3H), 6.90 (dd, 1H, ^3J = 8.9 Hz, ^4J = 2.6 Hz), 7.10 (d, 1H, ^4J = 2.6 Hz), 7.45 (d, 1H, ^3J = 8.9 Hz), 7.84 (s, 1H). **^{13}C-NMR** (DMSO-d_6, 101 MHz, 300 K): δ (ppm) = 28.9, 55.6, 102.68, 111.7, 112.7, 114.1, 128.4, 144.2, 149.3, 155.4, 171.9. **HRMS** (ESI): *m/z* calcd for $C_{11}H_{10}O_4$ [M-H]$^-$: 205.0506, found: 205.0506.

2-(6-Methoxybenzofuran-3-yl)acetic acid (18)

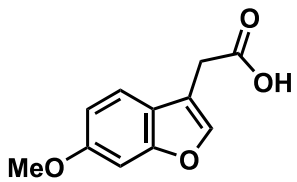

Following general procedure (III), 4-(chloromethyl)-7-methoxy-2*H*-chromen-2-one (206 mg, 917 µmol, 1.00 eq.) was suspended in $NaOH_{aq}$ (10 mL, 1 M, 10.0 mmol) and heated under reflux for 1 h. The clear orange solution was cooled to room temperature and acidified with 1 M HCl_{aq}. After stirring for 30 min, the resulting greyish precipitate was filtered off, washed with water and dried *in vacuo* to give the product (107 mg, 519 µmol, 56%). **^{1}H-NMR** (DMSO-d_6, 400 MHz, 298 K): δ (ppm) = 3.64 (s, 2H), 3.79 (s, 3H), 6.88 (dd, 1H, ^3J = 8.6 Hz, ^4J = 2.2 Hz), 7.16 (d, ^4J = 2.1 Hz), 7.46 (d, 1H, ^3J = 8.6 Hz), 7.76 (s, 1H), 12.41 (*br* s, 1H). **^{13}C-NMR** (DMSO-d_6, 101 MHz, 300 K): δ (ppm) = 29.0, 55.6, 95.9, 111.5, 113.8, 120.2, 120.9, 142.3, 155.5, 157.7, 171.9.

4-(1,3,4-Oxadiazol-2-yl)phenyl 2-(benzofuran-3-yl)acetate (19)

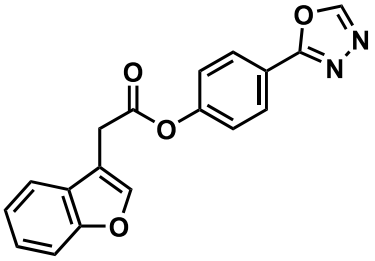

According to general procedure (I), 2-(benzofuran-3-yl)acetic acid (82.0 mg, 465 μmol, 1.00 eq.) was dissolved in dry CH_2Cl_2 (2.5 mL). To this solution EDCI (178 mg, 931 μmol, 2.00 eq.), DMAP (28.0 mg, 229 μmol, 0.50 eq.) and 4-(1,3,4-oxadiazol-2-yl)phenol (90.0 mg, 555 μmol, 1.20 eq.) were added. Afterwards, the mixture was stirred under argon atmosphere at room temperature for 21 h. Dilution with CH_2Cl_2 (5 mL) gave a yellow solution which was washed with saturated aqueous $NaHCO_3$ solution, water and brine and dried over Na_2SO_4. The solvent was evaporated under reduced pressure. The product (74.4 mg, 232 μmol, 50%) was isolated after column chromatography (SiO_2, 130 mL, 4 cm, hexane/ethyl acetate = 1:1) as a white solid. **^{1}H-NMR** ($CDCl_3$, 400 MHz, 298 K): δ (ppm) = 4.00 (d, 2H, ^4J = 1.1 Hz), 7.25 – 7.29 (m, 2H), 7.31 (dd, ^3J = 7.5 Hz, ^4J = 1.2 Hz), 7.35 (td, 1H, ^3J = 8.2, 7.8 Hz, ^4J = 1.5 Hz), 7.51 – 7.54 (m, 1H), 7.64 – 7.67 (m, 1H), 7.74 (s, 1H), 8.11 (d, 2H, ^3J = 8.9 Hz), 8.46 (s, 1H). **^{13}C-NMR** ($CDCl_3$, 101 MHz, 300 K): δ (ppm) = 30.2, 111.9, 112.4, 119.7, 121.5, 122.5, 123.0, 124.9, 127.5, 128.7, 143.3, 152.8, 153.5, 155.4, 164.2, 168.8. **HRMS** (ESI): *m/z* calcd for $C_{18}H_{12}N_2O_4$ $[M+H]^+$: 321.0868, found: 321.0868. **TLC**: R_f = 0.51 (hexane/ethyl acetate = 1:1).

4-(1,3,4-Oxadiazol-2-yl)phenyl 2-(5-methylbenzofuran-3-yl)acetate (20)

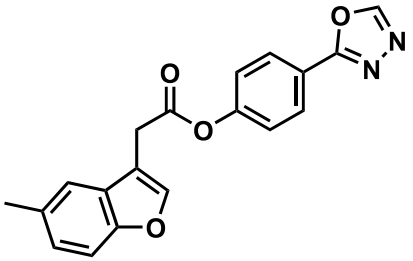

Following general procedure (I), 2-(5-methylbenzofuran-3-yl)acetic acid (100 mg, 526 μmol, 1.00 eq.) was dissolved in dry CH_2Cl_2 (4 mL). After addition of EDCI (151 mg, 790 μmol, 1.50 eq.), DMAP (32.0 mg, 262 μmol, 0.50 eq.) and 4-(1,3,4-oxadiazol-2-yl)phenol (102 mg, 629 μmol, 1.20 eq.) the resulting suspension was stirred at room temperature for 17 h under argon atmosphere. The reaction mixture was diluted with CH_2Cl_2 (12 mL), washed subsequently with saturated aqueous $NaHCO_3$ solution, water and brine and dried over Na_2SO_4. Afterwards, the

solvent was evaporated on a rotary evaporator under reduced pressure. Purification by column chromatography (SiO_2, 180 mL, 4 cm, hexane/ethyl acetate = 1:1) yielded the product (17.0 mg, 51.0 µmol, 10%) as a pale yellow solid. **^{1}H-NMR** ($CDCl_3$, 300 MHz, 298 K): δ (ppm) = 2.47 (s, 3H), 3.97 (d, 2H, ^4J = 1.0 Hz), 7.15 (dd, 1H, ^3J = 8.4 Hz, ^4J = 1.7 Hz), 7.25 – 7.30 (m, 2H), 7.40 (d, 1H, ^3J = 8.6 Hz), 7.41 – 7.43 (m, 1H), 7.69 (s, 1H), 8.11 (d, 2H, ^3J = 8.9 Hz), 8.46 (s, 1H). **^{13}C-NMR** ($CDCl_3$, 126 MHz, 300 K): δ (ppm) = 21.6, 30.1, 111.4, 112.0, 119.4, 121.4, 122.6, 126.2, 127.5, 128.7, 132.6, 143.4, 152.8, 153.5, 153.8, 164.2, 168.9. **HRMS** (ESI): *m/z* calcd for $C_{19}H_{14}N_2O_4$ $[M+H]^+$: 335.1023, found: 335.1025. **TLC**: R_f = 0.45 (hexane/ethyl acetate = 1:1).

4-(1,3,4-Oxadiazol-2-yl)phenyl 2-(5-methoxybenzofuran-3-yl)acetate (21)

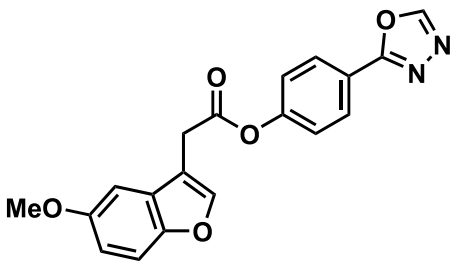

Following general procedure (I), 2-(5-methoxybenzofuran-3-yl)acetic acid (50.0 mg, 242 µmol, 1.00 eq.) was dissolved in dry CH_2Cl_2 (2 mL). Addition of EDCI (93.0 mg, 486 µmol, 2.00 eq.), DMAP (15.0 mg, 123 µmol, 0.50 eq.) and 4-(1,3,4-oxadiazol-2-yl)phenol (47.0 mg, 290 µmol, 1.20 eq.) gave a pale yellow solution which was stirred under argon atmosphere at room temperature for 16 h. After this time the reaction mixture was diluted with CH_2Cl_2 (4 mL), washed with saturated aqueous $NaHCO_3$ solution, water and brine and dried over Na_2SO_4. The organic solvent was removed under reduced pressure and the product (72.6 mg, 207 µmol, 85%) was obtained as a pale brown solid. **^{1}H-NMR** ($CDCl_3$, 400 MHz, 298 K): δ (ppm) = 3.86 (s, 3H), 3.96 (d, 2H, ^4J = 1.0 Hz), 6.95 (dd, 1H, ^3J = 8.9 Hz, ^4J = 2.5 Hz), 7.08 (d, 1H, ^4J = 2.5 Hz), 7.25 – 7.29 (m, 2H), 7.41 (dd, 1H, ^3J = 8.8 Hz, ^5J = 0.4 Hz), 7.71 (*br* s, 1H), 8.11 (d, 2H, ^3J = 8.9 Hz), 8.46 (s, 1H). **^{13}C-NMR** ($CDCl_3$, 101 MHz, 300 K): δ (ppm) = 30.2, 56.2, 102.2, 112.4, 112.4, 113.6, 121.5, 122.5, 128.0, 128.7, 144.1, 150.4, 152.8, 153.5, 156.3, 164.2, 168.7. **HRMS** (ESI): *m/z* calcd for $C_{19}H_{14}N_2O_5$ $[M+H]^+$: 351.0972, found: 351.0973. **TLC**: R_f = 0.44 (hexane/ethyl acetate = 1:1).

4-(1,3,4-Oxadiazol-2-yl)phenyl 2-(6-methoxybenzofuran-3-yl)acetate (22)

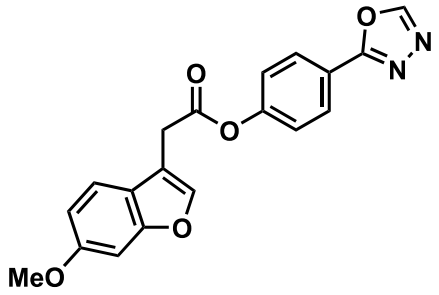

According to general procedure (I), 2-(6-methoxybenzofuran-3-yl)acetic acid (97.0 mg, 470 μmol, 1.00 eq.) was suspended in dry CH_2Cl_2 (2.5 mL). After addition of EDCI (180 mg, 942 μmol, 2.00 eq.), DMAP (29.0 mg, 237 μmol, 0.50 eq.) and 4-(1,3,4-oxadiazol-2-yl)phenol (91.0 mg, 561 μmol, 1.20 eq.), the reaction mixture was stirred under argon atmosphere at room temperature for 18 h. Following that, the mixture was diluted with CH_2Cl_2 (5 mL), washed with saturated aqueous $NaHCO_3$ solution, water and brine and dried over Na_2SO_4. The solvent was evaporated under reduced pressure and the crude product was purified by column chromatography (SiO_2, 130 mL, 4 cm, hexane/ethyl acetate = 1:1) to yield the product (38.1 mg, 109 μmol, 23%) as a white solid. **^{1}H-NMR** ($CDCl_3$, 400 MHz, 298 K): δ (ppm) = 3.87 (s, 3H), 3.96 (d, 2H, ^4J = 0.9 Hz), 6.93 (dd, 1H, ^3J = 8.6 Hz, ^4J = 2.2 Hz), 7.05 (d, 1H, ^4J = 2.2 Hz), 7.26 (d, 2H, ^3J = 8.8 Hz), 7.51 (d, 1H, ^3J = 8.6 Hz), 7.63 (s, 1H), 8.10 (d, 2H, ^3J = 8.8 Hz), 8.46 (s, 1H). **^{13}C-NMR** ($CDCl_3$, 101 MHz, 298 K): δ (ppm) = 30.2, 55.9, 96.3, 112.2, 112.3, 119.8, 120.8, 121.4, 122.6, 128.7, 142.3, 152.8, 153.5, 156.5, 158.5, 164.2, 168.8. **HRMS** (ESI): *m/z* calcd for $C_{19}H_{14}N_2O_5$ $[M+H]^+$: 351.0971, found: 351.0972. **TLC**: R_f = 0.46 (hexane/ethyl acetate = 1:1).

Methyl 2-(naphtho[2,1-*b*]furan-1-yl)acetate (23)

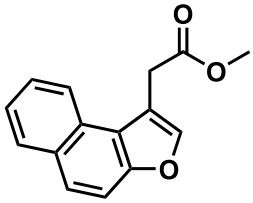

CH_3OH (15 mL) was cooled to 0 °C and concentrated H_2SO_4 (3 mL) was added dropwise. To the resulting clear solution was added 2-(naphtho[2,1-*b*]furan-1-yl)acetic acid (2.50 g, 11.1 mmol, 1.00 eq.) and the mixture was heated under reflux for 5 h. After cooling to room temperature the solvent was removed and the resulting mixture was taken up in CH_2Cl_2 (40 mL). The organic phase was washed with water (40 mL) aqueous $NaHCO_3$ solution (50 mL) and brine and dried over Na_2SO_4. After removing the solvent under reduced pressure the product (2.54 g, 10.6 mmol, 96%)

was obtained as a brownish oil which solidified in the freezer. **^{1}H-NMR** ($CDCl_3$, 400 MHz, 298 K): δ (ppm) = 3.75 (s, 3H), 4.09 (d, 2H, ^4J = 0.9 Hz), 7.49 (ddd, 1H, ^3J = 8.1, 7.0 Hz, ^4J = 1.2 Hz), 7.59 (ddd, 1H, ^3J = 8.3, 7.0 Hz, ^4J = 1.4 Hz), 7.65 (d, 1H, ^3J = 8.9 Hz), 7.74 (d, 1H, ^3J = 9.0 Hz), 7.76 (s, 1H), 7.96 (*br* d, 1H, ^3J = 8.1 Hz), 8.21 (*br* d, 1H, ^3J = 8.4 Hz). **^{13}C-NMR** ($CDCl_3$, 101 MHz, 300 K): δ (ppm) = 31.8, 52.5, 112.8, 114.9, 121.2, 123.0, 124.4, 126.0, 126.6, 128.5, 129.3, 130.9, 142.9, 153.6, 171.4. **HRMS** (APCI): *m/z* calcd for $C_{15}H_{12}O_3$ $[M+H]^+$: 241.0859, found: 241.0860. **TLC**: R_f = 0.29 (hexane/ethyl acetate = 10:1).

Methyl 2-(2-bromonaphtho[2,1-*b*]furan-1-yl)acetate (24)

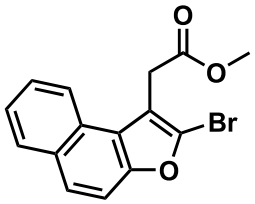

In a 25 mL round bottom flask methyl 2-(naphtho[2,1-*b*]furan-1-yl)acetate (440 mg, 1.85 mmol, 1.00 eq.) was dissolved in $CHCl_3$ (8 mL) and cooled to – 8 °C. In another round bottom flask *N*-bromosuccinimide (360 mg, 2.02 mmol, 1.09 eq.) was dissolved in CH_3CN (8 mL) and was added dropwise to the stirring solution methyl 2-(naphtho[2,1-*b*]furan-1-yl)acetate in $CHCl_3$. After 1 h at – 8 °C the reaction mixture was allowed to warm to room temperature and was then diluted with water (30 mL). This mixture was extracted with $CHCl_3$ (2 · 20 mL), the resulting organic layer was washed with water and brine, dried over Na_2SO_4 and concentrated under reduced pressure. Purification of the crude product by column chromatography (SiO_2, 180 mL, 4 cm, hexane/ethyl acetate = 10:1) gave the product (527 mg, 1.65 mmol, 90%) as a pale brown solid. **^{1}H-NMR** ($CDCl_3$, 300 MHz, 298 K): δ (ppm) = 3.72 (s, 3H), 4.04 (s, 2H), 7.50 (ddd, 1H, ^3J = 8.2, 6.9 Hz, ^4J = 1.2 Hz), 7.59 (*virt.* td, 1H, ^3J = 7.4, 7.0 Hz, ^4J = 1.5 Hz), 7.61 (d, 1H, ^3J = 8.9 Hz), 7.72 (d, 1H, ^3J = 9.0 Hz), 7.94 (*br* d, 1H, ^3J = 8.1 Hz), 8.15 (*br* d, 1H, ^3J = 8.4 Hz). **^{13}C-NMR** ($CDCl_3$, 75 MHz, 300 K): δ (ppm) = 32.45, 52.62, 77.16, 112.05, 114.59, 122.08, 122.81, 124.89, 126.04, 126.94, 127.43, 127.78, 129.32, 130.98, 153.50, 170.59. **HRMS** (APCI): *m/z* calcd for $C_{15}H_{11}BrO_3$ $[M+H]^+$: 318.9964, found: 318.9966. **TLC**: R_f = 0.37 (hexane/ethyl acetate = 10:1).

Methyl 2-(2-iodonaphtho[2,1-*b*]furan-1-yl)acetate (25)

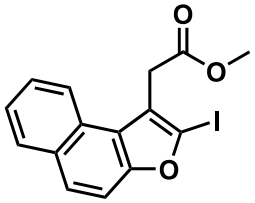

To a solution of methyl 2-(naphtho[2,1-*b*]furan-1-yl)acetate (314 mg, 1.31 mmol, 1.00 eq.) in 3 mL $CHCl_3$ a solution of *N*-iodosuccinimide (322 mg, 1.43 mmol, 1.10 eq.) in 3 mL CH_3CN was added under argon atmosphere at -10 °C. The solution was allowed to warm to room temperature and stirred for six days in the dark. Afterwards, the reaction mixture was diluted with 20 mL $CHCl_3$, extracted with saturated Na_2SO_3 solution and subsequently washed with water and brine (30 mL). The organic solvent was evaporated and the crude material was purified by flash chromatography (SiO_2, 200 mL, 3 cm, hexane/ethyl acetate = 20:1 → 15:1). The product (91.2 mg, 249 µmol, 19%) was isolated as white solid. **^{1}H-NMR** ($CDCl_3$, 400 MHz, 298 K) δ (ppm) =3.75 (s, 3H), 4.09 (d, 2H, ^4J = 1.0 Hz), 7.49 (ddd, 1H, ^3J = 8.1, 7.0 Hz, ^4J = 1.1 Hz), 7.59 (ddd, 1H, ^3J = 8.3, 7.0 Hz, ^4J = 1.3 Hz), 7.65 (d, 1H, ^3J = 8.9 Hz), 7.74 (d, 1H, ^3J = 9.0 Hz), 7.76 (s, 1H), 7.96 (d, 1H, ^3J = 8.3 Hz), 8.22 – 8.19 (m, 1H). **^{13}C-NMR** ($CDCl_3$, 126 MHz, 300 K); 34.24, 52.65, 99.43, 112.16, 121.74, 122.03, 122.82, 124.84, 126.11, 126.98, 127.09, 129.25, 130.79, 156.77, 170.75. **HRMS** (ESI) *m*/*z* calcd for $C_{15}H_{11}IO_3$ $[M+H]^+$: 366.9826, found: 366.9219. **TLC**: R_f = 0.28 (hexane/ethyl acetate = 10:1).

Methyl 2-(2-formylnaphtho[2,1-*b*]furan-1-yl)acetate (26)

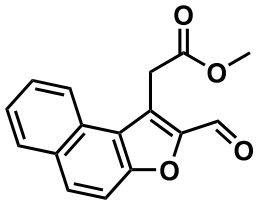

In a 10 mL round bottom flask methyl 2-(naphtho[2,1-*b*]furan-1-yl)acetate (150 mg, 624 µmol, 1.00 eq.) was dissolved in dry DMF (1.11 mL) and cooled to 0 °C. After addition of phosphoryl trichloride (552 mg, 3.60 mmol, 5.80 eq.) the reaction mixture was allowed to warm to room temperature and stirred for 7 h. The solution was then diluted with DMF (2.5 mL) and poured onto a mixture of saturated sodium acetate solution and ice water. After 30 min the mixture was extracted with ethyl acetate (3 · 15 mL), the organic layer was washed with water and brine and dried over Na_2SO_4. The organic solvent was removed under reduced pressure and the residue was purified by column chromatography (SiO_2, 230 mL, hexane/ethyl acetate = 5:1). The product

(72.1 mg, 269 μmol, 43%) was isolated as an orange solid. **^{1}H-NMR** ($CDCl_3$, 400 MHz, 298 K): δ (ppm) = 3.73 (s, 3H), 4.57 (s, 2H), 7.57 (ddd, 1H, ^3J = 8.1, 7.1 Hz, ^4J = 1.2 Hz), 7.65 – 7.70 (m, 2H), 7.95 (d, 1H, ^3J = 9.1 Hz), 7.99 (*br* d, 1H, ^3J = 8.1 Hz), 8.24 (*br* d, 1H, ^3J = 8.2 Hz), 10.1 (s, 1H). **^{13}C-NMR** ($CDCl_3$, 101 MHz, 300 K): δ (ppm) = 31.1, 52.8, 113.0, 122.1, 123.1, 124.3, 125.7, 128.0, 129.0, 129.9, 131.3, 131.6, 148.8, 154.8, 170.1, 180.7. **HRMS** (APCI): *m/z* calcd for $C_{16}H_{12}O_4$ $[M+H]^+$: 269.0808, found: 269.0809. **TLC**: R_f = 0.25 (hexane/ethyl acetate = 5:1).

Methyl 2-(2-cyanonaphtho[2,1-*b*]furan-1-yl)acetate (27)

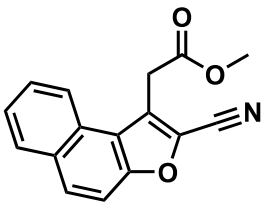

In a Schlenk tube, methyl 2-(2-formylnaphtho[2,1-*b*]furan-1-yl)acetate (101 mg, 376 μmol, 1.00 eq.), hydroxylamine hydrochloride (53.4 mg, 753 μmol, 6.22 eq.) and pyridine (282 mg, 3.57 mmol, 9.47 eq.) were combined and heated to 90 °C. Acetic anhydride (239 mg, 2.34 mmol, 2.00 eq.) was slowly added and the reaction mixture was stirred for additional 2 h at 95 °C. After this time, the mixture was poured on ice water. The resulting precipitate was taken up in EtOAc, and the aqueous phase was extracted with EtOAc (3 · 10 mL). The combined organic layers were washed with water and brine (20 mL), dried over Na_2SO_4 and concentrated under reduced pressure. Purification by column chromatography gave the product (94.6 mg, 366 μmol, 95%) as white solid. **^{1}H-NMR** ($CDCl_3$, 400 MHz, 298 K) δ (ppm) = 3.75 (s, 3H), 4.22 (s, 2H), 7.58 (ddd, 1H, ^3J = 8.2, 7.0 Hz, ^4J = 1.2 Hz), 7.64 (d, 1H, ^3J = 9.1 Hz), 7.67 (ddd,1H, ^3J = 8.4, 7.1 Hz, ^4J = 1.4 Hz), 7.93 (dt, 1H, ^3J = 9.1 Hz, ^4J = 0.6 Hz), 7.99 (ddt, 1H, ^3J = 8.1 Hz, ^4J = 1.3, 0.6 Hz), 8.15 (ddd, 1H, ^3J = 8.3 Hz, ^4J = 1.3, 0.7 Hz). **^{13}C-NMR** ($CDCl_3$, 101 MHz, 300 K) δ (ppm) = 31.93, 52.95, 111.62, 112.52, 120.20, 122.82, 125.86, 126.37, 127.49, 128.00, 128.11, 129.68, 130.85, 131.24, 154.78, 169.24. **HRMS** (ESI) *m/z* calcd for $C_{16}H_{11}NO_3$ $[M+H]^+$: 266.0812, found: 266.0767. **TLC**: R_f = 0.26 (hexane/ethyl acetate = 10:1).

2-(2-Iodonaphtho[2,1-*b*]furan-1-yl)acetic acid (28)

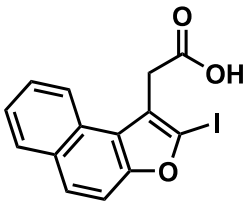

To a solution of methyl 2-(2-iodonaphtho[2,1-*b*]furan-1-yl)acetate (88.8 mg, 242 µmol, 1.00 eq.) in 1.6 mL dry THF were added 290 µL aqueous solution of LiOH (1 M, 291 µmol, 1.20 eq.) and 520 µL water. The resulting mixture was stirred at room temperature for 18 h. Afterwards, the reaction mixture was concentrated and acidified with HCl_{aq} (1 M) extracted with EtOAc (2 · 10 mL) and the combined organic layers were washed with water and brine (30 mL), dried over Na_2SO_4 and concentrated under reduced pressure. The product (81.3 mg, 231 µmol, 95%) was isolated as white solid. **^{1}H-NMR** (DMSO-d_6, 400 MHz, 298 K) δ (ppm) = 3.96 (s, 2H), 7.53 (ddd, 1H, ^3J = 8.1, 6.9 Hz, ^4J = 1.1 Hz), 7.63 (ddd, 1H, ^3J = 8.3, 7.0 Hz, 1.4 Hz), 7.79 (d, 1H, ^3J = 9.0 Hz), 7.82 (d, 1H, ^3J= 9.1 Hz), 8.05 (dd, 1H, ^3J = 8.1 Hz, ^4J = 1.3 Hz), 8.19 (d, 1H, ^3J = 8.3 Hz), 12.76 (s, 1H). **^{13}C-NMR** (DMSO-d_6, 126 MHz, 300 K) δ (ppm) = 33.59, 103.37, 112.04, 121.42, 122.46, 122.94, 124.79, 125.71, 126.50, 126.76, 128.99, 130.29, 155.72, 171.45. **HRMS** (ESI) m/z calcd for $C_{14}H_9IO_3$ $[M-H]^-$: 350.9524, found: 350.9523. **TLC**: R_f = 0.07 (hexane/ethyl acetate = 3:1 + 2 drops AcOH).

2-(2-Cyanonaphtho[2,1-*b*]furan-1-yl)acetic acid (29)

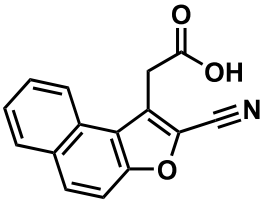

Methyl 2-(2-cyanonaphtho[2,1-*b*]furan-1-yl)acetate (76.6 mg, 289 µmol, 1.00 eq.) was dissolved in dry THF (1.9 mL). $LiOH_{aq}$ (346 µL, 1 m, 346 µmol, 1.20 eq.) and water (0.6 mL) were added and the resulting mixture was stirred for 18 h at room temperature. Then, the mixture was diluted with EtOAc (5 mL), acidified with HCl_{aq} (1 M) and extracted with EtOAc (3 · 10 mL). The combined organic layers were washed with water and brine (10 mL), dried over Na_2SO_4 and concentrated under reduced pressure. After column chromatography (SiO_2, 100 mL, 2.5 cm, hexane/ethyl acetate = 1:2 + 1% AcOH) the title compound (59.3 mg, 236 µmol, 82%) was isolated as yellow-brown solid. **^{1}H-NMR** (DMSO-d_6, 400 MHz, 298 K) δ (ppm) = 4.26 (s, 2H), 7.65 (ddd, 1H, ^3J = 8.0, 6.9 Hz, ^4J = 1.0 Hz), 7.75 (ddd, 1H, ^3J = 8.3, 7.1 Hz, ^4J = 1.3 Hz), 7.89 (d, 1H,

^3J = 9.1 Hz), 8.15 (d, 1H, ^3J = 8.5 Hz), 8.15 (d, 1H, ^3J = 9.3 Hz), 8.26 (d, 1H, ^3J = 8.2 Hz), 13.12 (s, 1H). **^{13}C-NMR** (DMSO-d_6, 101 MHz, 298 K) δ (ppm) = 31.44, 111.56, 112.47, 119.67, 123.03, 124.98, 125.83, 127.30, 127.92, 129.17, 129.40, 130.67, 130.94, 154.06, 170.15. **HRMS** (ESI) *m/z* calcd for $C_{15}H_9NO_3$ $[2M+H]^+$: 501.1092, found: 501.1090. **TLC**: R_f = 0.29 (hexane/ethyl acetate = 1:2 + 1% AcOH).

4-(1,3,4-Oxadiazol-2-yl)phenyl 2-(2-bromonaphtho[2,1-b]furan-1-yl)acetate (30)

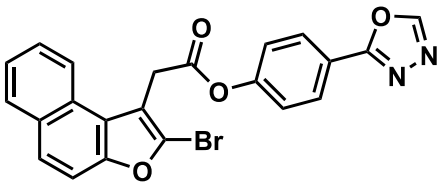

In a first attempt, **24** could not be separated from product resulting from *Sonogashira* coupling described below. Nonetheless, purification was successfully conducted after methyl ester cleavage and esterification with 4-(1,3,4-oxadiazol-2-yl)phenol. After column chromatography the title compound (22.8 mg, 51.0 μmol, 5% over steps) was isolated as pale yellow solid. **^{1}H-NMR** ($CDCl_3$, 400 MHz, 298 K): δ(ppm) = 4.32 (s, 2H), 7.21 (d, 2H, ^3J = 8.7 Hz), 7.54 (ddd, 1H, ^3J = 8.2, 7.0 Hz, ^4J = 1.2 Hz), 7.65 (ddd, 1H, ^3J = 8.3, 6.9 Hz, ^4J = 1.4 Hz), 7.65 (d, 1H, ^3J = 9.0 Hz), 7.76 (d, 1H, ^3J = 8.9 Hz), 7.99 (*br* d, 1H, ^3J = 8.2 Hz), 8.06 (d, 2H, ^3J = 8.7 Hz), 8.29 (*br* d, 1H, ^3J = 8.3 Hz), 8.44 (s, 1H). **^{13}C-NMR** ($CDCl_3$, 101 MHz, 300 K): δ(ppm) = 32.8, 112.2, 113.9, 121.5, 121.9, 122.5, 122.6, 125.1, 126.3, 127.1, 127.3, 128.2, 128.7, 129.6, 131.0, 152.8, 153.4, 153.6, 164.2, 168.2. **HRMS** (ESI): *m/z* calcd for $C_{22}H_{13}BrN_2O_4$ $[M+H]^+$: 449.0125, found: 449.0125. **TLC:** R_f = 0.33 (hexane/ethyl acetate = 2:1).

4-(1,3,4-Oxadiazol-2-yl)phenyl 2-(2-iodonaphtho[2,1-*b*]furan-1-yl)acetate (31)

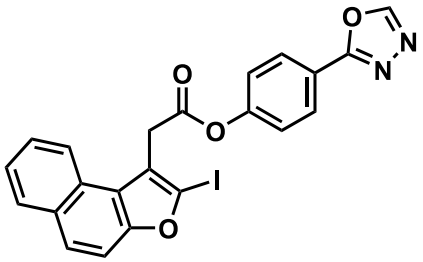

Following general procedure (I), 2-(2-iodonaphtho[2,1-*b*]furan-1-yl)acetic acid (51.4 mg, 146 μmol, 1.00 eq.) was dissolved in 2 mL dry CH_2Cl_2. EDCI (42.0 mg, 219 μmol, 1.50 eq.), DMAP (8.91 mg, 73.0 μmol, 0.50 eq.) and 4-(1,3,4-oxadiazol-2-yl)phenol (28.4 mg, 175 μmol, 1.20 eq.) were added and the resulting mixture was stirred at room temperature under argon atmosphere for 16 h. After this time 10 mL CH_2Cl_2 were added and the reaction mixture was washed with saturated $NaHCO_3$

solution water and brine (10 mL). The organic layer was dried over Na_2SO_4 and concentrated under reduced pressure. Purification by column chromatography (SiO_2, 110 mL, 2.5 cm, hexane/ethyl acetate = 2:1) yielded the title compound (53.0 mg, 107 µmol, 73%) as white solid. **^{1}H-NMR** ($CDCl_3$, 400 Hz, 298 K) δ (ppm) = 4.30 (s, 2H), 7.19 – 7.23(m, 2H), 7.53 (ddd, 1H, ^3J = 8.1, 7.0 Hz, ^4J = 1.1 Hz), 7.62 – 7.68 (m, 1H), 7.66 (d,1H ^3J = 9.0 Hz), 7.72 (d, 1H, ^3J = 8.9 Hz), 7.96 – 7.99 (m, 1H), 8.03 – 8.07 (m, 2H), 8.30 (dd, 1H, ^3J = 8.2 Hz, ^4J = 1.0 Hz), 8.44 (s, 1H). **^{13}C-NMR** ($CDCl_3$, 126 MHz, 300 K) δ (ppm) = 34.59, 99.85, 112.26, 121.35, 121.43, 121.58, 122.53, 122.60, 125.04, 126.37, 126.97, 127.14, 128.64, 129.50, 130.89, 152.79, 153.44, 156.92, 164.16, 168.32. **HRMS** (ESI) m/z calcd for $C_{22}H_{14}IN_2O_4$ $[M+H]^+$: 496.9993, found: 496.9993. **TLC**: R_f = 0.35 (hexane/ethyl acetate = 1:1).

4-(1,3,4-Oxadiazol-2-yl)phenyl 2-(2-cyanonaphtho[2,1-*b*]furan-1-yl)acetate (32)

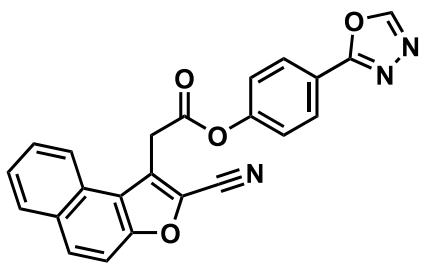

According to general procedure (I), 2-(2-cyanonaphtho[2,1-*b*]furan-1-yl)acetic acid (34.3 mg, 137 µmol, 1.00 eq.) was dissolved in dry CH_2Cl_2 (0.7 mL). Addition of EDCI (41.8 mg, 218 µmol, 1.50 eq.), DMAP (8.75 mg, 71.6 µmol, 0.50 eq.) and 4-(1,3,4-oxadiazol-2-yl)phenol (8.34 mg, 68.3 µmol, 1.20 eq.) gave a yellow solution, which was stirred at room temperature under argon atmosphere for 17 h. After this time, 10 mL CH_2Cl_2 were added, the organic phase was extracted with saturated $NaHCO_3$ solution, water and brine (10 mL) and dried over Na_2SO_4. The organic solvent was evaporated and the crude product was purified by column chromatography (SiO_2, 100 mL, 2.5 cm, hexane/ethyl acetate = 3:2). The title compound (14.3 mg, 36.2 µmol, 26%) was isolated as white solid. **^{1}H-NMR** ($CDCl_3$, 400 MHz, 298 K) δ (ppm) = 4.51 (s, 2H), 7.21 – 7.24 (m, 2H), 7.63 (ddd, 1H, ^3J = 8.2, 7.0 Hz, ^4J = 1.2 Hz), 7.68 (d, 1H, ^3J = 9.1 Hz), 7.73 (ddd, 1H, ^3J = 8.4, 7.0 Hz, ^4J = 1.4 Hz), 7.98 (dt, 1H, ^3J = 9.0 Hz, ^4J = 0.6 Hz), 8.03 (ddt, 1H, ^3J = 8.1 Hz, ^4J = 1.2, 0.6 Hz), 8.06 – 8.09 (m, 2H), 8.28 (dd, 1H, ^3J = 8.4 Hz, ^4J = 1.0 Hz), 8.45 (s, 1H). **^{13}C-NMR** ($CDCl_3$, 126 MHz, 300 K) δ (ppm) = 32.22, 111.55, 112.65, 120.02, 121.73, 122.42, 122.57, 126.10, 126.56, 126.63, 127.82, 128.27, 128.74, 129.95, 131.13, 131.32, 152.82, 153.14, 154.92, 164.06, 166.92.

HRMS (ESI) *m/z* calcd for $C_{23}H_{13}N_3O_4$ $[M+H]^+$: 396.0979, found: 396.0977. **TLC**: R_f = 0.28 (hexane/ethyl acetate = 1:1).

Methyl 2-(2-((trimethylsilyl)ethynyl)naphtho[2,1 *b*] furan-1-yl)acetate (33)

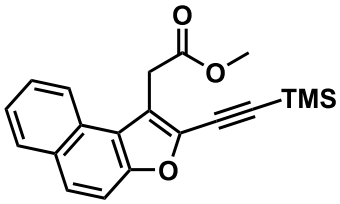

In a 50 mL Schlenk tube methyl 2-(naphtho[2,1-*b*]furan-1-yl)acetate (1.50 g, 4.70 mmol, 1.00 eq.), $Pd(PPh_3)_4$ (66.0 mg, 94.0 µmol, 0.018 eq.) and CuI (36.0 mg, 189 µmol, 0.27 eq.) were dissolved in dry THF (5 mL). Then, the resulting yellow solution was degassed by repeated freeze-pump-thaw cycles. Ethynyltrimethylsilane (951 mg, 9.40 mmol, 2.00 eq.) and triethylamine (508 mg, 5.17 mmol, 1.10 eq.) were added and the mixture was stirred at room temperature for 20 h. Afterwards, the reaction was diluted with EtOAc (25 mL) and subsequently washed with water and brine (20 mL each). The organic layer was dried over Na_2SO_4 and the residual solvent was removed by evaporation under reduced pressure. The resulting sticky brownish oil was purified by flash chromatography (SiO_2, 280 mL, 4 cm, hexane/ethyl acetate = 20:1) yielding the product (1.36 g, 4.05 mmol, 86%) as brown solid. **^{1}H-NMR** ($CDCl_3$, 300 MHz, 298 K): δ (ppm) = 0.32 (s, 9H), 3.72 (s, 3H), 4.15 (s, 2H), 7.49 (ddd, 1H ^3J = 8.1, 7.0 Hz, ^4J = 1.2 Hz,), 7.58 (d, 1H ^3J = 9.0 Hz,), 7.62 – 7.56 (m, 1H), 7.78 (d, 1H ^3J = 9.0 Hz,), 7.94 (d, 1H ^3J = 8.1 Hz,), 8.13 (d, 1H ^3J = 8.2 Hz,). **^{13}C-NMR** ($CDCl_3$, 101 MHz, 298 K): δ (ppm) = -0.09, 32.35, 52.55, 93.26, 105.37, 112.51, 120.28, 121.29, 122.99, 124.85, 127.02, 127.77, 128.11, 129.36, 131.09, 137.41, 152.75, 170.90. **HRMS** (ESI) *m/z* calcd for $C_{20}H_{20}O_3Si$ $[M+H]^+$: 337.1255, found: 337.1256. **TLC**: R_f = 0.45 (hexane/ethyl acetate = 10:1).

2-(2-Ethynylnaphtho[2,1-*b*]furan-1-yl)acetic acid (34)

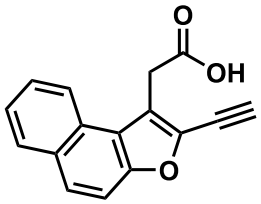

In a round bottom flask methyl 2-(2-((trimethylsilyl)ethynyl)naphtho[2,1 *b*] furan-1-yl)acetate (1.36 g, 4.05 mmol, 1.00 eq.) was dissolved in THF (24 mL). $LiOH_{aq}$ (4.86 mL, 1 M, 4.86 mmol) and water (7.1 mL) were added and the resulting solution was stirred at room temperature for 24 h. The organic solvent was removed under reduced pressure and the remaining residue was acidified with

1 M HCl_{aq}. The resulting suspension was extracted with EtOAc (3 · 20 mL), the organic layers were washed with water and brine, dried over Na_2SO_4 and concentrated under reduced pressure. The title compound (938 mg, 3.75 mmol, 93%) was isolated as brown solid. **^{1}H-NMR** (DMSO-d_6, 400 MHz, 298 K) δ (ppm) = 4.10 (s, 2H), 5.13 (s, 1H), 7.56 (ddd, 1H, ^3J = 8.1, 7.0 Hz, ^4J = 1.2 Hz), 7.66 (ddd, 1H, ^3J = 8.3, 7.0 Hz, ^4J = 1.4 Hz), 7.78 (d, 1H, ^3J = 9.0 Hz), 7.96 (d, 1H, ^3J = 9.0 Hz), 8.08 (d, 1H, ^3J = 7.9 Hz), 8.19 (d, 1H, ^3J = 8.4 Hz), 12.83 (s, 1H). **^{13}C-NMR** (DMSO-d_6, 101 MHz, 300 K) δ (ppm) = 31.50, 72.75, 90.49, 112.26, 120.68, 121.64, 122.99, 124.96, 126.99, 127.35, 127.83, 129.09, 130.49, 135.75, 151.90, 171.18. **HRMS** (ESI) *m/z* calcd for $C_{16}H_{10}O_3$ $[M-H]^-$: 249.0557, found: 249.0564. **TLC**: R_f = 0.11 (hexane/ethyl acetate = 5:1 + 2 drops AcOH).

4-(1,3,4-Oxadiazol-2-yl)phenyl 2-(2-ethynylnaphtho[2,1-*b*]furan-1-yl)acetate (35)

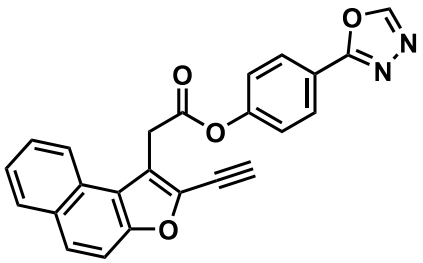

Following general procedure (I), 2-(2-ethynylnaphtho[2,1-*b*]furan-1-yl)acetic acid (100 mg, 400 μmol, 1.00 eq.) was dissolved in dry CH_2Cl_2 (2 mL) and EDCI (115 mg, 600 μmol, 1.50 eq.), DMAP (24.9 mg, 200 μmol, 0.50 eq.) and 4-(1,3,4-oxadiazol-2-yl)phenol (77.8 mg, 480 μmol, 1.20 eq.) were added. The resulting mixture was stirred at room temperature under argon atmosphere for 18 h and afterwards diluted with CH_2Cl_2 (2 mL). The organic phase was extracted with saturated $NaHCO_3$ solution, water and brine (10 mL) and dried over Na_2SO_4. After filtration and concentration under reduced pressure, the crude product was purified by column chromatography (SiO_2, 250 mL, 4 cm, hexane/ethyl acetate = 2:1). The product (77.5 mg, 197 μmol, 49%) was isolated as pale yellow solid. **^{1}H-NMR** ($CDCl_3$, 400 MHz, 298 K): δ (ppm) = 3.78 (s, 1H), 4.44 (s, 2H), 7.21 (d, 2H, ^3J = 8.9 Hz), 7.55 (ddd, 1H, ^3J = 8.1, 7.0 Hz, ^4J = 1.2 Hz), 7.63 (d, 1H, ^3J = 9.0 Hz), 7.66 (ddd, 1H, ^3J = 8.3, 7.0 Hz, ^4J = 1.3 Hz), 7.84 (d, 1H, ^3J = 9.0 Hz), 7.99 (*br* d, 1H, ^3J = 8.1 Hz), 8.06 (d, 2H, ^3J = 9.0 Hz), 8.29 (*br* d, 1H, ^3J = 8.2 Hz), 8.44 (s, 1H).**^{13}C-NMR** ($CDCl_3$, 101 MHz, 300 K): δ (ppm) = 32.5, 73.1, 87.0, 112.6, 120.1, 120.9, 121.4, 122.5, 122.7, 125.2, 127.3, 127.9, 128.2, 128.6, 129.6, 131.2, 136.9, 152.8, 153.0, 153.5, 168.3. **HRMS** (ESI): *m/z* calcd for $C_{24}H_{14}N_2O_4$ $[M+H]^+$: 395.1019, found: 395.1019. **TLC**: R_f = 0.25 (hexane/ethyl acetate = 2:1).

Phenyl 2-(2-ethynylnaphtho[2,1-*b*]furan-1-yl)acetate (36)

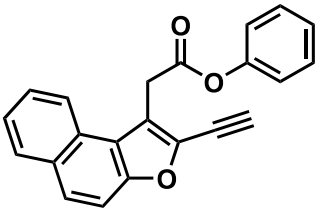

According to general procedure (I), 2-(2-ethynylnaphtho[2,1-*b*]furan-1-yl)acetic acid (50.0 mg, 200 μmol, 1.00 eq.) was dissolved in dry CH_2Cl_2 (1 mL). Addition of EDCI (57.5 mg, 300 μmol, 1.50 eq.), DMAP (12.2 mg, 100 μmol, 0.50 eq.) and phenol (18.8 mg, 240 μmol, 1.20 eq.) gave a light brown solution which was stirred at room temperature under argon atmosphere for 18 h. After this time, the reaction mixture was diluted with CH_2Cl_2 (1 mL) and washed saturated $NaHCO_3$ solution, water and brine (10 mL). The organic layer was dried over Na_2SO_4 and concentrated under reduced pressure. Purification by column chromatography (SiO_2, 250 mL, 4 cm, hexane/ethyl acetate = 10:1) gave the product (44.7 mg, 137 μmol, 68%) as pale-brown solid. **^{1}H-NMR** ($CDCl_3$, 500 MHz, 298 K) δ (ppm) = 3.77 (s, 1H), 4.40 (s, 2H), 7.01 – 7.03 (m, 2H), 7.17 – 7.20 (m, 1H), 7.29 – 7.32 (m, 2H), 7.53 (ddd, 1H, ^3J = 8.1, 6.9 Hz, ^4J = 1.2 Hz), 7.62 (d, 1H, ^3J = 9.0 Hz), 7.65 (ddd, 1H, ^3J = 8.3, 7.0 Hz, 1.4 Hz), 7.82 (d, 1H, ^3J = 9.0 Hz), 7.97 (d, 1H, ^3J = 8.2 Hz). **^{13}C-NMR** ($CDCl_3$, 101 MHz, 298 K) δ (ppm) = 32.50, 73.22, 76.84, 77.16, 77.36, 77.48, 86.84, 112.57, 120.59, 121.05, 121.53, 122.94, 125.06, 126.13, 127.21, 128.05, 128.10, 129.50, 129.53, 131.15, 136.81, 150.78, 153.01, 168.77. **HRMS** (ESI) *m/z* calcd for $C_{22}H_{14}O_3$ $[M+H]^+$: 327.1016, found: 327.1015. **TLC**: R_f = 0.33 (hexane/ethyl acetate = 10:1).

4-Methoxyphenyl 2-(2-ethynylnaphtho[2,1-*b*]furan-1-yl)acetate (37)

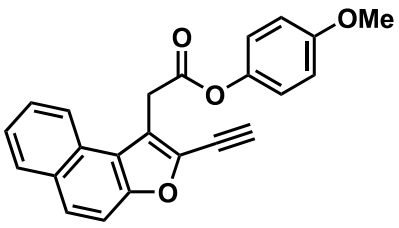

Following general procedure (I), 2-(2-ethynylnaphtho[2,1-*b*]furan-1-yl)acetic acid (50.0 mg, 200 μmol, 1.00 eq.) was dissolved in dry CH_2Cl_2 (1 mL). Addition of EDCI (57.5 mg, 300 μmol, 1.50 eq.), DMAP (12.0 mg, 100 μmol, 0.50 eq.) and 4-methoxyphenol (29.8 mg, 240 μmol, 1.20 eq.) led to a clear brown solution which was stirred at room temperature under argon atmosphere for 18 h. Afterwards, the reaction mixture was diluted with CH_2Cl_2 (1 mL) and extracted with saturated $NaHCO_3$ solution, water and brine (10 mL). After drying over Na_2SO_4 the organic solvent was

evaporated under reduced pressure. Purification by column chromatography (SiO_2, 250 mL, 4 cm, hexane/ethyl acetate = 10:1) yielded the product (51.3 mg, 144 μmol, 72%) as pale brown solid. **^{1}H-NMR** ($CDCl_3$, 500 MHz, 298 K) δ (ppm) = 3.78 (s, 3H), 3.79 (s, 1H), 4.40 (s, 2H), 6.86 – 6.82 (m, 2H), 6.97 – 6.94 (m, 2H), 7.55 (ddd, 1H, ^3J = 8.2, 6.9 Hz, ^4J = 1.2 Hz), 7.64 (d, 1H, ^3J = 8.9 Hz), 7.66 (ddd, 1H, ^3J = 8.4, 6.9 Hz, ^4J = 1.4 Hz), 7.84 (d, 1H, ^3J = 9.0 Hz), 7.99 (dd, 1H, ^3J = 8.1 Hz, ^4J =1.5 Hz), 8.32 (dd, 1H, ^3J = 8.4 Hz, ^3J = 1.0 Hz). **^{13}C-NMR** ($CDCl_3$, 101 MHz, 300 K) δ (ppm) = 32.44, 55.71, 73.23, 86.81, 112.57, 114.54, 120.67, 121.07, 122.28, 122.96, 125.04, 127.19, 128.05, 128.08, 129.49, 131.14, 136.77, 144.29, 153.00, 157.49, 169.14. **HRMS** (ESI) *m/z* calcd for $C_{23}H_{16}O_4$ $[M+H]^+$: 357.1121, found: 357.1121. **TLC**: R_f = 0.22 (hexane/ethyl acetate = 10:1).

Methyl 4-(2-(2-ethynylnaphtho[2,1-*b*]furan-1-yl)acetoxy)benzoate (38)

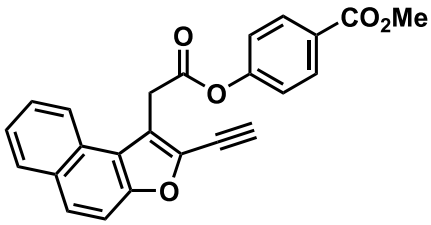

Following general procedure (I), 2-(2-ethynylnaphtho[2,1-*b*]furan-1-yl)acetic acid (50.0 mg, 200 μmol, 1.00 eq.) was dissolved in dry CH_2Cl_2 (1 mL). After addition of EDCI (57.5 mg, 300 μmol, 1.50 eq.), DMAP (12.2 mg, 100 μmol, 0.50 eq.) and methyl-4-hydroxybenzoate (36.5 mg, 240 μmol, 1.20 eq.) the mixture was stirred at room temperature under argon atmosphere for 18 h. Afterwards, the reaction mixture was diluted with CH_2Cl_2 (1 mL) and extracted with saturated $NaHCO_3$ solution, water and brine (10 mL). The organic layer was dried over Na_2SO_4 and concentrated under reduced pressure. The product (37.2 mg, 96.8 μmol, 48%) was isolated after column chromatography (SiO_2, 250 mL, 4 cm, hexane/ethyl acetate = 9:1) as an off-white solid. **^{1}H-NMR** ($CDCl_3$, 400 MHz, 298 K) δ (ppm) = 3.77 (s, 1H), 3.89 (s, 3H), 4.42 (s, 2H), 7.07 – 7.14 (m, 2H), 7.54 (ddd, 1H, ^3J = 8.1, 6.9 Hz, ^4J = 1.2 Hz), 7.63, d, 1H, ^3J = 8.9 Hz), 7.64 (ddd, 1H, ^3J = 8.3, 6.9 Hz, ^4J = 1.3 Hz), 7.83 (d, 1H, ^3J = 9.0 Hz), 7.98 (dd, 1H, ^3J = 8.2 Hz, ^4J = 1.2 Hz), 7.97 – 8.04 (m, 2H), 8.28 (dd, 1H, ^3J = 8.5 Hz, ^4J = 1.1 Hz). **^{13}C-NMR** ($CDCl_3$, 126 MHz, 300 K) δ (ppm) = 32.49, 52.37, 73.10, 86.98, 112.59, 120.19, 120.90, 121.58, 122.75, 125.13, 127.26, 127.93, 128.03, 128.19, 129.59, 131.14, 131.27, 136.83, 153.01, 154.27, 166.34, 168.29. **HRMS** (ESI) *m/z* calcd for $C_{24}H_{16}O_5$ $[M+H]^+$: 385.1071, found: 385.1070. **TLC**: R_f = 0.16 (hexane/ethyl acetate = 9:1).

4-Nitrophenyl 2-(2-ethynylnaphtho[2,1-*b*]furan-1-yl)acetate (39)

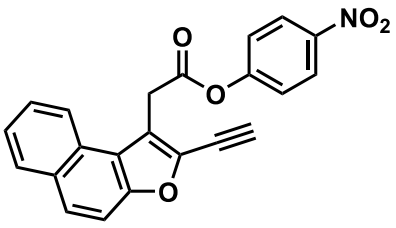

Following general procedure (I), 2-(2-ethynylnaphtho[2,1-*b*]furan-1-yl)acetic acid (50.0 mg, 200 μmol, 1.00 eq.) was dissolved in dry CH_2Cl_2 (1 mL) and EDCI (57.5 mg, 300 μmol, 1.50 eq.), DMAP (12.2 mg, 100 μmol, 0.50 eq.) and 4-nitrophenol (33.4 mg, 240 μmol, 1.20 eq.) were added. The resulting mixture was stirred at room temperature under argon atmosphere for 18 h. After this time, CH_2Cl_2 (1 mL) was added and the organic phase was extracted with saturated $NaHCO_3$ solution, water and brine (10 mL). The organic layer was dried over Na_2SO_4 and concentrated under reduced pressure. Purification by column chromatography (SiO_2, 250 mL, 4 cm, hexane/ethyl acetate = 17:3) yielded the product (21.0 mg, 56.6 μmol, 28%) as pale yellow solid. **^{1}H-NMR** ($CDCl_3$, 400 MHz, 298 K) δ (ppm) = 3.79 (s, 1H), 4.45 (s, 2H), 7.16 – 7.25 (m, 2H), 7.55 (ddd, 1H, ^3J = 8.1, 7.0 Hz, ^4J = 1.2 Hz), 7.64 (d, 1H, ^3J = 8.9 Hz), 7.62 – 7.69 (m, 1H), 7.84 (d, 1H, ^3J = 9.0 Hz), 7.99 (dd, 1H, ^3J = 8.1 Hz, ^4J = 1.2 Hz), 8.17 – 8.25 (m, 2H), 8.25 (dd, 1H, ^3J = 8.3 Hz, ^4J = 1.1 Hz). **^{13}C-NMR** ($CDCl_3$, 101 MHz, 300 K) δ (ppm) = 32.35, 72.87, 86.97, 112.50, 119.66, 120.64, 122.34, 122.43, 125.07, 125.20, 127.17, 127.72, 128.17, 129.56, 131.04, 135.27, 136.76, 152.91, 155.18, 167.79. **HRMS** (ESI) *m/z* calcd for $C_{22}H_{13}NO_5$ [M-H]$^-$: 370.0721, found: 370.0721. **TLC**: R_f = 0.33 (hexane/ethyl acetate = 17:3).

4-(Methylsulfonyl)phenyl 2-(2-ethynylnaphtho[2,1-*b*]furan-1-yl)acetate (40)

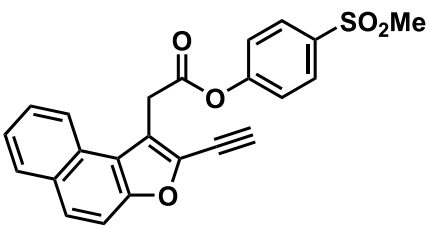

Following general procedure (I), 2-(2-ethynylnaphtho[2,1-*b*]furan-1-yl)acetic acid (102 mg, 408 μmol, 1.00 eq.) was dissolved in dry CH_2Cl_2 (5 mL), EDCI (117 mg, 612 μmol, 1.50 eq.), DMAP (24.9 mg, 204 μmol, 0.50 eq.) and 4-(methylsulfonyl)phenol (84.4 mg, 490 μmol, 1.20 eq.) were added and the resulting brown solution was stirred at room temperature under argon atmosphere for 22 h. Afterwards, CH_2Cl_2 (10 mL) was added and the organic phase was washed with saturated $NaHCO_3$ solution, water and brine (10 mL), dried over Na_2SO_4 and concentrated

under reduced pressure. Purification by column chromatography yielded the product (101 mg, 250 µmol, 61%) as brown solid. **^{1}H-NMR** ($CDCl_3$, 400 MHz, 298 K) δ (ppm) = 3.01 (s, 3H), 3.78 (s, 1H), 4.44 (s, 2H), 7.22 – 7.26 (m, 2H), 7.54 (ddd, 1H, ^{3}J = 8.1, 7.0 Hz, ^{4}J = 1.2 Hz), 7.64 (d, 1H, ^{3}J = 9.0 Hz), 7.60 – 7.69 (m, 1H), 7.84 (d, 1H, ^{3}J = 9.0 Hz), 7.89 – 7.93 (m, 2H), 8.26 (ddd, 1H, ^{3}J = 8.4 Hz, ^{4}J = 1.9, 0.7 Hz). **^{13}C-NMR** ($CDCl_3$, 126 MHz, 300 K) δ (ppm) = 32.47, 44.77, 73.02, 87.09, 112.63, 119.87, 120.79, 122.60, 122.70, 125.18, 127.28, 127.86, 128.28, 129.34, 129.68, 131.16, 136.87, 138.17, 153.04, 154.65, 168.14. **HRMS** (ESI) m/z calcd for $C_{23}H_{16}SO_5$ $[M+H]^+$: 405.0791, found: 405.0794. **TLC**: R_f = 0.49 (hexane/ethyl acetate = 1:1).

5.2.2 Biochemical methods

5.2.2.1 Protein purification

All proteins were expressed and purified according to general procedures in known literature.[36] The expression vectors for *H. sapiens* ClpP and *E. coli* ClpX were designed by Matthias Stahl and can be reviewed in the corresponding publication.

H. sapiens ClpP

For recombinant expression of *H. sapiens* ClpP (hClpP) C-terminal STREP-II tagged ClpP constructs (without mitochondrial recognition sequence 1-57) were cloned into pET301 expression vectors *via* Gateway® cloning technique (*Life Technologies*). For hClpP overexpression 4 L LB-medium containing ampicillin (1:1,000 from 100 mg/mL stock in ethanol/water 1:1) and chloramphenicol (1:1,000 from 34 mg/mL stock in ethanol) was inoculated with 40 mL overnight culture of *E. coli* Rosetta2 cells and grown at 37 °C under constant shaking. When an OD_{600} of 0.6 was reached expression was started by addition of isopropyl-*β*-D-thiogalactopyranoside (IPTG) (1:2,000 from 0.5 M stock in water) and cells were incubated at 25 °C for 20 h. Afterwards bacteria were pooled, centrifuged (6,000 g, 10 min, 4 °C), washed with PBS-buffer (140 mM NaCl, 10 mM Na_2HPO_4, 2.7 mM KCl, 1.8 mM KH_2PO_4, pH = 7.4), centrifuged again (6,000 g, 10 min, 4 °C) and stored at -20 °C until further use. For protein purification cells were resuspended in Strep binding buffer (100 mM Tris/HCl, 150 mM NaCl, 1mM EDTA, pH = 8.0) and lysed by sonication under constant cooling. Cell debris was pelletized by centrifugation (38,700 g, 30 min, 4 °C) and the supernatant was loaded on a pre-equilibrated 5 mL StrepTrap™ HP column (*GE Healthcare*) using an ÄKTA purifier 10 system (*GE Healthcare*). The column was washed with 25 mL Strep binding buffer before the protein was eluted with 20 mL Strep elution buffer (Strep binding buffer + 2.5 mM desthiobiotin). Fractions containing protein were pooled and concentrated to 1.5 mL using an Amicon® centrifugal filter (cut-off 10 kDa, 2,000 g, 4 °C).
Preparative size exclusion chromatography was performed on a HiLoad 16/60 Superdex 200 pg, (*GE Healthcare*) using hClpP storage buffer (20 mM HEPES, 100 mM NaCl, pH =7.0). Fractions containing protein were pooled, concentrated and stored in small aliquots at -80 °C. This method yielded 1.02 mg protein per liter bacterial medium.

E. coli ClpX

E. coli ClpX (EcClpX) was purified as described earlier.[36] For this 4 L LB-medium supplemented with ampicillin (1:1,000 from 100 mg/mL stock in ethanol/water (1:1)) was inoculated with 40 mL of an overnight culture of *E. coli* Rosetta2 (DE3) cells with a His6-TEV-EcClpX construct. Cells were grown to an OD_{600} of 0.6, then induced with IPTG (1:2,000 from 0.5 M stock in water) and

incubated at 25 °C for 20 h under constant shaking. Afterwards cells were pelleted (6,000 g, 10 min, 4 °C), washed with cold PBS-buffer, centrifuged again and stored at -20 °C until further use. For purification cells were resuspended in lysis buffer (50 mM HEPES, 300 mM KCl, 1 mM dithiothreitol (DTT), 10 mM imidazole, 5 mM $MgCl_2 \cdot 6H_2O$, 15% (v/v) glycerol, pH = 7.6) and lysed by sonication under permanent cooling. Cell debris was removed by centrifugation (38,700 g, 30 min, 4 °C) and the supernatant was loaded on a pre-equilibrated 5 mL HisTrap HP column (*GE Heaalthcare*). The column was washed with ten column volumes wash buffer (50 mM HEPES, 300 mM KCl, 1 mM DTT, 40 mM imidazole, 15% (v/v) glycerol, pH = 7.6) before the protein was eluted with 20 mL elution buffer (50 mM HEPES, 300 mM KCl, 1 mM DTT, 300 mM imidazole, 15% (v/v) glycerol, pH = 7.6). Fractions containing protein were pooled, concentrated (cut-off: 30 kDa, 2,000 g, 4 °C) and 1 mM EDTA was added. The His-tag was cleaved by addition of TEV-protease (2.5 mg/mL stock, 1:50 dilution per mg protein) and incubation overnight at 37 °C. When IP-MS indicated full conversion the crude protein was subjected to size exclusion chromatography. The protein solution was loaded on a pre-equilibrated HiLoad 16/60 Superdex 200 pg (*GE Healthcare*) using gel filtration buffer (50 mM HEPES, 300 mM KCl, 1 mM DTT, 5 mM $MgCl_2 \cdot 6H_2O$, 15% (v/v) glycerol, pH = 7.6). Fractions containing protein were pooled, concentrated and stored in aliquots at -80 °C (1.05 mg protein per liter bacterial suspension).

ssrA-eGFP

ssrA-tagged eGFP was purified as described previously.[269] In brief, *E. coli* KY2266 cells with a GFP construct containing a N-terminal Strep-II-tag and a C-terminal ssrA-tag from *E. coli* (AANDENYALAA) in a pDEST007 expression vector were grown in LB-medium and overexpression was induced by addition of anhydrotetracycline (0.2 mg/L). Purification was conducted using affinity chromatography (StrepTrap™ HP 5 mL, *GE Healthcare*) and size exclusion chromatography (HiLoad 16/60 Superdex 200 pg, *GE Healthcare*).

5.2.2.2 Peptidase activity assay

To investigate the potency of phenyl ester based inhibitors against the peptidolytic activity of hClpP the ability to cleave a fluorogenic tripeptide was assessed in a degradation assay, as described earlier.[75] For this, 1 µL inhibitor (100 mM DMSO stock, three different final concentrations: 100 µM, 10 µM, 1 µM) was aliquoted in triplicates in a black 96-well plate and incubated with 98 µL hClpP (final monomer concentration: 1.0 µM) in peptidase buffer (50 mM HEPES, 300 mM KCl, 1 mM DTT, 10% (v/v) glycerol, pH = 7.5) at 37 °C for 15 min. Measurement was started after addition of 1 µL fluorogenic substrate Suc-Leu-Tyr-AMC (200 µM final concentration) on a *Tecan Infinite 200 Pro* (excitation wavelength: λ = 380 nm, emission wavelength: λ = 430 nm). A linear

regression curve was fitted to the slope of the increasing fluorescence signal in the time interval t = 500 – 2,000 s with Microsoft Office Excel. DMSO treated samples were used as control and normalized to 100%. Residual activity of hClpP upon inhibitor treatment was determined by comparison with the DMSO control.

Determination of apparent IC_{50} values was performed by Markus Lakemeyer in the laboratories of Prof. Stephan A. Sieber at TU München.

Apparent IC_{50} values for the inhibition of ClpP peptidase activity were determined by peptidase activity assays as described above. For this, ClpP activity was measured after incubation with various concentrations of inhibitors. Fluorescence signals resulting from the cleavage of the fluorogenic substrate Suc-L-Y-AMC were measured on a *Tecan Infinte M200 pro* (excitation wavelength: λ = 380 nm; emission wavelength: λ = 440 nm). Nonlinear regression curves were generated from at least 6 replicates using *Microcal Origin 8.5* and *Prism 6.05*.

5.2.2.3 FITC-Casein assay

To assess the inhibitory potency on the proteolytic activity of hClpP, FITC-Casein assays were performed. ClpP alone is only capable to degrade small peptides, however for degradation of oligopeptides or proteins a chaperone of the AAA+ family (ATPases associated with diverse cellular activities) is needed which opens the pore to the proteolytic chamber and unfolds and directs the peptides to the peptidolytic core. The opening of the axial pore may also be triggered by small ADEP-fragments which leads to an indiscriminative degradation of substrate peptides.[98] For FITC-casein assays ClpP was initially incubated with inhibitors then with ADEP fragment. Proteolytic activity was measured by the degradation of FITC-casein substrate which leads to the release of fluorogenic FITC (fluorescein isothiocyanate). In a black 96-well plate 1 µL inhibitor was aliquoted in triplicates in three different concentrations (from 100 mM DMSO stock: 100 µM, 10 µM, 1 µM final concentration). As control nine wells were filled with 1 µL DMSO. ClpP buffer mix (final concentration of hClpP in assay 1.0 µM; assay buffer: 50 mM HEPES, 300 mM KCl, 1 mM DTT, 15% (v/v) glycerol, pH = 7.5) was pre-warmed at 37 °C and then 80 µL were aliquoted and incubated together with inhibitors for 15 min at 37 °C. Afterwards 1 µL ADEP fragment was added (1:100 from 1 mM DMSO stock, final assay concentration 10 µM) and incubated again for 15 min at 37 °C. Kinetic measurement was started after the addition of 20 µL casein mix (10 µM final concentration of Casein, 2 µM final concentration of FITC-casein). Fluorescence of the cleaved FITC was quantified over 120 min on a Tecan Infinite M200 pro (excitation wavelength: λ = 485 nm, emission wavelength: λ = 535 nm). The slope of the fluorescence over time signal was calculated in the time interval t = 420 – 900 s *via* linear regression with Microsoft Office Excel.

The residual activity of inhibitor treated protein was determined in comparison to DMSO treated control samples which were normalized to 100% activity.

5.2.2.4 Protease activity assay

GFP degradation assays were performed with *H. sapiens* ClpP and *E. coli* ClpX which are able to form a functional complex. The assay was performed with white flat-bottom 96-well plates in PZ-buffer (25 mM HEPES, 200 mM KCl, 5 mM $MgCl_2 \cdot 6H_2O$, 1 mM DTT, 10% (v/v) glycerol, pH = 7.6) at 37 °C. 0.6 µL inhibitor was aliquoted in triplicates and 59 µL enzyme-buffer mix (0.2 µM $hClpP_{14}$, 0.4 µM $EcClpX_6$; ATP-regeneration mix: 4 mM ATP, 16 mM creatine phosphate, 20 U/mL creatine phosphokinase) was added and incubated for 15 min at 37 °C. Fluorescence measurement was started after addition of 1 µL ssrA-GFP (final concentration: 0.4 µM) on a Tecan Infinite M200 Pro (excitation wavelength: λ = 485 nm, emission wavelength: λ = 535 nm). The slope of the decreasing fluorescence signal was calculated in the time interval t = 0 – 500 s *via* linear regression with Microsoft Office Excel. The residual activity of inhibitor treated protein was determined in comparison to DMSO treated control samples which were normalized to 100% activity

5.2.2.5 High resolution intact mass spectrometry

Target engagement and the degree of modification of wild-type hClpP by phenyl esters was investigated by incubation of hClpP with inhibitors **AV167** and **35** or DMSO as control, following measurement of intact protein masses of the enzyme-compound complex. For this, 1 µL compound (three different final concentrations 1 µM, 10 µM, 100 µM) was incubated with 99 µL hClpP (final concentration: 1 µM) in peptidase assay buffer (50 mM HEPES, 300 mM KCl, 1 mM DTT, 15% (v/v) glycerol, pH = 7.5) at room temperature for 1 h. Intact protein masses were subsequently measured on a LC-MS system consisting of a Dionex Ultimate 3000 HPLC (*Thermo Fisher Scientific Inc.*) coupled to a LTQ-FT Ultra mass spectrometer (*Thermo Fisher Scientific Inc.*) with an electrospray ionization source (capillary temperature 275 °C, spray voltage 4.2 kV, tube lens 110 V, capillary voltage 48 V, sheath gas flow 60 arb, aux gas flow 10 arb, sweep gas flow 0.2 arb). 2 µL of protein-inhibitor mix were on-line desalted by a Massprep desalting cartridge (*Waters*). The mass spectrometer was operated in positive mode at a resolution of *R* = 200,000 within a range of 600 – 2,000 m/z. Deconvolution was preformed using *Thermo Xcalibur Xtract* software and theoretical monoisotopic masses were reported.

5.2.2.6 Human cell culture

For cell based experiments all cell lines were thawed from cryo stocks and continuously cultivated in culture flasks (T-75, T175, *Sarstedt*) using an incubator (Autoflow, *Nuaire*, USA) operated at 37 °C with 5% CO_2 atmosphere. Sterile handling of cells was performed in a laminar flow cabinet (Herasafe KS, *Thermo Fisher Scientific Inc.*, USA). Prior to experiments, number of cells were determined using a Neubauer improved chamber (*LaborOptik Ltd.*), after incubation of a reference sample with Trypan blue (1:1).

Huh7

Hepato cellular carcinoma cells Huh7 (generously provided by Prof. Angelika Vollmar, Ludwigs-Maximilian Universität München, Department of Pharmacy – Center for Drug Research, originally purchased from the Japanese Collection of Research Bioresources (JCRB, Osaka, Japan)) were seeded in Dulbecco's modified Eagle's medium (DMEM, high glucose, 4.5 g/L glucose, *Sigma-Aldrich*) supplemented with 10% (v/v) heat-inactivated fetal bovine serum (FBS, *Sigma Aldrich*) and 2 mM L-glutamine (1:100 from 200 mM stock, *Sigma Aldrich*). Cells were split every 2-3 days to maintain a confluency between 50 – 80%. For this cells were first washed with pre-warmed PBS-buffer in order to remove dead cells and then detached by addition of Trypsin EDTA (1x) (1 mL for T-75 flask, 2 mL for T-175 flask; Trypsin EDTA (10x) solution diluted 1:10 in PBS-buffer, *GE Healthcare*). Cells were split 1:3 – 1:5 by addition of fresh medium. To facilitate cell attachment and growth all culture flasks and dishes were coated with collagen A containing solution (0.1 mg/mL Collagen A in PBS-buffer, pH = 3.5, *Merck*, L7220) prior to use.

Jurkat

Jurkat suspension cells (acute T cell leukemia, generously provided by Prof. Angelika Vollmar) were cultivated in Roswell Park Memorial Institute medium (RPMI 1640, *Sigma Aldrich*) supplemented with 10% (v/v) heat-inactivated FBS (*Sigma Aldrich*) and 2 mM L-glutamine (1:100 from 200 mM stock, *Sigma Aldrich*). Cell passaging was performed by centrifuging cells in medium (600 g, 6 min, 25 °C) before reconstituting them in fresh medium. Cells were split in a ratio of 1:3 – 1:5 to maintain a cell density between $0.1 \cdot 10^6$ and $1.0 \cdot 10^6$.

HL-60

HL-60 suspension cells (acute promyelocytic leukemia, generously provided by Prof. Angelika Vollmar) were reconstituted in Iscove's modified Dulbecco's medium (IMDM, *Sigma Aldrich*), supplemented with 10% (v/v) heat-inactivated FBS (*Sigma Aldrich*) and 2 mM L-glutamine (from

200 mM stock, *Sigma Aldrich*). Cells were split 1:3 – 1:5 every 2-3 days by centrifuging (600 g, 6 min, 25 °C) and exchange of old medium to maintain a cell density of $0.1 \cdot 10^6$ - $1.0 \cdot 10^6$.

K562

K562 suspension cells (chronic myelogenous leukemia, generously provided by Prof. Angelika Vollmar) were cultivated in RPMI 1640 medium (*Sigma Aldrich*) supplemented with 10% (v/v) heat-inactivated FBS (*Sigma Aldrich*) and 2 mM L-glutamine (1:100 from 200 mM stock, *Sigma Aldrich*). Cells were passaged every 2-3 days by centrifuging (600 g, 6 min, 25 °C) and diluting 1:3 – 1:5 with fresh medium.

5.2.2.7 Cell viability assays

Cell viability assays were conducted by Melanie M. Mandl and Martina Meßner in the laboratories of Prof. Angelika Vollmar at Ludwigs-Maximilan Universität München

Cell viability was investigated using CellTiter-Blue® Luminescent Cell Viability Assay (*Promega*) and was carried out according to the manufacturer's protocol. In brief, cells were seeded in 96-well plates and incubated with phenyl esters or DMSO for different time periods. Finally, cell viability was determined by addition of CellTiterBlue® reagent and incubation for two to four hours following fluorescence readout using *Tecan SpectraFluor Plus*.

5.2.2.8 Nicoletti assays

Apoptotic cell assessment was conducted by Melanie M. Mandl in the laboratories of Prof. Angelika Vollmar at Ludwigs-Maximilan Universität München

For the assessment of apoptotic cells upon treatment with phenyl esters cell death was measured as described by *Nicoletti et al.*[117] In brief, cells were treated with ClpP inhibitors for 48 h, then washed in cold PBS-buffer, pelleted (600 g, 5 min, 4 °C) and incubated with hypotonic fluorochrome solution containing propidium iodide (HFS-PI solution, 50 µg/mL, 4 °C, overnight). The amount of DNA within the cell depends on the stage of cell cycle and can be quantified by measuring the amount of DNA intercalating dye. The occurrence of a broad subG1 phase peak indicates apoptotic cells and was measured by flow cytometry (FACSCantoII, *BD Biosciences*). Analysis was conducted using FlowJo 7.6 analysis software and percentage of specific apoptosis was calculated with the formula

$$100 \times \frac{apoptosis_{experimental}(\%) - apoptosis_{spontaneous}(\%)}{100\% - apoptosis_{spontaneous}(\%)}$$

5.2.2.9 Cell migration assays

Cell migration assays were conducted by Melanie M. Mandl in the laboratories of Prof. Angelika Vollmar at Ludwigs-Maximilan Universität München

Migration assays were performed using boyden chambers with Transwell® permeable inserts (*Corning Inc.*, 6.5 mm polycarbonate membrane, 8.0 µm pore size). Compounds **35** or **40** were added to medium in the lower and upper compartment of the boyden chamber, while medium containing FBS was only added to the lower compartment. Cells were resuspended in medium without FBS (100,000 cells per insert) and added to the upper compartment. Cells migrated for 16 h and were stained afterwards with crystal violet. Four pictures per insert were taken and cells were counted and normalized to DMSO treated positive control. One chamber without FBS-gradient served as negative control.

5.2.2.10 Western Blot experiments

Western blot experiments were conducted by Melanie M. Mandl in the laboratories of Prof. Angelika Vollmar at Ludwigs-Maximilan Universität München

Proteins separated by SDS-PAGE were transferred to a nitrocellulose membrane (Hybond-ECL, *Amersham Bioscience*) by tank blotting (tank buffer: 48 mM Tris base, 39 mM Glycine, 20% (v/v) MeOH, ddH_2O) at 4 °C, 100 V for 90 min. Membranes were blocked with 5% (w/v) non-fat dry milk powder (*Carl Roth*) and incubated at 4 °C overnight or at room temperature for 2 h with the respective primary antibody. Afterwards, membranes were washed with PBS-T (PBS-buffer with 0.5% (v/v) Tween-20®, pH = 7.6) and incubated with the corresponding horseradish peroxidase (HRP)-conjugated secondary antibody at room temperature for 1 h. Protein bands were visualized using enhanced chemiluminescence solution (ECL, 100 mM Tris, 2.5 mM Luminol, 1 mM *p*-Coumaric acid, 17 µM H_2O_2, H_2O, pH = 8.5) and *ChemiDoc Touch Imaging System*. As loading control, the stain-free technology (*Bio Rad*) was used. This technique enables a quantification of the whole lane protein, and therefore can be used for the normalization of protein bands.[270]

5.2.2.11 *In situ* and *in vitro* labeling experiments

General remarks for labeling in human cell lines

For analytical gel-based labeling cells were seeded in 6-well plates (*Sarstedt*) with each well representing one state for further analysis. Before compound treatment adherent cells were grown in 2 mL medium until a confluency of 70 – 80% was reached. For suspension cells 150,000 cells/mL were seeded in 2 mL medium and used immediately.

Labeling in adherent cell lines

Adherent cells were seeded in 6-well plates and allowed to grow to a confluency of 70 – 80%. Prior to seeding each well was pre-incubated with collagen A solution (0.1 mg/mL in PBS-buffer, pH = 3.5, *Merck*, L7220) according to the manufacturer's protocol. For labeling experiments cells were washed with 1 mL warm PBS-buffer then 1 mL medium (DMEM, 2 mM L-glutamine, no FBS) with probe (various concentrations, stock solution in DMSO, max. 0.1% (v/v) DMSO) was added and incubated at 37 °C for 1 h.

Labeling in suspension cell lines

For labeling experiments in suspension cell lines 999 µL medium (RPMI, 2 mM L-glutamine, no FBS) containing 300,000 cells were seeded in each well of a 6-well plate. 1 µL probe (various concentrations, stock solution in DMSO, max. 0.1% (v/v) DMSO) was added to each well and distributed by pipetting up and down. Cells were incubated at 37 °C for 1 h.

Cell harvest and lysis

Following incubation with probes suspension cells were harvested, pelletized (600 g, 6 min, 4 °C) and washed with 1 mL cold PBS-buffer. Cells were lysed by addition of 100 µL lysis buffer (1% (v/v) 4-nonylphenyl polyethylene glycol substitute (NP-40), 1% (w/v) sodium deoxycholate in PBS-buffer, pH = 7.4) and were incubated on ice for 15 min. For adherent cells, washing was performed in each well before scraping. Cells were lysed by addition of 100 µL lysis buffer to each well and were further incubated for 15 min on ice after transfer to reaction tubes. The cytosolic fraction was recovered by centrifugation (45 min, 21,100 g, 4 °C) and the pelletized insoluble fraction was further washed with 200 µL ice-cold PBS-buffer, centrifuged (20 min, 21,100 g, 4 °C) and solubilized in 100 µL 0.2% (w/v) SDS in PBS-buffer by sonication (10 s, 10% intensity, Sonopuls GM 2070, *Bandelin*).

Click reaction and SDS-PAGE

For visualization of labeled proteins, a fluorescent dye was attached to the probe-enzyme complex *via* copper(I)-catalyzed alkyne-azide cycloaddition (*Click* reaction). Cytosolic and membrane fractions were analyzed separately. For each state, 100 µL cytosolic or membrane fraction was incubated with 10 µL *Click* master mix (2 µL tetramethylrhodamine 5-carboxamido-(6-azidohexanyl), 5-isomer (TAMRA-N_3, 5 mM in DMSO, *Life Technologies*), 2 µL Tris(2-carboxyethyl)phosphine (TCEP, 52 mM in ddH_2O) and 6 µL Tris((1-benzyl-4-triazolyl)methyl)amine (TBTA ligand, 1.67 mM in 80% (v/v) *t*-BuOH, 20% (v/v) DMSO). *Click* reaction was started by addition of 2 µL $CuSO_4$ (50 mM in ddH_2O) and samples were incubated in

the dark at room temperature for 1 h. Afterwards the reaction was quenched by addition of 110 µL Laemmli buffer (2x) (63 mM Tris-HCl, 2% (v/v) glycerol, 139 mM sodium dodecylsulfate (SDS), 0.0025% (v/v) bromophenol blue, 5% (v/v) 2-mercaptoethanol). Proteins were separated by SDS polyacrylamide gel electrophoresis. For this, 12.5% polyacrylamide gels were loaded with 40 µL sample and were run for 2.5 h at 150 V, 500 mA. To determine protein size, 10 µL fluorescence standard (*Invitrogen™ Novex™ Benchmark™*) and Roti®Mark Standard (*Carl Roth*) were loaded in separate pockets of the gel. Fluorescence gels were analyzed with an image reader LAS-4000 (*Fujifilm Life Science*, USA) with a 575DF20 filter and ImageQuant LAS-4000 control software. For visualization of total protein amount loaded, gels were stained with coomassie staining solution (0.25% (w/v) Coomassie brilliant blue R-250, 9.20% (v/v) acetic acid, 45.4% ethanol in ddH_2O) and incubated under constant shaking at room temperature overnight. Excess coomassie stain in the gel was removed by coomassie destaining solution (10% (v/v) acetic acid, 20% (v/v) ethanol in ddH_2O) which was removed and renewed every two hours. Gels were analyzed with image reader LAS-4000 and ImageQuant™ software version 1.2.

Labeling of recombinant H. sapiens ClpP

For labeling of recombinantly expressed hClpP 1 µL probe (**35**, solution in DMSO) was incubated with 49 µL hClpP (1.02 µM, final concentration: 1 µM) in hClpP SEC-buffer (20 mM HEPES, 100 mM NaCl, pH = 7.0) at room temperature for 1 h. Afterwards *Click* chemistry was conducted as described above with 5 µL *Click* master mix (1 µL TAMRA-N_3, 5 mM in DMSO (*Life Technologies*), 1 µL TCEP, 52 mM in ddH_2O and 3 µL TBTA ligand, 1.67 mM in 80% (v/v) *t*-BuOH, 20% (v/v) DMSO). The reaction was initiated with 1 µL $CuSO_4$ (50 mM in ddH_2O) and samples were incubated in the dark at room temperature for 1 h. Then, 56 µL Laemmli buffer (2x) was added and proteins were visualized by SDS-PAGE.

Labeling in E. coli expression strain

To substantiate that ClpP can also be addressed by phenyl ester probes in a more complex environment labeling was conducted in *E. coli* Rosetta2 expression strain. For this, 100 mL LB-medium containing ampicillin (1:1,000 from 100 mg/mL stock in ethanol/water 1:1) and chloramphenicol (1:1,000 from 34 mg/mL stock in ethanol) was inoculated with 1 mL overnight culture and was grown until OD_{600} reached 0.6 at 37 °C. Then the bacteria culture was split in two parts and in one half expression was induced by addition of 50 µL IPTG (0.5 M stock in water). The other half was not induced and served as a control. After incubation for further 3 h at 37 °C bacteria were harvested by centrifugation (6,000 g, 10 min, 4 °C) and were diluted with PBS-buffer to an OD_{600} of 40. 198 µL bacteria suspension was treated with 2 µL probe (3 mM in DMSO, final

concentration 30 µM, max. 1% (v/v) DMSO) or DMSO and was incubated under constant shaking at 25 °C for 1 h. Afterwards bacteria were centrifuged (6,000 g, 10 min, 4 °C), washed once with 200 µL ice-cold PBS-buffer, centrifuged and stored at -20 °C. Cells were resuspended in 200 µL ice-cold PBS-buffer and were lysed by sonication (2x 20 s, 80% intensity, Sonopuls, *Bandelin*). Cell debris was separated by centrifugation (21,100 g, 45 min, 4 °C) and 100 µL cytosolic fraction was used for *Click* reaction using 10 µL master mix (2 µL TAMRA-N_3, 5 mM in DMSO (*Life Technologies*), 1 µL TCEP, 52 mM in ddH_2O and 3 µL TBTA ligand, 1.67 mM in 80% (v/v) *t*-BuOH, 20% (v/v) DMSO). *Click* reaction was started by addition of 2 µL $CuSO_4$ (50 mM in ddH_2O) and proceeded for 1 h at room temperature in the dark. Afterwards 110 µL Laemmli buffer was added and proteins were separated by SDS-PAGE.

5.2.2.12 MS-based labeling experiments

Labeling in Jurkat cell line

Cells were grown in RPMI medium supplemented with 10% (v/v) heat-inactivated FBS and 2 mM L-glutamine in T175 culture flasks (*Sarstedt*). For preparative labeling experiments cells were washed with warm PBS-buffer, centrifuged (600 g, 6 min, RT), reconstituted in medium without FBS and counted using a Neubauer improved counting chamber (*LaborOptik Ltd.*). $2.9 \cdot 10^6$ cells/mL were seeded in each well of a 6-well plate leading to $\approx 17 \cdot 10^6$ cells per replicate. Labeling was conducted in four technical replicates per state. For this purpose, 1 µL of **35** in DMSO (20 µM final concentration) or DMSO as control were added to each well and were incubated for 1 h at 37 °C and 5% CO_2. Afterwards cells were harvested by gently scraping the surface of each well and transferring the cell suspension into centrifuge tubes, following a centrifugation step (600 g, 6 min, 4 °C), washing with ice-cold PBS-buffer and incubation with lysis buffer.

Labeling in Huh7 cell line

Huh7 cells were grown on TC150 dishes (*Sarstedt*) in DMEM medium supplemented with 10% (v/v) heat-inactivated FBS and 2 mM L-glutamine to a confluency of ≈ 70 – 80%. Prior to seeding culture dishes were coated with collagen A (0.1 mg/mL in PBS pH = 3.5, *Merck*, L7220) according to manufacturer's protocol. For labeling experiments cells were washed once with warm PBS-buffer, then 12 mL labeling medium (DMEM, with 2 mM L-glutamine, without FBS) with probe (20 µM final concentration of **35** or **D3** in DMSO, max. 0.1% DMSO) or DMSO was added and cells were incubated for 1 h at 37 °C with 5% CO_2. Afterwards, medium was removed, cells were washed with 10 mL ice-cold PBS-buffer, gently scraped off and resuspended in 1 mL lysis buffer.

Cell lysis and BCA assay

Cell pellets were incubated with 1 mL lysis buffer for 30 min (1 h for Huh7) on ice. Cytosolic fraction was obtained by pelletizing membranes and nuclei (21,000 g, 45 min, 4 °C). Protein concentration of cytosolic fractions were determined *via* BCA-assay using the Roti®Quant kit (*Carl Roth*). For this, 20 µL cell lysate from each replicate was diluted with 180 µL ddH_2O and 50 µL protein solution was pipetted in a transparent 96-well plate in triplicates. A dilution series of bovine serum albumin (BSA, *Sigma Aldrich*) was aliquoted in the same manner. 100 µL BCA-mix (reagent 1: reagent 2 = 15:1, Roti®Quant universal, *Carl Roth*) was added and incubated at 60 °C for 15 min. Afterwards, the absorption was measured on a *Tecan Infinite M Nano+* (absorbance wavelength: λ = 492 nm) and protein concentration was determined by comparison to the calibration curve of standard BSA. Protein concentration was adjusted by addition of lysis buffer to a final concentration of 1 – 2 mg protein/mL.

Click chemistry, protein precipitation

In the case of labeling with **35** in Jurkat and Huh7 cells *Click* chemistry was performed with 900 µL cytosolic fraction and 60 µL click mastermix (20 µL Biotin-PEG-N_3 10 mM in DMSO (*Jena Bioscience*), 10 µL TCEP 52 mM in H_2O, 30 µL TBTA ligand (1.67 mM in 80% (v/v) *t*-BuOH, 20% (v/v) DMSO)) and finally 10 µL $CuSO_4$ (50 mM in ddH_2O) at room temperature for 1 h. For labeling with **D3** in Huh7 cells 900 µL cytosolic cell lysate per replicate were incubated for 1 h at room temperature with 43 µL click mastermix consisting of the following components: 3 µL biotin-PEG-N_3 10 mM in DMSO, 10 µL TCEP 52 mM in H_2O, 30 µL TBTA ligand (1.67 mM in 80% (v/v) *t*-BuOH, 20% (v/v) DMSO)). Click reaction was started by addition of 20 µL $CuSO_4$ (50 mM in ddH_2O). Protein precipitation was achieved by addition of four volumes acetone (-80 °C) and incubation over night at -20 °C. Precipitated proteins were pelletized by centrifugation (21,000 g, 15 min, 4 °C) and resuspended in 200 µL methanol (-80 °C, LC-MS grade) by sonication. The supernatant was discarded, the protein pellet was taken up in 500 µL PBS-buffer containing 0.2% (w/v) SDS and dissolved by sonication. Remaining precipitate was discarded after centrifugation (10,000 g, 10 min, 4 °C) and supernatant was used for the enrichment step.

Enrichment, reduction, alkylation and digestion

For protein enrichment 50 µL avidin-agarose beads suspension (*Sigma-Aldrich*, A9207) per sample was washed three times (1 mL 0.4% (w/v) SDS/PBS-buffer, centrifugation 400 g, 2 min, RT) and incubated with protein solution under continuous mixing at room temperature for 1 h in LoBind *Eppendorf* tubes. Afterwards beads were centrifuged (400 g, 3 min, RT) and subsequently washed three times with 0.2% (w/v) SDS/PBS-buffer and five times with PBS-buffer to remove

unspecifically bound proteins. 30 – 50 µL Protein-Avidin beads suspension in PBS-buffer were successively reduced, and digested by addition of 25 µL digestion buffer (5 ng/µL Trypsin (in 50 mM acetic acid), 50 mM Tris-HCl, 2 M urea, 1 mM DTT from fresh 1 M stock in water, pH = 8.0) and incubation at room temperature for 30 min with continuous shaking at 600 rpm (Thermomixer comfort 5355, *Eppendorf*). Alkylation and further digestion of proteins was performed by addition of 100 µL alkylation buffer (50 mM Tris-HCl, 2 M urea, 5.5 mM iodoacetamide (IAA, freshly prepared from 550 mM stock in H_2O), pH = 8.0) following incubation overnight at 25 °C with continuous shaking at 600 rpm (Thermomixer comfort 5355, *Eppendorf*). Digestion was stopped by adjusting the pH to 2 – 3 with 10% (v/v) aqueous formic acid (FA) to a final concentration of 1% FA. Beads were centrifuged (16,000 g, 3 min, RT) and supernatant was desalted using Sep-Pak® C18 columns (50 mg sorbent per cartridge, 55 – 105 µm particle size, WAT054955, *Waters*). In brief, columns were washed once with 1 mL acetonitrile (MeCN), once with 500 µL elution buffer (80% (v/v) MeCN, 19.5% (v/v) H_2O, 0.5% (v/v) FA) and three times with 1 mL 0.1% (v/v) FA in H_2O. Samples were loaded and eluted in LoBind *Eppendorf* tubes with 250 µL elution buffer after washing twice with 1 mL 0.1% (v/v) FA and once with 250 µL 0.5% (v/v) FA. Samples were dried by speedvac solvent removal and stored at -80 °C until further analysis.

Sample preparation for LC-MS/MS measurement

For MS-analysis peptide samples were dissolved in 25 – 40 µL 1% (v/v) FA in H_2O, sonicated twice for 10 min and filtered with 0.22 µm Ultrafree-MC® centrifugal filters (*Merck*, UFC30GVNB) equilibrated with 1% (v/v) FA in H_2O. Filtrates were transferred into MS vials and analyzed by LC-MS/MS.

Data acquisition by LC-MS/MS

Measurement on Orbitrap Fusion

Samples from labeling in Huh7 cells with **35** or **D3** were analyzed with an UltiMate 3000 nano HPLC system (*Dionex*) using Acclaim C18 PepMap100 (75 µm ID x 2 cm) trap and Acclaim PepMap RSLC C18 (75 µm ID x 50 cm) separation columns in an EASY-spray setting coupled to an Orbitrap Fusion (*Thermo Fisher Scientific Inc.*). 5 µL peptide samples (8 µL for **35**) were loaded on the trap and washed with 0.1% (v/v) TFA, then transferred to the analytical column (buffer A: H_2O with 0.1% (v/v) FA, buffer B: MeCN with 0.1% (v/v) FA, flow 0.3 µL/min, gradient: to 5% buffer B in 7 min, from 5% to 22% buffer B in 105 min, then to 32% buffer B in 10 min, to 90% buffer B in 10 min and hold at 90% buffer B for 10 min, then to 5% buffer B in 0.1 min and hold 5% buffer B for 9.9 min) and ionized by nanospray ionization (NSI) with spray voltage of 1.7 kV (2.1 kV for **35**) and capillary temperature of 275 °C. Orbitrap Fusion was operated in a TOP speed

data dependent mode. Full scan acquisition was performed in the orbitrap at a resolution of R = 120,000 and an AGC target of 2e5 in a scan range of 300 – 1500 m/z with a maximum injection time of 50 ms. Monoisotopic precursor selection as well as dynamic exclusion (dynamic exclusion duration: 60 s, mass tolerance low/high 10 ppm) was enabled. Precursors with charge states 2 - 7 and intensities greater than 5e3 were selected for fragmentation. Isolation was performed in the quadrupole using a window of 1.6 m/z. Precursors were analyzed to an AGC target of 1e5 and a maximum injection time of 50 ms with "inject ions for all available parallelizable time" set to true. Peptide fragments were generated by higher-energy collisional dissociation (HCD) with a collision energy of 30% and detected in the orbitrap with ion trap scan rate set to rapid.

Measurement on Q Exactive Plus

Samples from labeling in Jurkat cells with **35** were analyzed with an UltiMate 3000 nano HPLC system (*Dionex*) using Acclaim C18 PepMap100 (75 µm ID x 2 cm) trap and Acclaim PepMap RSLC C18 (75 µm ID x 50 cm) separation columns in an EASY-spray setting coupled to a Q Exactive Plus (*Thermo Fisher Scientific Inc.*). 5 µL peptide samples were loaded on the trap and washed with 0.1% (v/v) TFA, then transferred to the analytical column (buffer A: H_2O with 0.1% (v/v) FA, buffer B: MeCN with 0.1% (v/v) FA, flow 0.3 µL/min, gradient: to 5% buffer B in 7 min, from 5% to 22% buffer B in 105 min, then to 32% buffer B in 10 min, to 90% buffer B in 10 min and hold at 90% buffer B for 10 min, then to 5% buffer B in 0.1 min and hold 5% buffer B for 9.9 min) and ionized at spray voltage of 2.0 kV and a capillary temperature of 275 °C. Q Exactive Plus was operated in a TOP12 data dependent mode with full scan acquisition in the orbitrap at a resolution of R = 140,000 and an AGC target of 3e6 in a scan range of 300 – 1500 m/z with a maximum injection time of 80 ms. Monoisotopic precursor selection as well as dynamic exclusion (dynamic exclusion duration: 60 s) was enabled. Precursors with charge states >1 and intensities greater than 1e4 were selected for fragmentation. Isolation was performed in the quadrupole using a window of 1.6 m/z. Precursors were analyzed in a scan range of 200 – 2,000 m/z to an AGC target of 1e5 and a maximum injection time of 100 ms. Peptide fragments were generated by higher-energy collisional dissociation (HCD) with a normalized collision energy of 27% and detected in the orbitrap.

Data processing: general comments

MS-data were analyzed using MaxQuant software (versions 1.5.5.0 and 1.6.0.1). Peptides were identified by comparison of MS/MS spectra against Uniprot human reference proteome (taxon identifier 9606, canonical version, without isoforms, for **D3** labeling: downloaded 2017/03/13, for **35** labeling: downloaded 2017/07/18) using Andromeda search engine. MaxQuant settings were

largely set on default. Carbamidomethylation of cysteines was used as fixed modifications and methionine oxidation and N-terminal acetylation were included as modifications in protein quantification. Trypsin/P was set as digestion enzyme and min. peptide length was set to 7. False discovery rate for proteins, sites and PSM was set to 0.01. Match between runs was enabled with a matching window of 0.7 min and alignment time window of 20 min.

Statistical analysis of proteomics data

Resulting data was further statistically analyzed with Perseus software (version 1.6.0.1). ProteinGroups files were loaded to Perseus, following $\log_2$-transformation and filtering by categorical columns. Protein groups satisfying the criteria of 'only identified by site', 'reverse' and 'potential contaminants' were excluded. Matrices were further filtered based on valid values (min. valids 50%), excluding protein groups that appear in less than half of all replicates. Missing values were replaced by imputation from normal distribution (width 0.3, down shift 0.9, total matrix). GO annotation downloaded from Uniprot and categorical annotation of probe treated samples and DMSO control was performed. To analyze the data two-sided student's *t*-tests with DMSO as single control group and Benjamini-Hochberg false discovery rate correction (FDR 0.05) were applied. Volcano plots were generated by plotting student's *t*-test difference (probe/DMSO) against *t*-test p-value (probe/DMSO).

5.3 Experimental part for chapter 3

5.3.1 Chemical Synthesis

Chemical synthesis was conducted by Tuan-Anh Nguyen in the laboratories of Prof. Kathrin Lang at TU München

Chemical synthesis was conducted as previously described and slightly modified.[149]

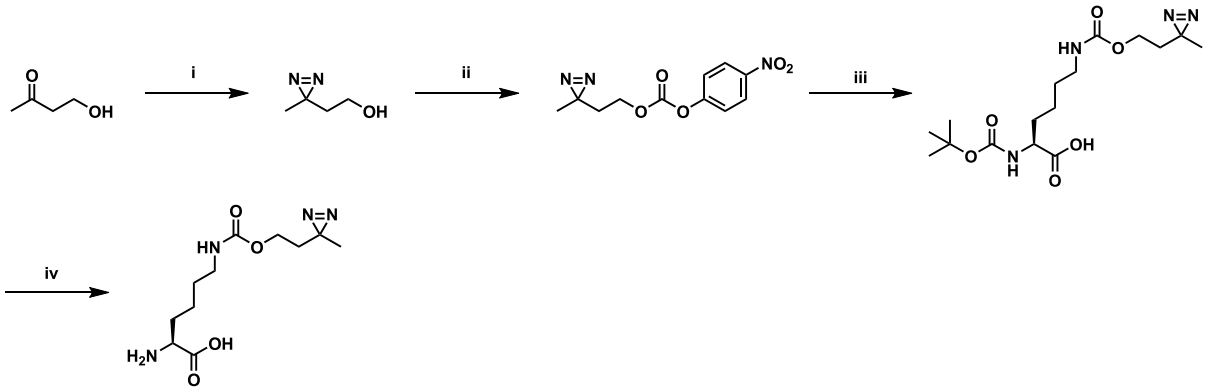

Figure 5.1 i) 1.) NH_3 (7 M in MeOH, 5.44 eq.), NH_2OSO_3H (1.11 eq.), 0 °C, 3 h, then RT o/n, 2.) I_2, NEt_3 (1.28 eq.), 0 °C, 3 h, MeOH, 42% over two steps; ii) 4-nitrophenyl carbonochloridate (1.20 eq.), pyridine (1.20 eq.), 0 °C to RT, o/n, DCM, 62%; iii) N-Boc-L-lysine (1.20 eq.), NEt_3 (2.00 eq.) RT, o/n, dioxane, 60%; iv) TFA (7.00 eq.) RT, 3 h, DCM, 96%.

5.3.2 Biochemical Methods

5.3.2.1 Cloning and protein overexpression

Cloning and protein overexpression was conducted by Tuan-Anh Nguyen in the laboratories of Prof. Kathrin Lang at TU München

Plasmids for bacterial expression were constructed with pET301_hClpP vectors bearing a C-terminal StrepII-tag and lacking the N-terminal 56 amino acid signal sequence. This was cloned into the pPylt backbone with a C-terminal His_6-tag applying Gibson cloning protocol as recommended by *New England BioLabs Inc.* Respective amber codon (TAG) positions were introduced *via* site-directed ligase independent mutagenesis (SLIM) methodology.[271]

Plasmids required for mammalian cell experiments were generated as follows. pRK5SV40_hClpP vectors from above-mentioned expressions containing the N-teminal 56-amino acid mitochondrial targeting sequence and bearing a C-terminal FLAG-tag was cloned into a pET17 helper vector. FLAG-tag was replacement by HA-tag was conducted *via* SLIM methodology as well as appropriate introduction of TAG positions. TAG-hClpP-HA constructs were amplified with primers bearing a XbaI and BamHI prior and after the gene of interest and were cloned into the SE325 backbone using standard restriction cloning protocol.[272]

Expression and purification of hClpP-TAG-H_6 for biochemical assays was conducted as follows. After co-transformation of pBK_Mb_PylRS_D171 (which encodes the synthetase for diaziK, Kanamycin^R) and pPylt_-56aa-hClpP-TAG-H_6 (Tetracycline^R) in *E. coli* DH10*β* cells and culturing overnight in LB medium with 1x antibiotic strength, culture was diluted into 2xYT to an OD_{600} = 0.05 with 1x antibiotics and incubated at 37 °C at 200 rpm. At OD_{600} ≈ 0.3, dK UAA was added to a final concentration of 1 mM (from 100 mM stock solution in 100 mM TFA in H_2O, filtered 0.2 μm). At OD_{600} ≈ 0.6, protein expression was induced with arabinose (0.02% (w/v) final concentration) at 37 °C, 200 rpm. After 3 h (for wt hClpP) or 18 h (for amber suppressed hClpP), cells were harvested by centrifugation (4200 rpm, 15 min, 4 °C). For SDS-PAGE analysis of amber suppressed hClpP, 1 mL of culture was harvested, pellet resuspended in 1x Laemmli buffer (normalised according to OD_{600} values; per OD_{600} = 1, 100 μL 1x SDS), boiled, pelleted and loaded onto a 15% SDS gel.

For protein purification, pellets were resuspended in lysis buffer (50 mM Tris/HCl, pH = 7.5, RT), 100 mM KCl, 10% (v/v) glycerol) and sonicated on ice, lysate cleared by centrifugation (13500 g, 35 min, 4 °C) and supernatant was subjected to HisTrap purification on GE Äkta system with increasing imidazole concentration (lysis buffer, 20 mM to 300 mM imidazole). Appropriate

fractions were analysed *via* 15% SDS-PAGE, pooled, concentrated and rebuffered (SEC buffer: 20 mM HEPES, pH = 7 (6 °C), 100 mM NaCl) and thereafter flash frozen and stored at -80 °C until further use.

5.3.2.2 Peptidase activity assay with ClpP mutants

Peptidase assays with hClpP mutants were largely conducted as described in chapter 5.2.2.2. Mutants SH1-7 were diluted in peptidase assay buffer (50 mM HEPES, 300 mM KCl, 1 mM DTT, 15% (v/v) glycerol, pH = 7.5) to a final enzyme concentration of 1 μM $hClpP_{monomer}$ (71.4 nM $hClpP_{14}$) in 98 μL buffer. Proteins were pipetted in a black 96-well plate and pre-incubated at 37 °C for 15 min. Fluorescence measurement was started immediately after addition of 1 μL AMC-substrate (Suc-Leu-Tyr-AMC, 20 mM stock in DMSO, final concentration 200 μM) at 37 °C on a Tecan Infinite M Nano+ (excitation wavelength: λ = 380 nm, emission wavelength: λ = 430 nm). Fluorescence data were plotted against time and the slope in the interval t = 300 – 1330 s was determined *via* linear regression using Microsoft Office Excel. Residual activity of hClpP mutants was determined by comparison to wild-type hClpP which was normalized to 100% activity.

5.3.2.3 Protease activity assay with ClpP mutants

Protease activity of hClpP mutants SH1-7 in combination with EcClpX was performed as described in chapter 5.2.2.4. ClpP and ClpX were diluted in PZ-buffer (25 mM HEPES, 200 mM KCl, 5 mM $MgCl_2 \cdot 6H_2O$, 1 mM DTT, 10% (v/v) glycerol, pH = 7.6). ATP-Regeneration mix (final concentration: 4 mM ATP, 16 mM creatine phosphate, 20 U/mL creatine phosphokinase) was added to yield final protein concentration of 0.2 μM $hClpP_{14}$ and 0.4 μM $EcClpX_6$. 60 μL protein solution per mutant was aliquoted in triplicates in a white 96-well plate and incubated at 37 °C for 15 min before 1 μL ssrA-eGFP (24 μM stock solution, final concentration 0.4 μM) was added. Fluorescence was measured on a Tecan Infinite M200 Pro (excitation wavelength: λ = 485 nm, emission wavelength: λ = 535 nm) at 37 °C over a time period of 60 min. The slope of the decreasing fluorescence signal was determined in the time interval t = 0 – 100 s by linear regression using Microsoft Office Excel. The residual activity of ClpP mutants was determined by comparison with wild-type hClpP which was normalized to 100% activity.

5.3.2.4 High resolution intact protein mass experiments

Validation of correct masses of recombinantly expressed hClpP mutants was conducted by high resolution intact protein mass spectrometry. For this, protein was diluted in water (LC-MS grade) to a concentration of 1 μM in 50 μL and was subsequently measured on a Dionex Ultimate 3000 HPLC (*Thermo Fisher Scientific Inc.*) coupled to a LTQ-FT Ultra mass spectrometer (*Thermo Fisher*

Scientific Inc.) with an electrospray ionization source (capillary temperature 275 °C, spray voltage 4.2 kV, tube lens 110 V, capillary voltage 48 V, sheath gas flow 60 arb, aux gas flow 10 arb, sweep gas flow 0.2 arb). 5 µL protein solution was on-line desalted by a Massprep desalting cartridge (*Waters*) and the mass spectrometer was operated in positive mode at a resolution of R = 200,000 within a range of 600 – 2,000 m/z. Deconvolution was preformed using *Thermo Xcalibur Xtract* software and theoretical monoisotopic masses were reported.

5.3.2.5 Human cell culture

Cells were cultivated by Tuan-Anh Nguyen in the laboratories of Prof. Kathrin Lang at TU München

For trapping experiments Hek293T wild-type cells (generously provided by Prof. Matthias Feige) were first transfected with plasmids encoding mutant ClpPs. For this, transfection optimization was performed in 12-well and 6-well plates with 10^5 cells and $5 \cdot 10^5$ cells/mL respectively (12-well plate: 1 mL, 6-well plate: 2 mL). 10 cm dishes with $3.5 \cdot 10^6$ cells/mL and total volume of 10 mL were used for proteomics experiments (triplicates for +UV and –UV). 24 h after seeding, media was replaced with DMEM supplemented with 2 mM dK (neutralization of pH was accomplished by addition of 1 M $NaOH_{aq}$). Plasmids SE325_+56aa_hClpP_TAG_HA and SE323_Mm_D171PylRS_4xtRNA (plasmid ratio 3:1) were incubated with Opti-MEM™ (*Gibco™, Fisher Scientific*) and poly(ethyleneimine) (PEI, *Sigma*) in stoichiometry as indicated in Table 5.5 for 15 min at RT prior to transfection. After 40-44 h post-transfection cells were washed 3 times with PBS (1 well volume, each) and cells were submitted to UV-light exposure (λ = 365 nm, 15 W, Vilber, VL-215.L) under permanent cooling on ice or were immediately harvested by scraping. Cells were pelleted (700 g, 4 °C, 15 min), flash frozen in liquid nitrogen and stored for limited time periods at -20 °C until further use.

Table 5.5 Parameters for transfection of mutant ClpP in Hek293T.

Dish type	*Total amount of DNA per well [µg]*	*Opti-MEM™ per well [µL]*	*PEI (1mg/mL) per well [µL]*
12 well	1	150	4
6 well	2	200	9
10 cm dish	10	1000	30

5.3.2.6 MS-based trapping experiments

In situ trapping and enrichment

Cells were thawn on ice, resuspended in 1 mL lysis buffer (50 mM Tris/HCl, 150 mM NaCl, 1 mM $MgCl_2 \cdot 6H_2O$, 1% (v/v) 4-Nonylphenyl-polyethylene glycol (NP-40), 5% (v/v) glycerol, pH = 7.4 at 4 °C) and incubated for 30 min at 4 °C. Afterwards membranes and cell debris were separated by centrifugation (21,100 g, 20 min, 4 °C). For protein enrichment, 30 µL monoclonal

HA-antibody agarose beads suspension (A2095, isotype IgG1, *Merck*) per replicate in LoBind Eppendorf tubes were equilibrated with 1 mL wash buffer (50 mM Tris/HCl, 150 mM NaCl, 0.05% (v/v) NP-40, 5% (v/v) glycerol, pH = 7.4 at 4 °C) and centrifuged at 1,000 g for 1 min at 4 °C. 500 µL cytosolic fraction were incubated with equilibrated beads for 3 h at 4 °C on a rotating wheel. Afterwards beads were centrifuged at 1,000 g for 1 min at 4 °C. The supernatant was discarded and beads were washed two times each with 1 mL wash buffer and two times each with 1 mL basic buffer (50 mM Tris/HCl, 150 mM NaCl, pH = 7.4 at 4 °C) to remove unspecifically bound proteins.

Digestion, reduction, alkylation

Digestion and reduction of enriched proteins was perfomed by addition of 25 µL digestion buffer I (5 ng/µL (in 50 mM acetic acid), 50 mM Tris/HCl, 2 M urea, 1 mM DTT (freshly prepared and diluted 1:1,000 from 1 M stock) pH = 8.0) and incubated for 30 min. Afterwards, alkylation of free cysteines and further digestion was conducted by addition of 100 µL digestion buffer II (5.5 mM IAA (freshly prepared and diluted 1:100 from 550 mM stock), 50 mM Tris/HCl, 2 M urea, pH = 8.0, following incubation for 16 – 19 h at 25 °C with continuous mixing at 650 rpm in a thermoshaker (Thermomixer comfort 5355, *Eppendorf*).

Desalting and sample preparation

Digestion was stopped by adjusting the pH to 2 – 3 *via* addition of 17.5 µL 10% (v/v) formic acid in water. Peptide solutions were desalted by stage tips with two-layered C18 material (*SDC-XC*, *3M*) according to a published protocol.[273] In brief, per replicate two layers of C18 material were packed into a 200 µL pipet tip and washed with 70 µL MeOH, 70 µL 80% (v/v) MeCN, 0.5% (v/v) FA and 3x 70 µL 0.5% (v/v) FA (centrifugation: 1,000 g, 1-2 min, RT). Samples were loaded and centrifuged at 1,000 g for 1-2 min at RT. Beads were washed with 70 µL 0.5% (v/v) FA and the washing solution was also loaded onto the C18 material. Samples were desalted by washing two times with 70 µL 0.5% (v/v) FA. Elution of peptides was conducted with 2x 30 µL 80% (v/v) MeCN, 0.5% (v/v) FA into fresh LoBind Eppendorf tubes followed by speedvac assisted solvent removal. Samples were stored at -80 °C until further use. For LC-MS/MS measurement sample peptides were dissolved in 25 µL 1% (v/v) aqueous FA and sonicated 3x 5 min with centrifugation for 1 min at 17,000 g in between. Dissolved peptides were filtered using 0.22 µm Ultrafree-MC® centrifugal filters (UFC30GVNB, *Merck*) pre-equilibrated with 300 µL 1% (v/v) FA. Filtrates were transferred to MS-vials prior to LC-MS/MS analysis.

Data acquisition on Orbitrap Fusion

Peptide samples from substrate enrichment experiments were analyzed with an UltiMate 3000 nano HPLC system (*Dionex*) using an Acclaim C18 PepMap100 (75 µm ID x 2 cm) trap and an Acclaim PepMap RSLC C18 (75 µm ID x 50 cm) separation column in EASY-spray setting coupled to an Orbitrap Fusion (*Thermo Fisher Scientific Inc.*). 1-5 µL peptide sample (see Table 5.6) were loaded on the trap and washed with 0.1% (v/v) TFA, then transferred to the analytical column (buffer A: H_2O with 0.1% (v/v) FA, buffer B: MeCN with 0.1% (v/v) FA, flow as indicated in Table 5.6, gradient: to 5% buffer B in 7 min, from 5% to 22% buffer B in 105 min, then to 32% buffer B in 10 min, to 90% buffer B in 10 min and hold at 90% buffer B for 10 min, then to 5% buffer B in 0.1 min and hold 5% buffer B for 9.9 min) and ionized by nanospray ionization (NSI) with capillary temperature of 275 °C. Spray voltage was applied as indicated in Table 5.6. Orbitrap Fusion was operated in a TOP speed data dependent mode. Master scan acquisition was carried out in the orbitrap at a resolution of R = 120,000, an AGC target of 2.0e5 in a scan range of 300 – 1500 m/z and a maximum injection time of 50 ms. Monoisotopic Peak Determination was set to "Peptide" and dynamic exclusion was enabled with dynamic exclusion duration set to 60 s with a mass tolerance (low/high) of 10 ppm. Precursors with a charge state of 2 – 7 and intensities greater than 5.0e3 were submitted to fragmentation by higher collisional dissociation (HCD). Isolation of precursors was performed in the Quadrupole with an isolation window of 1.6 m/z. Detection was carried out in the ion trap to an AGC target of 1.0e4 with first mass set to 120 m/z, Ion Trap Scan Rate set to "Rapid" and "Inject Ions for All Available Parallelizable Time" set to true. Maximum Ion Injection Time was set to 100 ms and peptide fragments were generated by HCD with a collision energy of 30%.

Table 5.6 Mass spectrometry instrument parameters for enriched samples.

Samplename	*Injection volume [µL]*	*Flow [µL/min]*	*Spray voltage [kV]*
SH1 dK	5	0.3	1.87
SH2 dK	5	0.4	1.77
SH3 dK	5	0.4	1.77
SH4 dK	5	0.4	1.77
SH5 dK	5	0.4	1.77
SH6 dK	5	0.4	1.77
SH7 dK	5	0.4	1.77
SH2 dK Rot	1	0.4	1.77
SH7 dK Rot	1	0.4	1.77

Data processing

MS-data were processed using Andromeda search engine of MaxQuant (MQ) Software (version 1.6.0.1). For identification of peptides, MS/MS spectra were searched against a Uniprot reference proteome (taxon identifier 9606, canonical version, without isoforms, downloaded 2017/07/18). MaxQuant settings were largely set on default with Label-free quantification (LFQ) enabled and Trypsin as digestion enzyme with a maximum of 2 missed cleavages and a minimum peptide length of 7 amino acids. Methionine oxidation and N-terminal acetylation were set as variable modifications with a maximum number of 5 modifications per peptide and carbamidomethylation of cysteines was used as fixed modification. Second peptide search was enabled as well as match between runs with a matching time window of 0.7 min and an alignment time window of 20 min. For identification false discovery rate on the PSM, protein and site level was set to 0.01.

Statistical MS-data analysis

MaxQuant data were further statistically processed with Perseus software (version 1.6.2.3). ProteinGroups table was loaded into the program with LFQ intensities of all replicates as main column. Rows were filtered based on categorical columns omitting values that met the criterium of "reverse", "potential contaminant" and "only identified by site". After $\log_2$ transformation, matrices were further filtered based on valid values. Proteins with less than 50% of valid values in LFQ intensity compared to all replicates were excluded. Remaining missing values were inserted by imputation from a normal distribution (width: 0.3, down shift: 1.2 – 1.8). Categorical annotation of UV-irradiated (+UV) and non-treated (-UV) samples was performed before data were analyzed by two-sided student's *t*-test with –UV as single control group with Benjamini-Hochberg false discovery rate correction (FDR 0.05). Additionally, GO-term annotations with GOBP, GOMF and GOCC, downloaded from Uniprot were added.

5.4 Experimental part for chapter 4

5.4.1 Chemical Synthesis

(Z)-2-methyl-4-(3,4,5-trimethoxybenzylidene)oxazol-5(4*H*)-one (41)

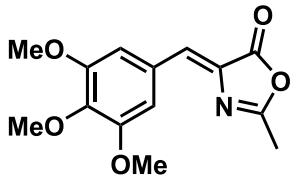

N-acetylglycine (4.95 g, 42.3 mmol, 1.00 eq.) and sodium acetate (3.47 g, 42.3 mmol, 1.00 eq.) were suspended in acetic anhydride (30 mL) and stirred at room temperature for 30 min. 3,4,5-Trimethoxybenzaldehyde (8.30 g, 42.3 mmol, 1.00 eq.) was added and the resulting mixture was heated at 80 °C for 6 h. When TLC showed no remaining starting material, the brownish suspension was cooled to room temperature. 600 mL ethanol/water (1:2) was added and the resulting suspension was stirred for another 30 min. The precipitate was filtered and further washed with ethanol/water (1:2) before lyophilisation yielded the title compound (7.20 g, 26.0 mmol, 61%) as a yellow solid. **^{1}H-NMR** ($CDCl_3$, 300 MHz, 300 K): δ (ppm) = 7.40, (s, 2H), 7.05 (q, ^4J = 0.5 Hz, 1H), 3.92 (s, 3H), 3.92 (s, 6H), 2.40 (*virt.* d, 3H, E/Z-isomers). **^{13}C-NMR** ($CDCl_3$, 75 MHz, 300 K): δ (ppm) = 168.0, 165.8, 153.4, 141.3, 131.9, 131.6, 128.7, 109.8, 61.2, 56.4, 15.9. **HRMS** (ESI): *m/z* calcd for $C_{14}H_{15}NO_5$ $[M+H]^+$: 278.1023, found: 278.1023. **TLC**: R_f = 0.65 (0.5% MeOH/DCM).

Methyl-(Z)-2-acetamido-3-(3,4,5-trimethoxyphenyl)acrylate (42)

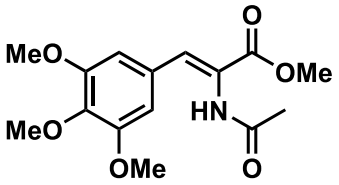

To a solution of sodium acetate (2.96 g, 36.1 mmol, 2.00 eq.) in methanol (100 mL) (Z)-2-methyl-4-(3,4,5-trimethoxybenzylidene)oxazol-5(4*H*)-one (5.00 g, 18.0 mmol, 1.00 eq.). The resulting mixture was stirred at room temperature for 4 h. Afterwards, the solvent was removed and the residue was dissolved in EtOAc (40 mL) and washed with water (50 mL). The aqueous phase was further extracted with EtOAc (3 · 50 mL) and the resulting organic phases were combined, washed with brine (50 mL) and dried over Na_2SO_4. After solvent removal, the product (4.99 g, 16.1 mmol, 89%) was isolated as a yellow solid. **^{1}H-NMR** ($CDCl_3$, 400 MHz, 300 K): δ (ppm) = 7.33 (s, 1H), 7.11 (s, 1H), 6.73 (s, 2H), 3.85 (d, *J* = 10.2 Hz, 6H), 3.82 (s, 6H), 2.15 (s, 3H). **^{13}C-NMR** ($CDCl_3$, 101 MHz, 300 K): δ (ppm) = 168.9, 165.9, 153.2, 139.4, 133.1, 129.1, 125.1 123.6, 107.3, 61.0, 56.2,

52.8, 23.5. **HRMS** (ESI): *m/z* calcd for $C_{15}H_{19}NO_6$ $[M+H]^+$: 310.1285, found: 310.1285. **TLC**: R_f = 0.35 (0.5% MeOH/DCM).

Rac-Methyl-2-acetamido-3-(3,4,5-trimethoxyphenyl)-propanoate (43)

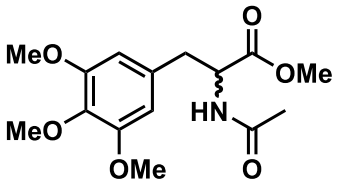

In a 1 L Schlenk flask activated palladium on charcoal (Pd/C, 10% (w/w), 800 mg) was degassed and a solution of methyl-(Z)-2-acetamido-3-(3,4,5-trimethoxyphenyl)acrylate (7.46 g, 24.1 mmol, 1.00 eq.) in methanol (200 mL) was added. The resulting mixture was stirred under H_2-atmosphere for 7 days until TLC showed complete conversion. Afterwards, the reaction mixture was filtered over Celite® and the solvent was removed *in vacuo* to yield the title compound (7.21 g, 23.2 mmol, 96%) as a colorless solid. **^{1}H-NMR** ($CDCl_3$, 500 MHz, 300 K): δ (ppm) = 6.30 (s, 2H), 5.91 (d, ^3J = 7.7 Hz, 1H), 4.87 (dt, ^3J = 7.6, 5.8 Hz, 1H), 3.83 (s, 3H), 3.82 (s, 6H), 3.74 (s, 3H), 3.13 - 3.02 (m, 2H) 2.01 (s, 3H). **^{13}C-NMR** ($CDCl_3$, 75 MHz, 300 K): δ (ppm) = 172.2, 169.7, 153.4, 137.3, 131.6, 106.3, 61.0, 56.3, 53.3, 52.5, 38.3, 23.4. **HRMS** (ESI): *m/z* calcd for $C_{15}H_{21}NO_6$ $[M+H]^+$: 312.1442, found: 3112.1441. **TLC**: R_f = 0.20 (hexane/ethyl acetate = 3:1).

(*S*)-2-Acetamido-3-(3,4,5-trimethoxyphenyl)propanoicacid ((*S*)-44) and (*R*)-Methyl-2-acetamido-4-(3,4,5-trimethoxyphenyl)propanoate ((*R*)-44)

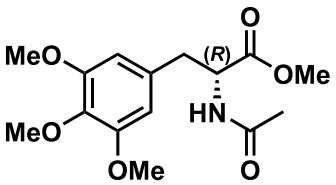

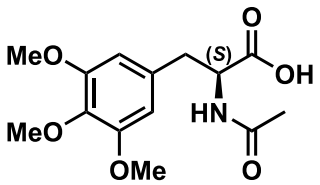

Finely ground methyl 2-acetamido-3-(3,4,5-trimethoxyphenyl)propanoate (2.00 g, 6.42 mmol, 1.00 eq.) was suspended in aqueous $NaHCO_3$-buffer (0.2 M, 69 mL, pH = 8.4) and heated to 37 °C. Alcalase® (0.5 mL, Protease from *Bacillus licheniformis*, >2.4 U/g, *Sigma Aldrich*) was added and the reaction was monitored by HPLC-MS. During the reaction, the pH value was adjusted by addition of 2 M $NaOH_{aq}$. When half-maximal conversion was reached the reaction was stopped by increasing the pH to 9 and the aqueous phase was extracted with CH_2Cl_2 (3 · 80 mL). The organic extracts were combined, washed with brine (100 mL) and the solvent was removed to yield (*R*)-methyl ester (911 mg, 2.93 mmol, 47%) as a white solid. For the (*S*)-enantiomer the aqueous phase of the reaction mixture was acidified with 2 M HCl_{aq} (7 mL) to a pH value of 1 and stirred for

30 min. After extraction with EtOAc (3 · 80 mL) the combined organic phase was washed with brine (100 mL) and the solvent was removed. The (*S*)-enantiomer (889 mg, 2.99 mmol, 47%) was isolated as a wheat-colored solid.

(44): **^{1}H-NMR** ($CDCl_3$, 400 MHz, 298 K): δ (ppm) = 6.39 (s, 2H), 6.11 (d, ^{3}J = 7.2 Hz, 1H), 4.82 (q, ^{3}J = 6.3 Hz, 1H), 3.83 (s, 3H), 3.82 (s, 6H), 3.27 – 2.89 (m, 2H), 2.02 (s, 3H). **^{13}C-NMR** ($CDCl_3$, 101 MHz, 300 K): δ (ppm) = 174.0, 171.4, 153.4, 137.2, 131.6, 106.5, 61.0, 56.3, 53.6, 37.5, 23.0. **HRMS** (ESI): *m/z* calcd for $C_{14}H_{19}NO_6$ $[M+H]^+$: 298.1285, found: 298.1284. **TLC**: R_f = 0.04 (hexane/ethyl acetate = 1:2 + 0.1% AcOH).

(45) **^{1}H-NMR** ($CDCl_3$, 400 MHz, 298 K): δ (ppm) = 6.30 (s, 2H), 5.91 (d, ^{3}J = 7.3 Hz, 1H), 4.87 (dt, ^{3}J = 7.7, 5.7 Hz, 1H), 3.83 (s, 3H), 3.82 (s, 6H), 3.75 (s, 3H), 3.07 (dd, ^{3}J = 5.8 Hz, ^{2}J = 1.9 Hz, 2H), 2.01 (s, 3H).**^{13}C-NMR** ($CDCl_3$, 101 MHz, 300 K): δ (ppm) = 172.2, 169.7, 153.4, 137.3, 131.6, 106.3, 61.0, 56.2, 53.3, 52.5, 38.2, 23.3. **HRMS** (ESI): *m/z* calcd for $C_{15}H_{21}NO_6$ $[M+H]^+$: 312.1442, found: 312.1441. **TLC**: R_f = 0.18 (hexane/ethyl acetate = 1:2 + 0.1% AcOH).

(*R*)-2-((tert-butoxycarbonyl)amino)-3-(3,4,5-trimethoxyphenyl)propanoic acid (45)

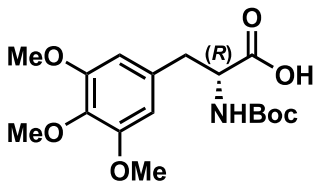

To a solution of methyl (*R*)-2-acetamido-3-(3,4,5-trimethoxyphenyl)propanoate (895.7 mg, 2.88 mmol, 1.00 eq.) in THF (25 mL) was added di-*tert*-butyldicarbonate (1.26 g, 5.75 mmol, 2.00 eq.) and the resulting mixture was stirred at 80 °C for 3 h. The reaction mixture was cooled down and aqueous LiOH (20 mL, 2 M) was added. Stirring for further 3 h resulted in a pale yellow emulsion. The organic solvent was removed and the remaining aqueous layer was acidified with concentrated HCl until a pH of 11 was reached. The aqueous phase was extracted with hexane (3 · 20 mL) and afterwards the pH was adjusted to 2 – 3 by addition of concentrated HCl. The white precipitate was filtered and lyophilized to yield the product (667 mg, 1.88 mmol, 65%) as a colorless solid. **^{1}H-NMR** (CD_3CN, 400 MHz, 298 K): δ (ppm) = 6.52 (s, 2H), 4.34 (td, ^{3}J = 8.8, 4.8 Hz, 1H), 3.78 (s, 3H), 3.68 (s, 6H), 3.09 (dd, ^{2}J = 13.9, 4.8 Hz, 3H), 2.81 (dd, ^{2}J = 13.9, ^{3}J = 9.2 Hz, 1H), 1.35 (s, 9H).**^{13}C-NMR** (CD_3CN, 101 MHz, 300 K): δ (ppm) = 174.1, 156.5, 154.1, 137.7, 134.1, 107.6, 80.0, 60.8, 56.7, 55.7, 38.4, 28.5. **HRMS** (ESI): *m/z* calcd for $C_{17}H_{25}NO_7$ $[M-H]^-$: 354.1558, found:.354.1561. **TLC**: R_f = 0.08 (3% MeOH/DCM = 1:2 + 0.1% AcOH).

Methyl (*R*)-4-((2-((*tert*-butoxycarbonyl)amino)-3-(3,4,5-trimethoxyphenyl)propanoyl)oxy) benzoate (46)

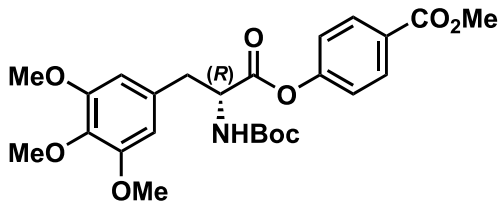

In a dried 25 mL Schlenk flask (*R*)-2-((tert-butoxycarbonyl)amino)-3-(3,4,5-trimethoxyphenyl)-propanoic acid (500 mg, 1.41 mmol, 1.00 eq.) was dissolved in anhydrous CH_2Cl_2 (18 mL) and cooled to 0 °C. Subsequently, methyl 4-hydroxybenzoate (225 mg, 1.48 mmol, 1.05 eq.), EDCI (283 mg, 1.48 mmol, 1.05 eq.), 1-hydroxybenzotriazol monohydrate (323 mg, 2.11 mmol, 1.50 eq.) and diisopropylethylamine (364 mg, 2.81 mmol, 2.00 eq.) were added. The resulting mixture was allowed to warm to room temperature while stirring for 20 h. Afterwards the resulting suspension was diluted with CH_2Cl_2 (20 mL) and the organic layer was washed with 5% (w/v) aqueous citric acid (3 · 20 mL), 5% (w/v) aqueous $NaHCO_3$ solution (3 · 20 mL) and brine (25 mL). After drying over Na_2SO_4 the solvent was removed under reduced pressure. Flash column chromatography (SiO_2, 40 mL, 2 cm, hexane/ethyl acetate = 100% → 20%) yielded the title compound (351 mg, 717 µmol, 51%) as an off-white solid. **^{1}H-NMR** ($CDCl_3$, 500 MHz, 298 K): δ (ppm) = 8.06 (d, ^3J = 8.6 Hz, 2H), 7.09 (d, ^3J = 8.5 Hz, 2H), 6.42 (s, 2H), 5.07 (d, ^3J = 7.9 Hz, 1H), 4.79 (q, ^3J = 7.0 Hz, 1H), 3.91 (s, 3H), 3.84 (s, 3H), 3.81 (s, 6H), 3.17 (d, ^3J = 6.2 Hz, 2H), 1.45 (s, 9H). **^{13}C-NMR** ($CDCl_3$, 101 MHz, 298 K): δ (ppm) = 170.3, 166.3, 155.2, 154.0, 153.5, 137.5, 131.3, 131.3, 128.2, 121.4, 106.5, 80.5, 61.0, 56.3, 54.9, 52.4, 38.8, 28.5. **HRMS** (ESI): *m/z* calcd for $C_{25}H_{31}NO_9$ $[M+H]^+$: 490.2072, found: 490.2071. **TLC**: R_f = 0.19 (hexane/ethyl acetate = 3:1).

Methyl (*R*)-4-((2-amino-3-(3,4,5-trimethoxyphenyl)propanoyl)oxy)benzoate TFA-salt (47)

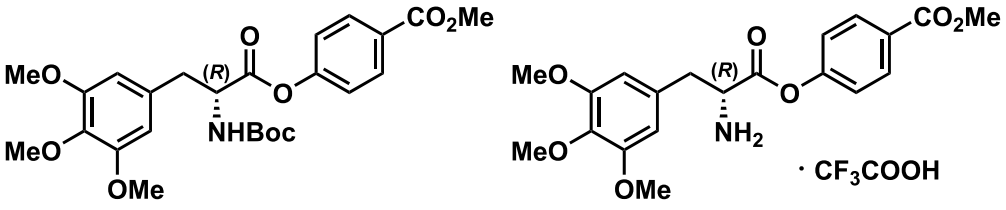

Under an argon atmosphere methyl (*R*)-4-((2-((tert-butoxycarbonyl)amino)-3-(3,4,5-trimethoxy-phenyl)propanoyl)oxy) benzoate (328 mg, 669 µmol, 1.00 eq.) was dissolved in anhydrous CH_2Cl_2 (5 mL) and cooled to 0 °C. Trifluoracetic acid (TFA, 500 µL, 6.49 mmol, 9.70 eq.) was added and the resulting mixture was stirred at 0 °C for 9 h. After warming to room temperature, the organic solvent was removed and the residue was taken up in CH_3CN/H_2O (1:1) and lyophilized. The

product (326 mg, 648 µmol, 97%) was isolated as a colorless solid. **^{1}H-NMR** (DMSO-d_6, 500 MHz, 298 K): δ (ppm) = 8.62 (s, 2H), 8.31 – 7.93 (m, 2H), 7.47 – 7.18 (m, 2H), 6.67 (s, 2H), 4.66 (t, ^3J = 6.7 Hz, 1H), 3.87 (s, 6H), 3.75 (s, 3H), 3.64 (s, 3H), 3.23 (dd, ^3J = 6.7, 2.1 Hz, 2H). **^{13}C-NMR** (DMSO-d_6, 101 MHz, 298 K): δ (ppm) = 167.5, 165.3, 153.1, 153.0, 136.8, 131.1, 129.7, 127.9, 121.7, 106.9, 59.9, 55.8, 53.4, 52.3, 36.1. **^{19}F-NMR** (DMSO-d_6, 376 MHz, 300 K, internal reference: C_6F_6: -161.64 ppm): δ (ppm) = –73.9. **HRMS** (ESI): *m/z* calcd for $C_{20}H_{23}NO_7$ $[M+H]^+$: 390.1547, found: 390.1548. **TLC**: R_f = 0.65 (10% MeOH/CH_2Cl_2).

(4-Azidophenyl)methanol (48)

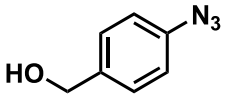

(4-Aminophenyl)methanol (1.00 g, 8.12 mmol, 1.00 eq.) was dissolved in 2 M H_2SO_4 (13 mL) and cooled to 0 °C to give a yellow-brown solution. Sodium nitrite (840 mg, 12.2 mmol, 1.50 eq.) dissolved in water (6.5 mL) was added slowly under stirring. After 15 min sodium azide (791 mg, 12.2 mmol, 1.50 eq.) dissolved in water (6.5 mL) was added dropwise and the resulting mixture was warmed to room temperature. The reaction mixture was extracted with diethyl ether (3 · 20 mL) and the combined organic phases were washed with brine (25 mL) dried over Na_2SO_4 and the solvent was removed under reduced pressure to give the title compound (1.17 g, 7.85 mmol, 97%) as a brown solid. **^{1}H-NMR** ($CDCl_3$, 500 MHz, 298 K): δ (ppm) = 7.36 – 7.32 (m, 2H), 7.03 – 7.00 (m, 2H), 4.65 (s, 2H), 1.87 (s, 1H). **^{3}C-NMR** ($CDCl_3$, 75 MHz, 298 K): δ (ppm) = 139.52, 137.72, 128.66, 119.25, 64.83. **TLC**: R_f = 0.69 (hexane/ethyl acetate = 1:3).

5-Benzyl 1-(*tert*-butyl) (*tert*-butoxycarbonyl)-D-glutamate (49)

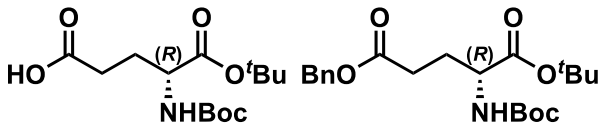

A solution of (*R*)-5-(benzyloxy)-2-((*tert*-butoxycarbonyl)amino)-5-oxopentanoic acid (2.00 g, 5.93 mmol, 1.00 eq.) in ice-cold anhydrous CH_2Cl_2 (4 mL) was added over 5 min to a cooled solution of EDCI (1.14 g, 5.93 mmol, 1.00 eq.), dimethylaminopyridine (36.0 mg, 296 µmol, 0.05 eq.) and *tert*-butanol (2.82 mL, 2.23 g, 30.1 mmol, 5.07 eq.) in CH_2Cl_2 (16 mL). The reaction mixture was stirred at 0 °C for 1 h before it was warmed to room temperature and stirred for another 22 h. The reaction mixture was diluted with 25 mL CH_2Cl_2 after TLC indicated that all starting material was consumed. The organic phase was washed with saturated aqueous $NaHCO_3$ solution (50 mL), water (50 mL) and brine (50 mL), dried over Na_2SO_4, filtered and concentrated

under reduced pressure. After purification by column chromatography (SiO_2, 2.8 L, 7.5 cm, hexane/ethyl acetate = 5:1) the product (826 mg, 2.10 mmol, 35%) was obtained as colorless oil which solidified after storage at -20 °C. **^{1}H-NMR** ($CDCl_3$, 300 MHz, 300 K): δ (ppm) = 7.38 – 7.32 (m, 5H), 5.12 (s, 2H), 5.05 (s, 1H), 4.21 (q, ^3J = 7.8 Hz, 1H), 2.55 – 2.34 (m, 2H), 2.18 (dq, ^3J = 14.1, 6.5 Hz, 1H), 2.00 – 1.85 (m, 1H), 1.46 (s, 9H), 1.43 (s, 9H). **^{13}C-NMR** ($CDCl_3$, 126 MHz, 300 K): δ (ppm) = 172.9, 171.5, 155.5, 135.9, 128.7, 128.4, 128.4, 82.4, 79.9, 66.6, 53.5, 30.5, 28.5, 28.3, 28.1. **HRMS** (ESI): *m/z* calcd for $C_{21}H_{31}NO_6$ $[M+H]^+$: 394.2224, found: 394.2224. **TLC**: R_f = 0.51 (hexane/ethyl acetate = 3:1).

(*R*)-5-(*tert*-butoxy)-4-((*tert*-butoxycarbonyl)amino)-5-oxopentanoic acid (50)

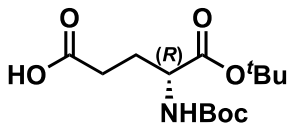

In a heated 100 mL Schlenk flask palladium on charcoal (Pd/C, activated, 10% (w/w), 188 mg, 0.07 eq.) was degassed two times. 5-Benzyl 1-(*tert*-butyl) (*tert*-butoxycarbonyl)-D-glutamate (993 mg, 2.52 mmol, 1.00 eq.) dissolved in methanol (10 mL) was added and the mixture was stirred under an atmosphere of H_2 at room temperature for 19 h. Afterwards the reaction mixture was diluted with EtOAc (30 mL) and filtered through a plug of Celite®. The filtrate was concentrated *in vacuo* to yield the title compound (765 mg, 2.52 mmol, >99%) as pale yellow solid. **^{1}H-NMR** ($CDCl_3$, 500 MHz, 298 K): δ (ppm) = 5.15 (d, ^3J = 8.1 Hz, 1H), 4.26 – 4.17 (m, 1H), 2.44 (qt, ^3J = 16.3, 7.3 Hz, 2H), 2.16 (dt, ^3J = 19.6, 6.7 Hz, 1H), 1.91 (dt, ^3J = 12.8, 6.3 Hz, 1H), 1.47 (s, 9H), 1.44 (s, 9H). **^{13}C-NMR** ($CDCl_3$, 126 MHz, 300 K): δ (ppm) = 177.4, 171.4, 155.8, 82.6, 80.3, 53.3, 30.3, 28.4, 28.1. **HRMS** (ESI): *m/z* calcd for $C_{14}H_{25}NO_6$ $[M+H]^+$: 304.1755, found: 304.1756. **TLC**: R_f = 0.23 (hexane/ethyl acetate = 3:1).

5-(4-azidobenzyl) 1-(*tert*-butyl) (*tert*-butoxycarbonyl)-D-glutamate (51)

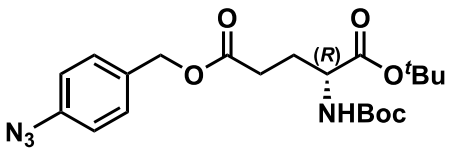

To a solution of (*R*)-5-(*tert*-butoxy)-4-((*tert*-butoxycarbonyl)amino)-5-oxopentanoic acid (584 mg, 1.92 mmol, 1.00 eq.) in anhydrous CH_2Cl_2 (19 mL) was added EDCI (738 mg, 3.85 mmol, 1.00 eq.), DMAP (118 mg, 966 µmol, 0.50 eq.) and then (4-azidophenyl)methanol (287 mg, 1.92 mmol, 1.00 eq.). The resulting mixture was stirred at room temperature for 21 h and was afterwards concentrated under reduced pressure. Purification by flash chromatography (SiO_2, 40 g,

40 mL/min, hexane/ethyl acetate 10% → 20% (5 min) → 50% (2 min) → 100% (2 min)) afforded the product (645 mg, 1.48 mmol, 77%) as yellow oil. **^{1}H-NMR** ($CDCl_3$, 500 MHz, 298 K): δ (ppm) = 7.34 (dd, ^3J = 8.7 Hz, ^4J = 2.0 Hz, 2H), 7.03 – 6.99 (m, 2H), 5.08 (d, ^2J = 4.2 Hz, 2H), 4.21 (q, ^3J = 7.4 Hz, 1H), 2.51 – 2.35 (m, 2H), 2.16 (dq, ^3J = 14.3, 6.6, 6.0 Hz, 1H), 1.96 – 1.83 (m, 1H), 1.45 (s, 9H), 1.43 (s, 9H). **^{13}C-NMR** ($CDCl_3$, 126 MHz, 300 K): δ (ppm) = 172.8, 171.4, 155.5, 140.2, 132.7, 130.1, 119.3, 82.4, 79.9, 65.9, 53.4, 30.4, 28.4, 28.2, 28.1. **HRMS** (ESI): *m/z* calcd for $C_{21}H_{30}N_4O_6$ $[M+H]^+$: 435.2238, found: 435.2239. **TLC**: R_f = 0.57 (hexane/ethyl acetate = 3:1).

5-(4-azidobenzyl) 1-(*tert*-butyl) D-glutamate (52)

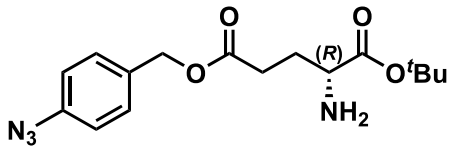

5-(4-azidobenzyl) 1-(*tert*-butyl) (*tert*-butoxycarbonyl)-D-glutamate (619 mg, 1.43 mmol, 1.00 eq.) was dissolved in anhydrous CH_2Cl_2 (9 mL) and cooled to 0 °C. Trifluoroacetic acid (1.06 mL, 1.58 g, 9.70 eq.) was added and the resulting mixture was stirred at 0 °C for 1.5 h and at room temperature for further 6 h. The solvent was removed under reduced pressure and the residue was dissolved in CH_3CN/water (1:1) and lyophilized to give the crude product as a brown solid. RP-HPLC (P2, 21 min, 30-60% B, λ = 253 nm) afforded the TFA-salt of the title compound (348.2 mg, 777 μmol, 54%) as a dark yellow solid. **^{1}H-NMR** ($CDCl_3$, 300 MHz, 300 K): δ (ppm) = 8.32 (s, 2H), 7.45 – 7.39 (m, 2H), 7.16 – 7.10 (m, 2H), 5.09 (s, 2H), 3.95 (t, ^3J = 6.7 Hz, 1H), 2.69 – 2.38 (m, 2H), 2.13 – 1.92 (m, 2H), 1.44 (s, 9H). **^{13}C-NMR** ($CDCl_3$, 126 MHz, 300 K): δ (ppm) = 171.5, 168.3, 139.3, 132.9, 130.1, 119.2, 83.3, 65.3, 51.6, 29.1, 27.5, 25.3. **HRMS** (ESI): *m/z* calcd for $C_{16}H_{22}N_4O_4$ $[M+H]^+$: 335.1714, found: 335.1715. **TLC**: R_f = 0.08 (hexane/ethyl acetate = 1:1).

5-(4-Azidobenzyl) 1-(*tert*-butyl) ((prop-2-yn-1-yloxy)carbonyl)-D-glutamate (53)

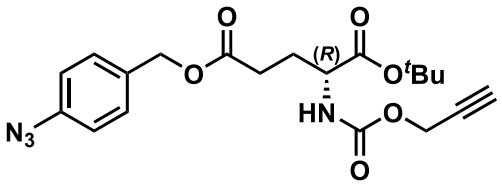

In a heated Schlenk flask 5-(4-azidobenzyl) 1-(*tert*-butyl) D-glutamate (326 mg, 726 μmol, 1.00 eq.) was dissolved in anhydrous CH_2Cl_2 (3.6 mL), cooled to 0 °C and $NaHCO_3$ (182 mg, 2.16 mmol, 2.98 eq.) was added. Propargyl chloroformate (74.0 μL, 98.4 mg, 763 μmol, 1.05 eq.) was added using a Hamilton® syringe and the mixture was stirred at 0 °C for 2.5 h. After this time another 1.05 eq. of propargylformate was added and the reaction continued for further 3 h. When TLC

indicated full conversion the mixture was diluted with CH_2Cl_2 (20 mL), filtered and concentrated under reduced pressure. The crude brown oil was purified by RP-HPLC (P2, 16 min, 60-90% D, λ = 251 nm) which afforded the product (204 mg, 489 μmol, 67%) as a pale yellow oil. **^{1}H-NMR** ($CDCl_3$, 500 MHz, 298 K): δ (ppm) = 7.37 – 7.31 (m, 2H), 7.05 – 6.98 (m, 2H), 5.40 (d, ^3J = 8.0 Hz, 1H), 5.08 (s, 2H), 4.73 – 4.61 (m, 2H), 4.27 (td, ^3J = 8.0, 4.9 Hz, 1H), 2.52 – 2.34 (m, 3H), 2.26 – 2.15 (m, 1H), 1.96 (dtd, ^3J = 14.3, 8.4, 6.1 Hz, 1H), 1.46 (s, 9H). **^{13}C-NMR** ($CDCl_3$, 126 MHz, 300 K): δ (ppm) = 172.7, 170.8, 155.1, 140.2, 132.6, 130.1 119.3, 82.8, 78.1, 75.0, 66.0, 53.9, 52.9, 30.3, 28.1, 28.0. **HRMS** (ESI): *m/z* calcd for $C_{20}H_{24}N_4O_6$ $[M+H]^+$: 417.1769, found: 417.1775. **TLC**: R_f = 0.79 (hexane/ethyl acetate = 1:1).

(*R*)-5-((4-azidobenzyl)oxy)-5-oxo-2-(((prop-2-yn-1-yloxy)carbonyl)amino)pentanoic acid (54)

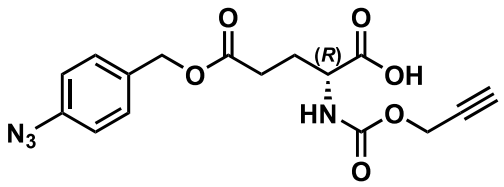

For deprotection of the ester 5-(4-azidobenzyl) 1-(*tert*-butyl) ((prop-2-yn-1-yloxy)carbonyl)-D-glutamate (143 mg, 342 μmol, 1.00 eq.) was dissolved in anhydrous CH_2Cl_2 (2 mL) and cooled to 0 °C. Trifluoroacetic acid (250 μL, 373 mg, 3.32 mmol, 9.70 eq.) was added and the reaction was stirred at 0 °C for 4 h. The solvent was removed under reduced pressure and the crude product was purified by RP-HPLC (1. run: P2, 20 min, 30-80% B, λ =252 nm, 2. run: P1, 20 min, 25-50% D, λ =252 nm). The product (27.4 mg, 76.0 μmol, 22%) was isolated as pale yellow oil. **^{1}H-NMR** ($CDCl_3$, 500 MHz, 298 K): δ (ppm) = 7.37 – 7.31 (m, 2H), 7.07 – 6.99 (m, 2H), 5.51 (d, ^3J = 8.0 Hz, 1H), 5.09 (s, 2H), 4.74 – 4.62 (m, 2H), 4.43 (td, ^3J = 8.0, 5.1 Hz, 1H), 2.60 – 2.43 (m, 2H), 2.48 (t, ^4J = 2.3 Hz, 1H), 2.28 (dtd, ^2J = 14.6 Hz, ^3J = 7.4, 5.0 Hz, 1H), 2.05 (dq, ^2J = 14.7 Hz, ^3J = 7.4 Hz, 1H). **^{13}C-NMR** ($CDCl_3$, 126 MHz, 300 K): δ (ppm) = 175.1, 172.9, 155.3, 140.4, 132.4, 130.2, 119.3, 77.9, 75.2, 66.3, 53.3, 53.2, 30.4, 27.4. **HRMS** (ESI): *m/z* calcd for $C_{16}H_{16}N_4O_6$ $[M+H]^+$: 361.1143, found: 361.1140. **TLC**: R_f = 0.18 (hexane/ethyl acetate = 1:2, + 0.2% AcOH).

Methyl 4-(((*R*)-2-((*R*)-5-((4-azidobenzyl)oxy)-5-oxo-2-(((prop-2-yn-1-yloxy)carbonyl)amino)pentanamido)-3-(3,4,5-trimethoxyphenyl)propanoyl)oxy)benzoate (Trap1)

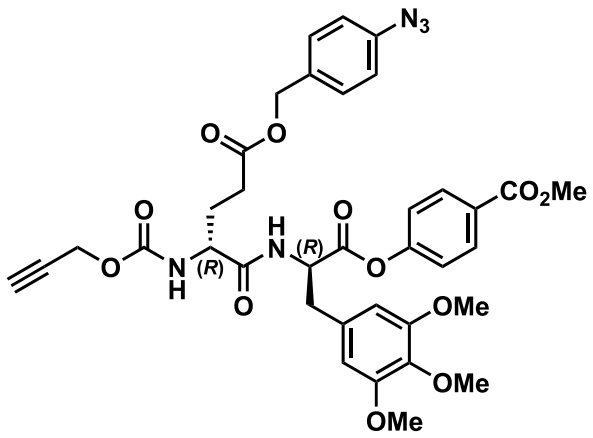

A solution of methyl (*R*)-4-((2-amino-3-(3,4,5-trimethoxyphenyl) propanoyl)oxy)benzoate 2,2,2-trifluoroacetate (37.5 mg, 74.5 μmol, 1.00 eq.) and (*R*)-5-oxo-2-(((prop-2-yn-1-yloxy)carbonyl)-amino)-5-((4-(3-(trifluoromethyl)-3*H*-diazirin-3-yl)benzyl)oxy)pentanoic acid (29.5 mg, 81.9 μmol, 1.10 eq.) in anhydrous DMF (1 mL) was cooled to 0 °C. (1-cyano-2-ethoxy-2-oxoethyliden-aminooxy)dimethylamino-morpholino-carbenium hexafluorophos-phate (35.1 mg, 81.9 μmol, 1.10 eq.) and diisopropylethylamine (25.3 μL, 19.3 mg, 149 μmol, 2.00 eq.) were added and the mixture was stirred and allowed to warm to room temperature overnight (22 h). The solvent was co-evaporated with toluene (5 ml) to yield the crude product as yellow-brown oil. The residue was taken up in CH_2Cl_2 (4 mL), washed subsequently with 5% (w/v) aqueous citric acid (3 · 2 mL), saturated $NaHCO_3$ solution (3 · 2 mL) and brine (5 mL), dried over $MgSO_4$ and concentrated under reduced pressure. The crude product was purified by column chromatography in a glas pipet (SiO_2, 5 mL, 0.5 cm, hexane/ethyl acetate = 3:2) to obtain the title compound (12.6 mg, 17.2 μmol, 23%) as a colorless solid. **^{1}H-NMR** ($CDCl_3$, 500 MHz, 301 K): δ (ppm) = 8.08 – 8.01 (m, 2H), 7.34 – 7.27 (m, 2H), 7.12 – 7.05 (m, 2H), 7.03 – 6.96 (m, 2H), 6.93 (d, ^3J = 7.3 Hz, 1H), 6.43 (*virt.* d, ^3J = 10.5 Hz, 2H), 5.66 (d, ^3J = 7.6 Hz, 1H), 5.05 (s, 2H), 5.02 (q, 3J = 6.6 Hz, 1H), 4.65 (*virt.* t, ^2J = 2.3 Hz, 2H), 4.30 (q, ^3J = 7.3 Hz, 1H), 3.92 (s, 3H), 3.83 (*virt.* d, ^3J = 5.3 Hz, 3H), 3.82 (s, 6H), 3.26 – 3.14 (m, 2H), 2.61 – 2.43 (m, 2H), 2.46 (t, ^4J = 2.3 Hz, 1H), 2.15 – 2.06 (m, 1H), 1.96 (dq, ^2J = 12.9 Hz, ^3J = 6.9 Hz, 1H). **^{13}C-NMR** ($CDCl_3$, 126 MHz, 301 K): δ (ppm) = 173.5, 173.4, 171.1, 169.6, 166.3, 166.2, 155.4, 153.9, 153.6, 140.4, 137.5, 132.3, 132.3, 131.4, 130.9, 130.8, 130.2, 130.1, 128.3, 121.4, 121.3, 119.3, 106.3, 78.0, 75.1, 66.3, 61.0, 56.3, 54.0, 53.8, 53.1, 53.0, 52.5, 38.3, 30.3, 28.3. **HRMS** (ESI): *m/z* calcd for $C_{36}H_{37}N_5O_{12}$ $[M+H]^+$: 723.2512, found: 732.2507. **TLC**: R_f = 0.8 (hexane/ethyl acetate = 1:2).

((4-Bromobenzyl)oxy)(*tert*-butyl)dimethylsilane (55)

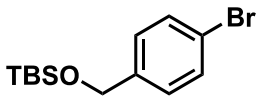

In an argon flushed flask (4-Bromophenyl)methanol (25.0 g, 134 mmol, 1.00 eq.) was dissolved in CH_2Cl_2 (250 mL) and *tert*-butyldimethylsilyl chloride (22.2 g, 147 mmol, 1.10 eq.) and imidazol (18.2 g, 267 mmol, 2.00 eq.) was added and the resulting mixture was stirred at room temperature for 21 h. Afterwards the reaction mixture was diluted with ice water and the organic layer was washed subsequently with saturated NH_4Cl solution (150 mL) and brine (150 mL). The organic phase was dried over Na_2SO_4 and the solvent was removed under reduced pressure to give the crude product (40.2 g, 134 mmol, >99%) as a colorless oil which was used without further purification. **^{1}H-NMR** ($CDCl_3$, 400 MHz, 298 K): δ (ppm) = 7.47 – 7.43 (m, 2H), 7.22 – 7.18 (m, 2H), 4.68 (s, 2H), 0.94 (s, 9H), 0.10 (s, 6H). **^{13}C-NMR** ($CDCl_3$, 101 MHz, 298 K): δ (ppm) = 140.6, 131.4, 127.9, 120.7, 64.5, 26.1, 18.5, -5.1. **TLC**: R_f = 0.67 (hexane/ethyl acetate = 25:1).

1-(4-(((*tert*-butyldimethylsilyl)oxy)methyl)phenyl)-2,2,2-trifluoroethan-1-one (56)

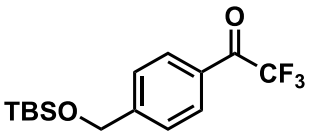

In a 500 mL Schlenk flask ((4-bromobenzyl)oxy)(tert-butyl)dimethylsilane (19.6 g, 64.9 mmol, 1.00 eq.) was dissolved in anhydrous THF (300 mL) and cooled to -78 °C. *n*-Butyl lithium (2.5 M, 54.5 mL, 136 mmol, 2.10 eq.) was added over 10 min. The resulting mixture was stirred at -78 °C for 30 min before adding methyl trifluormethylacetate (17.4 g, 13.6 mL, 136 mmol, 2.10 eq.). The reaction mixture was quenched after 3 h by warming to room temperature and addition of saturated NH_4Cl solution (150 mL). The organic phase was separated and the aqueous layer was extracted with EtOAc (3 · 50 mL). The combined organic phases were washed with brine (250 mL), dried over Na_2SO_4, filtered and the solvent was removed under reduced pressure to give a yellow oil and a colorless precipitate. The product was purified by column chromatography (SiO_2, 2.12 L, 7.5 cm, hexane/ethyl acetates = 40:1) to yield the title compound (19.1 g, 59.9 mmol, 92%) as a pale yellow oil. **^{1}H-NMR** ($CDCl_3$, 500 MHz, 300 K): δ (ppm) = 8.08 – 8.02 (m, 2H), 7.54 – 7.47 (m, 2H), 4.83 (s, 2H), 0.96 (s, 9H), 0.13 (s, 6H). **^{13}C-NMR** ($CDCl_3$, 75 MHz, 300 K): δ (ppm) = 180.3 (q, ^2J = 34.8 Hz), 150.2, 130.4 (q, ^3J = 3.1 Hz), 128.8, 126.3, 116.9 (q, ^1J = 291.4 Hz), 64.4, 26.0, 18.5 - 5.2. **^{19}F-NMR** ($CDCl_3$, 376 MHz, 300 K, internal reference: C_6F_6: -161.64 ppm): δ (ppm) = –71.2.

HRMS (ESI): *m/z* calcd for $C_{15}H_{21}F_3O_2Si$ [M-H]$^-$: 317.1190, found: 317.1195. **TLC**: R_f = 0.42 (hexane/ethyl acetate = 25:1).

(*E*/*Z*)-1-(4-(((*tert*-butyldimethylsilyl)oxy)methyl)phenyl)-2,2,2-trifluoroethan-1-one oxime (57)

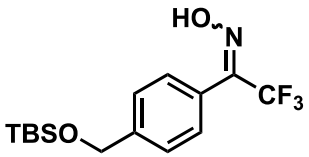

1-(4-(((*tert*-Butyldimethylsilyl)oxy)methyl)phenyl)-2,2,2-trifluoroethan-1-one (19.0 g, 59.8 mmol, 1.00 eq.) was dissolved in a mixture of anhydrous pyridine (173 mL) and anhydrous ethanol (81 mL). Hydroxylamine hydrochloride (4.57 g, 65.8 mmol, 1.10 eq.) was added under argon and the resulting mixture was heated at 80 °C for 19 h. Afterwards the solvent was removed and the residue was taken up in Et_2O (250 mL), washed with water (6 · 100 mL), 0.1 M HCl_{aq} (200 mL) and saturated $NaHCO_3$ solution (100 mL) and dried over Na_2SO_4. The solvent was removed under reduced pressure to give the crude product as a colorless oil which was further purified by column chromatography (SiO_2, 3.5 L, 7.5 cm, hexane/ethyl acetate =15:1 → 10:1). The title compound (7.28 g, 21.8 mmol, 37%) was isolated as a pale yellow oil. **^{1}H-NMR** ($CDCl_3$, 300 MHz, 298 K): δ (ppm) = 9.12 (s, 1H), 7.56 – 7.47 (m, 2H), 7.48 – 7.41 (m, 2H), 4.80 (s, 2H), 0.97 (s, 9H), 0.13 (s, 6H). **^{13}C-NMR** ($CDCl_3$, 75 MHz, 300 K): δ (ppm) = 147.8 (q, ^2J = 32.2 Hz), 144.3, 128.8, 126.1, 124.6, 120.8 (q, ^3J = 274.8 Hz) 64.6, 26.1, 25.8, 18.6, -3.5, -5.2. **^{19}F-NMR** ($CDCl_3$, 376 MHz, 300 K, internal reference: C_6F_6: -161.64 ppm): δ (ppm) = –66.4. **HRMS** (ESI): *m/z* calcd for $C_{15}H_{22}F_3NO_2Si$ [M-H]$^-$: 332.1299, found: 332.1300. **TLC**: R_f = 0.38 (hexane/ethyl acetate = 10:1).

(*E*/*Z*)-1-(4-(((*tert*-butyldimethylsilyl)oxy)methyl)phenyl)-2,2,2-trifluoroethan-1-one *O*-tosyl oxime (58)

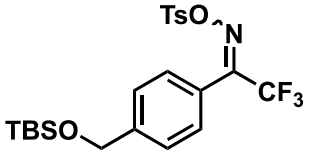

To a stirred solution of (E/Z)-1-(4-(((*tert*-butyldimethylsilyl)oxy)methyl)phenyl)-2,2,2-trifluoroethan-1-one oxime (7.13 g, 21.4 mmol, 1.00 eq.) in anhydrous CH_2Cl_2 (45 mL) under an inert atmosphere was added dimethyl-aminopyridine (235 mg, 1.92 mmol, 0.09 eq.), triethylamine (3.87 mL, 2.81 g, 27.8 mmol, 2.47 eq.) and *p*-tosyl choride (4.89 g, 25.7 mmol, 2.00 eq.) at 0 °C. The colorless slurry was warmed to room temperature and stirred for further 2.5 h. The reaction was quenched by addition of water (25 mL): The phases were separated and the organic layer was

additionally washed with water (2 · 25 mL) and brine (30 mL), dried over Na_2SO_4, filtered and concentrated. The crude yellow oil was further purified by column chromatography (SiO_2 2.3 L, 7.5 cm, hexane/ethyl acetate = 10:1) to yield the title compound (8.41 g, 17.2 mmol, 81%) as a pale yellow oil. **^{1}H-NMR** ($CDCl_3$, 500 MHz, 300 K): δ (ppm) = 7.92 – 7.86 (m, 2H), 7.46 – 7.40 (m, 2H), 7.42 – 7.35 (m, 4H), 4.78 (s, 2H), 2.48 (s, 3H), 0.96 (s, 9H), 0.12 (s, 6H). **^{13}C-NMR** ($CDCl_3$, 126 MHz, 300 K): δ (ppm) = 154.1 (q, ^2J = 33.3 Hz), 146.2, 145.7, 131.3, 130.0, 129.4, 128.9, 128.6, 126.1, 123.0, 119.8 (q, ^3J = 277.7 Hz), 64.4, 26.0, 21.9, 18.5, -5.2. **^{19}F-NMR** ($CDCl_3$, 376 MHz, 300 K, internal reference: C_6F_6: -161.64 ppm): δ (ppm) = -61.4, -66.5 (mixture of E/Z-isomers, integral ratio: 1:4). **TLC**: R_f = 0.36 (hexane/ethyl acetate = 10:1).

3-(4-(((*tert*-butyldimethylsilyl)oxy)methyl)phenyl)-3-(trifluoromethyl)diaziridine (59)

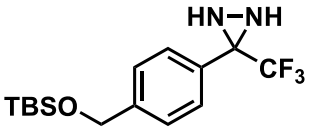

A stirred solution of (*E*/*Z*)-1-(4-(((*tert*-butyldimethylsilyl)oxy)methyl)phenyl)-2,2,2-trifluoroethan-1-one O-tosyl oxime (7.39 g, 15.1 mmol, 1.00 eq.) in 7 M ammonia in methanol (20 mL) was cooled to –50 °C and stirred for 1 h. After TLC showed full consumption of starting material excess ammonia was flushed out of the flask by a continuous N_2-stream. The residue was diluted with EtOAc, washed with water (100 mL), saturated $NaHCO_3$ solution (100 mL) and brine (100 mL). The organic solvent was dried over Na_2SO_4, filtered and concentrated. Purification by column chromatography (SiO_2, 3.7 L,.7.5 cm, hexane/ethyl acetate = 40:1 → 10:1) gave the title compound (2.60 g, 7.83 mmol, 52%) as yellow oil. **^{1}H-NMR** ($CDCl_3$, 500 MHz, 300 K): δ (ppm) = 7.58 (d, ^3J = 8.0 Hz, 2H), 7.38 (d, ^3J = 8.4 Hz, 2H), 4.76 (s, 2H), 2.76 (br s, 1H), 2.20 (br s, 1H), 0.95 (s, 9H), 0.11 (s, 6H). **^{13}C-NMR** ($CDCl_3$, 126 MHz, 300 K): δ (ppm) = 143.9, 130.3, 128.2, 126.3, 123.7 (q, ^3J = 278.3 Hz), 64.5, 58.1 (q, ^2J = 35.9 Hz), 26.1, 18.5, -5.2. **^{19}F-NMR** ($CDCl_3$, 376 MHz, 300 K, internal reference: C_6F_6: -161.64 ppm): δ (ppm) = -75.5. **HRMS** (ESI): *m*/*z* calcd for $C_{15}H_{23}F_3N_2OSi$ $[M+H]^+$: 333.1605, found: 333.1604. **TLC**: R_f = 0.34 (hexane/ethyl acetate = 10:1).

3-(4-(((*tert*-butyldimethylsilyl)oxy)methyl)phenyl)-3-(trifluoromethyl)-3*H*-diazirine (60)

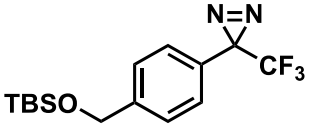

In a dark fumehood, to a stirred solution of 3-(4-(((*tert*-butyldimethylsilyl)oxy)methyl)phenyl)-3-(trifluoromethyl)diaziridine in methanol (4.8 mL) and anhydrous triethylamine (1.66 mL, 1.20 g,

11.9 mmol, 1.66 eq.) was added iodine (2.42 g, 9.53 mmol, 1.32 eq.) portion wise until a red color persisted. The reaction mixture was stirred for further 4.5 h and was quenched by addition of 5% (w/v) aqueous citric acid (5 mL). 5% (w/v) aqueous $Na_2S_2O_5$ solution (10 mL) was added and the organic phase was separated, dried over Na_2SO_4 and concentrated under reduced pressure. The crude product was purified by column chromatography (SiO_2, 1.5 L, 4 cm, hexane/ethyl acetate = 20:1) to give the title compound (1.86 g, 5.64 mmol, 79%) as a yellow oil. **^{1}H-NMR** ($CDCl_3$, 500 MHz, 300 K): δ (ppm) = 7.39 – 7.33 (m, 2H), 7.39 – 7.14 (m, 2H), 4.75 (s, 2H), 0.94 (d, J = 0.8 Hz, 9H), 0.10 (d, J = 0.8 Hz, 6H). **^{13}C-NMR** ($CDCl_3$, 126 MHz, 300 K): δ (ppm) = 143.5, 127.7, 126.5, 126.4, 122.3 (q, ^2J = 274.7 Hz), 64.4, 28.6 (q, ^3J = 40.3 Hz), 26.0, 18.5, -5.2. **^{19}F-NMR** ($CDCl_3$, 376 MHz, 300 K, internal reference: C_6F_6: -161.64 ppm): δ (ppm) = -65.2. **TLC**: R_f = 0.40 (hexane/ethyl acetate = 100:1).

4-(3-trifluoromethyl-3*H*-diazirin-3-yl)benzyl alcohol (61)

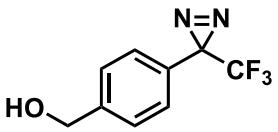

In a dark fume hood and under an argon atmosphere 3-(4-(((*tert*-butyldimethylsilyl)oxy)methyl) phenyl)-3-(trifluoromethyl)-3*H*-diazirine (1.78 g, 5.40 mmol, 1.00 eq.) was treated with tetrabutylammonium fluoride (1 M in THF, 6.54 mL, 6.54 mmol, 1.21 eq.) at room temperature. The reaction mixture was stirred for 30 min until TLC showed full conversion. Afterwards, the reaction mixture was diluted with diethyl ether (40 mL), washed with water (3 · 15 mL) and brine (20 mL), dried over Na_2SO_4, filtered and concentrated. The resulting crude product was further purified by column chromatography (SiO_2, 1 L, 4 cm, hexane/ethyl acetate = 4:1) to yield the title compound (1.05 g, 4.87 mmol, 90%) as a yellow oil. **^{1}H-NMR** ($CDCl_3$, 500 MHz, 300 K): δ (ppm) = 7.39 – 7.33 (m, 2H), 7.18 (d, ^3J = 8.1 Hz, 2H), 4.67 (s, 2H), 2.21 (s, 1H). **^{13}C-NMR** ($CDCl_3$, 126 MHz, 300 K): δ (ppm) = 142.6, 128.4, 127.2, 126.8, 122.2 (q, ^2J = 274.7 Hz), 64.5 (q, ^3J = 40.5 Hz), 28.5. **^{19}F-NMR** ($CDCl_3$, 376 MHz, 300 K, internal reference: C_6F_6: -161.64 ppm): δ (ppm) = -65.1. **HRMS** (ESI): m/z calcd for $C_9H_7F_3N_2O$ [M+FA-H]$^-$: 261.0493, found: 261.0494. **TLC**: R_f = 0.27 (hexane/ethyl acetate = 4:1).

1-(*tert*-butyl) 5-(4-(3-(trifluoromethyl)-3*H*-diazirin-3-yl)benzyl) (*tert*-butoxycarbonyl)-D-glutamate (62)

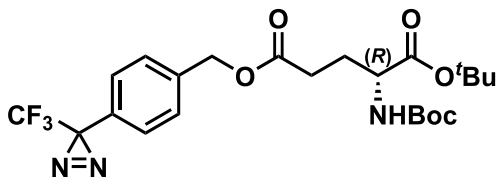

(*R*)-5-(*tert*-Butoxy)-4-((*tert*-butoxycarbonyl)amino)-5-oxopentanoic acid (350 mg, 1.15 mmol, 1.00 eq.) was dissolved in anhydrous CH_2Cl_2 (12 mL) under argon atmosphere. EDCI (442 mg, 2.31 mmol, 2.00 eq.), DMAP (70.5 mg, 1.58 mmol, 0.50 eq.) and 4-(3-trifluoromethyl-3*H*-diazirin-3-yl)benzyl alcohol (299 mg, 1.38 mmol, 1.20 eq.) was added and the mixture was stirred at room temperature for 22 h. The solvent was removed under reduced pressure and the residue was purified by column chromatography (SiO_2, 1.2 L, 3 cm, hexane/ethyl acetate =10:1). The title compound (396 mg, 789 µmol, 69%) was isolated as a yellow oil. **^{1}H-NMR** ($CDCl_3$, 500 MHz, 300 K): δ (ppm) = 7.42 – 7.35 (m, 2H), 7.22 – 7.16 (m, 2H), 5.14 (d, ^2J = 12.8 Hz, 1H), 5.10 (d, ^2J = 12.8 Hz, 1H), 5.06 (d, ^3J = 7.4 Hz, 1H), 4.21 (q, ^3J = 7.3 Hz, 1H), 2.48 (ddd, ^2J = 15.9 Hz, ^3J = 9.1, 6.7 Hz, 1H), 2.40 (ddd, ^2J = 16.6 Hz, ^3J = 9.0, 6.0 Hz, 1H), 2.17 (dq, ^2J = 13.8 Hz, ^{3}J = 6.3 Hz, 1H), 1.91 (dddd, ^2J = 14.1 Hz, ^3J = 9.0, 8.2, 6.0 Hz, 1H), 1.45 (s, 9H), 1.43 (s, 9H). **^{13}C-NMR** ($CDCl_3$, 126 MHz, 300 K): δ (ppm) = 172.7, 171.4, 155.5, 137.7, 129.2, 128.6, 126.8, 122.2 (q, ^3J = 274.7 Hz), 82.4, 80.0, 65.6, 53.4, 30.3, 28.4, 28.2, 28.1. **^{19}F-NMR** ($CDCl_3$, 376 MHz, 300 K, internal reference: C_6F_6: -161.64 ppm): δ (ppm) = -65.1. **HRMS** (ESI): *m/z* calcd for $C_{23}H_{30}F_3N_3O_6$ $[M+H]^+$: 502.2160, found: 502.2167. **TLC**: R_f = 0.39 (hexane/ethyl acetate = 4:1).

1-(*tert*-butyl) 5-(4-(3-(trifluoromethyl)-3*H*-diazirin-3-yl)benzyl) D-glutamate (63)

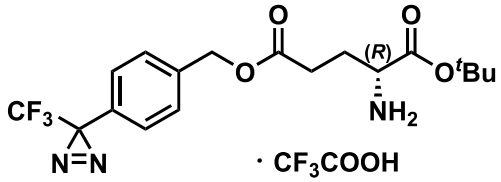

For deprotection of the amine 1-(*tert*-butyl) 5-(4-(3-(trifluoromethyl)-3*H*-diazirin-3-yl)benzyl) (*tert*-butoxycarbonyl)-D-glutamate (363 mg, 724 µmol, 1.00 eq.) was dissolved in anhydrous CH_2Cl_2 (4.7 mL) and cooled to 0 °C. Trifluoroacetic acid (540 µL, 805 mg, 7.03 mmol, 9.70 eq.) was added and the resulting mixture was stirred at 0 °C for 5 h and afterwards at room temperature for 1 h. The solvent was removed under reduced pressure and the crude product was purified by RP-HPLC (P2, 21 min, 30-70% B, λ = 222 nm) to give the product (215 mg, 418 µmol, 58%) as a colorless solid in form of the TFA-salt. **^{1}H-NMR** (DMSO-d_6, 500 MHz, 300 K): δ (ppm) = 8.26 (s, 3H),

7.54 – 7.48 (m, 2H), 7.34 – 7.28 (m, 2H), 5.16 (s, 2H), 3.95 (t, ^3J = 6.7 Hz, 1H), 2.62 (ddd, ^2J = 17.2 Hz, ^3J = 8.8, 6.3 Hz, 1H), 2.56 – 2.44 (m, 1H), 2.02 (dddd, ^2J = 19.1, 14.4 Hz, ^3J = 8.5, 7.1 Hz, 2H), 1.44 (s, 9H). **^{13}C-NMR** (DMSO-d_6, 126 MHz, 300 K): δ (ppm) = 171.5, 168.3, 138.5, 128.8, 127.3, 126.7, 121.9 (q, ^1J = 276.1 Hz), 83.3, 65.0, 51.6, 29.0, 28.1 (q, ^2J = 40.1 Hz), 27.5, 25.2. **^{19}F-NMR** (DMSO-d_6, 376 MHz, 300 K, internal reference: C_6F_6: -161.64 ppm): δ (ppm) = -63.7, -72.5 (TFA). **HRMS** (ESI): *m/z* calcd for $C_{18}H_{23}F_3N_3O_4$ $[M+H]^+$: 402.1635, found: 402.1639. **TLC**: R_f = 0.16 (hexane/ethyl acetate = 1:1).

1-(*tert*-butyl) 5-(4-(3-(trifluoromethyl)-3*H*-diazirin-3-yl)benzyl) ((prop-2-yn-1-yloxy)carbonyl)-D-glutamate (64)

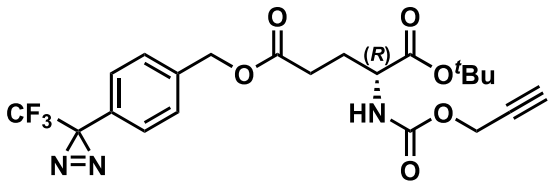

1-(*tert*-Butyl) 5-(4-(3-(trifluoromethyl)-3H-diazirin-3-yl)benzyl) D-glutamate 2,2,2-trifluoro-acetate (157 mg, 305 µmol, 1.00 eq.) was dissolved in anhydrous CH_2Cl_2 (6 mL) and cooled to 0 °C under an inert atmosphere. $NaHCO_3$ (76.4 mg, 909 µmol, 2.98 eq.) was added to the stirring solution and propargyl chloroformate (91.0 µL, 111 mg, 321 µmol, 3.05 eq.) was added dropwise with a Hamilton® syringe. The reaction mixture was allowed to warm to room temperature and was stirred for 4 h. After this time additional 2.05 eq. propargylchloroformate was added and the reaction continued for further 3 h. The mixture was diluted with CH_2Cl_2 (20 mL), filtered and concentrated under reduced pressure. The colorless oil was further purified by RP-HPLC (P2, 18 min, 60-98% B, λ = 225 nm) to give the product (132 mg, 272 µmol, 89%) as a colorless oil. **^{1}H-NMR** ($CDCl_3$, 500 MHz, 300 K): δ (ppm) = 7.40 – 7.36 (m, 2H), 7.21 – 7.17 (m, 2H), 5.40 (d, ^3J = 8.0 Hz, 1H), 5.12 (s, 2H), 4.72 – 4.62 (m, 2H), 4.28 (td, ^3J = 7.9, 4.9 Hz, 1H), 2.46 (t, ^4J = 2.6 Hz, 1H), 2.52 – 2.35 (m, 2H), 2.25 – 2.17 (m, 1H), 1.96 (dddd, ^2J = 14.1, ^3J = 8.8, 7.9, 6.1 Hz, 1H), 1.46 (s, 9H). **^{13}C-NMR** ($CDCl_3$, 126 MHz, 300 K): δ (ppm) = 172.5, 170.7, 155.1, 137.6, 129.2, 128.6, 126.9, 122.2 (q, ^1J = 274.7 Hz), 82.9, 78.1, 75.0, 65.7, 53.9, 52.9, 30.2, 28.4 (q, ^2J = 40.4 Hz) 28.1, 28.0. **^{19}F-NMR** ($CDCl_3$, 376 MHz, 300 K, internal reference: C_6F_6: -161.64 ppm): δ (ppm) = -65.1. **HRMS** (ESI): *m/z* calcd for $C_{22}H_{24}F_3N_3O_6$ $[M+H]^+$: 484.1690, found: 484.1695. **TLC**: R_f = 0.60 (hexane/ethyl acetate = 3:1).

(*R*)-5-oxo-2-(((prop-2-yn-1-yloxy)carbonyl)amino)-5-((4-(3-(trifluoromethyl)-3*H*-diazirin-3-yl)benzyl)oxy)pentanoic acid (65)

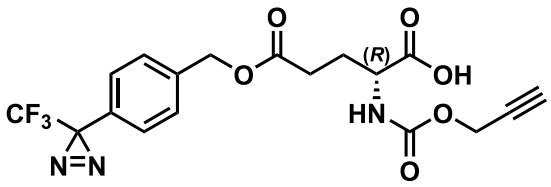

For deprotection of the *tert*-butyl ester a solution of 1-(*tert*-butyl) 5-(4-(3-(trifluoromethyl)-3*H*-diazirin-3-yl)benzyl) ((prop-2-yn-1-yloxy)carbonyl)-D-glutamate (99.8 mg, 206 μmol, 1.00 eq.) in anhydrous CH_2Cl_2 (1.4 mL) was cooled to 0 °C. Trifluoroacetic acid (153 μL, 228 mg, 2.00 mmol, 9.70 eq.) was added and the reaction mixture was stirred at 0 °C for 7.5 h. The solvent was removed under reduced pressure and the residue was purified by RP-HPLC (P2, 21 min, 20-60% D, λ = 222 nm). After lyophilization the product (74.1 mg, 173 μmol, 84%) was isolated as a pale yellow oil. **^{1}H-NMR** ($CDCl_3$, 500 MHz, 300 K): δ (ppm) = 7.39 – 7.35 (m, 2H), 7.20 (d, ^3J = 8.0 Hz, 2H), 5.51 (d, ^3J = 8.0 Hz, 1H), 5.13 (s, 2H), 4.73 – 4.62 (m, 2H), 4.44 (td, ^3J = 8.0, 5.0 Hz, 1H), 2.61 – 2.44 (m, 2H), 2.47 (t, ^4J = 2.1 Hz, 1H), 2.34 – 2.23 (m, 1H), 2.11 – 1.99 (m, 1H). **^{13}C-NMR** ($CDCl_3$, 101 MHz, 300 K): δ (ppm) = 175.7, 172.7, 155.4, 137.5, 129.3, 128.7, 126.9, 122.2 (q, ^1J = 274.8 Hz), 83.0, 77.9, 75.2, 65.9, 53.3, 53.2, 30.3, 28.5 (q, ^2J = 40.6 Hz), 28.1, 27.4. **^{19}F-NMR** ($CDCl_3$, 376 MHz, 300 K, internal reference: C_6F_6: -161.64 ppm): δ (ppm) = -65.1. **HRMS** (ESI): *m/z* calcd for $C_{18}H_{16}F_3N_3O_6$ $[M+H]^+$: 428.1064, found: 428.1069. **TLC**: R_f = 0.25 (hexane/ethyl acetate = 1:1 + 0.25% AcOH).

Methyl 4-(((*R*)-2-((*R*)-5-oxo-2-(((prop-2-yn-1-yloxy)carbonyl)amino)-5-((4-(3-(trifluoromethyl)-3*H*-diazirin-3-yl)benzyl)oxy)pentanamido)-3-(3,4,5-trimethoxyphenyl)propanoyl)oxy)benzoate (Trap2)

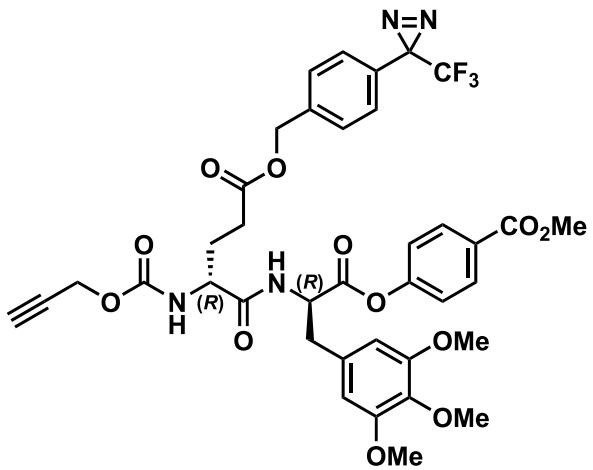

A solution of methyl (*R*)-4-((2-amino-3-(3,4,5-trimethoxyphenyl) propanoyl)oxy)benzoate 2,2,2-trifluoroacetate (52.4 mg, 104 μmol, 1.00 eq.) and (*R*)-5-oxo-2-(((prop-2-yn-1-yloxy)carbonyl)-

amino)-5-((4-(3-(trifluoromethyl)-3*H*-diazirin-3-yl)benzyl)oxy)pentanoic acid (48.9 mg, 115 μmol, 1.10 eq.) in anhydrous DMF (1 mL) was cooled to 0 °C. While stirring 1-cyano-2-ethoxy-2-oxoethyliden-aminooxy)dimethylamino-morpholino-carbenium hexafluorophosphate (49.0 mg, 115 μmol, 1.10 eq.) and diisopropylethylamine (35.4 μL, 26.9 mg, 208 μmol, 2.00 eq.) were added and the resulting mixture was allowed to warm to room temperature overnight (21 h). Toluene (5 mL) was added and the solvents were co-evaporated resulting in a yellow oil which was diluted with CH_2Cl_2 (5 mL). The organic phase was washed subsequently with 5% (w/v) aqueous citric acid (3 · 3 mL), saturated $NaHCO_3$ solution (3 · 3 mL) and brine (5 mL), dried over Na_2SO_4 and concentrated under reduced pressure. The crude yellow product was purified by column chromatography (1st column: glas pipet, SiO_2, 5 mL, 0.5 cm, hexane/ethyl acetate = 3:2; 2nd column: SiO_2 400 mL, 2 cm, 2% MeOH/DCM; 3rd column: SiO_2, 490 mL, 2 cm, 0.5% MeOH/DCM → 1% MeOH/DCM) to give the title compound (47.6 mg, 59.6 μmol, 57%) as a pale yellow solid. **^{1}H-NMR** ($CDCl_3$, 500 MHz, 298 K): δ (ppm) = 8.09 – 8.02 (m, 2H), 7.39 – 7.31 (m, 2H), 7.18 (dd, ^3J = 8.0, 4.3 Hz, 2H), 7.10 (dq, *J* = 9.3, 2.5 Hz, 2H), 6.78 (dd, *J* = 38.4, 7.1 Hz, 1H), 6.43 (d, *J* = 9.4 Hz, 2H), 5.64 (dd, *J* = 38.8, 7.7 Hz, 1H), 5.10 (d, *J* = 5.0 Hz, 2H), 5.02 (p, *J* = 7.4, 6.9 Hz, 1H), 4.65 (t, *J* = 2.6 Hz, 1H), 4.66 – 4.60 (m, 1H), 4.28 (p, *J* = 6.8 Hz, 1H), 3.92 (s, 3H), 3.83 (d, *J* = 4.8 Hz, 3H), 3.81 (d, *J* = 6.5 Hz, 6H), 3.26 – 3.14 (m, 2H), 2.63 – 2.46 (m, 2H), 2.46 (dq, *J* = 5.2, 2.7 Hz, 1H), 2.39 (dt, *J* = 17.4, 6.4 Hz, 0H), 2.16 – 2.05 (m, 1H), 1.96 (ddt, *J* = 14.5, 11.3, 7.5 Hz, 1H). **^{13}C-NMR** (CD_3CN, 101 MHz, 300 K): δ (ppm) = 173.4 (d, *J* = 3.3 Hz), 172.3, 170.7, 166.8 (d, *J* = 2.0 Hz), 156.2, 155.2 (d, *J* = 7.3 Hz), 154.3 (d, *J* = 2.2 Hz), 139.7 (d, *J* = 2.1 Hz), 137.8, 133.3, 133.1, 131.9 (d, *J* = 1.2 Hz), 129.3 (d, *J* = 4.8 Hz), 129.1, 129.0 (d, *J* = 1.6 Hz), 127.6, 123.2 (q, *J* = 274.3 Hz), 122.7 (d, *J* = 5.4 Hz), 107.5 (d, *J* = 9.6 Hz), 79.4, 76.0 (d, *J* = 2.6 Hz), 66.0 (d, *J* = 2.6 Hz), 60.8, 56.7, 55.1, 55.1, 53.2 (d, *J* = 4.0 Hz), 52.8, 37.8 (d, *J* = 3.0 Hz), 30.7 (d, *J* = 7.9 Hz), 29.2 (q, *J* = 39.5 Hz), 28.1. **HRMS** (ESI): *m/z* calcd for $C_{38}H_{37}F_3N_4O_{12}$ $[M+H]^+$: 799.2428, found: 799.2433. **TLC**: R_f = 0.27 (2% MeOH/CH_2Cl_2).

5.4.2 Biochemical Methods

5.4.2.1 Protein expression

Proteins SaClpP and SaClpX were graciously provided by Barbara Eyermann. Vector design and overexpression of these proteins was conducted according to previous reports.[24,228]

S. aureus ClpP

In brief, *E. coli* BL21 (DE3) cells carrying a ClpP construct with a C-terminal Strep-II tag were grown in LB-medium and overexpression was initiated by addition of 0.5 M IPTG. Cells were harvested after incubation for 4 h at 37 °C, lysed and the supernatant was subjected to affinity and size exclusion chromatography in the same way as with hClpP, described in chapter 5.2.2.

S. aureus ClpX

A His6-TEV-SaClpX construct was cloned in a pET300 vector and the protein was overexpressed in *E. coli* BL21 (DE3) cells after addition of 0.5 M IPTG at 25 °C overnight. Purification was conducted in the same manner as EcClpX in chapter 2 by affinity purification with a HisTrap HP 5 mL column. Following cleavage of the His-tag with TEV-protease the resulting crude protein was further purified by size exclusion chromatography using the same buffer system as described in chapter 5.2.2.

5.4.2.2 Peptidase activity assay

For investigation of the influence of phenyl esters on the peptidolytic activity of SaClpP a fluorometric assay with an artificial peptide substrate was conducted. For this compounds were aliquoted in a black 96-well plate and residual protein activity was compared to a DMSO control after addition of the fluorogenic substrate. In detail, 0.6 µL of compounds **Trap1** and **Trap2**, dissolved in DMSO, were pipetted in triplicates, 58.4 µL protein solution (0.14 µM $SaClpP_{monomer}$ concentration in EP buffer (100 mM NaCl, 100 mM HEPES, pH = 7.0) or PZ buffer (200 mM KCl, 25 mM HEPES, 5 mM $MgCl_2 \cdot 6H_2O$, 1 mM DTT, 10% (v/v) glycerol, pH = 7.6)) was added and incubated at 32 °C for 15 min. Afterwards, 1 µL substrate (Ac-Ala-hArg-2-Aoc-ACC, 200 µM final concentration, *Bachem*) was added and the resulting increase in fluorescence was measured on a Tecan Infinite F200 Pro (excitation wavelength: λ = 380 nm, emission wavelength: λ = 430 nm). The fluorescence signal was plotted against time and the initial slope in the interval t = 200 – 1200 s was determined *via* linear regression using Microsoft Office Excel. Residual activity of compound treated ClpP was determined by comparison to the DMSO control.

5.4.2.3 Protease activity assay

ClpP on its own is not able to degrade large proteins or oligopeptide but is dependent on a chaperone of the AAA+-family. In *S. aureus* this function can be adopted by proteins ClpA and ClpX.[274] To assess the residual protease activity after compound treatment with phenyl ester traps **Trap1** and **Trap2** a GFP-based degradation assay was used. For this 0.6 µL compound, dissolved in DMSO, was pipetted in a white 96-well plate, 58.4 µL enzyme mix (2.8 µM $SaClpP_{monomer}$, 2.4 µM $SaClpX_{monomer}$, in PZ-buffer with ATP-regeneration mix: 4mM ATP, 16 mM creatine phosphate and 20 U/mL creatine phosphokinase) was added and incubated at 32 °C for 15 min. The decline in fluorescence was measured after addition of 1 µL ssrA-tagged eGFP (24 µM stock, final concentration 0.4 µM) on a *Tecan Infinite F200 Pro* (excitation wavelength: λ = 485 nm, emission wavelength: λ = 535 nm). To eliminate perturbing effects due to thermal equilibration in the beginning the decreasing fluorescence signal in the interval t = 120 – 480 s was utilized for linear regression fitting with Microsoft Office Excel. The residual protein activity was determined by comparison to DMSO treated control samples which were normalized to 100% activity. Compound **AV170** was used as a positive control.[75]

5.4.2.4 High resolution intact protein mass spectrometry

Modification of SaClpP by phenyl ester traps **Trap1** and **Trap2** was determined by high resolution intact protein mass spectrometry in a similar manner as described in chapter 5.2.2.5. Briefly, 1 µL compound (three different final concentrations 1 µM, 10 µM, 100 µM) was incubated with 99 µL SaClpP (1 µM final concentration) in EP-buffer (100 mM HEPES, 100 mM NaCl, pH = 7.0) or PZ-buffer (25 mM HEPES, 200 mM KCl, 5 mM $MgCl_2 \cdot 6H_2O$, 1 mM DTT, 10% (v/v) glycerol, pH = 7.6) at room temperature for 1 h. 2 µL sample was on-line desalted by a Massprep desalting cartridge (*Waters*) and measured on the same instrument as mentioned above (capillary temperature 275 °C, spray voltage 4.2 kV, tube lens 120 V, capillary voltage 48 V, sheath gas flow 60 arb, aux gas flow 10 arb, sweep gas flow 0.0 arb) in positive mode at a resolution of R = 200,000 in a range of 600 – 2,000 m/z. Deconvolution was performed with *Xcalibur Xtract* software and theoretical monoisotopic masses were plotted.

5.4.2.5 Gel-based labeling experiments

Labeling in S. aureus NCTC8325 and lysis

For analytical labeling 50 mL B-medium (1% (w/v) peptone, 0.5% (w/v) NaCl, 0.5% (w/v) yeast, 0.1% (w/v) K_2HPO_4) was inoculated 1:100 with 0.5 mL overnight culture of the respective bacterial strain. Cells were grown until stationary phase + 1 h and were harvested by centrifugation (6,000 g, 10 min, 4 °C), washed with 10 mL ice-cold PBS-buffer and pelletized (6,000 g, 10 min,

4 °C). Bacteria were diluted to OD_{600} = 40 and 198 µL bacteria suspension were incubated with 2 µL probe (1:100 from DMSO stock solution) or DMSO as control in the dark at room temperature for 1 h. Afterwards bacteria were pelletized (6,000 g, 10 min, 4 °C), washed once with 500 µL ice-cold PBS-buffer (6,000 g, 10 min, 4 °C) and stored at -80 °C until further use. Cell lysis was achieved by sonication (4x 30 s, cooling break after each sonication step, 75% intensity, Sonopuls, *Bandelin*) in 200 µL ice-cold PBS-buffer and lysates were separated from cell debris by centrifugation (13,000 g, 30 min, 4 °C). Membrane fractions were solubilized with 200 µL 0.4% (w/v) SDS/PBS-buffer and sonication (10 s, 10% intensity).

Click reaction and SDS-PAGE

For visualization of labeled proteins, a fluorescent dye was attached to the probe-enzyme complex *via* copper(I)-catalyzed alkyne-azide cycloaddition (*Click* reaction). Cytosolic and membrane fractions were analyzed separately in the same manner as described in chapter 2. In brief, for each state, 100 µL cytosolic or membrane fraction was incubated with 10 µL click master mix (composition as described above). *Click* reaction was started by addition of 2 µL $CuSO_4$ (50 mM in ddH_2O) and samples were incubated in the dark at room temperature for 1 h. Afterwards the reaction was quenched by addition of 110 µL Laemmli buffer and proteins were separated by SDS polyacrylamide gel electrophoresis. For this, 12.5% polyacrylamide gels were loaded with 50 µL sample and were run for 2.5 h at 150 V, 500 mA. To determine protein size, 10 µL fluorescence standard (*Invitrogen™ Novex™ Benchmark™*) and Roti®Mark Standard (*Carl Roth*) were loaded in separate pockets of the gel. Fluorescence gels were analyzed with an image reader LAS-4000 (*Fujifilm Life Science*, USA) with a 575DF20 filter using ImageQuant LAS-4000 control software. For visualization of total protein amount loaded, gels were stained with coomassie staining solution (0.25% (w/v) Coomassie brilliant blue R-250, 9.20% (v/v) acetic acid, 45.4% ethanol in ddH_2O) and incubated under constant shaking at room temperature overnight. Excess coomassie stain in the gel was removed by coomassie destaining solution (10% (v/v) acetic acid, 20% (v/v) ethanol in ddH_2O) which was removed and renewed every two hours. Gels were analyzed with image reader LAS-4000 and ImageQuant™ software version 1.2.

5.4.2.6 *In vitro* trapping experiments

In vitro trapping experiments were conducted in 96-well plates with varying concentrations of probe and in different buffer systems. For this, the setup of GFP degradation assay, described in chapter 5.4.4 was adapted. 58.4 µL enzyme buffer mix (2.8 µM $SaClpP_{monomer}$, 2.4 µM $SaClpX_{monomer}$ in EP-buffer, PZ-buffer or PZ-buffer without DTT with ATP-regeneration mix: 4mM ATP, 16 mM creatine phosphate and 20 U/mL creatine phosphokinase) was added to 1 µL compound **Trap1**

or **Trap2** and incubated at 32 °C for 15 min. Control samples without **Trap1** or **Trap2**, SaClpP, SaClpX or GFP were included. 1 µL ssrA-tagged eGFP was added and incubated for 2 min. Afterwards samples were irradiated with UV-light (λ = 365 nm, *Philips TL-D BLB*, 18W) for 30 min under permanent cooling. Again, control samples without UV-irradiation were included. For visualization, a fluorescence dye was attached to the probes by *Click* chemistry. In detail, 5 µL click master mix (1 µL TAMRA-N_3 (5 mM), 1 µL TCEP (52 mM in ddH_2O), 3 µL TBTA ligand (1.67 mM in 80% (v/v) *t*-BuOH, 20% (v/v) DMSO) was added and the reaction was started by addition of 1 µL $CuSO_4$ (50 mM in ddH_2O). Samples were incubated in the dark at room temperature for 1 h before the reaction was quenched by addition of 53 µL Laemmli buffer. SDS-PAGE was performed to visualize photocrosslinked proteins.

For western blot analysis gels were prepared as described in chapter 5.2.2.10 using anti-GFP HRP-conjugate antibodies (*Abcam*, Camabridge, UK, dilution 1:5,000). Chemiluminescence readout was conducted after incubation with ECL-substrate (ECL, 100 mM Tris, 2.5 mM Luminol, 1 mM *p*-Coumaric acid, 17 µM H_2O_2, H_2O, pH = 8.5) on an image reader LAS-4000 (*Fujifilm Life Science*, USA) using ImageQuant LAS-4000 control software.

5.4.2.7 Gel-based trapping experiments

Labeling and photocrosslinking in S .aureus NCTC8325

For *in situ* trapping experiments 50 mL B-medium was inoculated with 500 µL overnight culture of *S. aureus* NCTC8325 and bacteria were grown until stationary phase + 1 h. Cells were harvested by centrifugation (6,000 g, 10 min, 4 °C), washed once with 10 mL PBS-buffer, centrifuged (6,000 g, 10 min, 4 °C) and diluted with PBS-buffer to an OD_{600} = 40. 198 µL bacterial suspension were incubated with 2 µL probe (from DMSO solution, max. 1% DMSO) in the dark at room temperature for 1 h. DMSO treated bacteria were used as control. For photocrosslinking, bacteria were diluted with 800 µL PBS-buffer, transferred to 12-well plates and irradiated with UV-light (λ = 365 nm, *Philips TL-D BLB*, 18W) under permanent cooling.

Lysis, Click chemistry and SDS-PAGE

Afterwards bacteria were harvested by centrifugation (6,000 g, 10 min, 4 °C), washed once with 500 µL ice-cold PBS-buffer, centrifuged (6,000 g, 10 min, 4 °C) and stored at -80 °C until further use. Lysis was performed in 200 µL ice-cold PBS-buffer by sonication (4x 30 s, 75% intensity, Sonopuls, *Bandelin*) with permanent cooling. Samples were centrifuged (10,000 g, 30 min, 4 °C) the cytosolic fraction was separated and the membrane fraction was washed once with 200 µL ice-cold PBS-buffer, centrifuged (6,000 g, 10 min, 4 °C) and solubilized in 200 µL 0.4% (w/v) SDS/PBS-

buffer. *Click* chemistry was performed as described above with 100 µL sample volume. The reaction was quenched by addition of 110 µL Laemmli buffer and proteins were separated by SDS-PAGE as described above.

Western Blot analysis

For western blot analysis proteins were separated by SDS-PAGE and were afterwards transferred to a methanol-activated PVDF (polyvinylidene fluoride) membrane for 50 min at 15 V. Blotting was performed with blotting buffer (48 mM Tris/HCl, 39 mM glycine, 0.0375% SDS, 20% MeOH) *via* a Bio-Rad Trans-Blot SD semi-dry transfer cell setup. Unoccupied parts of the membrane were blocked for 45 min using 5% (w/v) BSA (bovine serum albumin) in PBS-T (PBS-buffer with 0.5% (v/v) Tween-20®). Membranes were washed and incubated with serum derived from rabbits immunized with tagfree SaClpP (dilution: 1:1,000 in blocking buffer) overnight at 4 °C as described previously.[223] After washing with PBS-T membranes were incubated for 1 h at RT with secondary antibody (goat anti-rabbit HRP-conjugate, dilution: 1:10,000 in blocking buffer). Chemiluminescene was measured after addition of ECL substrate (ECL, 100 mM Tris, 2.5 mM Luminol, 1 mM *p*-Coumaric acid, 17 µM H_2O_2, H_2O, pH = 8.5) using an image reader LAS-4000 (*Fujifilm Life Science*, USA) with ImageQuant LAS-4000 control software.

5.4.2.8 MS-based labeling experiments

Labeling in S. aureus NCTC8325

100 mL B-medium divided into two 250 mL flasks with four baffles was inoculated with 500 µL overnight culture of *S. aureus NCTC8325* each and was incubated at 37 °C under constant shaking until the bacteria suspension reached an OD_{600} between 5.5 and 6.5. Bacteria were pooled, centrifuged (6,000 g, 10 min, 4 °C), the pellet was washed with 10 mL ice-cold PBS-buffer, centrifuged again (6,000 g, 10 min, 4 °C) and the bacteria pellet was diluted in cold PBS-buffer to an OD_{600} = 40. 990 µL of this bacteria suspension were further incubated with 10 µL probe **Trap1** or **Trap2** in triplicates (1 mM stock concentration in DMSO, final concentration: 10 µM) in the dark at 25 °C for 1 h under constant shaking at 400 rpm (Thermomixer comfort 5355, *Eppendorf*). As a negative control 990 µL bacteria suspension were treated with 10 µL DMSO in triplicates in the same manner.

Lysis and Click reaction

Bacteria samples were harvested by centrifugation (6,000 g, 10 min, 4 °C), the supernatant was discarded and the bacteria pellet was washed twice with 1 mL ice-cold PBS-buffer (6,000 g, 10 min, 4 °C). Cells were resuspended in 1 mL PBS and incubated with 5 µL lysostaphin solution

(10 mg/mL in 20 mM sodium acetate buffer, pH = 4.5, recombinant lysostaphin from *Staphylococcus simulans*, L9043, *Sigma Aldrich*) at 37 °C for 30 min with constant shaking at 1,400 rpm (Thermomixer comfort 5355, *Eppendorf*). 20 µL 20% (w/v) SDS/PBS was subsequently added and remaining DNA was solubilized by applying shear force by sonication (20 s, 10% intensity, Sonopuls, *Bandelin*). Remaining precipitate was pelletized by centrifugation (21,000 g, 30 min, 25 °C) and 20 µL of the supernatant was diluted with 180 µL ddH_2O for quantification of protein amount by BCA-assay.

BCA-assay

20 µL cell lysate was diluted with 180 µL ddH_2O and 50 µL protein solution were pipetted in a transparent 96-well plate in triplicates. A dilution series of bovine serum albumin (BSA, *Sigma Aldrich*) was aliquoted in the same manner. 100 µL BCA-mix (reagent 1: reagent 2 = 15:1, Roti®Quant universal, *Carl Roth*) was added and incubated at 60 °C for 15 min. Afterwards, the absorption was measured on a *Tecan Infinite M Nano+* (absorbance wavelength: λ = 492 nm) and protein concentration was determined by comparison to the calibration curve of standard BSA.

Click chemistry, protein precipitation, enrichment, reduction, alkylation and digestion

Protein concentration of bacteria cell lysates was adjusted to 1 – 2 mg protein/mL by addition of PBS-buffer. Click chemistry was performed with 940 µL lysate and 60 µL Click master mix (10 µL Biotin-PEG-N_3 10 mM (*Jena Bioscience*), 20 µL TCEP 52 mM, in H_2O, 30 µL TBTA ligand (1.67 mM in 80% (v/v) *t*-BuOH, 20% (v/v) DMSO)). The reaction was started by addition of 10 µL $CuSO_4$ (50 mM in ddH_2O) and incubated in the dark at room temperature for 1 h. Afterwards proteins were precipitated by addition of 4 mL acetone (-80 °C) and were incubated overnight at -20 °C. On the next day proteins were pelletized by centrifugation (21,000 g, 15 min, 4 °C), resuspended in 200 µL methanol (-80 °C, LC-MS grade, *Fisher Scientific*) by sonication (5 s, 10% intensity, Sonopuls, *Bandelin*) and centrifuged again (21,000 g, 15 min, 4 °C). This step was repeated and afterwards proteins were solubilized in 500 µL 0.2% (w/v) SDS/PBS-buffer at room temperature by sonication and centrifuged again (10,000 g, 1 min, RT). Prior to enrichment 50 µL avidin-agarose bead suspension (*Sigma Aldrich*, A9207) per sample was washed three times with 1 mL 0.4% (w/v) SDS/PBS-buffer (centrifugation 400 g, 2 min, RT). Solubilized proteins were incubated with avidin-agarose beads in LoBind *Eppendorf* tubes at room temperature for 1 h under continuous mixing. Afterwards beads were washed three times with 1 mL 0.2% (w/v) SDS/PBS-buffer (centrifugation: 400 g, 1 min, RT) and five times with 1 mL PBS-buffer (centrifugation: 400 g, 1 min, RT). Afterwards 25 µL digestion buffer I (2 M urea, 50 mM Tris-HCl, 5 ng/µL Trypsin (in 50 mM acetic acid, *Promega*), 1 mM DTT from 1 M stock in ddH_2O, pH = 8.0) was added

and samples were incubated for 30 min at 25 °C under constant shaking at 450 rpm (Thermomixer comfort 5355, *Eppendorf*). Then, 100 µL digestion buffer II (2 M urea, 50 mM Tris-HCl, 5 mM IAA, pH = 8.0) was added and samples were incubated overnight at 25 °C under constant shaking at 450 rpm (Thermomixer comfort 5355, *Eppendorf*).

Desalting and sample preparation

Digestion was stopped by adjusting the pH to 2 – 3 with 10% (v/v) aqueous formic acid (FA) to a final concentration of 1% FA. The bead suspension was centrifuged (13,000 g, 2 min, RT) and the supernatant was desalted with pre-equilibrated SepPak® C18 columns (50 mg sorbent per cartridge, 55 – 105 µm particle size, WAT054955, *Waters*). Briefly, columns were equilibrated with 1 mL MeCN, washed once with 500 µL elution buffer (80% MeCN, 19.5% H_2O, 0.5% FA) and three times with 1 mL 0.1% (v/v) aqueous FA. Samples were loaded and columns were again washed three times with 1 mL 0.1% (v/v) aqueous FA and once with 250 µL 0.5% (v/v) aqueous FA. Peptides were eluted in LoBind tubes by adding three times 250 µL elution buffer. Samples were dried by speedvac solvent removal and stored at -80 °C until further analysis. For LC-MS analysis peptide samples were dissolved in 25 µL 1% (v/v) aqueous FA, sonicated three times for 5 min and filtered with 0.22 µm Ultrafree-MC® centrifugal filters (*Merck*, UFC30GVNB) which were equilibrated with 1% (v/v) aqueous FA. Filtrates were transferred to MS vials and analyzed by LC-MS/MS.

Data acquisition on Q Exactive Plus

Samples from labeling with phenyl ester probes **Trap1** and **Trap2** were analyzed with an UltiMate 3000 nano HPLC system (*Dionex*) using Acclaim c18 PepMap100 (75 µm ID x 2 cm) trap columns and Acclaim PepMap RSLC C18 (75 µm ID x 50 cm) separation columns in an EASY-spray setting coupled to a Q Exactive Plus (*Thermo Fisher Scientific Inc.*). 1 µL peptide samples were injected on the trap column and washed with 0.1% aqueous TFA, then transferred to the analytical column (buffer A: 0.1% (v/v) FA in H_2O, buffer B: 0.1% (v/v) FA in MeCN, flow 0.4 µL/min, gradient: to 5% buffer B in 7 min, from 5% to 22% buffer B in 105 min, then to 32% buffer B in 10 min, to 90% buffer B in 10 min and hold at 90% buffer B for 10 min, then to 5% buffer B in 0.1 min and hold 5% buffer B for 9.9 min) and ionized at spray voltage of 1.9 kV and a capillary temperature of 275 °C.Q Exactive Plus was operated in TOP12 data dependent mode with full scan acquisition in the orbitrap at a resolution of R = 140,000 with an AGC target of 3e6 in a scan range of 300 – 1,500 m/z and a maximum injection time of 80 ms. Monoisotopic precursor selection and dynamic exclusion (dynamic exclusion duration: 60 s) was enabled and precursors with a charge state >1 and intensities greater than 1e4 were selected for fragmentation. Precursor

ions were isolated in the quadrupole applying a window of 1.6 m/z and were analyzed at a resolution of $R = 17{,}500$ in a scan range of 200 – 2,000 m/z to an AGC target of 1e5 and a maximum injection time of 100 ms. Peptide fragments were generated by higher-energy collional dissociation (HCD) with a normalized collisional energy (nce) of 27% and were detected in the orbitrap.

Data Processing: general comments

For further analysis of MS-data MaxQuant software (version 1.6.0.1) was used. Peptides were identified by comparison of MS/MS spectra against an *in silico* digested reference proteome (Uniprot, taxon identifier 93061, canonical version, without isoforms, downloaded 2019/06/28) using Andromeda search engine. MaxQuant settings were set to a large extent on default with carbamidomethylation of cysteines as fixed modifications and methionine oxidation and N-terminal acetylation as modifications in protein quantification. Trypsin was set as digestion enzyme and min. peptide length was set to 7. False discovery rate for proteins, sites and PSM was set to 0.01. Second peptide search as well as match between runs with a matching window of 0.7 min and alignment time window of 20 min was enabled.

Statistical analysis of proteomics data

Resulting data were further processed with Perseus software (version 1.6.2.3) and statistically analyzed. For this, ProteinGroups files were loaded into Perseus, LFQ-intensities were selected as main columns which were then $\log_2$-transformed and filtered by categorical columns. Proteins conforming with the criteria 'only identified by site', 'reverse' and 'potential contaminant' were excluded. Matrices were further filtered based on valid values in the main columns (min. valid values 50%), excluding protein groups that appear in less than half of all replicates. Missing values were imputed from a normal distribution (width 0.3, down-shift 1.8, total matrix) to enable statistical evaluation. Categorical annotation of probe treated samples and DMSO control was performed before a two-sided student's *t*-test was conducted with DMSO as single control group and Benjamini-Hochberg false discovery rate correction (FDR 0.05). Scatter plots were created by plotting student's *t*-test difference (probe/DMSO, $\log_2$-scale) against *t*-test p-value (probe/DMSO, $\log_{10}$-scale).

5.4.2.9 MS-based trapping experiments

For identification of new ClpP substrates bacteria were incubated with phenyl ester trap molecules which covalently label the peptidase and are able to crosslink substrate proteins upon UV-irradiation. Labeling was conducted as described in chapter 5.4.2.8. First, 990 µL bacteria

suspension (OD_{600} = 40, in PBS-buffer) was incubated in two triplicates each with 10 µL **Trap1** or **Trap2** (1 mM stock solution in DMSO, final concentration: 10 µM) in the dark at 25 °C for 1 h with constant shaking at 450 rpm (Thermomixer comfort 5355, *Eppendorf*). Bacteria were centrifuged (6,000 g, 10 min, 4 °C) the supernatant was discarded and cells were washed with 1 mL ice-cold PBS-buffer and centrifuged again (6,000 g, 10 min, 4 °C). Bacteria pellets were resuspended in 2 mL PBS-buffer and samples of one triplicate of each phenyl ester trap treated samples was transferred to wells of a 6-well plate and irradiated with UV-light (λ = 365 nm, *Philips TL-D BLB*, 18W) for 15 min under permanent cooling. Control samples were incubated for the same time in 2 mL *Eppendorf* tubes at 4 °C. Afterwards samples were centrifuged (6,000 g, 10 min, 4 °C) the supernatant was discarded and bacteria were resuspended in 1 mL ice-cold PBS-buffer. 5 µL lysostaphin solution (10 mg/mL in 20 mM sodium acetate buffer, pH = 4.5, recombinant lysostaphin from *Staphylococcus simulans*, L9043, *Sigma Aldrich*) was added and bacteria were incubated at 37 °C for 30 min with constant shaking at 1,400 rpm (Thermomixer comfort 5355, *Eppendorf*). Afterwards 20 µL 20% (v/v) SDS/PBS-buffer was added and the lysate was sonicated (10 s, 10% intensity, RT, Sonopuls, *Bandelin*). Remaining cell debris was pelletized by centrifugation (10,000 g, 30 min, RT). Protein concentration was adjusted to 1 – 2 mg protein/mL by BCA-assay and *Click* chemistry was performed as described in chapter 5.4.2.8. *Click* reaction was quenched by addition of 4 mL acetone (-80 °C) and precipitated proteins were stored overnight at -20 °C. Enrichment, reduction, alkylation and digestion steps were conducted as described above and remaining peptide solutions were desalted with SepPak® C18 columns applying the protocol described in chapter 5.4.2.8. Samples were lyophilized and stored at -80 °C until further LC-MS/MS analysis.

Data acquisition on Orbitrap Fusion

For LC-MS analysis peptide samples were dissolved in 25 µL 1% (v/v) aqueous FA, sonicated three times for 5 min and filtered with 0.22 µm Ultrafree-MC® centrifugal filters (*Merck*, UFC30GVNB) which were equilibrated with 1% (v/v) aqueous FA. Filtrates were transferred to MS vials and analyzed by LC-MS/MS. Samples were analyzed with an UltiMate 3000 nano HPLC system (*Dionex*) using Acclaim C18 PepMap100 (75 µm ID x 2 cm) trap and Acclaim PepMap RSLC C18 (75 µm ID x 50 cm) separation columns in an EASY-spray setting coupled to an Orbitrap Fusion (*Thermo Fisher Scientific Inc.*). 1 µL peptide sample was loaded on the trap and washed with 0.1% (v/v) TFA, then transferred to the analytical column (buffer A: H_2O with 0.1% (v/v) FA, buffer B: MeCN with 0.1% (v/v) FA, flow 0.4 µL/min, gradient: to 5% buffer B in 7 min, from 5% to 22% buffer B in 105 min, then to 32% buffer B in 10 min, to 90% buffer B in 10 min and hold at 90% buffer B for 10 min, then to 5% buffer B in 0.1 min and hold 5% buffer B for 9.9 min) and

ionized by nanospray ionization (NSI) with spray voltage of 1.8 kV and capillary temperature of 275 °C. Orbitrap Fusion was operated in a TOP speed data dependent mode. Full scan acquisition was performed in the orbitrap at a resolution of R = 120,000 and an AGC target of 2.0e5 in a scan range of 300 – 1500 m/z with a maximum injection time of 50 ms. Monoisotopic peak determination was set to 'peptides' and dynamic exclusion (dynamic exclusion duration: 60 s, mass tolerance low/high 10 ppm) was enabled. Precursors with charge states 2 - 7 and intensities greater than 5.0e3 were selected for fragmentation. Isolation was performed in the quadrupole using a window of 1.6 m/z and precursors were analyzed to an AGC target of 1.0e4 and a maximum injection time of 100 ms with "inject ions for all available parallelizable time" set to true. Peptide fragments were generated by higher-energy collisional dissociation (HCD) with a collision energy of 30% and detected in the ion trap with scan rate set to 'rapid' and first mass set to 120 m/z.

Data processing and statistical analysis

Analysis of raw data was performed with MaxQuant software (version 1.6.0.1) as described in chapter 5.4.2.8. Resulting data sets were further statistically analyzed with Perseus software (version 1.6.2.3). For this, Protein groups files were loaded and LFQ intensities were selected as main columns. After $\log_2$ transformation, protein groups were filtered excluding those satisfying the criteria 'potential contaminants','reverse' and 'only identified by sites'. Further filtering eliminated protein groups that featured only 50% or less valid values in the main columns. Missing values were replaced by imputation from a normal distribution (width: 0.3, down shift: 1.5, total matrix). After categorical annotation of LFQ intensities to groups +UV and –UV a two sided student's *t*-test was applied with –UV as the single control group and Benjamini-Hochberg false discovery rate correction (FDR 0.05). Scatter plots were created by plotting student's *t*-test difference (+UV vs. –UV, $\log_2$-scale) against student's *t*-test p-value ($\log_{10}$-scale).

6 Bibliography

1. Sender, R., Fuchs, S. & Milo, R. Are We Really Vastly Outnumbered? Revisiting the Ratio of Bacterial to Host Cells in Humans. *Cell* **164**, 337–340 (2016).
2. Sender, R., Fuchs, S. & Milo, R. Revised Estimates for the Number of Human and Bacteria Cells in the Body. *PLoS Biol.* **14**, 1–14 (2016).
3. Nelson, D. L. & Cox, M. M. *Principles of Biochemistry*. (W. H. Freeman and Company, 2008).
4. Pryde, K. R., Taanman, J. W. & Schapira, A. H. A LON-ClpP Proteolytic Axis Degrades Complex I to Extinguish ROS Production in Depolarized Mitochondria. *Cell Rep.* **17**, 2522–2531 (2016).
5. Wang, W., Zhao, F., Ma, X., Perry, G. & Zhu, X. Mitochondria dysfunction in the pathogenesis of Alzheimer's disease: recent advances. *Mol. Neurodegener.* **15**, 30 (2020).
6. Haider, L. *et al.* Oxidative damage in multiple sclerosis lesions. *Brain* **134**, 1914–1924 (2011).
7. Kim, I., Rodriguez-Enriquez, S. & Lemasters, J. J. Selective degradation of mitochondria by mitophagy. *Arch. Biochem. Biophys.* **462**, 245–253 (2007).
8. Quirós, P. M., Langer, T. & López-Otín, C. New roles for mitochondrial proteases in health, ageing and disease. *Nat. Rev. Mol. Cell Biol.* **16**, 345–359 (2015).
9. Varabyova, A., Stojanovski, D. & Chacinska, A. Mitochondrial protein homeostasis. *IUBMB Life* **65**, 191–201 (2013).
10. Lu, B. *et al.* The ATP-dependent Lon protease of Mus musculus is a DNA-binding protein that is functionally conserved between yeast and mammals. *Gene* **306**, 45–55 (2003).
11. Peters, J. M., Franke, W. W. & Kleinschmidt, J. A. Distinct 19 S and 20 S subcomplexes of the 26 S proteasome and their distribution in the nucleus and the cytoplasm. *J. Biol. Chem.* **269**, 7709–7718 (1994).
12. Coux, O., Tanaka, K. & Goldberg, A. L. Structure and Functions of the 20S and 26S Proteasome. *Annu. Rev. Biochem.* **65**, 801–847 (1996).
13. Thrower, J. S., Hoffman, L., Rechsteiner, M. & Pickart, C. M. Recognition of the polyubiquitin proteolytic signal. *EMBO J.* **19**, 94–102 (2000).
14. Nobel Prize Awardees in Chemistry, 2004. *Nobel Prize Commitee* (2004).
15. Paramore, A. & Frantz, S. Bortezomib. *Nat. Rev. Drug Discov.* **2**, 611–612 (2003).
16. Sakamoto, K. M. *et al.* Protacs: Chimeric molecules that target proteins to the Skp1–Cullin–F box complex for ubiquitination and degradation. *Proc. Natl. Acad. Sci.* **98**, 8554–8559 (2001).
17. Bross, P., Andresen, B. S., Knudsen, I., Kruse, T. A. & Gregersen, N. Human ClpP protease: cDNA sequence, tissue-specific expression and chromosomal assignment of the gene. *FEBS Lett.* **377**, 249–252 (1995).
18. Kessel, M. *et al.* Homology in Structural Organization Between E. coli ClpAP Protease and the Eukaryotic 26 S Proteasome. *J. Mol. Biol.* **250**, 587–594 (1995).
19. Wong, K. S. & Houry, W. A. Chemical Modulation of Human Mitochondrial ClpP: Potential Application in Cancer Therapeutics. *ACS Chem. Biol.* **14**, 2349–2360 (2019).
20. Jacques, S. *et al.* Imipridone Anticancer Compounds Ectopically Activate the ClpP Protease and Represent a New Scaffold for Antibiotic Development. *Genetics* **214**, (2020).
21. Kang, S. G., Maurizi, M. R., Thompson, M., Mueser, T. & Ahvazi, B. Crystallography and mutagenesis point to an essential role for the N-terminus of human mitochondrial ClpP. *J. Struct. Biol.* **148**, 338–352 (2004).
22. Kang, S. G., Maurizi, M. R., Thompson, M., Mueser, T. & Ahvazi, B. Crystallography and mutagenesis point to an essential role for the N-terminus of human mitochondrial ClpP. *J. Struct. Biol.* **148**, 338–352 (2004).
23. Gur, E., Ottofueling, R. & Dougan, D. Machines of Destruction – AAA+ Proteases and the Adaptors That Control Them. in *Regulated Proteolysis in Microorganisms* (ed. Dougan, D. A.) **66**, 3–33 (Springer Netherlands, 2013).
24. Gersch, M., List, A., Groll, M. & Sieber, S. A. Insights into structural network responsible

for oligomerization and activity of bacterial virulence regulator caseinolytic protease P (ClpP) protein. *J. Biol. Chem.* **287**, 9484–9494 (2012).
25. Geiger, S. R., Böttcher, T., Sieber, S. A. & Cramer, P. A Conformational Switch Underlies ClpP Protease Function. *Angew. Chemie Int. Ed.* **50**, 5749–5752 (2011).
26. Ye, F. *et al.* Helix Unfolding/Refolding Characterizes the Functional Dynamics of Staphylococcus aureus Clp Protease. *J. Biol. Chem.* **288**, 17643–17653 (2013).
27. Wang, J., Hartling, J. A. & Flanagan, J. M. The Structure of ClpP at 2.3 Å Resolution Suggests a Model for ATP-Dependent Proteolysis. *Cell* **91**, 447–456 (1997).
28. Kang, S. G., Dimitrova, M. N., Ortega, J., Ginsburg, A. & Maurizi, M. R. Human mitochondrial ClpP is a stable heptamer that assembles into a tetradecamer in the presence of ClpX. *J. Biol. Chem.* **280**, 35424–35432 (2005).
29. Glynn, S. E., Nager, A. R., Baker, T. A. & Sauer, R. T. Dynamic and static components power unfolding in topologically closed rings of a AAA+ proteolytic machine. *Nat. Struct. Mol. Biol.* **19**, 616–622 (2012).
30. Gersch, M. *et al.* AAA+ chaperones and acyldepsipeptides activate the ClpP protease via conformational control. *Nat. Commun.* **6**, 6320 (2015).
31. Gatsogiannis, C., Balogh, D., Merino, F., Sieber, S. A. & Raunser, S. Cryo-EM structure of the ClpXP protein degradation machinery. *Nat. Struct. Mol. Biol.* **26**, 946–954 (2019).
32. Glynn, S. E., Martin, A., Nager, A. R., Baker, T. A. & Sauer, R. T. Structures of Asymmetric ClpX Hexamers Reveal Nucleotide-Dependent Motions in a AAA+ Protein-Unfolding Machine. *Cell* **139**, 744–756 (2009).
33. Ripstein, Z. A., Vahidi, S., Houry, W. A., Rubinstein, J. L. & Kay, L. E. A processive rotary mechanism couples substrate unfolding and proteolysis in the ClpXP degradation machinery. *Elife* **9**, e52158 (2020).
34. Cordova, J. C., Olivares, A. O. & Lang, M. J. Mechanically Watching the ClpXP Proteolytic Machinery. in *Optical Tweezers: Methods and Protocols* (ed. Gennerich, A.) 317–341 (Springer New York, 2017). doi:10.1007/978-1-4939-6421-5_12
35. Malik, I. T. *et al.* Functional Characterisation of ClpP Mutations Conferring Resistance to Acyldepsipeptide Antibiotics in Firmicutes. *ChemBioChem* **21**, 1997–2012 (2020).
36. Stahl, M. *et al.* Selective Activation of Human Caseinolytic Protease P (ClpP). *Angew. Chemie - Int. Ed.* **57**, 14602–14607 (2018).
37. Ishizawa, J. *et al.* Mitochondrial ClpP-Mediated Proteolysis Induces Selective Cancer Cell Lethality. *Cancer Cell* **35**, 721-737.e9 (2019).
38. Brötz-Oesterhelt, H. *et al.* Dysregulation of bacterial proteolytic machinery by a new class of antibiotics. *Nat. Med.* **11**, 1082–1087 (2005).
39. Leung, E. *et al.* Activators of Cylindrical Proteases as Antimicrobials: Identification and Development of Small Molecule Activators of ClpP Protease. *Chem. Biol.* **18**, 1167–1178 (2011).
40. Ishizawa, J. *et al.* Mitochondrial ClpP-Mediated Proteolysis Induces Selective Cancer Cell Lethality. *Cancer Cell* **35**, 721-737.e9 (2019).
41. Cravatt, B. F., Wright, A. T. & Kozarich, J. W. Activity-Based Protein Profiling: From Enzyme Chemistry to Proteomic Chemistry. *Annu. Rev. Biochem.* **77**, 383–414 (2008).
42. Sadaghiani, A. M., Verhelst, S. H. L. & Bogyo, M. Tagging and detection strategies for activity-based proteomics. *Curr. Opin. Chem. Biol.* **11**, 20–28 (2007).
43. Kam, C. M., Abuelyaman, A. S., Li, Z., Hudig, D. & Powers, J. C. Biotinylated isocoumarins, new inhibitors and reagents for detection, localization, and isolation of serine proteases. *Bioconjug. Chem.* **4**, 560–567 (1993).
44. Abuelyaman, A. S., Hudig, D., Woodard, S. L. & Powers, J. C. Fluorescent Derivatives of Diphenyl [1-(N-Peptidylamino)alkyl]phosphonate Esters: Synthesis and Use in the Inhibition and Cellular Localization of Serine Proteases. *Bioconjug. Chem.* **5**, 400–405 (1994).
45. Speers, A. E., Adam, G. C. & Cravatt, B. F. Activity-Based Protein Profiling in Vivo Using a Copper(I)-Catalyzed Azide-Alkyne [3 + 2] Cycloaddition. *J. Am. Chem. Soc.* **125**, 4686–

4687 (2003).
46. Speers, A. E. & Cravatt, B. F. Chemical Strategies for Activity-Based Proteomics. *ChemBioChem* **5**, 41–47 (2004).
47. Greenbaum, D., Medzihradszky, K. F., Burlingame, A. & Bogyo, M. Epoxide electrophiles as activity-dependent cysteine protease profiling and discovery tools. *Chem. Biol.* **7**, 569–581 (2000).
48. Sieber, S. A. & Nodwell, M. B. *Activity-based Protein Profiling. Topics in Current Chemistry* (Springer-Verlag Berlin Heidelberg, 2012). doi:10.1007/978-3-642-28378-9
49. Liu, Y., Patricelli, M. P. & Cravatt, B. F. Activity-based protein profiling: The serine hydrolases. *Proc. Natl. Acad. Sci.* **96**, 14694–14699 (1999).
50. Pan, Z. *et al.* Development of activity-based probes for trypsin-family serine proteases. *Bioorg. Med. Chem. Lett.* **16**, 2882–2885 (2006).
51. Kato, D. *et al.* Activity-based probes that target diverse cysteine protease families. *Nat. Chem. Biol.* **1**, 33–38 (2005).
52. Weerapana, E. *et al.* Quantitative reactivity profiling predicts functional cysteines in proteomes. *Nature* **468**, 790–795 (2010).
53. Zanon, P. R. A., Lewald, L. & Hacker, S. M. Isotopically Labeled Desthiobiotin Azide (isoDTB) Tags Enable Global Profiling of the Bacterial Cysteinome. *Angew. Chemie Int. Ed.* **59**, 2829–2836 (2020).
54. Köhn, M. & Breinbauer, R. The Staudinger Ligation—A Gift to Chemical Biology. *Angew. Chemie Int. Ed.* **43**, 3106–3116 (2004).
55. Blackman, M. L., Royzen, M. & Fox, J. M. Tetrazine Ligation: Fast Bioconjugation Based on Inverse-Electron-Demand Diels−Alder Reactivity. *J. Am. Chem. Soc.* **130**, 13518–13519 (2008).
56. Rostovtsev, V. V., Green, L. G., Fokin, V. V. & Sharpless, K. B. A stepwise huisgen cycloaddition process: Copper(I)-catalyzed regioselective 'ligation' of azides and terminal alkynes. *Angew. Chemie - Int. Ed.* **41**, 2596–2599 (2002).
57. Lang, K. & Chin, J. W. Bioorthogonal reactions for labeling proteins. *ACS Chem. Biol.* **9**, 16–20 (2014).
58. Chaiet, L. & Wolf, F. J. The properties of streptavidin, a biotin-binding protein produced by Streptomycetes. *Arch. Biochem. Biophys.* **106**, 1–5 (1964).
59. Wright, M. H. & Sieber, S. A. Chemical proteomics approaches for identifying the cellular targets of natural products. *Nat. Prod. Rep.* **33**, 681–708 (2016).
60. Brunner, J. New photolabeling and crosslinking methods. *Annu. Rev. Biochem.* **62**, 483–514 (1993).
61. Kotzyba-Hibert, F., Kapfer, I. & Goeldner, M. Recent Trends in Photoaffinity Labeling. *Angew. Chemie Int. Ed. English* **34**, 1296–1312 (1995).
62. Smith, E. & Collins, I. Photoaffinity labeling in target- and binding-site identification. *Future Med. Chem.* **7**, 159–183 (2015).
63. Kleiner, P., Heydenreuter, W., Stahl, M., Korotkov, V. S. & Sieber, S. A. A Whole Proteome Inventory of Background Photocrosslinker Binding. *Angew. Chemie Int. Ed.* **56**, 1396–1401 (2017).
64. Nishi, Y., Hamamoto, K., Kajiyama, M. & Kawamura, I. The Perrault syndrome: Clinical report and review. *Am. J. Med. Genet.* **31**, 623–629 (1988).
65. Jenkinson, E. M. *et al.* Perrault syndrome is caused by recessive mutations in CLPP, encoding a mitochondrial ATP-dependent chambered protease. *Am. J. Hum. Genet.* **92**, 605–613 (2013).
66. Gispert, S. *et al.* Loss of mitochondrial peptidase Clpp leads to infertility, hearing loss plus growth retardation via accumulation of CLPX, mtDNA and inflammatory factors. *Hum. Mol. Genet.* **22**, 4871–4887 (2013).
67. Cole, A. *et al.* Inhibition of the Mitochondrial Protease ClpP as a Therapeutic Strategy for Human Acute Myeloid Leukemia. *Cancer Cell* **27**, 864–876 (2015).

68. Larkin, K. & Byrd, J. C. Antagonizing ClpP: A New Power Play in Targeted Therapy for AML. *Cancer Cell* **27**, 747–749 (2015).
69. Škrtić, M. *et al.* Inhibition of Mitochondrial Translation as a Therapeutic Strategy for Human Acute Myeloid Leukemia. *Cancer Cell* **20**, 674–688 (2011).
70. Lagadinou, E. D. *et al.* BCL-2 inhibition targets oxidative phosphorylation and selectively eradicates quiescent human leukemia stem cells. *Cell Stem Cell* **12**, 329–341 (2013).
71. Böttcher, T. & Sieber, S. A. B-Lactones As Privileged Structures for the Active-Site Labeling of Versatile Bacterial Enzyme Classes. *Angew. Chemie - Int. Ed.* **47**, 4600–4603 (2008).
72. Böttcher, T. & Sieber, S. A. β-lactones as specific inhibitors of ClpP attenuate the production of extracellular virulence factors of Staphylococcus aureus. *J. Am. Chem. Soc.* **130**, 14400–14401 (2008).
73. Staub, I. & Sieber, S. A. B-Lactams As Selective Chemical Probes for the in Vivo Labeling of Bacterial Enzymes Involved in Cell Wall Biosynthesis, Antibiotic Resistance, and Virulence. *J. Am. Chem. Soc.* **130**, 13400–13409 (2008).
74. Gersch, M. *et al.* The mechanism of caseinolytic protease (ClpP) inhibition. *Angew. Chemie - Int. Ed.* **52**, 3009–3014 (2013).
75. Hackl, M. W. *et al.* Phenyl Esters Are Potent Inhibitors of Caseinolytic Protease P and Reveal a Stereogenic Switch for Deoligomerization. *J. Am. Chem. Soc.* **137**, 8475–8483 (2015).
76. Gronauer, T. F. *et al.* Design and synthesis of tailored human caseinolytic protease P inhibitors. *Chem. Commun.* **54**, 9833–9836 (2018).
77. Gersch, M. *et al.* Barrel-shaped ClpP Proteases Display Attenuated Cleavage Specificities. *ACS Chem. Biol.* **11**, 389–399 (2016).
78. Moreno-cinos, C., Goossens, K., Salado, I. G. & Veken, P. Van Der. ClpP Protease , a Promising Antimicrobial Target. *Int. J. Mol. Sci.* **20**, 2232 (2019).
79. Moreno-Cinos, C. *et al.* α-Amino Diphenyl Phosphonates as Novel Inhibitors of Escherichia coli ClpP Protease. *J. Med. Chem.* **62**, 774–797 (2019).
80. Szyk, A. & Maurizi, M. R. Crystal structure at 1.9 Å of E. coli ClpP with a peptide covalently bound at the active site. *J. Struct. Biol.* **156**, 165–174 (2006).
81. Mundra, S. *et al.* Bioorganic & Medicinal Chemistry A novel class of Plasmodial ClpP protease inhibitors as potential antimalarial agents. *Bioorg. Med. Chem.* **25**, 5662–5677 (2017).
82. Gersch, M., Kolb, R., Alte, F., Groll, M. & Sieber, S. A. Disruption of Oligomerization and Dehydroalanine Formation as Mechanisms for ClpP Protease Inhibition. *J. Am. Chem. Soc.* **136**, 1360–1366 (2014).
83. Khan, K. M. *et al.* Synthesis and in vitro leishmanicidal activity of some hydrazides and their analogues. *Bioorg. Med. Chem.* **11**, 1381–1387 (2003).
84. Wertz, S., Kodama, S. & Studer, A. Aminierung von Benzoxazolen und 1,3,4-Oxadiazolen mit 2,2,6,6-Tetramethylpiperidin-N-oxoammonium-tetrafluoroborat als organischem Oxidationsmittel. *Angew. Chemie* **123**, 11713–11717 (2011).
85. Abd-El-Aziz, A. S. *et al.* Synthesis of novel coumarin and benzocoumarin derivatives and their biological and photophysical studies. *J. Heterocycl. Chem.* **44**, 1287–1301 (2007).
86. Piloto, A. M., Costa, S. P. G. & Gonçalves, M. S. T. A naphtho[2,1-b]furan as a new fluorescent label: synthesis and spectral characterisation. *Tetrahedron Lett.* **46**, 4757–4760 (2005).
87. Rappoport, Z. *CRC Handbook of Tables for Organic Compounds Identification*. (CRC Press, Inc., 1984).
88. Stahl, M. & Sieber, S. A. An amino acid domino effect orchestrates ClpP's conformational states. *Curr. Opin. Chem. Biol.* **40**, 102–110 (2017).
89. van Eis, M., Matt, P. & Wagner, J. Indolymaleimide derivatives. **WO2008/747**, (2008).
90. Ando, K. *et al.* Preparation of 2-, 3-, 4- and 7-(2-alkylcarbamoyl-1-alkylvinyl)benzo[b]furans and their BLT1 and/or BLT2 inhibitory activities. *Org. Biomol. Chem.* **6**, 296–307 (2008).
91. Chan, J. H.-T., Elix, J. A. & Ferguson, B. A. Annelated Furans. XVII The Wittig Reaction of Benzofuranones. *Aust. J. Chem.* **28**, 1097–1111 (1975).

92. Bobošíková, M. *et al.* The oxidative rearrangement of furan-2-carboximidamides: preparation and properties of 2-acylaminofurans. *J. Chem. Soc. Perkin Trans. 1* 680–689 (2001). doi:10.1039/b010010m
93. Ki, D. P. *et al.* Lacosamide isothiocyanate-based agents: Novel agents to target and identify lacosamide receptors. *J. Med. Chem.* **52**, 6897–6911 (2009).
94. Reno, M. J., Stevens, K. L., Waterson, A. G. & Zhang, Y. Chemical Compounds. 1–130 (2005).
95. Kirstein, J. *et al.* The antibiotic ADEP reprogrammes CIP, switching it from a regulated to an uncontrolled protease. *EMBO Mol. Med.* **1**, 37–49 (2009).
96. Kang, S. G. *et al.* Functional Proteolytic Complexes of the Human Mitochondrial ATP-dependent Protease, hClpXP. *J. Biol. Chem.* **277**, 21095–21102 (2002).
97. Kang, S. G., Dimitrova, M. N., Ortega, J., Ginsburg, A. & Maurizi, M. R. Human Mitochondrial ClpP Is a Stable Heptamer That Assembles into a Tetradecamer in the Presence of ClpX. *J. Biol. Chem.* **280**, 35424–35432 (2005).
98. Carney, D. W. *et al.* A simple fragment of cyclic acyldepsipeptides is necessary and sufficient for ClpP activation and antibacterial activity. *Chembiochem Commun.* **15**, 2216–2220 (2014).
99. Twining, S. S. Fluorescein isothiocyanate-labeled casein assay for proteolytic enzymes. *Anal. Biochem.* **143**, 30–34 (1984).
100. Kim, Y. I., Burton, R. E., Burton, B. M., Sauer, R. T. & Baker, T. A. Dynamics of substrate denaturation and translocation by the ClpXP degradation machine. *Mol. Cell* **5**, 639–648 (2000).
101. Karzai, A. W., Roche, E. D. & Sauer, R. T. The SsrA-SmpB system for protein tagging, directed degradation and ribosome rescue. *Nat. Struct. Biol.* **7**, 449–455 (2000).
102. Tornøe, C. W., Christensen, C. & Meldal, M. Peptidotriazoles on solid phase: [1,2,3]-Triazoles by regiospecific copper(I)-catalyzed 1,3-dipolar cycloadditions of terminal alkynes to azides. *J. Org. Chem.* **67**, 3057–3064 (2002).
103. Huisgen, R. Kinetics and Mechanism of 1,3-Dipolar Cycloadditions. *Angew. Chemie Int. Ed. English* **2**, 633–645 (1963).
104. Rickert, D. E. Metabolism of nitroaromatic compounds. *Drug Metab. Rev.* **18**, 23–53 (1987).
105. Jacques, S. *et al.* Imipridone Anticancer Compounds Ectopically Activate the ClpP Protease and Represent a New Scaffold for Antibiotic Development. *Genetics* **214**, 1103–1120 (2020).
106. Keilhauer, E. C., Hein, M. Y. & Mann, M. Accurate Protein Complex Retrieval by Affinity Enrichment Mass Spectrometry (AE-MS) Rather than Affinity Purification Mass Spectrometry (AP-MS). *Mol. Cell. Proteomics* **14**, 120–135 (2015).
107. Doré, S. *et al.* Bilirubin, formed by activation of heme oxygenase-2, protects neurons against oxidative stress injury. *Proc. Natl. Acad. Sci.* **96**, 2445 (1999).
108. Wang, X. *et al.* Transmembrane Protein 230 Mediates a Poly(ADP-ribose) Polymerase-1-Linked Apoptosis. *Front. Aging Neurosci.* **12**, 235 (2020).
109. Emdad, L. *et al.* AEG-1/MTDH/LYRIC: A Promiscuous Protein Partner Critical in Cancer, Obesity, and CNS Diseases. *Adv. Cancer Res.* **131**, 97–132 (2016).
110. Yang, Y. S. & Strittmatter, S. M. The reticulons: A family of proteins with diverse functions. *Genome Biol.* **8**, 1–10 (2007).
111. Wan, Q. *et al.* Reticulon 3 mediates Bcl-2 accumulation in mitochondria in response to endoplasmic reticulum stress. *Apoptosis* **12**, 319–328 (2007).
112. Neve, E. P. A. *et al.* Amidoxime reductase system containing cytochrome b 5 type B (CYB5B) and MOSC2 is of importance for lipid synthesis in adipocyte mitochondria. *J. Biol. Chem.* **287**, 6307–6317 (2012).
113. Plitzko, B. *et al.* The involvement of mitochondrial amidoxime reducing components 1 and 2 and mitochondrial cytochrome b5in N-reductive metabolism in human cells. *J. Biol. Chem.* **288**, 20228–20237 (2013).
114. Jakobs, H. H. *et al.* The N-reductive system composed of mitochondrial Amidoxime Reducing Component (mARC), Cytochrome b5 (CYB5B) and Cytochrome b5 Reductase

(CYB5R) is regulated by fasting and high fat diet in mice. *PLoS One* **9**, 1–11 (2014).
115. Seth, R. B., Sun, L., Ea, C. K. & Chen, Z. J. Identification and characterization of MAVS, a mitochondrial antiviral signaling protein that activates NF-κB and IRF3. *Cell* **122**, 669–682 (2005).
116. Bulletin, Technical for CellTiter-Blue ® Cell Viability Assay. 1–15 (2016).
117. Nicoletti, I., Migliorati, G., Pagliacci, M. C., Grignani, F. & Riccardi, C. a Rapid and Simple Method for Measuring Thymocyte Apoptosis By Propidium Iodide Staining and Flow-Cytometry. *J. Immunol. Methods* **139**, 271–279 (1991).
118. Riccardi, C. & Nicoletti, I. Analysis of apoptosis by propidium iodide staining and flow cytometry. *Nat. Protoc.* **1**, 1458–1461 (2006).
119. Boyden, S. The chemotactic effect of mixtures of antibody and antigen on polymorphonuclear leucocytes. *J. Exp. Med.* **115**, 453–466 (1962).
120. Chen, H. C. Boyden chamber assay. *Methods Mol. Biol.* **294**, 15–22 (2005).
121. Haynes, C. M. & Ron, D. The mitochondrial UPR – protecting organelle protein homeostasis. *J. Cell Sci.* **123**, 3849–3855 (2010).
122. Brötz-Oesterhelt, H. *et al.* Dysregulation of bacterial proteolytic machinery by a new class of antibiotics. *Nat. Med.* **11**, 1082–1087 (2005).
123. Weinandy, F. *et al.* A β-lactone-based antivirulence drug ameliorates Staphylococcus aureus skin infections in mice. *ChemMedChem* **9**, 710–713 (2014).
124. Tan, J. *et al.* De Novo Design of Boron-Based Peptidomimetics as Potent Inhibitors of Human ClpP in the Presence of Human ClpX. *J. Med. Chem.* **62**, 6377–6390 (2019).
125. Shpilka, T. & Haynes, C. M. The mitochondrial UPR: mechanisms, physiological functions and implications in ageing. *Nat. Rev. Mol. Cell Biol.* **19**, 109–12 (2018).
126. Letts, J. A. & Sazanov, L. A. Clarifying the supercomplex: The higher-order organization of the mitochondrial electron transport chain. *Nat. Struct. Mol. Biol.* **24**, 800–808 (2017).
127. Dröse, S. & Brandt, U. Molecular Mechanisms of Superoxide Production by the Mitochondrial Respiratory Chain. in *Mitochondrial Oxidative Phosphorylation: Nuclear-Encoded Genes, Enzyme Regulation, and Pathophysiology* (ed. Kadenbach, B.) 145–169 (Springer New York, 2012). doi:10.1007/978-1-4614-3573-0_6
128. Haynes, C. M., Yang, Y., Blais, S. P., Neubert, T. A. & Ron, D. The Matrix Peptide Exporter HAF-1 Signals a Mitochondrial UPR by Activating the Transcription Factor ZC376.7 in C. elegans. *Mol. Cell* **37**, 529–540 (2010).
129. Voos, W., Jaworek, W., Wilkening, A. & Bruderek, M. Protein quality control at the mitochondrion. *Essays Biochem.* **60**, 213–225 (2016).
130. Al-Furoukh, N. *et al.* ClpX stimulates the mitochondrial unfolded protein response (UPRmt) in mammalian cells. *Biochim. Biophys. Acta - Mol. Cell Res.* **1853**, 2580–2591 (2015).
131. Esencan, E. *et al.* Impaired Mitochondrial Stress Response due to CLPP Deletion Is Associated with Altered Mitochondrial Dynamics and Increased Apoptosis in Cumulus Cells. *Reprod. Sci.* **27**, 621–630 (2020).
132. Haynes, C. M., Petrova, K., Benedetti, C., Yang, Y. & Ron, D. ClpP Mediates Activation of a Mitochondrial Unfolded Protein Response in C. elegans. *Dev. Cell* **13**, 467–480 (2007).
133. Bhandari, V. *et al.* The role of ClpP protease in bacterial pathogenesis and human diseases. *ACS Chem. Biol.* **13**, 1413–1425 (2018).
134. Flynn, J. M., Neher, S. B., Kim, Y. I., Sauer, R. T. & Baker, T. A. Proteomic discovery of cellular substrates of the ClpXP protease reveals five classes of ClpX-recognition signals. *Mol. Cell* **11**, 671–683 (2003).
135. Fischer, F., Langer, J. D. & Osiewacz, H. D. Identification of potential mitochondrial ClpXP protease interactors and substrates suggests its central role in energy metabolism. *Sci. Rep.* **5**, 1–13 (2015).
136. Roux, K. J., Kim, D. I., Raida, M. & Burke, B. A promiscuous biotin ligase fusion protein identifies proximal and interacting proteins in mammalian cells. *J. Cell Biol.* **196**, 801–810 (2012).

137. Choi-Rhee, E., Schulman, H. & Cronan, J. E. Promiscuous protein biotinylation by Escherichia coli biotin protein ligase. *Protein Sci.* **13**, 3043–3050 (2004).
138. Fux, A., Korotkov, V. S., Schneider, M., Antes, I. & Sieber, S. A. Chemical Cross-Linking Enables Drafting ClpXP Proximity Maps and Taking Snapshots of In Situ Interaction Networks. *Cell Chem. Biol.* **26**, 48-59.7 (2019).
139. Szczepanowska, K. *et al.* CLPP coordinates mitoribosomal assembly through the regulation of ERAL 1 levels. *EMBO J.* **35**, 2566–2583 (2016).
140. Szczepanowska, K. *et al.* A salvage pathway maintains highly functional respiratory complex I. *Nat. Commun.* **11**, 1643–1661 (2020).
141. Seo, J. H. *et al.* The Mitochondrial Unfoldase-Peptidase Complex ClpXP Controls Bioenergetics Stress and Metastasis. *PLoS Biol* **14**, e1002507 (2016).
142. Deepa, S. S. *et al.* Down-regulation of the mitochondrial matrix peptidase ClpP in muscle cells causes mitochondrial dysfunction and decreases cell proliferation. *Free Radic. Biol. Med.* **91**, 281–292 (2016).
143. Liu, X., Salokas, K., Weldatsadik, R. G., Gawriyski, L. & Varjosalo, M. Combined proximity labeling and affinity purification−mass spectrometry workflow for mapping and visualizing protein interaction networks. *Nat. Protoc.* **15**, 3182–3211 (2020).
144. Liu, C. C. & Schultz, P. G. Adding New Chemistries to the Genetic Code. *Annu. Rev. Biochem.* **79**, 413–444 (2010).
145. Dumas, A., Lercher, L., Spicer, C. D. & Davis, B. G. Designing logical codon reassignment-Expanding the chemistry in biology. *Chem. Sci.* **6**, 50–69 (2015).
146. Nguyen, T. A., Cigler, M. & Lang, K. Expanding the Genetic Code to Study Protein–Protein Interactions. *Angew. Chemie - Int. Ed.* **57**, 14350–14361 (2018).
147. Hao, B. *et al.* Reactivity and Chemical Synthesis of L-Pyrrolysine— the 22nd Genetically Encoded Amino Acid. *Chem. Biol.* **11**, 1317–1324 (2004).
148. Ai, H. wang, Shen, W., Sagi, A., Chen, P. R. & Schultz, P. G. Probing Protein-Protein Interactions with a Genetically Encoded Photo-crosslinking Amino Acid. *ChemBioChem* **12**, 1854–1857 (2011).
149. Chou, C., Uprety, R., Davis, L., Chin, J. W. & Deiters, A. Genetically encoding an aliphatic diazirine for protein photocrosslinking. *Chem. Sci.* **2**, 480–483 (2011).
150. Zhang, M. *et al.* A genetically incorporated crosslinker reveals chaperone cooperation in acid resistance. *Nat. Chem. Biol.* **7**, 671–677 (2011).
151. Kang, S. G., Maurizi, M. R., Thompson, M., Mueser, T. & Ahvazi, B. Crystallography and mutagenesis point to an essential role for the N-terminus of human mitochondrial ClpP. *J. Struct. Biol.* **148**, 338–352 (2004).
152. Field, J. *et al.* Purification of a RAS-responsive adenylyl cyclase complex from Saccharomyces cerevisiae by use of an epitope addition method. *Mol. Cell. Biol.* **8**, 2159–2165 (1988).
153. Szklarczyk, D. *et al.* STRING v11: protein–protein association networks with increased coverage, supporting functional discovery in genome-wide experimental datasets. *Nucleic Acids Res.* **47**, D607–D613 (2019).
154. Szczepanowska, K. *et al.* CLPP coordinates mitoribosomal assembly through the regulation of ERAL 1 levels . *EMBO J.* **35**, 2566–2583 (2016).
155. Seo, J. H. *et al.* The Mitochondrial Unfoldase-Peptidase Complex ClpXP Controls Bioenergetics Stress and Metastasis. *PLoS Biol.* **14**, 1–21 (2016).
156. Sciacovelli, M. *et al.* The Mitochondrial Chaperone TRAP1 Promotes Neoplastic Growth by Inhibiting Succinate Dehydrogenase. *Cell Metab.* **17**, 988–999 (2013).
157. Ruzzenente, B. *et al.* LRPPRC is necessary for polyadenylation and coordination of translation of mitochondrial mRNAs. *EMBO J.* **31**, 443–456 (2012).
158. Cole, A. *et al.* Inhibition of the Mitochondrial Protease ClpP as a Therapeutic Strategy for Human Acute Myeloid Leukemia. *Cancer Cell* **27**, 864–876 (2015).
159. Towbin, H., Staehelin, T. & Gordon, J. Electrophoretic transfer of proteins from

polyacrylamide gels to nitrocellulose sheets: procedure and some applications. *Proc. Natl. Acad. Sci.* **76**, 4350–4354 (1979).
160. Picotti, P. & Aebersold, R. Selected reaction monitoring–based proteomics: workflows, potential, pitfalls and future directions. *Nat. Methods* **9**, 555–566 (2012).
161. Haapanen, O. & Sharma, V. A modeling and simulation perspective on the mechanism and function of respiratory complex I. *Biochim. Biophys. Acta - Bioenerg.* **1859**, 510–523 (2018).
162. Howard, M. J., Lim, W. H., Fierke, C. A. & Koutmos, M. Mitochondrial ribonuclease P structure provides insight into the evolution of catalytic strategies for precursor-tRNA 5' processing. *Proc. Natl. Acad. Sci. U. S. A.* **109**, 16149–16154 (2012).
163. Wynn, R. M. *et al.* Molecular mechanism for regulation of the human mitochondrial branched-chain α-ketoacid dehydrogenase complex by phosphorylation. *Structure* **12**, 2185–2196 (2004).
164. González-Mariscal, I. *et al.* The mitochondrial phosphatase PPTC7 orchestrates mitochondrial metabolism regulating coenzyme Q10 biosynthesis. *Biochim. Biophys. Acta - Bioenerg.* **1859**, 1235–1248 (2018).
165. Gourdoupis, S., Nasta, V., Calderone, V., Ciofi-Baffoni, S. & Banci, L. IBA57 Recruits ISCA2 to Form a [2Fe-2S] Cluster-Mediated Complex. *J. Am. Chem. Soc.* **140**, 14401–14412 (2018).
166. Sheftel, A. D. *et al.* The human mitochondrial ISCA1, ISCA2, and IBA57 proteins are required for [4Fe-4S] protein maturation. *Mol. Biol. Cell* **23**, 1157–1166 (2012).
167. Maize, K. M., Wagner, C. R. & Finzel, B. C. Structural characterization of human histidine triad nucleotide binding protein 2 (hHint2), a member of the histidine triad (HIT) superfamily. *FEBS J.* **180**, 3389–3398 (2013).
168. Seo, J. H. *et al.* The Mitochondrial Unfoldase-Peptidase Complex ClpXP Controls Bioenergetics Stress and Metastasis. *PLoS Biol.* **14**, 1–21 (2016).
169. Seiferling, D. *et al.* Loss of CLPP alleviates mitochondrial cardiomyopathy without affecting the mammalian UPR mt . *EMBO Rep.* **17**, 953–964 (2016).
170. Hofsetz, E., Demir, F., Szczepanowska, K., Kukat, A. & Jayachandran, N. The mouse heart mitochondria N terminome provides insights into ClpXP-mediated proteolysis. *Mol. Cell. Proteomics* 1–40 (2020). doi:https://doi.org/10.1074/mcp.RA120.002082
171. O'Hara, A. M. & Shanahan, F. The gut flora as a forgotten organ. *EMBO Rep.* **7**, 688–693 (2006).
172. Ziebandt, A. K. *et al.* The influence of agr and σB in growth phase dependent regulation of virulence factors in Staphylococcus aureus. *Proteomics* **4**, 3034–3047 (2004).
173. Bassler, B. L. How bacteria talk to each other: Regulation of gene expression by quorum sensing. *Curr. Opin. Microbiol.* **2**, 582–587 (1999).
174. Cheng, A. G. *et al.* Contribution of coagulases towards Staphylococcus aureus disease and protective immunity. *PLoS Pathog.* **6**, 19–20 (2010).
175. Ligon, B. L. Penicillin: Its Discovery and Early Development. *Semin. Pediatr. Infect. Dis.* **15**, 52–57 (2004).
176. Davies, J. & Davies, D. Origins and evolution of antibiotic resistance. *Microbiol. Mol. Biol. Rev.* **74**, 417–433 (2010).
177. Lakemeyer, M., Zhao, W., Mandl, F. A., Hammann, P. & Sieber, S. A. Thinking Outside the Box—Novel Antibacterials To Tackle the Resistance Crisis. *Angew. Chemie - Int. Ed.* **57**, 14440–14475 (2018).
178. Ogston, A. *Micrococcus* Poisoning. *J. Anat. Physiol.* **17**, 24–58 (1882).
179. van Belkum, A. *et al.* Co-evolutionary aspects of human colonisation and infection by Staphylococcus aureus. *Infect. Genet. Evol.* **9**, 32–47 (2009).
180. Rosenbach, F. J. Mikroorganismen bei den Wundinfectionskrankheiten des Menschen. *Mikroorganismen bei den Wundinfectionskrankheiten des Menschen* 1 (1884).
181. Frees, D., Qazi, S. N. A., Hill, P. J. & Ingmer, H. Alternative roles of ClpX and ClpP in Staphylococcus aureus stress tolerance and virulence. *Mol. Microbiol.* **48**, 1565–1578 (2003).

182. Bhakdi, S. & Tranum-Jensen, J. Alpha-Toxin of Staphylococcus aureus. *Microbiol. Rev.* **55**, 733–751 (1991).
183. Maheswaran, S. K. & Lindorfer, R. K. Staphylococcal beta-hemolysin. II. Phospholipase C activity of purified beta-hemolysin. *J. Bacteriol.* **94**, 1313–1319 (1967).
184. Tam, K. & Torres, V. J. Staphylococcus aureus Secreted Toxins and Extracellular Enzymes. *Microbiol. Spectr.* **7**, 640–668 (2019).
185. Alonzo, F. & Torres, V. J. The Bicomponent Pore-Forming Leucocidins of Staphylococcus aureus. *Microbiol. Mol. Biol. Rev.* **78**, 199–230 (2014).
186. Seilie, E. S. & Bubeck Wardenburg, J. Staphylococcus aureus pore-forming toxins: The interface of pathogen and host complexity. *Semin. Cell Dev. Biol.* **72**, 101–116 (2017).
187. Spaan, A. N., Van Strijp, J. A. G. & Torres, V. J. Leukocidins: Staphylococcal bi-component pore-forming toxins find their receptors. *Nat. Rev. Microbiol.* **15**, 435–447 (2017).
188. Koop, G. *et al.* Identification of LukPQ, a novel, equid-adapted leukocidin of Staphylococcus aureus. *Sci. Rep.* **7**, 1–10 (2017).
189. Vrieling, M. *et al.* LukMF' is the major secreted leukocidin of bovine Staphylococcus aureus and is produced in vivo during bovine mastitis. *Sci. Rep.* **6**, 1–12 (2016).
190. Yamada, T. *et al.* Leukotoxin family genes in Staphylococcus aureus isolated from domestic animals and prevalence of lukM-lukF-PV genes by bacteriophages in bovine isolates. *Vet. Microbiol.* **110**, 97–103 (2005).
191. Rosenstein, R. & Götz, F. Staphylococcal lipases: Biochemical and molecular characterization. *Biochimie* **82**, 1005–1014 (2000).
192. Doery, H. M., Magnusson, B. J., Gulasekharam, J. & Pearson, J. E. The properties of phospholipase enzymes in staphylococcal toxins. *J. Gen. Microbiol.* **40**, 283–296 (1965).
193. Hanakawa, Y. *et al.* Enzymatic and Molecular Characteristics of the Efficiency and Specificity of Exfoliative Toxin Cleavage of Desmoglein 1. *J. Biol. Chem.* **279**, 5268–5277 (2004).
194. Nishifuji, K., Sugai, M. & Amagai, M. Staphylococcal exfoliative toxins: 'Molecular scissors' of bacteria that attack the cutaneous defense barrier in mammals. *J. Dermatol. Sci.* **49**, 21–31 (2008).
195. Hu, C., Xiong, N., Zhang, Y., Rayner, S. & Chen, S. Functional characterization of lipase in the pathogenesis of Staphylococcus aureus. *Biochem. Biophys. Res. Commun.* **419**, 617–620 (2012).
196. Friedrich, R. *et al.* Staphylocoagulase is a prototype for the mechanism of cofactor-induced zymogen activation. *Nature* **425**, 535–539 (2003).
197. Kroh, H. K., Panizzi, P. & Bock, P. E. Von Willebrand factor-binding protein is a hysteretic conformational activator of prothrombin. *Proc. Natl. Acad. Sci. U. S. A.* **106**, 7786–7791 (2009).
198. Grella, D. K. & Castellino, F. J. Activation of human plasminogen by staphylokinase. Direct evidence that preformed plasmin is necessary for activation to occur. *Blood* **89**, 1585–1589 (1997).
199. Spaulding, A. R. *et al.* Staphylococcal and streptococcal superantigen exotoxins. *Clin. Microbiol. Rev.* **26**, 422–447 (2013).
200. Rödström, K. E. J., Elbing, K. & Lindkvist-Petersson, K. Structure of the Superantigen Staphylococcal Enterotoxin B in Complex with TCR and Peptide–MHC Demonstrates Absence of TCR–Peptide Contacts. *J. Immunol.* **193**, 1998–2004 (2014).
201. Kimber, I. *et al.* Toxic Shock Syndrome: Characterization of Human Immune Responses to TSST-1 and Evidence for Sensitivity Thresholds. *Toxicol. Sci.* **134**, 49–63 (2013).
202. Deisenhofer, J. Crystallographic Refinement and Atomic Models of a Human Fc Fragment and Its Complex with Fragment B of Protein A from Staphylococcus aureus at 2.9- and 2.8-Å Resolution. *Biochemistry* **20**, 2361–2370 (1981).
203. Goodyear, C. S. & Silverman, G. J. Death by a B cell superantigen: In vivo VH-targeted apoptotic supraclonal B cell deletion by a staphylococcal toxin. *J. Exp. Med.* **197**, 1125–1139

(2003).
204. Foster, T. J. The MSCRAMM Family of Cell-Wall-Anchored Surface Proteins of Gram-Positive Cocci. *Trends Microbiol.* **27**, 927–941 (2019).
205. Yan, H., Wang, Q., Teng, M. & Li, X. The DNA-binding mechanism of the TCS response regulator ArlR from Staphylococcus aureus. *J. Struct. Biol.* **208**, (2019).
206. Giraudo, A. T., Raspanti, C. G., Calzolari, A. & Nagel, R. Characterization of a Tn551-mutant of Staphylococcus aureus defective in the production of several exoproteins. *Can. J. Microbiol.* **40**, 677–681 (1994).
207. Yarwood, J. M., McCormick, J. K. & Schlievert, P. M. Identification of a novel two-component regulatory system that acts in global regulation of virulence factors of Staphylococcus aureus. *J. Bacteriol.* **183**, 1113–1123 (2001).
208. Fournier, B., Klier, A. & Rapoport, G. The two-component system ArlS-ArlR is a regulator of virulence gene expression in Staphylococcus aureus. *Mol. Microbiol.* **41**, 247–261 (2001).
209. Dunman, P. M. *et al.* Transcription Profling-Based Identication of Staphylococcus aureus Genes Related by the agr and/or sarA Loci. *J. Bacteriol.* **183**, 7341–7353 (2001).
210. George, E. A. & Muir, T. W. Molecular mechanisms of agr quorum sensing in virulent staphylococci. *ChemBioChem* **8**, 847–855 (2007).
211. Mcnamara, P. J., Milligan-Monroe, K. C., Khalili, S. & Proctor, R. A. Identification, cloning, and initial characterization of rot, a locus encoding a regulator of virulence factor expression in Staphylococcus aureus. *J. Bacteriol.* **182**, 3197–3203 (2000).
212. Krysiak, J. *et al.* Quantitative Map of β-Lactone-Induced Virulence Regulation. *J. Proteome Res.* **16**, 1180–1192 (2017).
213. Oogai, Y. *et al.* Expression of virulence factors by Staphylococcus aureus grown in Serum. *Appl. Environ. Microbiol.* **77**, 8097–8105 (2011).
214. Schelin, J., Cohn, M. T., Frisk, B. & Frees, D. A Functional ClpXP Protease is Required for Induction of the Accessory Toxin Genes, tst, sed, and sec. *Toxins (Basel).* **12**, 1–15 (2020).
215. Geisinger, E., Adhikari, R. P., Jin, R., Ross, H. F. & Novick, R. P. Inhibition of rot translation by RNAIII, a key feature of agr function. *Mol. Microbiol.* **61**, 1038–1048 (2006).
216. Janzon, L., Löfdahl, S. & Arvidson, S. Identification and nucleotide sequence of the delta-lysin gene, hld, adjacent to the accessory gene regulator (agr) of Staphylococcus aureus. *MGG Mol. Gen. Genet.* **219**, 480–485 (1989).
217. Benito, Y. *et al.* Probing the structure of RNAIII, the Staphylococcus aureus agr regulatory RNA, and identification of the RNA domain involved in repression of protein A expression. *RNA* **6**, 668–679 (2000).
218. Bloes, D. A. *et al.* Phenol-Soluble Modulin Peptides Contribute to Influenza A Virus-Associated Staphlococcus aureus Pneumonia. *Infect. Immun.* **85**, 1–9 (2017).
219. Michel, A. *et al.* Global regulatory impact of ClpP protease of Staphylococcus aureus on regulons involved in virulence, oxidative stress response, autolysis, and DNA repair. *J. Bacteriol.* **188**, 5783–5796 (2006).
220. Frees, D., Sørensen, K. & Ingmer, H. Global virulence regulation in Staphylococcus aureus: Pinpointing the roles of C1pP and C1pX in the sar/agr regulatory network. *Infect. Immun.* **73**, 8100–8108 (2005).
221. Böttcher, T. & Sieber, S. A. β-Lactones as Privileged Structures for the Active-Site Labeling of Versatile Bacterial Enzyme Classes. *Angew. Chemie Int. Ed.* **47**, 4600–4603 (2008).
222. Bottcher, T. & Sieber, S. a. beta-Lactones as Specific Inhibitors of ClpP Attenuate the Production of Extracellular Virulence Factors of Staphylococcus aureus. *J. Am. Chem. Soc.* **130**, 14400–14401 (2008).
223. Hackl, M. W. *et al.* Phenyl Esters Are Potent Inhibitors of Caseinolytic Protease P and Reveal a Stereogenic Switch for Deoligomerization. *J. Am. Chem. Soc.* **137**, 8475–8483 (2015).
224. Lakemeyer, M. *et al.* Tailored Peptide Phenyl Esters Block ClpXP Proteolysis by an Unusual Breakdown into a Heptamer–Hexamer Assembly. *Angew. Chemie - Int. Ed.* **58**, 7127–7132 (2019).

225. Joshi, S. A., Hersch, G. L., Baker, T. A. & Sauer, R. T. Communication between ClpX and ClpP during substrate processing and degradation. *Nat. Struct. Mol. Biol.* **11**, 404–411 (2004).
226. Kim, Y. I. *et al.* Molecular determinants of complex formation between Clp/Hsp 100 ATPases and the ClpP peptidase. *Nat. Struct. Biol.* **8**, 230–233 (2001).
227. Lee, B. G. *et al.* Structures of ClpP in complex with acyldepsipeptide antibiotics reveal its activation mechanism. *Nat. Struct. Mol. Biol.* **17**, 471–478 (2010).
228. Gersch, M. *et al.* AAA+ chaperones and acyldepsipeptides activate the ClpP protease via conformational control. *Nat Commun* **6**, (2015).
229. Feng, J. *et al.* Trapping and proteomic identification of cellular substrates of the ClpP protease in staphylococcus aureus. *J. Proteome Res.* **12**, 547–558 (2013).
230. More, S. S. & Vince, R. Design, synthesis and biological evaluation of glutathione peptidomimetics as components of anti-Parkinson prodrugs. *J. Med. Chem.* **51**, 4581–4588 (2008).
231. Hu, T. & Panek, J. S. Enantioselective synthesis of the protein phosphatase inhibitor (-)-motuporin. *J. Am. Chem. Soc.* **124**, 11368–11378 (2002).
232. Spletstoser, J. T., Flaherty, P. T., Himes, R. H. & Georg, G. I. Synthesis and anti-tubulin activity of a 3'-(4-Azidophenyl)-3'- dephenylpaclitaxel photoaffinity probe. *J. Med. Chem.* **47**, 6459–6465 (2004).
233. Zheng, G. *et al.* Structural Modifications to Tetrahydropyridine-3-carboxylate Esters en Route to the Discovery of M5-Preferring Muscarinic Receptor Orthosteric Antagonists. *J. Med. Chem.* **56**, 1693–1703 (2013).
234. Ramesh, R., Chandrasekaran, Y., Megha, R. & Chandrasekaran, S. Base catalyzed cyclization of N-aryl and N-alkyl-O-propargyl carbamates to 4-alkylidene-2-oxazolidinones. *Tetrahedron* **63**, 9153–9162 (2007).
235. Güixens-Gallardo, P., Hocek, M. & Perlíková, P. Inhibition of non-templated nucleotide addition by DNA polymerases in primer extension using twisted intercalating nucleic acid modified templates. *Bioorg. Med. Chem. Lett.* **26**, 288–291 (2016).
236. Nakamoto, K. & Ueno, Y. Diazirine-containing RNA photo-cross-linking probes for capturing microRNA targets. *J. Org. Chem.* **79**, 2463–2472 (2014).
237. Kumar, A. B., Tipton, J. D. & Manetsch, R. 3-Trifluoromethyl-3-aryldiazirine photolabels with enhanced ambient light stability. *Chem. Commun.* **52**, 2729–2732 (2016).
238. Smith, D. P. *et al.* Trifluoromethyldiazirine: An effective photo-induced cross-linking probe for exploring amyloid formation. *Chem. Commun.* 5728–5730 (2008).
239. Woo, K. M., Chung, W. J., Ha, D. B., Goldberg, A. L. & Chung, C. H. Protease Ti from Escherichia coli requires ATP hydrolysis for protein breakdown but not for hydrolysis of small peptides. *J. Biol. Chem.* **264**, 2088–2091 (1989).
240. Heck, A. J. R. & Van Den Heuvel, R. H. H. Investigation of intact protein complexes by mass spectrometry. *Mass Spectrom. Rev.* **23**, 368–389 (2004).
241. Baker, N. D., Griffin, R. J., Irwin, W. J. & Slack, J. A. The reduction of aryl azides by dithiothreitol: a model for bioreduction of aromatic azido-substituted drugs. *Int. J. Pharm.* **52**, 231–238 (1989).
242. KVN, R. R. *et al.* Isolation, purification and characterization of glucokinase from Staphylococcus aureus. *J. Pharm. Res.* **6**, 205–209 (2013).
243. Delvillani, F., Papiani, G., Dehó, G. & Briani, F. S1 ribosomal protein and the interplay between translation and mRNA decay. *Nucleic Acids Res.* **39**, 7702–7715 (2011).
244. Hampele, I. C. *et al.* Structure and function of the dihydropteroate synthase from Staphylococcus aureus. *J. Mol. Biol.* **268**, 21–30 (1997).
245. Uniprot. No Title. Available at: https://www.uniprot.org/uniprot/P60430. (Accessed: 15th October 2020)
246. Sibbald, M. J. J. B. *et al.* Mapping the Pathways to StaphylococcalPathogenesis by Comparative Secretomics. *Microbiol. Mol. Biol. Rev.* **70**, 755–788 (2006).
247. Nygaard, P. & Sxlid, H. H. Nucleotide metabolism. in *Encyclopedia of Microbiology* 296–307

(Elsevier Inc., 2009). doi:10.1016/B978-0-444-64046-8.00008-2
248. Tosi, T. *et al.* Inhibition of the Staphylococcus aureus c-di-AMP cyclase DacA by direct interaction with the phosphoglucosamine mutase GlmM. *PLoS Pathog.* **15**, 1–28 (2019).
249. Jolly, L. *et al.* The femR315 gene from Staphylococcus aureus, the interruption of which results in reduced methicillin resistance, encodes a phosphoglucosamine mutase. *J. Bacteriol.* **179**, 5321–5325 (1997).
250. Corrigan, R. M., Abbott, J. C., Burhenne, H., Kaever, V. & Gründling, A. C-di-amp is a new second messenger in staphylococcus aureus with a role in controlling cell size and envelope stress. *PLoS Pathog.* **7**, e1002217 (2011).
251. Komatsuzawa, H. *et al.* The gate controlling cell wall synthesis in Staphylococcus aureus. *Mol. Microbiol.* **53**, 1221–1231 (2004).
252. Recsei, P. A., Gruss, A. D. & Novick, R. P. Cloning, sequence, and expression of the lysostaphin gene from Staphylococcus simulans. *Proc. Natl. Acad. Sci. U. S. A.* **84**, 1127–1131 (1987).
253. Salazar, O. & Asenjo, J. A. Enzymatic lysis of microbial cells. *Biotechnol. Lett.* **29**, 985–994 (2007).
254. Uniprot. No Title. Available at: https://www.uniprot.org/uniprot/Q2G0V7. (Accessed: 16th October 2020)
255. Laczkovich, I. *et al.* Increased flexibility in the use of exogenous lipoic acid by Staphylococcus aureus. *Mol. Microbiol.* **109**, 150–168 (2018).
256. Brown, M. J., Russo, B. C., O'Dee, D. M., Schmitt, D. M. & Nau, G. J. The contribution of the glycine cleavage system to the pathogenesis of Francisella tularensis. *Microbes Infect.* **16**, 300–309 (2014).
257. Douce, R., Bourguignon, J., Neuburger, M. & Rébeillé, F. The glycine decarboxylase system: A fascinating complex. *Trends Plant Sci.* **6**, 167–176 (2001).
258. Smith, E. J., Visai, L., Kerrigan, S. W., Speziale, P. & Foster, T. J. The Sbi protein is a multifunctional immune evasion factor of Staphylococcus aureus. *Infect. Immun.* **79**, 3801–3809 (2011).
259. Zhang, L., Rosander, A., Jacobsson, K., Lindberg, M. & Frykberg, L. Expression of staphylococcal protein Sbi is induced by human IgG. *FEMS Immunol. Med. Microbiol.* **28**, 211–218 (2000).
260. Frees, D. *et al.* New insights into staphylococcus aureus stress tolerance and virulence regulation from an analysis of the role of the ClpP protease in the strains Newman, COL, and SA564. *J. Proteome Res.* **11**, 95–108 (2012).
261. Luo, Y. Alanylated lipoteichoic acid primer in Bacillus subtilis. *F1000Research* **5**, 1–20 (2016).
262. Perego, M. *et al.* Incorporation of D-alanine into lipoteichoic acid and wall teichoic acid in Bacillus subtilis: Identification of genes and regulation. *Journal of Biological Chemistry* **270**, 15598–15606 (1995).
263. Stapleton, M. R. *et al.* Characterization of IsaA and SceD, two putative lytic transglycosylases of Staphylococcus aureus. *J. Bacteriol.* **189**, 7316–7325 (2007).
264. Lopes, A.-A. *et al.* crossm Roles of Lytic Transglycosylases in Biofilm Formation and. *Antimicrob. Agents Chemother.* **63**, 1–11 (2019).
265. Clarke, S. R. *et al.* Identification of in vivo-expressed antigens of Staphylococcus aureus and their use in vaccinations for protection against nasal carriage. *J. Infect. Dis.* **193**, 1098–1108 (2006).
266. Lorenz, U. *et al.* Human antibody response during sepsis against targets expressed by methicillin resistant Staphylococcus aureus. *FEMS Immunol. Med. Microbiol.* **29**, 145–153 (2000).
267. Tweten, R. K., Christianson, K. K. & Iandolo, J. J. Transport and processing of staphylococcal alpha-toxin. *J. Bacteriol.* **156**, 524–528 (1983).
268. Stahl, M. *et al.* Selektive Aktivierung der humanen caseinolytischen Protease P (ClpP). *Angew. Chemie* **130**, 14811–14816 (2018).

269. Dahmen, M., Vielberg, M. T., Groll, M. & Sieber, S. A. Structure and mechanism of the caseinolytic protease ClpP1/2 heterocomplex from listeria monocytogenes. *Angew. Chemie - Int. Ed.* **54**, 3598–3602 (2015).
270. Colella, A. D. *et al.* Comparison of Stain-Free gels with traditional immunoblot loading control methodology. *Anal. Biochem.* **430**, 108–110 (2012).
271. Chiu, J., March, P. E., Lee, R. & Tillett, D. Site-directed, Ligase-Independent Mutagenesis (SLIM): a single-tube methodology approaching 100% efficiency in 4 h. *Nucleic Acids Res.* **32**, e174 (2004).
272. Schmied, W. H., Elsässer, S. J., Uttamapinant, C. & Chin, J. W. Efficient Multisite Unnatural Amino Acid Incorporation in Mammalian Cells via Optimized Pyrrolysyl tRNA Synthetase/tRNA Expression and Engineered eRF1. *J. Am. Chem. Soc.* **136**, 15577–15583 (2014).
273. Rappsilber, J., Ishihama, Y. & Mann, M. Stop And Go Extraction tips for matrix-assisted laser desorption/ionization, nanoelectrospray, and LC/MS sample pretreatment in proteomics. *Anal. Chem.* **75**, 663–670 (2003).
274. Frees, D. *et al.* Clp ATPases are required for stress tolerance, intracellular replication and biofilm formation in Staphylococcus aureus. *Mol. Microbiol.* **54**, 1445–1462 (2004).

7 List of abbreviations

Å	*unit of distance, Ångström*
ABP	activity-based probe
ABPP	activity-based protein profiling
ADEP	acyldepsipeptide
ACC	7-amino-4-carbamoylmethylcoumarin
AMC	7-amin-4-methylcoumarin
AML	acute myeloid leukemia
ATP	adenosine triphosphate
BCA	bicinchoninic acid
BioID	proximity-dependent biotin identification
BSA	bovine serum albumin
°C	*unit of temperature, degree Celsius*
calcd	calculated
COMU	[(1-Cyano-2-ethoxy-2-oxoethylidenaminooxy)dimethylamino-morpholino-carbenium-hexafluorophosphat]
CuAAC	Copper(I)-catalyzed azide-alkyne cycloaddition
Da	*atomic mass unit, Dalton*
dd	doubly deionized
DCM	dichloromethane
DIPEA	diisopropylethylamine
DMAP	dimethylaminopyridine
DMF	dimethylformamide
DMEM	Dulbecco's modified Eagle's medium
DMSO	dimethylsulfoxide
DNA	deoxyribonucleic acid
DNP	2,4-dinitrophenylhydrazine
DTT	dithiothreitol
ECL	enhanced chemiluminescence
E. coli	*Escherichia coli*
EDCI	1-ethyl-3-(3-dimethylaminopropyl)carbodiimide hydrochloride
EDTA	ethylenedimamine
eq.	equivalent
ESI	electron spray ionization
Et	ethyl
et al.	*et alii*
ETC	electron transport chain
EtOAc	ethyl acetate
EtOH	ethanol
FA	formic acid
FBS	fetal bovine serum
FDR	false discovery rate
FITC	fluorescein-5-isothiocyanate
FRET	Förster resonance energy transfer
g	*unit of mass, gram*
GO	gene ontology
h	*hour, unit of time*
H	*unit of frequency, Hertz*
HEPES	4-(2-hydroxyethyl)-1-piperazineethanesulfonic acid
HOBT	hydroxybenzotriazole
HPLC	high-performance liquid chromatography
H. sapiens	*Homo sapiens*
HR-MS	high-resolution mass spectrometry
HRP	horse-radish peroxidase
IAA	iodoacetamide
IBS	iodosuccinimide
IC_{50}	half maximal inhibitory concentration
IMDM	Iscove's modified Dulbecco's medium
IP-MS	intact protein mass spectrometry
IPTG	isopropyl-*β*-D-thiogalactopyranoside
J	coupling constant
K	*unit of temperature, Kelvin*
L	*unit of volume, liter*
LB	lysogenic broth
LC-MS	liquid chromatography coupled with mass spectrometry
LFQ	label-free quantification
M	*unit of concentration, mol per liter*
mol	*unit of amount of substance, mole*
Me	methyl
MeCN	acetonitrile
MeOH	methanol
min	*unit of time, minute*

mRNA	messenger ribonucleic caid
MS	mass spectrometry
MS/MS	tandem mass spectrometry
^{mt}UPR	mitochondrial unfolded protein response
m/z	mass to charge
NADH	nicotinamide adenine dinucleotide
n-BuLi	*n*-butyl lithium
NEt_3	Triethylamine
NBS	*N*-bromosuccinimide
NMR	nuclear magnetic resonance
OD	optical density
o/n	overnight
PBS	phosphate buffered saline
PDB	protein databank
PEG	polyethylene glycol
pH	*potentia Hydrogenii*
PPh_3	triphenylphosphine
PPi	protein-protein interaction
ppm	*part per million*
PSM	peptide spectrum matches
p-TsCl	*para*-toluenesulfonyl chloride
PVDF	polyvinylidene fluoride
py	pyridine
R_f	retention factor
rpm	rotation per minute
RhN_3	rhodamine azide
ROS	reactive oxygen species
RP-HPLC	reversed-phase high performance liquid chromatography
RPMI	Roswell Park Memorial Institute
RT	room temperature
s	*unit of time, second*
SAR	structure activity relationship
S. aureus	*Staphylococcus aureus*
SD	standard deviation
SDS-PAGE	sodium dodecyl sulfate polyacrylamide gel electrophoresis
SEC	size exclusion chromatography
SRM	selected reaction monitoring
SLIM	site-directed ligase independent mutagenesis
STRING	Search tool for the retrieval of interacting genes/proteins
TAMRA	tetramethylrhodamine 5-carboxamido-(6-azidohexanyl)
TBAF	tetrabutyl ammonium fluoride
TBDMSCl	*tert*-butyldimethylsilyl chloride
TBTA	tris(benzyltriazolylmethyl)amine
TCA	tricarboxylic acid
TCEP	tris(2-carboxyethyl)phosphine
TEV	tobacco etch virus
TFA	trifluoroacetic acid
THF	tetrahydrofurane
TLC	thin layer chromatography
TMS	trimethylsilyl
Tris	tris(hydroxymethyl)aminomethane
tRNA	transfer ribonucleic acid
UAA	unnatural amino acid
UMP	uracil monophosphate
UV	ultra violet
V	*unit of voltage, Volt*
(v/v)	volume/volume
WB	western blot
wt	wild-type
(w/v)	weight/volume

8 Appendices

8.1 Supplementary figures and tables

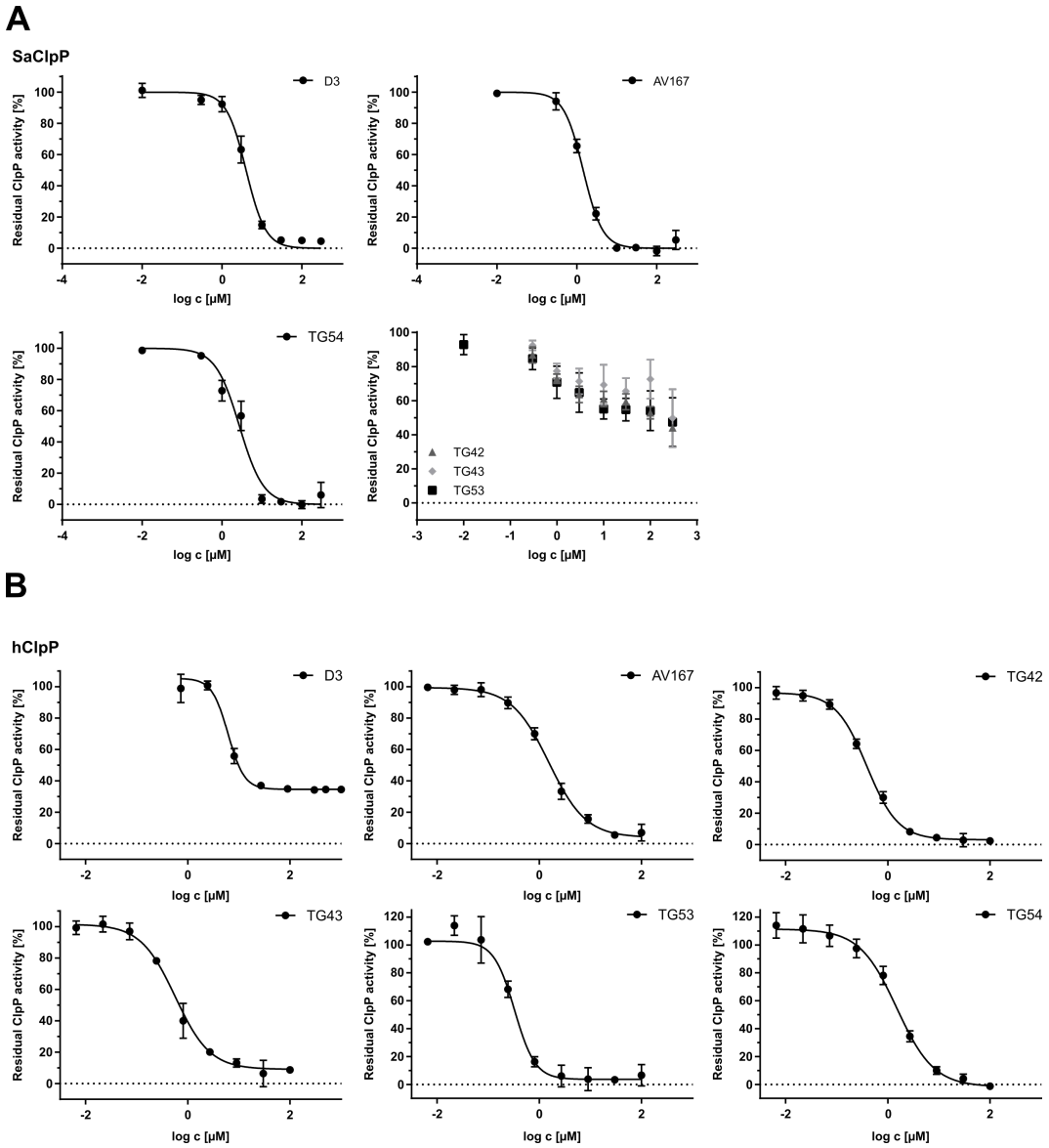

Figure 8.1 A) Raw data for determination of apparent IC_{50} values for phenyl esters with SaClpP. 1 µM SaClpP was incubated with varying concentrations of phenyl esters for 15 min at 32 °C prior to addition of fluorogenic substrate Suc-L-Y-AMC (200 µM). Curves were generated by fitting a nonlinear regression curve to the data points representing results from at least six replicates (mean ± SD). B) Raw data for determination of apparent IC_{50} values of phenyl esters with hClpP. Compounds were incubated with 1 µM hClpP for 15 min at 37 °C prior to addition of substrate. Curves were generated by fitting a nonlinear regression curve to the data points representing results from at least six replicates (mean ± SD).

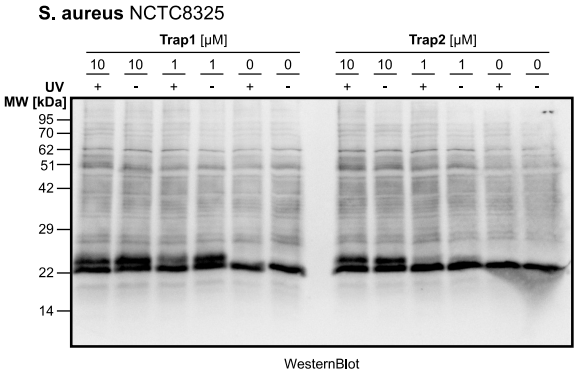

Figure 8.2 Full western blot for Figure 4.17.

Trapping experiments with ClpP mutants in Hek293T cells

Table 8.1 Significantly enriched proteins from trapping experiments in Hek293T cells with ClpP mutant SH1 (log_2 ratio > 1, $–log_{10}$ t-test p-value > 1.30). For annotation of known substrates recent literature references [20,40,135,140,154,158,170] were taken into account and proteins are marked with "+". Proteins that do not show previous connection to ClpP are labeled with "-".

Protein names	Gene name	Enrichment factor (log_2)	p-value t-test ($-log_{10}$)	Annotated as substrate
10 kDa heat shock protein, mitochondrial	HSPE1	2.528060913	2.357710492	-
Dihydrolipoyllysine-residue succinyltransferase component of 2-oxoglutarate dehydrogenase complex, mitochondrial	DLST	2.465864182	2.80002771	+
39S ribosomal protein L13, mitochondrial	MRPL13	2.259292603	2.699404838	+
Serine beta-lactamase-like protein LACTB, mitochondrial	LACTB	2.176890055	2.572455941	-
Clathrin light chain B	CLTB	2.020890554	2.431020243	-
Clathrin light chain A	CLTA	1.966786702	2.557270996	-
Acetyltransferase component of pyruvate dehydrogenase complex	DLAT	1.89736557	3.709135937	+
Clathrin heavy chain;Clathrin heavy chain 1	CLTC	1.736051559	2.961035244	-
Mitochondrial import receptor subunit TOM22 homolog	TOMM22	1.710225423	1.440738034	-
Hsc70-interacting protein	ST13	1.659377416	1.952781386	-
Pyruvate dehydrogenase protein X component, mitochondrial	PDHX	1.573442459	2.736985754	+
Protein scribble homolog	SCRIB	1.551549276	3.539765357	-
Unconventional myosin-Id	MYO1D	1.484951655	1.64892459	-
Stress-induced-phosphoprotein 1	STIP1	1.29959933	2.367580932	+
Non-specific protein-tyrosine kinase	YES1	1.120776494	1.381649232	-
Malate dehydrogenase;Malate dehydrogenase, mitochondrial	MDH2	1.095053355	2.650466362	+
Enoyl-CoA hydratase, mitochondrial	ECHS1	1.090739568	1.345539571	+
Histone-arginine methyltransferase CARM1	CARM1	1.032866796	2.484322024	-

Table 8.2 Significantly enriched proteins from trapping experiments in Hek293T cells with ClpP mutant SH2 (log_2 ratio > 1, $–log_{10}$ t-test p-value > 1.30). For annotation of known substrates recent literature references [20,40,135,140,154,158,170] were taken into account and proteins are marked with "+". Proteins that do not show previous connection to ClpP are labeled with "-".

Protein names	Gene name	Enrichment factor (log_2)	p-value t-test ($-log_{10}$)	Annotated as substrate
Heterogeneous nuclear ribonucleoprotein U-like protein 2	HNRNPUL2	6.518294017	3.110163196	-
Heterogeneous nuclear ribonucleoprotein A/B	HNRNPAB	4.536731084	3.787498035	-
Lupus La protein	SSB	4.239100138	3.281673152	-
RNA-binding motif, single-stranded-interacting protein 1	RBMS1	4.080912272	3.334308368	-
Threonine synthase-like 1	THNSL1	4.00594902	2.76971573	+
Nuclease-sensitive element-binding protein 1	YBX1	3.788115819	2.647808991	-
5-3 exoribonuclease 2	XRN2	3.784579595	1.987684658	-
Polyadenylate-binding protein 2	PABPN1	3.684401194	5.265217984	-
Polyadenylate-binding protein 4	PABPC4	3.624721527	3.165265389	-
Heterogeneous nuclear ribonucleoprotein D-like	HNRNPDL	3.583220164	2.000476081	-
Glycine cleavage system H protein, mitochondrial	GCSH	3.544822693	2.06076592	+
Heterogeneous nuclear ribonucleoprotein D-like	HNRNPDL	3.502468745	4.691630576	-
Spermatid perinuclear RNA-binding protein	HEL162	3.452546438	4.487742728	-
Heterogeneous nuclear ribonucleoprotein D0	HNRPD	3.413604736	4.007088155	-
Probable tRNA pseudouridine synthase 2	TRUB2	3.179822286	2.300139499	-
THUMP domain-containing protein 1	THUMPD1	3.174427032	2.603579596	-
Polyadenylate-binding protein	PABPC1	3.137008031	1.753759417	-
Zinc finger CCCH-type antiviral protein 1	ZC3HAV1	2.919965108	2.420918282	-
10 kDa heat shock protein, mitochondrial	HSPE1	2.761142095	3.09089524	-
Heterogeneous nuclear ribonucleoprotein Q	SYNCRIP	2.755172729	4.298819047	-
28S ribosomal protein S28, mitochondrial	MRPS28	2.729255676	3.446636279	+
RNA-binding protein Musashi homolog 2	MSI2	2.702177684	2.971068803	-
Isoleucine--tRNA ligase, mitochondrial	IARS2	2.593344371	2.965459546	+
Insulin-like growth factor 2 mRNA-binding protein 2	IGF2BP2	2.534356435	2.700772355	-
ATP-dependent RNA helicase DHX36	DHX36	2.501374563	4.009703465	-
28S ribosomal protein S34, mitochondrial	MRPS34	2.4945666	3.644553291	-
28S ribosomal protein S6, mitochondrial	MRPS6	2.381146113	2.339273589	+
39S ribosomal protein L1, mitochondrial	MRPL1	2.373535792	1.615456931	+
Heterogeneous nuclear ribonucleoprotein U	HNRNPU	2.367306391	3.13102073	-
Enoyl-CoA hydratase, mitochondrial	ECHS1	2.342359543	3.047345112	+
Probable E3 ubiquitin-protein ligase makorin-2	MKRN2	2.319894155	3.55549555	-
39S ribosomal protein L3, mitochondrial	MRPL3	2.30510203	2.612886642	-
28S ribosomal protein S23, mitochondrial	MRPS23	2.268669128	1.625540672	+
Insulin-like growth factor 2 mRNA-binding protein 3	IGF2BP3	2.225276311	2.443275937	-
G-rich sequence factor 1	GRSF1	2.191397985	2.477793642	+
Dihydrolipoyl dehydrogenase;Dihydrolipoyl dehydrogenase, mitochondrial	DLD	2.153752009	2.769800596	+
39S ribosomal protein L15, mitochondrial	MRPL15	2.151285172	2.905576994	+
28S ribosomal protein S18b, mitochondrial	MRPS18B	2.08224678	2.633008426	+
Insulin-like growth factor 2 mRNA-binding protein 1	IGF2BP1	2.064293543	2.941183194	-
La-related protein 1	LARP1	2.006263097	2.120226653	-
Dihydrolipoyllysine-residue succinyltransferase component of 2-oxoglutarate dehydrogenase complex, mitochondrial	DLST	2.002729416	1.877540646	+
39S ribosomal protein L11, mitochondrial	MRPL11	2.002288183	2.247417398	-
28S ribosomal protein S9, mitochondrial	MRPS9	1.978295008	2.517465445	+
39S ribosomal protein L4, mitochondrial	MRPL4	1.969324112	5.952863687	-
Heterogeneous nuclear ribonucleoprotein L	HNRNPL	1.955095927	2.677170871	-
39S ribosomal protein L43, mitochondrial	MRPL43	1.823653539	3.138160528	+
2-oxoglutarate dehydrogenase, mitochondrial	OGDH	1.819985708	2.856320033	+
28S ribosomal protein S5, mitochondrial	MRPS5	1.779591242	2.439905779	+
Lipoamide acyltransferase component of branched-chain alpha-keto acid dehydrogenase complex, mitochondrial	DBT	1.758091609	3.175318594	-
Heat shock protein 75 kDa, mitochondrial	TRAP1	1.741571426	3.627208492	+
Pyruvate dehydrogenase protein X component, mitochondrial	PDHX	1.727851868	3.730399994	+
28S ribosomal protein S16, mitochondrial	MRPS16	1.673002879	3.86417554	+
Constitutive coactivator of PPAR-gamma-like protein 1	FAM120A	1.664419174	2.432006898	-
Acetyltransferase component of pyruvate dehydrogenase complex	DLAT	1.646781286	2.619956461	+
28S ribosomal protein S31, mitochondrial	MRPS31	1.642515182	2.495011687	+
NF-kappa-B-repressing factor	NKRF	1.629261017	2.198007411	-
39S ribosomal protein L21, mitochondrial	MRPL21	1.614315033	2.751716284	+

39S ribosomal protein L13, mitochondrial	MRPL13	1.536867778	1.761671464	+
39S ribosomal protein L45, mitochondrial	MRPL45	1.51011912	2.818758442	+
Acetyl-CoA acetyltransferase, mitochondrial	ACAT1	1.493288676	4.410884257	+
Cytochrome b-c1 complex subunit 1, mitochondrial	UQCRC1	1.483260473	2.589449466	+
Protein deglycase DJ-1	PARK7	1.470893224	1.40334102	-
28S ribosomal protein S22, mitochondrial	MRPS22	1.408541361	3.16183956	+
Interleukin enhancer-binding factor 3	ILF3	1.39076678	3.376662231	-
Heterogeneous nuclear ribonucleoprotein K	HNRPK	1.387111028	4.044415826	-
Leucine-rich PPR motif-containing protein, mitochondrial	LRPPRC	1.363213857	3.179289191	+
Heterogeneous nuclear ribonucleoprotein A0	HNRNPA0	1.350752513	3.024946219	-
SRA stem-loop-interacting RNA-binding protein, mitochondrial	SLIRP	1.34758695	2.431424984	+
Heterogeneous nuclear ribonucleoprotein R	HNRNPR	1.34037145	2.4306181	-
40S ribosomal protein S17	RPS17	1.305379232	3.539899275	-
39S ribosomal protein L51, mitochondrial	MRPL51	1.294469198	3.03400986	-
Williams-Beuren syndrome chromosomal region 16 protein	WBSCR16	1.292111715	1.659171632	+
39S ribosomal protein L39, mitochondrial	MRPL39	1.289264679	6.064794061	+
Pentatricopeptide repeat domain-containing protein 3, mitochondrial	PTCD3	1.275725047	2.906635339	+
28S ribosomal protein S26, mitochondrial	MRPS26	1.262624741	3.15316929	+
RNA-binding motif protein, X chromosome	RBMX	1.254060109	1.732152367	-
Protein ELYS	AHCTF1	1.225773493	1.577281647	-
Interleukin enhancer-binding factor 2	ILF2	1.18741099	1.811837932	-
28S ribosomal protein S11, mitochondrial	MRPS11	1.187133153	2.377316847	+
39S ribosomal protein L17, mitochondrial	MRPL17	1.182820002	3.031551281	+
Far upstream element-binding protein 3	FUBP3	1.172859828	1.804180042	-
28S ribosomal protein S29, mitochondrial	DAP3	1.166245143	1.970002487	+
Cysteine desulfurase, mitochondrial	NFS1	1.087621053	2.13564208	+
L-2-hydroxyglutarate dehydrogenase, mitochondrial	L2HGDH	1.063916524	1.589935736	-
39S ribosomal protein L44, mitochondrial	MRPL44	1.001045227	1.504273452	+

Table 8.3 Significantly enriched proteins from trapping experiments in Hek293T cells with ClpP mutant SH3 (log_2 ratio > 1, $–log_{10}$ t-test p-value > 1.30). For annotation of known substrates recent literature references [20,40,135,140,154,158,170] were taken into account and proteins are marked with "+". Proteins that do not show previous connection to ClpP are labeled with "-".

Protein names	Gene name	Enrichment factor (log_2)	p-value t-test ($-log_{10}$)	Annotated as substrate
26S proteasome non-ATPase regulatory subunit 10	PSMD10	2.599224091	3.099309091	-
Low molecular weight phosphotyrosine protein phosphatase	ACP1	2.394634883	2.20235606	-
Cytochrome c oxidase subunit 5A, mitochondrial	COX5A	1.666353861	2.481374747	+
L-2-hydroxyglutarate dehydrogenase, mitochondrial	L2HGDH	1.296777725	2.262133108	-
Acetyltransferase component of pyruvate dehydrogenase complex	DLAT	1.292052587	1.997436201	+
Dihydrolipoyllysine-residue succinyltransferase component of 2-oxoglutarate dehydrogenase complex, mitochondrial	DLST	1.283274333	2.210274591	+
Pyruvate dehydrogenase protein X component, mitochondrial	PDHX	1.192612966	3.005726645	+
Vimentin	HEL113	1.184209188	2.364686983	+
SEC23-interacting protein	SEC23IP	1.117851893	1.597814887	-
Tubulin alpha-1A chain;Tubulin alpha-3C/D chain;Tubulin alpha-3E chain	TUBA1A	1.113746643	1.816653826	-
MAP7 domain-containing protein 1	MAP7D1	1.087779363	1.465578942	-
Lipoamide acyltransferase component of branched-chain alpha-keto acid dehydrogenase complex, mitochondrial	DBT	1.006003698	3.013900794	-

Table 8.4 Significantly enriched proteins from trapping experiments in Hek293T cells with ClpP mutant SH4 (log_2 ratio > 1, $–log_{10}$ t-test p-value > 1.30). For annotation as known substrate recent literature references [20,40,135,140,154,158,170] were taken into account.

Protein names	Gene name	Enrichment factor (log_2)	p-value t-test ($-log_{10}$)	Annotated as substrate
Glycine cleavage system H protein, mitochondrial	GCSH	3.83144188	3.39578492	+
Cytochrome c oxidase subunit 4 isoform 1, mitochondrial	COX4I1	2.07114728	3.26673057	+
Low molecular weight phosphotyrosine protein phosphatase	ACP1	1.80448977	1.30789463	-
10 kDa heat shock protein, mitochondrial	HSPE1	1.68412463	2.08915157	-
Inorganic pyrophosphatase 2, mitochondrial	PPA2	1.62349447	2.91607884	+
Lipoamide acyltransferase component of branched-chain alpha-keto acid dehydrogenase complex, mitochondrial	DBT	1.56262271	2.99743635	-
Mitochondrial import inner membrane translocase subunit Tim8 B	TIMM8B	1.42010689	3.72810838	-
Stress-induced-phosphoprotein 1	STIP1	1.37785149	2.74930439	+
Polyadenylate-binding protein 2	PABPN1	1.31002935	1.34611824	-
Growth arrest and DNA damage-inducible proteins-interacting protein 1	GADD45GIP1	1.22106043	1.4733748	-
Mitochondrial import inner membrane translocase subunit Tim13	TIMM13	1.18352318	2.32393757	-
Pyruvate dehydrogenase protein X component, mitochondrial	PDHX	1.05083529	3.76064284	+
Heat shock protein 75 kDa, mitochondrial	TRAP1	1.01244863	3.36180087	+

Table 8.5 Significantly enriched proteins from trapping experiments in Hek293T cells with ClpP mutant SH5 (log_2 ratio > 1, $–log_{10}$ t-test p-value > 1.30). For annotation of known substrates recent literature references [20,40,135,140,154,158,170] were taken into account and proteins are marked with "+". Proteins that do not show previous connection to ClpP are labeled with "-".

Protein names	Gene name	Enrichment factor (log_2)	p-value t-test ($-log_{10}$)	Annotated as substrate
Protein deglycase DJ-1	PARK7	2.57212321	2.39455614	-
Lipoamide acyltransferase component of branched-chain alpha-keto acid dehydrogenase complex, mitochondrial	DBT	2.52292633	3.0810378	-
L-2-hydroxyglutarate dehydrogenase, mitochondrial	L2HGDH	2.40566762	1.6841459	-
Pyruvate dehydrogenase protein X component, mitochondrial	PDHX	1.88935089	3.07300658	+
Proteasome activator complex subunit 3	PSME3	1.80785497	2.90815977	-
Acetyltransferase component of pyruvate dehydrogenase complex	DLAT	1.74389521	2.96192323	+
Dihydrolipoyllysine-residue succinyltransferase component of 2-oxoglutarate dehydrogenase complex, mitochondrial	DLST	1.62713242	2.04765556	+
2-oxoglutarate dehydrogenase, mitochondrial	OGDH	1.41948636	4.23615689	+
Mitochondrial import receptor subunit TOM70	TOMM70A	1.4188385	2.55492142	-
Dihydrolipoyl dehydrogenase;Dihydrolipoyl dehydrogenase, mitochondrial	DLD	1.3963871	2.67590128	+
Acetyl-CoA acetyltransferase, mitochondrial	ACAT1	1.3935407	3.05525474	+
Pyruvate dehydrogenase E1 component subunit alpha	PDHA1	1.36758105	2.68051774	-

Coiled-coil domain-containing protein 80	CCDC80	1.16726494	1.46698247	-

Table 8.6 Significantly enriched proteins from trapping experiments in Hek293T cells with ClpP mutant SH6 (log_2 ratio > 1, $–log_{10}$ t-test p-value > 1.30). For annotation of known substrates recent literature references [20,40,135,140,154,158,170] were taken into account and proteins are marked with "+". Proteins that do not show previous connection to ClpP are labeled with "-".

Protein names	Gene names	Enrichment factor (log_2)	p-value t-test ($-log_{10}$)	Annotated as substrate
39S ribosomal protein L39, mitochondrial	MRPL39	3.69523875	2.87025648	+
Mitochondrial import receptor subunit TOM40 homolog	TOMM40	3.61561521	3.17518351	-
SRA stem-loop-interacting RNA-binding protein, mitochondrial	SLIRP	2.97568321	1.65137757	+
Cleavage and polyadenylation specificity factor subunit 4	CPSF4	2.9491717	2.7285779	-
Small nuclear ribonucleoprotein G	SNRPG	2.80916087	2.04616458	-
Tripeptidyl-peptidase 1	TPP1	2.78866768	1.32640606	-
Transducin beta-like protein 3	TBL3	2.78135109	1.43187895	-
Lipoamide acyltransferase component of branched-chain alpha-keto acid dehydrogenase complex, mitochondrial	DBT	2.37619591	3.14234269	-
Septin-2	SEPT2	2.26404635	2.4847726	-
Mitochondrial import receptor subunit TOM6 homolog	TOMM6	2.14990807	1.42698883	+
Short/branched chain specific acyl-CoA dehydrogenase, mitochondrial	ACADSB	2.05969874	3.37409558	+
26S proteasome non-ATPase regulatory subunit 4	PSMD4	1.93259303	2.5893379	+
Pyruvate dehydrogenase protein X component, mitochondrial	PDHX	1.77110227	4.17378336	+
Acetyltransferase component of pyruvate dehydrogenase complex	DLAT	1.65835698	3.3096671	+
Mitochondrial import receptor subunit TOM5 homolog	TOMM5	1.62214979	2.86460387	-
Nucleoporin Nup43	NUP43	1.62046878	1.42195773	-
Dihydrolipoyllysine-residue succinyltransferase component of 2-oxoglutarate dehydrogenase complex, mitochondrial	DLST	1.518013	3.07525562	+
Plasminogen activator inhibitor 1 RNA-binding protein	SERBP1	1.43370883	1.71404677	-
Enoyl-CoA hydratase, mitochondrial	ECHS1	1.40692139	2.27185593	+
10 kDa heat shock protein, mitochondrial	HSPE1	1.394804	1.56747413	-
rRNA methyltransferase 2, mitochondrial	HEL97	1.27911504	2.2129185	-
Cyclin-dependent kinase 4	CDK4	1.20119413	3.4476943	-
Mitochondrial import receptor subunit TOM22 homolog	TOMM22	1.15445201	2.30656297	-
Heat shock protein 75 kDa, mitochondrial	TRAP1	1.08820279	2.82503219	+

Table 8.7 Significantly enriched proteins from trapping experiments in Hek293T cells with ClpP mutant SH7 (log_2 ratio > 1, $–log_{10}$ t-test p-value > 1.30). For annotation of known substrates recent literature references [20,40,135,140,154,158,170] were taken into account and proteins are marked with "+". Proteins that do not show previous connection to ClpP are labeled with "-".

Protein names	Gene names	Enrichment factor (log_2)	p-value t-test ($-log_{10}$)	Annotated as substrate
Enoyl-CoA hydratase, mitochondrial	ECHS1	7.08297412	6.14249209	+
10 kDa heat shock protein, mitochondrial	HSPE1	5.22580592	1.72892543	-
Isovaleryl-CoA dehydrogenase, mitochondrial	IVD	5.19725927	3.41344426	+
Hydroxyacyl-coenzyme A dehydrogenase, mitochondrial	HADH	4.82912254	4.47425768	+
Malate dehydrogenase;Malate dehydrogenase, mitochondrial	MDH2	4.56429545	5.94513238	+
Sepiapterin reductase	SPR	4.56307348	3.7642302	-
99,3% Presequence Protease, pitrilysin metallopeptidase	PITRM1	4.4543368	5.58843754	+
Aconitate hydratase, mitochondrial	ACO2	4.26304881	4.06072425	+
Isocitrate dehydrogenase [NADP], mitochondrial	IDH2	4.13931402	3.85969321	+
Short/branched chain specific acyl-CoA dehydrogenase, mitochondrial	ACADSB	3.87617238	2.68326046	+
Acetyl-CoA acetyltransferase, mitochondrial	ACAT1	3.68018341	4.93766787	+
Citrate synthase;Citrate synthase, mitochondrial	CS	3.55343119	5.48344718	+
Acetyltransferase component of pyruvate dehydrogenase complex	DLAT	3.54185422	1.80263618	+
Polyribonucleotide nucleotidyltransferase 1, mitochondrial	PNPT1	3.53656324	5.08480506	+
Isocitrate dehydrogenase [NAD] subunit, mitochondrial;Isocitrate dehydrogenase [NAD] subunit alpha, mitochondrial	IDH3A	3.50106875	3.3788779	+
Single-stranded DNA-binding protein;Single-stranded DNA-binding protein, mitochondrial	SSBP1	3.35598755	3.86522097	+
Serine hydroxymethyltransferase;Serine hydroxymethyltransferase, mitochondrial	SHMT2	3.34568469	5.2228862	+
Dihydrolipoyllysine-residue succinyltransferase component of 2-oxoglutarate dehydrogenase complex, mitochondrial	DLST	3.28835551	3.95726853	+
Tyrosine--tRNA ligase, mitochondrial;Tyrosine--tRNA ligase	YARS2	3.21464602	2.86100621	+
Dihydrolipoyl dehydrogenase;Dihydrolipoyl dehydrogenase, mitochondrial	DLD	3.1332798	4.18157035	+
2-oxoglutarate dehydrogenase, mitochondrial	OGDH	3.05487124	3.66429743	+
Acyl-coenzyme A thioesterase 1;Acyl-coenzyme A thioesterase 2, mitochondrial	ACOT1	2.97574298	3.16847496	+
Lipoamide acyltransferase component of branched-chain alpha-keto acid dehydrogenase complex, mitochondrial	DBT	2.96562449	2.48880334	-
Electron transfer flavoprotein subunit beta	ETFB	2.90824827	2.26341865	+
Fumarate hydratase, mitochondrial	FH	2.86964989	2.44974423	-
Mitochondrial ribonuclease P protein 1	TRMT10C	2.78555107	1.87222244	+
Mitochondrial import receptor subunit TOM70	TOMM70A	2.76650874	1.39449238	-
Acyl-CoA dehydrogenase family member 9, mitochondrial	ACAD9	2.71775881	4.27364214	+
Protein deglycase DJ-1	PARK7	2.71552658	1.65359826	-
Heat shock protein 75 kDa, mitochondrial	TRAP1	2.70960172	3.19950177	+
Cob(I)yrinic acid a,c-diamide adenosyltransferase, mitochondrial	MMAB	2.69214185	2.97033291	-
Pyruvate dehydrogenase protein X component, mitochondrial	PDHX	2.63960838	3.00161336	+
Isoleucine--tRNA ligase, mitochondrial	IARS2	2.61310514	3.81692843	+
Leucine-rich PPR motif-containing protein, mitochondrial	LRPPRC	2.56129265	2.89057994	+
ATP synthase subunit d, mitochondrial	ATP5H	2.55917295	1.38680909	+
Glutaminase kidney isoform, mitochondrial	GLS	2.5211792	2.01331491	+
3-hydroxyacyl-CoA dehydrogenase type-2	HSD17B10	2.46673584	4.53563713	+
ATP synthase F(0) complex subunit B1, mitochondrial	ATP5F1	2.35659091	1.82896105	-
Mitochondrial intermediate peptidase	MIPEP	2.28592555	2.47335817	+
Glycine--tRNA ligase	GARS	2.27018166	1.59514186	+
Aldehyde dehydrogenase, mitochondrial	ALDH2	2.2700901	3.4454459	-
Aspartate--tRNA ligase, mitochondrial	DARS2	2.26568476	2.72366543	-
NAD-dependent malic enzyme, mitochondrial	ME2	2.16055552	3.58115927	-
Monofunctional C1-tetrahydrofolate synthase, mitochondrial	MTHFD1L	2.1106542	3.40480894	+
Electron transfer flavoprotein subunit alpha, mitochondrial	ETFA	1.99602763	4.13475842	+
ATP synthase subunit beta;ATP synthase subunit beta, mitochondrial	ATP5B	1.99509048	3.31934939	+
Hydroxymethylglutaryl-CoA lyase, mitochondrial	HMGCL	1.94898097	1.65773869	+
ATP synthase mitochondrial F1 complex assembly factor 2	ATPAF2	1.93302917	1.60720171	-
NADH dehydrogenase [ubiquinone] 1 alpha subcomplex subunit 6	NDUFA6	1.90193367	1.82497091	+

Pyruvate dehydrogenase E1 component subunit alpha, mitochondrial	PDHA1	1.89166832	3.68221395	+
Ornithine aminotransferase, mitochondrial	OAT	1.83684095	2.7689186	+
Isocitrate dehydrogenase [NAD] subunit, mitochondrial	IDH3B	1.83460172	3.62711305	+
Succinyl-CoA ligase [ADP/GDP-forming] subunit alpha, mitochondrial	SUCLG1	1.83005333	4.50265362	+
Medium-chain specific acyl-CoA dehydrogenase, mitochondrial	ACADM	1.81834157	4.32905502	+
Complex III assembly factor LYRM7	LYRM7	1.74750392	1.82877052	+
Glycine dehydrogenase (decarboxylating), mitochondrial	GLDC	1.65087446	1.52630458	+
2,4-dienoyl-CoA reductase, mitochondrial	DECR1	1.62497393	1.49161777	+
Mitochondrial import inner membrane translocase subunit TIM44	TIMM44	1.61522675	2.26591336	+
G-rich sequence factor 1	GRSF1	1.60489273	2.3446218	+
ATP synthase subunit g, mitochondrial	ATP5L	1.57912763	1.53196088	-
Delta(3,5)-Delta(2,4)-dienoyl-CoA isomerase, mitochondrial	ECH1	1.57240359	2.11907915	+
ATP synthase subunit O, mitochondrial	ATP5O	1.54561996	2.93276679	-
39S ribosomal protein L44, mitochondrial	MRPL44	1.54289563	2.88366699	+
Cytoplasmic dynein 1 light intermediate chain 1	DYNC1LI1	1.47920227	1.35880247	-
3-hydroxyisobutyrate dehydrogenase;3-hydroxyisobutyrate dehydrogenase, mitochondrial	HIBADH	1.45746994	2.16669445	-
Probable leucine--tRNA ligase, mitochondrial	LARS2	1.41318893	1.96446322	+
Glutamate dehydrogenase;Glutamate dehydrogenase 1, mitochondrial	GLUD1	1.39283371	3.3153833	+
Aspartate aminotransferase;Aspartate aminotransferase, mitochondrial	GOT2	1.38335546	1.97231956	+
28S ribosomal protein S28, mitochondrial	MRPS28	1.33673096	2.01300666	+
28S ribosomal protein S27, mitochondrial	MRPS27	1.3307972	2.73975322	-
3-hydroxyisobutyryl-CoA hydrolase, mitochondrial	HIBCH	1.30554263	2.89547207	-
Ran GTPase-activating protein 1	RANGAP1	1.25149218	1.7788858	-
28S ribosomal protein S34, mitochondrial	MRPS34	1.22402382	1.5503205	-
39S ribosomal protein L1, mitochondrial	MRPL1	1.22068787	1.7740464	+
Cytosol aminopeptidase	LAP3	1.2072506	1.48275179	-
Methylcrotonoyl-CoA carboxylase beta chain, mitochondrial	MCCC2	1.13636843	3.04760163	+
SRA stem-loop-interacting RNA-binding protein, mitochondrial	SLIRP	1.12037404	1.84222529	+
Ubiquitin carboxyl-terminal hydrolase;Probable ubiquitin carboxyl-terminal hydrolase FAF-X	USP9X	1.05227025	1.31671925	-
ATP synthase subunit alpha;ATP synthase subunit alpha, mitochondrial	ATP5A1	1.00348409	3.88912011	+

Trapping experiments with rotenone treated Hek293T cells

Table 8.8 Significantly enriched proteins from trapping experiments in rotenone treated Hek293T cells with ClpP mutant SH2 (log_2 ratio > 1, $–log_{10}$ t-test p-value > 1.30). Proteins that were enriched only in rotenone treated samples and no other ClpP mutants are marked as follows: "+" indicates positive and "-" indicates no unique enrichment.

Protein names	Gene names	Enrichment factor (log_2)	p-value t-test ($-log_{10}$)	Unique for rotenone treated samples
CDKN2A-interacting protein	CDKN2AIP	5.829336166	4.040013777	+
Glycine cleavage system H protein, mitochondrial	GCSH	5.622687658	3.547040595	-
THUMP domain-containing protein 1	THUMPD1	4.467810313	2.25853187	-
L-2-hydroxyglutarate dehydrogenase, mitochondrial	L2HGDH	3.54887708	2.627576481	-
RNA-binding protein Musashi homolog 1	MSI1	3.508930206	3.157466777	+
RNA-binding protein Musashi homolog 2	MSI2	3.060661316	2.923710133	-
Threonine synthase-like 1	THNSL1	2.965991338	2.611644794	-
Heterogeneous nuclear ribonucleoprotein U-like protein 2	HNRNPUL2	2.948937734	3.977559625	-
Polyadenylate-binding protein 2	PABPN1	2.659805934	2.594563442	-
Inorganic pyrophosphatase 2, mitochondrial	PPA2	2.637054443	1.517691785	-
Heterogeneous nuclear ribonucleoprotein D-like	HNRNPDL	2.558508555	2.11972959	-
Protein phosphatase PTC7 homolog	PPTC7	2.429484685	2.367260172	+
Heterogeneous nuclear ribonucleoprotein A/B	HNRNPAB	2.380776087	3.285908114	-
NAD-dependent malic enzyme, mitochondrial	ME2	2.338485718	2.705599794	-
RNA-binding motif, single-stranded-interacting protein 1	RBMS1	2.317210515	4.040859241	-
39S ribosomal protein L53, mitochondrial	MRPL53	2.278296153	1.644229884	+
39S ribosomal protein L52, mitochondrial	MRPL52	2.268756866	1.684215422	+
39S ribosomal protein L33, mitochondrial	MRPL33	2.196620941	3.921010963	+
Dihydrolipoyl dehydrogenase	DLD	2.178907394	3.568975709	-
Pyruvate dehydrogenase protein X component, mitochondrial	PDHX	2.133876801	3.274047919	-
Heterogeneous nuclear ribonucleoprotein D-like	HNRNPDL	1.989514669	2.604936259	-
Probable E3 ubiquitin-protein ligase makorin-2	MKRN2	1.952359517	3.091680264	-
Putative transferase CAF17, mitochondrial	IBA57	1.927953084	2.28678109	+
5-3 exoribonuclease 2	XRN2	1.894339879	2.899070362	-
RNA-binding motif, single-stranded-interacting protein 2	RBMS2	1.76350975	2.731841921	+
Scaffold attachment factor B2	SAFB2	1.705375671	2.6444863	+
Heterogeneous nuclear ribonucleoprotein D0	HNRPD	1.705236435	2.88015151	-
Enoyl-CoA hydratase, mitochondrial	ECHS1	1.640617371	2.209923076	-
3-hydroxyacyl-CoA dehydrogenase type-2	HSD17B10	1.62707456	3.046260469	+
Heterogeneous nuclear ribonucleoprotein L-like	HNRNPLL	1.5285333	1.787033256	-
Dihydrolipoyllysine-residue succinyltransferase component of 2-oxoglutarate dehydrogenase complex, mitochondrial	DLST	1.46873792	2.346542802	-
Acetyltransferase component of pyruvate dehydrogenase complex	DLAT	1.389623642	2.174352815	-
Leucine-rich PPR motif-containing protein, mitochondrial	LRPPRC	1.369992574	3.256026935	-
39S ribosomal protein L11, mitochondrial	MRPL11	1.355416616	2.657172419	-
Heterogeneous nuclear ribonucleoprotein Q	SYNCRIP	1.348293304	2.908116296	-
10 kDa heat shock protein, mitochondrial	HSPE1	1.346793493	2.380939534	-
Acetyl-CoA acetyltransferase, mitochondrial	ACAT1	1.346787135	2.900621023	-
Heat shock protein 75 kDa, mitochondrial	TRAP1	1.285238902	3.443833745	-
Hsc70-interacting protein	ST13	1.213008881	2.343873193	-
Isoleucine--tRNA ligase, mitochondrial	IARS2	1.210509618	2.172471039	-
ATP synthase mitochondrial F1 complex assembly factor 2	ATPAF2	1.207989375	2.36997155	-
2-oxoglutarate dehydrogenase, mitochondrial	OGDH	1.207115173	3.257591742	-
ATP-dependent RNA helicase DHX36	DHX36	1.187526067	2.20148615	-
Presequence protease, mitochondrial	PITRM1	1.16511027	2.587880206	-
Lipoamide acyltransferase component of branched-chain alpha-keto acid dehydrogenase complex, mitochondrial	DBT	1.144769669	2.845733961	-
39S ribosomal protein L54, mitochondrial	MRPL54	1.111061732	1.658340646	+
39S ribosomal protein L2, mitochondrial	MRPL2	1.111005147	2.507914069	+
39S ribosomal protein L18, mitochondrial	MRPL18	1.10972023	2.994042816	+
2-oxoisovalerate dehydrogenase subunit alpha, mitochondrial	BCKDHA	1.109059652	1.593489521	+
39S ribosomal protein L44, mitochondrial	MRPL44	1.096445719	3.076966717	-
Lupus La protein	SSB	1.095890681	2.815146607	-
Mitochondrial ribonuclease P protein 1	TRMT10C	1.090220133	1.630214209	+
THUMP domain-containing protein 3	THUMPD3	1.081604004	1.871894752	+

Polyadenylate-binding protein	PABPC4	1.064692815	2.757012728	-
Zinc finger protein ubi-d4	DPF2	1.047100703	1.477201208	+
39S ribosomal protein L39, mitochondrial	MRPL39	1.037794749	2.360246654	-

Table 8.9 Significantly enriched proteins from trapping experiments in rotenone treated Hek293T cells with ClpP mutant SH7 (log_2 ratio > 1, $–log_{10}$ t-test p-value > 1.30). Proteins that were enriched only in rotenone treated samples and no other ClpP mutants are marked as follows: "+" indicates positive and "-" indicates no unique enrichment.

Protein names	Gene names	Enrichment factor (log_2)	p-value t-test ($-log_{10}$)	Unique for rotenone treated samples
Enoyl-CoA hydratase, mitochondrial	ECHS1	5.274079005	2.003698056	-
10 kDa heat shock protein, mitochondrial	HSPE1	3.559659958	2.416902285	-
Tyrosine--tRNA ligase, mitochondrial;Tyrosine--tRNA ligase	YARS2	3.065404256	2.676012595	-
Malate dehydrogenase;Malate dehydrogenase, mitochondrial	MDH2	2.600123723	2.538980576	-
Kappa-casein	CSN3	2.359725952	3.196187718	+
Single-stranded DNA-binding protein;Single-stranded DNA-binding protein, mitochondrial	SSBP1	2.081043879	3.129474044	-
Polyribonucleotide nucleotidyltransferase 1, mitochondrial	PNPT1	1.964795431	1.332356849	-
Isovaleryl-CoA dehydrogenase, mitochondrial	IVD	1.945773443	2.242487823	-
Cyclin-dependent kinase 4	CDK4	1.944344203	1.647243029	+
Presequence protease, mitochondrial	PITRM1	1.935722987	2.271304681	-
Inorganic pyrophosphatase 2, mitochondrial	PPA2	1.739587784	2.006109134	-
Tubulin beta chain	TUBB	1.616382599	1.715995809	-
Histidine triad nucleotide-binding protein 2, mitochondrial	HINT2	1.565341949	2.158128659	+
Citrate synthase;Citrate synthase, mitochondrial	CS	1.521754583	2.614555541	-
Putative transferase CAF17, mitochondrial	IBA57	1.488054911	1.419573126	+
Mitochondrial import receptor subunit TOM40 homolog	TOMM40	1.405598323	1.483859403	-
Acetyltransferase component of pyruvate dehydrogenase complex	DLAT	1.354489009	3.254700786	-
Hydroxyacyl-coenzyme A dehydrogenase, mitochondrial	HADH	1.331139247	2.839319267	-
Acyl-CoA dehydrogenase family member 9, mitochondrial	ACAD9	1.292857488	2.455665811	-
Mitochondrial ribonuclease P protein 1	TRMT10C	1.282247543	2.355294345	-
Aconitate hydratase, mitochondrial	ACO2	1.259790421	2.855714637	-
Heat shock protein 75 kDa, mitochondrial	TRAP1	1.242417653	3.172907231	-
Host cell factor 1	HCFC1	1.204651515	1.306021892	+
SRA stem-loop-interacting RNA-binding protein, mitochondrial	SLIRP	1.125771205	3.272002454	-
NADH dehydrogenase [ubiquinone] flavoprotein 2, mitochondrial	NDUFV2	1.117319743	1.840864095	+
Glutamate dehydrogenase;Glutamate dehydrogenase 1, mitochondrial	GLUD1	1.045743306	2.092659677	-
Poly [ADP-ribose] polymerase 1	PARP1	1.03410085	1.622107904	+
5-AMP-activated protein kinase catalytic subunit alpha-2;5-AMP-activated protein kinase catalytic subunit alpha-1	PRKAA1	1.022970835	2.443330979	+

8.2 Selected ^{1}H-NMR and ^{13}C-NMR spectra for chapter 2

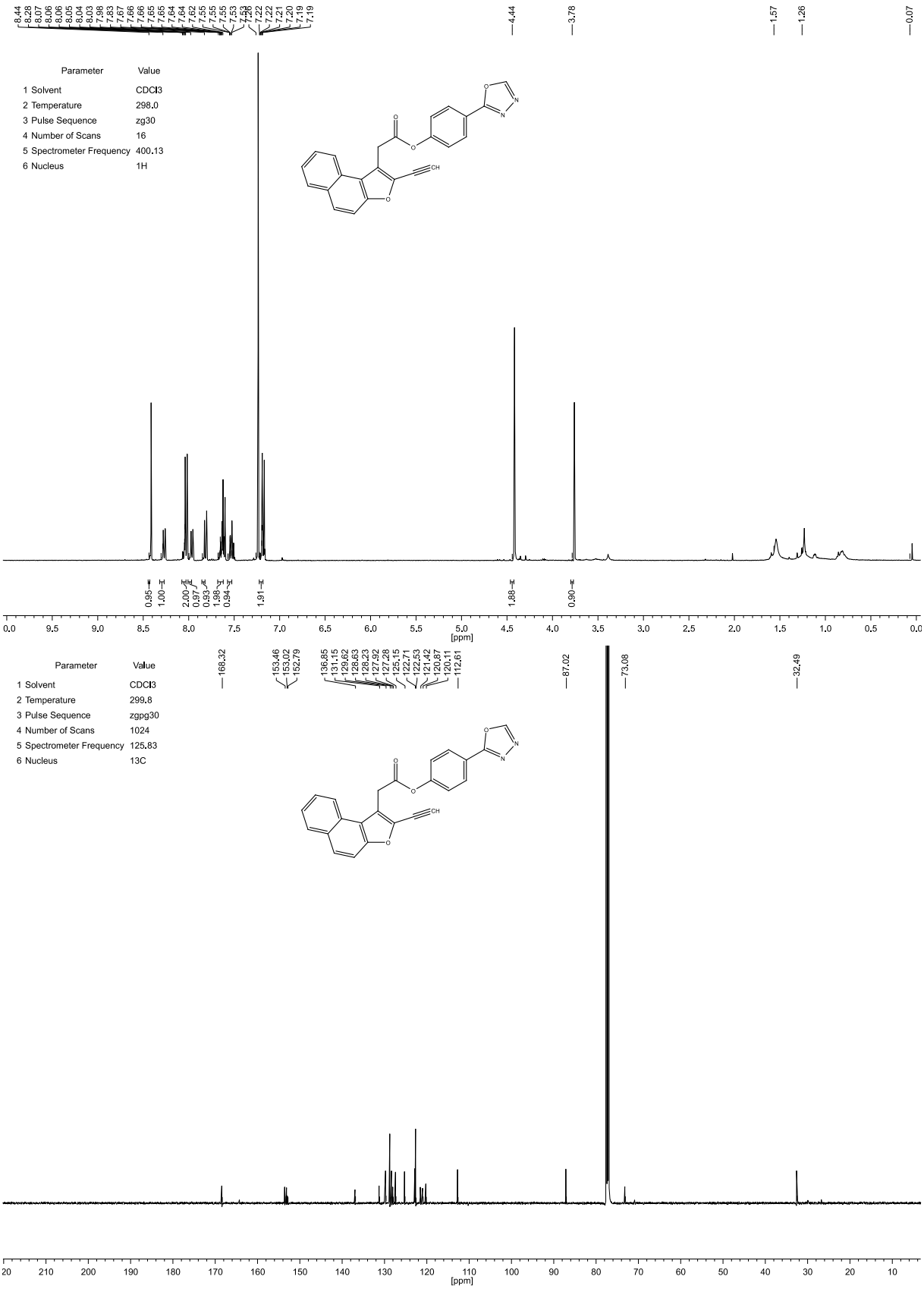

Figure 8.3 ^{1}H-NMR and ^{13}C-NMR spectrum of **35**.

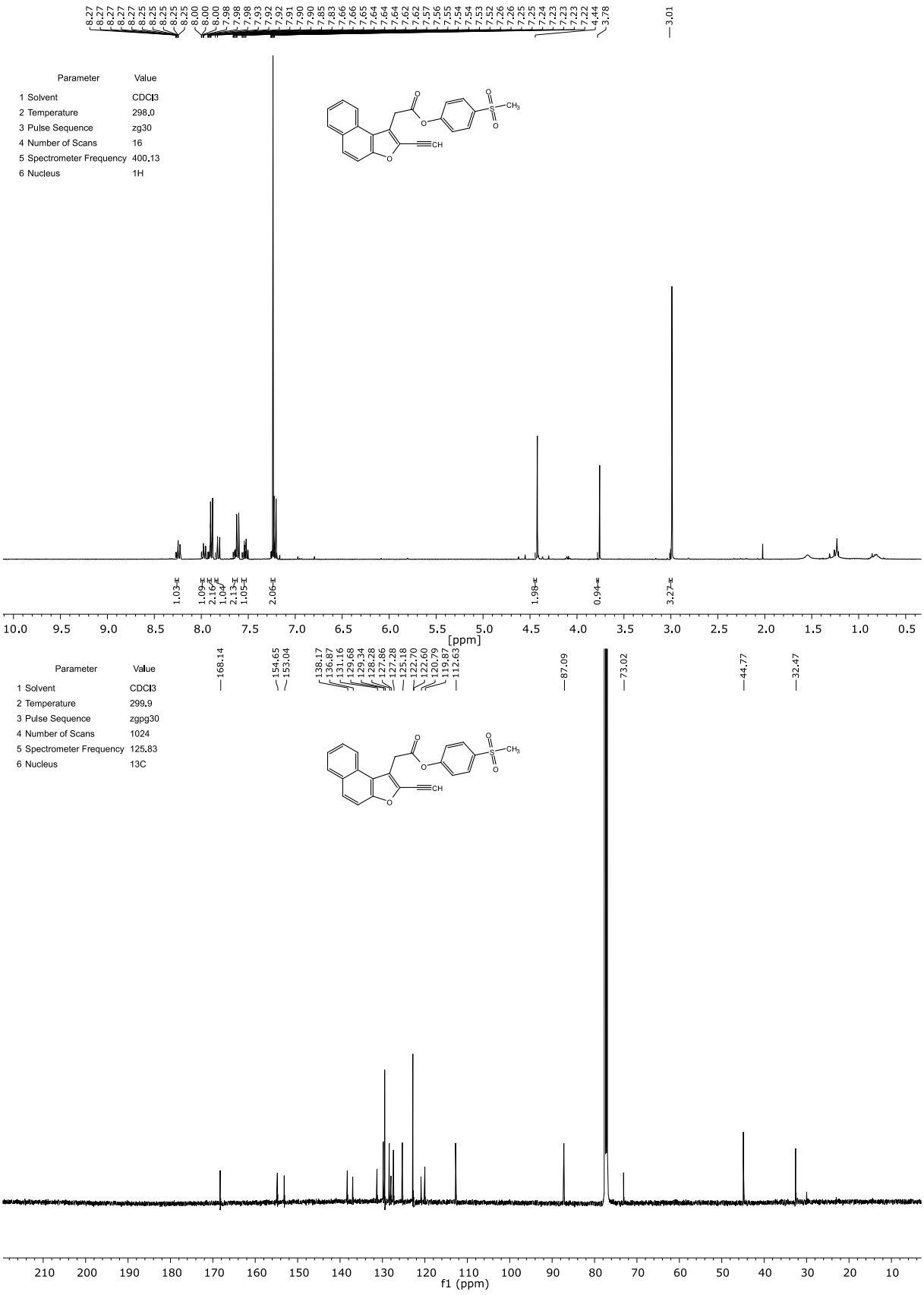

Figure 8.4 ^{1}H-NMR and ^{13}C-NMR spectrum of **40**.

8.3 Selected ^{1}H-NMR and ^{13}C-NMR spectra for chapter 4

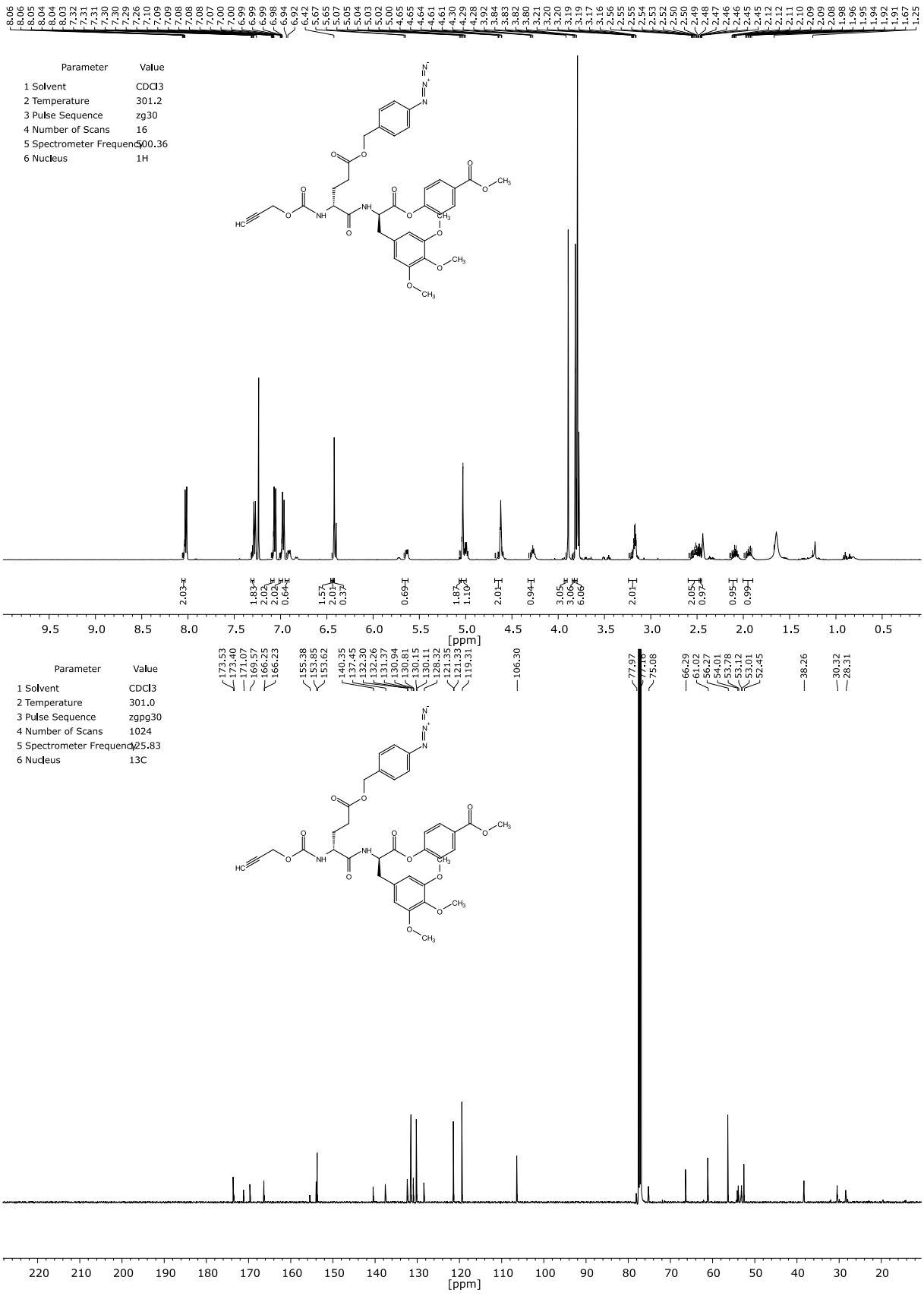

Figure 8.5 ^{1}H-NMR and ^{13}C-NMR spectrum of **Trap1**.

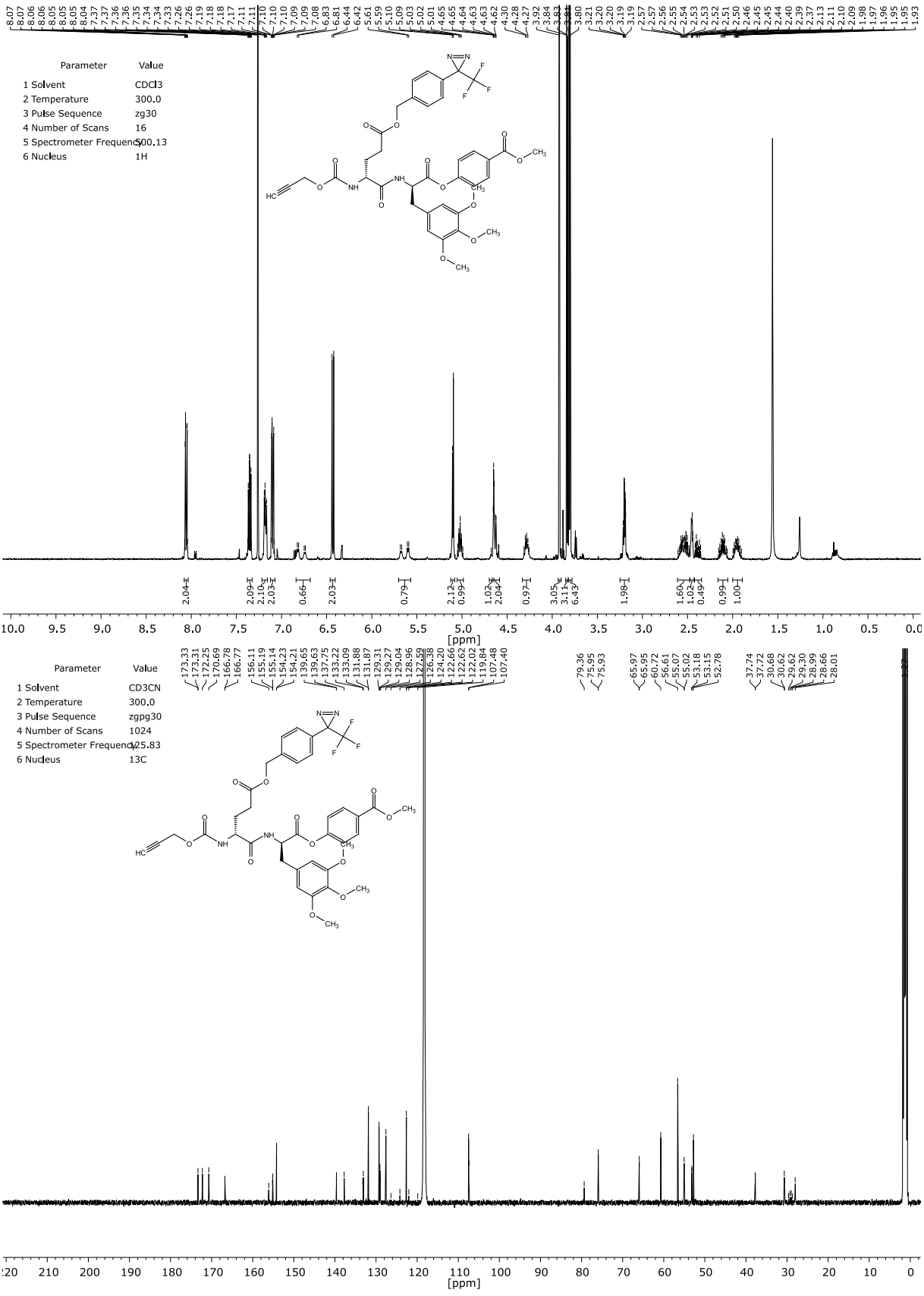

Figure 8.6 ^{1}H-NMR and ^{13}C-NMR spectrum of **Trap2**.

9 Licenses

JOHN WILEY AND SONS LICENSE
TERMS AND CONDITIONS

Nov 22, 2020

This Agreement between Thomas Gronauer ("You") and John Wiley and Sons ("John Wiley and Sons") consists of your license details and the terms and conditions provided by John Wiley and Sons and Copyright Clearance Center.

License Number	4954310301133
License date	Nov 22, 2020
Licensed Content Publisher	John Wiley and Sons
Licensed Content Publication	Angewandte Chemie International Edition
Licensed Content Title	Tailored Peptide Phenyl Esters Block ClpXP Proteolysis by an Unusual Breakdown into a Heptamer–Hexamer Assembly
Licensed Content Author	Markus Lakemeyer, Eva Bertosin, Friederike Möller, et al
Licensed Content Date	Apr 17, 2019
Licensed Content Volume	58
Licensed Content Issue	21
Licensed Content Pages	6
Type of use	Dissertation/Thesis
Requestor type	University/Academic
Format	Print and electronic
Portion	Figure/table
Number of figures/tables	1
Will you be translating?	No
Title	Design and synthesis of novel inhibitors for human protease ClpXP and substrate identification of human and S. aureus ClpXP
Institution name	Technical University Munich
Expected presentation date	Jan 2021
Portions	Graph from Figure 2c
Requestor Location	Thomas Gronauer Lichtenbergstrasse 4 Garching, 85748 Germany Attn: Technical University Munich
Publisher Tax ID	EU826007151
Total	0.00 EUR

Terms and Conditions

TERMS AND CONDITIONS

This copyrighted material is owned by or exclusively licensed to John Wiley & Sons, Inc. or one of its group companies (each a"Wiley Company") or handled on behalf of a society with which a Wiley Company has exclusive publishing rights in relation to a particular work (collectively "WILEY"). By clicking "accept" in connection with completing this licensing transaction, you agree that the following terms and conditions apply to this transaction (along with the billing and payment terms and conditions established by the Copyright Clearance Center Inc., ("CCC's Billing and Payment terms and conditions"), at the time that

SPRINGER NATURE LICENSE
TERMS AND CONDITIONS

Nov 22, 2020

This Agreement between Thomas Gronauer ("You") and Springer Nature ("Springer Nature") consists of your license details and the terms and conditions provided by Springer Nature and Copyright Clearance Center.

License Number	4954310116621
License date	Nov 22, 2020
Licensed Content Publisher	Springer Nature
Licensed Content Publication	Nature Structural & Molecular Biology
Licensed Content Title	Clarifying the supercomplex: the higher-order organization of the mitochondrial electron transport chain
Licensed Content Author	James A Letts et al
Licensed Content Date	Oct 5, 2017
Type of Use	Thesis/Dissertation
Requestor type	academic/university or research institute
Format	print and electronic
Portion	figures/tables/illustrations
Number of figures/tables /illustrations	1
High-res required	no
Will you be translating?	no
Circulation/distribution	50000 or greater
Author of this Springer Nature content	no
Title	Design and synthesis of novel inhibitors for human protease ClpXP and substrate identification of human and S. aureus ClpXP
Institution name	Technical University Munich
Expected presentation date	Jan 2021
Portions	Figure 1
Requestor Location	Thomas Gronauer Lichtenbergstrasse 4 Garching, 85748 Germany Attn: Technical University Munich
Total	0.00 EUR

Terms and Conditions

Springer Nature Customer Service Centre GmbH
Terms and Conditions

This agreement sets out the terms and conditions of the licence (the **Licence**) between you and **Springer Nature Customer Service Centre GmbH** (the **Licensor**). By clicking 'accept' and completing the transaction for the material (**Licensed Material**), you also confirm your acceptance of these terms and conditions.

1. Grant of License

1. 1. The Licensor grants you a personal, non-exclusive, non-transferable, world-wide licence to reproduce the Licensed Material for the purpose specified in your order only. Licences are granted for the specific use requested in the order and for no other use, subject to the conditions below.